A CONSIDERATION OF CYCLE SELECTION FOR MESO-SCALE DISTRIBUTED SOLAR-THERMAL POWER

A Thesis
Presented to
The Academic Faculty

by

Suzanne Price

In Partial Fulfillment
of the Requirements for the Degree
Master of Science in the
Mechanical Engineering

Georgia Institute of Technology
August 2009

A CONSIDERATION OF CYCLE SELECTION FOR MESO-SCALE DISTRIBUTED SOLAR-THERMAL POWER

Approved by:

Professor J. Rhett Mayor, Advisor
Woodruff School of Mechanical Engineering
Georgia Institute of Technology

Professor Srinivas Garimella
Woodruff School of Mechanical Engineering
Georgia Institute of Technology

Professor Sheldon Jeter
Woodruff School of Mechanical Engineering
Georgia Institute of Technology

Date Approved: 1 July 2009

To my parents,

for their unending love and support.

ACKNOWLEDGEMENTS

I would like to express my gratitude to my academic and research advisor, Dr. J. Rhett Mayor. Without his support, guidance, and enthusiasm, I would not have successfully completed this thesis. Over the course of the past two years, I have further developed my engineering skills as Dr. Mayor continually engages me in discussion about "why" a solution is valid and not just "how" I arrived at the solution.

I would also like to thank my thesis review committee, Dr. Srinivas Garimella and Dr. Sheldon Jeter, for their guidance throughout my studies at Georgia Tech. Their expertise has contributed to a deeper understanding of thermodynamics and heat transfer.

I am grateful for my outstanding research group colleagues, Alex, Andrew, Angela, and Jacob, who have provided an abundance of support from technical brainstorming to a funny picture that makes me laugh. The fun times of Friday wrap-up lunches to burning inanimate objects with the Fresnel lenses will not be forgotten.

Finally, I wish to thank my parents, my sister and my fiancé for their love and support. My parents have always encouraged me to dream big and go after lofty goals. Without my parents encouragement, I would not have developed into the person I am today. I would like to graciously say "thank you" to my sister for the countless phone calls and cards from her students that brightened my day. And finally, I am grateful for my fiancé, Jordan, for supporting me through the rewards and struggles of undergraduate and graduate school.

TABLE OF CONTENTS

LIST OF TABLES

LIST OF FIGURES

NOMENCLATURE

A	Area $[m^2]$
AFUE	Annual Fuel Utilization Efficiency [%]
C	Cost [$]
CAT	Closest approach temperature
CP	Constant pressure specific heat $[\frac{kJ}{kg-K}]$
CRSTP	Central receiving solar-thermal power
DIPPR	Design Institute for Physical Properties
DSG	Direct steam generation
EIA	Energy Information Agency
EOS	Equation of state
EES	Engineering Equation Solver
g	Graviatational constant $[[\frac{m^2}{sec}]$
h	Heat transfer coefficient $[\frac{W}{m^2-K}]$
h	Specific enthalpy $[\frac{kJ}{kg}]$
K	Loss factor
k	Thermal conductivity $[\frac{W}{m-K}]$
$\dot{\boldsymbol{m}}$	Mass flow rate $[\frac{kg}{sec}]$
NREL	National Renewable Energy Laboratory
OECD	Organization for Economic Cooperation and Development
ORC	Organic Rankine cycle
P	Pressure [kPa or MPa]
PTC	Parabolic trough collector
PV	Photovoltaic
q	Heat Transfer per unit mass $[\frac{kJ}{kg}]$
$\dot{\boldsymbol{Q}}$	Heat transfer rate $[kW]$
Qu	Quality
PCSAFT	Perturbed Chain Statistical Associating Fluid Theory
R	Thermal resistance $[\frac{K}{W}]$

Ra	Rayleigh number
s	Specific entropy $[\frac{kJ}{kg-K}]$
T	Temperature [C or K]
t	time [sec]
$\dot{\boldsymbol{W}}$	Power [kW]
X	Concentration
Z	Cost-to-efficiency ratio [\$/%]

Greek Characters

$\boldsymbol{\alpha}$	Thermal diffusivity $[\frac{m^2}{sec}]$
$\boldsymbol{\beta}$	Thermal expansion coefficient $[\frac{1}{K}]$
$\boldsymbol{\delta}$	Thickness [mm]
$\boldsymbol{\eta}$	Efficiency
$\boldsymbol{\epsilon}$	Effectiveness
$\boldsymbol{\nu}$	Kinematic viscosity $[\frac{m^2}{sec}]$

Subscripts

act	Actual
B	Basic
D	Dilute
G	Generator
HX	Heat exchanger
P	Pump
s	Ideal
ss	Source,Sink
ST	Shell & Tube
T	Turbine
V	Vapor
WF	Working Fluid

SUMMARY

Thermodynamic and thermoeconomic aspects of 12.5 kW residential solar-thermal power generating systems suitable for distributed, decentralized power generation paradigm are presented in this thesis. The design of a meso-scale power system greatly differs from centralized power generation. As a result, this thesis provides guidance in the selection of the power cycle and operating parameters suitable for meso-scale power generation.

Development of standard thermodynamic power cycle computer simulations provides means for evaluation of the feasibility of meso-scale solar-thermal power generation. The thermodynamic power cycles considered in this study are the Rankine cycle, the organic Rankine cycle with toluene, R123, and ethylbenzene as working fluids, the Kalina cycle, and the Maloney-Robertson cycle. From a strictly thermodynamic perspective, the cycles are evaluated based on first- and second-law efficiencies. Additionally, the study includes economic feasibility through thermoeconomic characterization that encompasses a meso-scale cost model for solar-thermal power generation systems.

Key results from this study indicate that a R123 organic Rankine cycle is the most cost-effective cycle implementation for operating conditions in which the maximum temperature is limited below 240 °C. For temperatures greater than 240 °C and less than 375 °C, the toluene and ethylbenzne organic Rankine cycles outperform the other cycles. The highest first law efficiency of 28% of the Kalina cycle exceeds all other cycles at temperatures between 375 °C and 500 °C. However, when including thermodynamic and thermoeconomic performance, the Maloney-Robertson and Kalina cycles have poor performance on a cost-to-efficiency basis.

CHAPTER 1

INTRODUCTION

The goal of this effort has been to enhance the understanding of thermodynamic power cycle selection for meso-scale solar-thermal power generation. For this study, meso-scale power generation is defined to be power levels near 12.5 kW peak with average levels around 5 to 7 kW. By establishing enhanced guidelines for cycle selection based on thermoeconometric principles, this thesis aims to contribute to the advancement of a feasible, commercially viable meso-scale solar-thermal power generation technology that supports a paradigm shift to distributed, sustainable power generation infrastructure capable of addressing growing societal needs for a less expensive, clean energy supply.

The Energy Information Administration (EIA) presents an annual report, the International Energy Outlook, aimed to characterize international production of and consumption of energy. The 2008 report predicts a 50% increase in energy demand over the next 40 years, including an 80% increase in the energy needs of developing nations that are not a part of the Organization for Economic Cooperation and Development(OECD). Increased demand for energy is met with an increase in coal, liquid fuels and natural gas with a small contribution in the increase of renewable and nuclear technologies (Figure 1). The liquids category in Figure 1 includes " petroleum-derived fuels and non-petroleum-derived fuels, such as ethanol and biodiesel, coal-to-liquids, and gas-to-liquids. Petroleum coke, which is a solid, is included. Also included are natural gas liquids, crude oil consumed as a fuel, and liquid hydrogen". The increase in energy generation is met with an increase use of liquids and coal. The use of renewable sources, including hydropower, is expected to grow only 2% between now

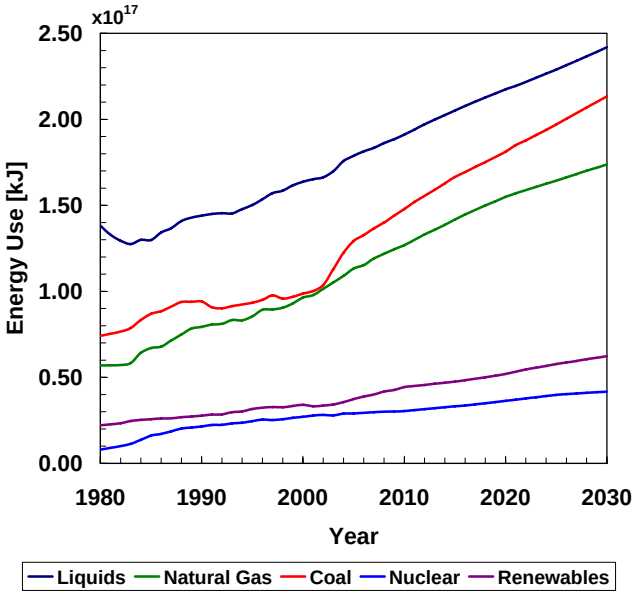

Figure 1: EIA projected Total Energy Usage characterized by Fuel Source [11]

and 2030 (Figure 2). Coinciding with the increase use of fossil fuel based power, the EIA estimates that 2030 carbon-dioxide emissions will increase 51% compared to the levels in 2000 (Figure 3). Furthermore, predictions in the Energy Outlook for 2008 indicate that the 2030 carbon dioxide emission from developing nations will exceed that of developed nations by 72%. [11]

The EIA Outlook for 2008 does not forecast a large increase in the use of renewable energy technologies; however, it is imperative to continue ongoing research in the alternative energy sector that will lead to lower-cost, lower-carbon emitting technologies to fulfill the increasing global energy needs. Likewise, development of these technologies will create cost-competitive technologies that can be utilized by developing nations and potentially offset the 72% increase in carbon dioxide emissions that is anticipated to ensue from the ongoing growth in these nations.

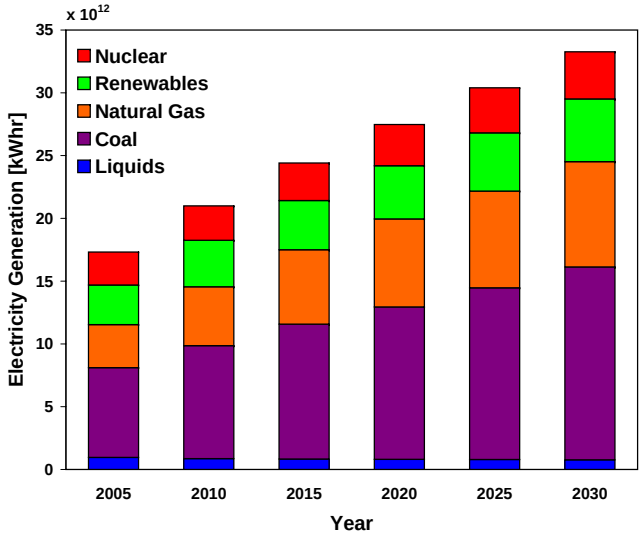

Figure 2: EIA projected Fuel Usage by Source for Electricity Generation [11]

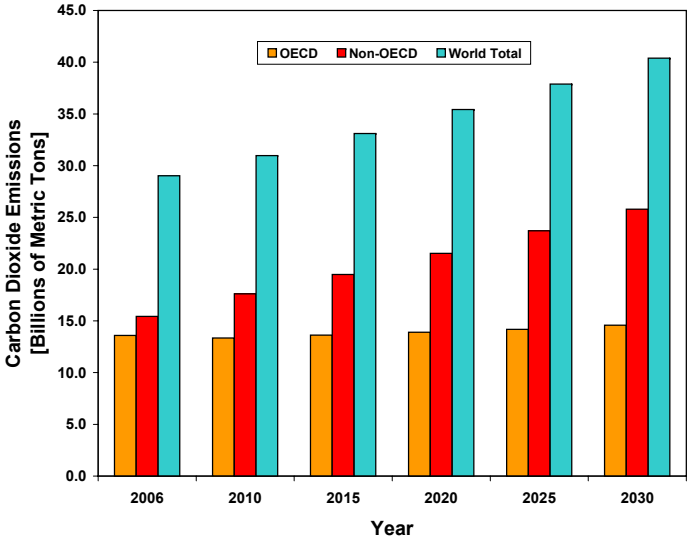

Figure 3: EIA projected Carbon-Dioxide Emissions [11]

1.1 Overview of Solar Power Technologies

Solar power generation is achieved by converting radiative energy from the sun into electricity. In this section, various methods for generating solar power are presented. The current focus of residential solar power generation in the United States is photovoltaic cells while the centralized power plants are solar-thermal technologies.

Photovoltaic (PV) cells are devices that implement the photovoltaic effect. The photovoltaic effect was first studied in 1839 by French physicist A. E. Becquerel [21]. PV cells convert sunlight directly into electricity without the use of a heat engine. The first PV solar cell was created in 1883 by Charles Fritts and it was less than 1% efficient. The modern PV solar cells were created by researchers at RCA and Bell Laboratories in 1954 [21]. One of the early applications of these new PV cells in the 1950s was the US satellite Vanguard in 1958 [72].

Modern day PV technologies apply the photovoltaic effect through the use of p-n type semi-conducting materials. Photonic energy incident on the PV cell excites electrons in the semi-conducting material. When the increase in energy is larger than the band gap of the semiconductor, electrons move freely in the conduction band. Then a p-n junction is used to convert the electon flow in the conduction band to a current. PV cells have not become a mainstream application because of the low conversion efficiencies and high cost. Commercially available cells typically are 10% to 15% efficient [54] and estimated total installed costs at various power levels are listed in Table 1. Recent technological advancements in the creation of silion PV cells have increased the efficiency to 40% [20]; however, these cells are not commercially availble and have a capital cost at $3 per Watt not including the support structures, tracking devices or control systems [57].

Solar-thermal technologies are not used for power generation at the residential level but are a main source of large-scale solar power generation. Governmental research dedicated to the development of large-scale solar-thermal power began in

Table 1: Cost of PV Cells at Various Power Levels [69]

Power Level [kW]	Cost per Watt
0.75	\$12
2	\$8-\$10
5	\$6-\$8

1974 when the Solar Energy Industries Association was formed. The Solar Energy Research Institute was formed in 1977 and later became the National Renewable Energy Laboratory (NREL).

Solar One in Barstow, California was the first operational large scale solar-thermal system. It came online in 1983. Solar One is a central receiving solar-thermal power (CRSTP) plant. CRSTP plants use mirrors, or heliostats, to focus sunlight at a central receiver. Since many heliostats are focused onto one central receiver, temperatures of 1000°C can be obtained and steam production will support 10 to 1000 MW of power output from standard steam power cycles. Solar One in California was shut down in 1988 after proof-of-concept was established then recommissioned as Solar Two in 1995 to test improvements to the system including more collection area and different collection fluids. Solar Two was decommissioned in 1999.

Currently, PS10 in Spain is an operational CRSTP plant. PS10 is located in Sanlúcar la Mayor, Sevilla, Spain. It has a capacity of 11 MW and has storage capacity that allows full production for 30 minutes in the absence of sunlight as well as natural gas back-up to deliver 12 to 15% of full load. PS10 has 624 Sanlucar-120 heliostats that each provide 120 square meters of collection area. The heliostat field reflects sunlight to the receiving tower where 92% of the sunlight collected is converted to steam4(b)). The steam is expanded through a turbine to produce usable energy [1].

A parabolic trough collector (PTC) is an alternative to a point source heliostat CRSTP plant. PTCs create a concentrated line source at a lower concentration ratio. Often times, multifaceted PTC and compound parabolic concentrators are used to

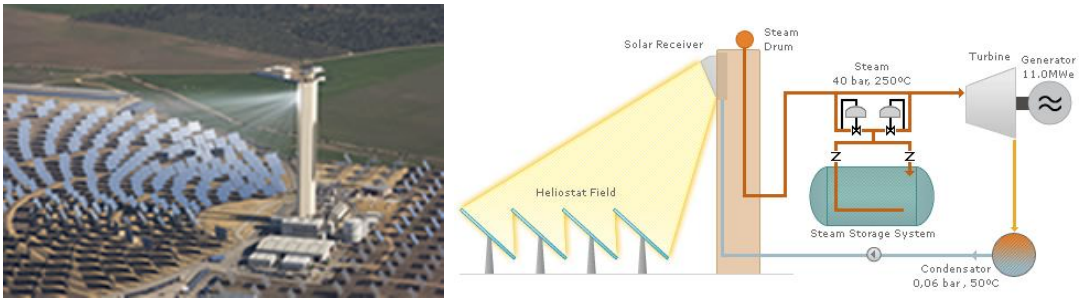

(a) (b)

Figure 4: PS10 in Sanlúcar la Mayor, Sevilla [1]

increase concentration ratio of the focused light. PTCs can be used in a dual-loop heat exchange process for power generation or for direct steam generation (DSG). In the dual-loop heating method, a thermally capacitive fluid is heated by the concentrated sunlight. After reaching temperature, a heat exchange process with the working fluid provides the source heat for the power cycle. In dual-loop implementation, the working fluid from the power cycle is not directly heated by the concentrated sunlight. DSG technologies use the concentrated sunlight to generate steam directly in the flow tubes of the PTCs. The steam is then transported to the turbines where it is expanded to produce work.

Nevada Solar One Plant located in Boulder City, Nevada is an example of a dual loop system. This plant has been in operation since June 2007 and the solar collecting area is 1,619,000 square meters (0.625 square miles). Nevada Solar One has 760 PTCs coated with a reflective material and an additional 182,000 mirrors to concentrate sunlight onto 18,240 flow tubes positioned at the focal length of the PTCs (Figure 5). The thermally capacitive fluid in the flow tubes reaches temperatures up to 390°C (735°F) and then it is used to provide the source heat for steam generation. The steam then expands through turbines to produce 64 MW of energy [2].

Direct Steam Generation (DSG) within the flow pipes of the PTCs offers another mode of large-scale power generation. At this time, there is ongoing development at la Platforma Solar de Almeria in Spain with DSG technologies with the Direct Solar

Figure 5: PTCs for Nevada Solar One [2]

Figure 6: Suncatcher Solar Parabolic Dish Stirling Energy System by SES [64]

Steam Project [48]. The test facilities for DSG were built in 1997 and include 40 parabolic troughs with 3000 square meters of collector length [80]. Absorber tubes with an outer diameter of 70 mm run 550 m and heat the flow to 400°C at 100 bar of pressure. The publication by Zaraz *et al.* [80] in 2004 provides proof of concept for DSG technologies. In 2008, Eck *et al.* [15] reported on continuing research with three steam separator design for DSG technologies in la Platforma Solar de Almeria.

Parabolic dish collectors coupled with Stirling Engines are able to produce meso-scale power at 5 to 100 kW. The first solar powered Stirling Engine, Vangaurd I, was developed by Advanco Corporation in 1984 [21]. An 11 m parabolic dish with a concentration ratio of 2100 focused sunlight onto a Stirling engine that reached 800°C with a power output of 25 kW. Today, the Suncatcher produced by Stirling

Energy Systems is a commercially available, 25kW solar Stirling engine with dual axis tracking shown in Figure 6 [64].

Fresnel lenses are an alternative collection technique to provide concentrated solar energy for a solar-thermal system. Fresnel lens are made by collapsing a concave lens onto a flat surface as seen in Figure 7. The reduced material equates to reduced weight for the tracking structure but the distinct edges created by the facets increase sunlight reflection and blocking [21]. Field tests on and methods for optimization of flat Fresnel lens applications for PV cells have been presented in literature [34, 5, 79]. Additionally, a 5896 kg (13,000 pound) Fresnel lens assembly was developed and built in 1983 by Entech, Inc for solar-thermal applications [56]. In 2001, Leutz and Gordon completed the design and testing of a domed non-imaging Fresnel lens for solar-thermal or PV applications [40]. These lenses provide an optical concentration of 13.67 and a fairly uniform illumination over the spot area but have poor spectral matching [40]. The spectral matching is important in PV applications. In low concentration needs, the domed Fresnel lens does not require a tracking device. One of the main economic disadvantages of the domed Fresnel lens is the cost of $4-$5 per Watt [40]. Microarrays of Fresnel lenses are used for consumer electronics displays and optical communications devices [9, 37, 81] and the fabrication techniques may provide means of cost reduction for meso-scale power generation systems.

1.2 Uniqueness of Meso-Scale Power Generation

The main design constraints at the meso-scale encompass the macro-scale challenges as well as unique considerations only applicable to meso-scale. The challenges specific to the meso-scale are

1. Impact of Collection Site

2. Large Dynamic Fluctuations in Demand

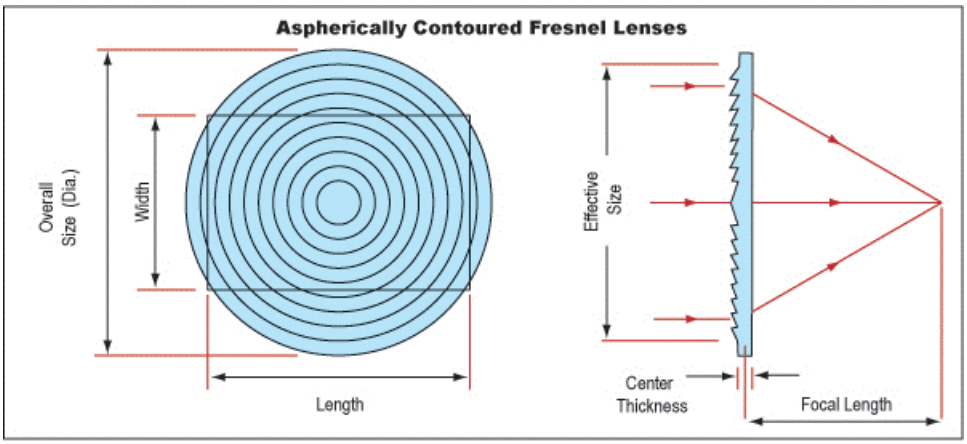

Figure 7: Fresnel Lens Diagram from Edmund Optics [16]

3. Cost Competitiveness

A more detailed discussion of the effects of each of these design considerations at the meso-scale follows in this section.

1.2.1 Impact of Collection Site

With distributed power generation, the users are spread across the world where the incoming solar radiation varies with latitude and season. Therefore, the site is not selected base on the ability to optimize the amount of incoming sunlight as with large-scale centralized solar power plants. The wide variation in collection sites leads to two anticipated operating modes for meso-scale solar-thermal power generation: a pressure-based set of operating parameters and a temperature-based set of operating parameters. The pressure-based parameters are constrained by the maximum turbine pressure because enough sunlight is collected to reach the maximum operating temperature. The upper pressure limit is defined by the residential building codes and other applicable safety standards. On the other hand, the temperature-based design is applicable in areas such as a city where shading of the collector is likely or in areas farther from the equator where a smaller incident angle with the sun contributes to a lower amount of the incoming radiation. As a result of decreased light reaching the

collector, the temperature of the stream heated by the collector is decreased. Therefore, the maximum cycle pressure is limited by the achievable saturation temperature of the working fluid.

In order to determine which system constraints are appropriate for the location of interest, examination of the average incident radiation data from a source such as the METSTAT global direct technique maintained by the NREL is required [53]. The NREL METSTAT hourly solar radiation for the equinoxes and solstices for 2005 for the cities of Atlanta, Georgia, Tucson, Arizona and Bangor, Maine are presented in Figure 8. The design for this meso-scale system is subject to the temperature-based operating parameters for a collection site in Atlanta and Bangor where there is a lower amount of incoming radiation. Tucson has a higher average peak insulation and appears to have fewer fluctuations in the radiation reaching the earth's surface and reaching a higher operating will not be problematic; as a result, the pressure-based constraints apply.

1.2.2 Large Dynamic Fluctuations

This study considers two end-use applications for the meso-scale solar-thermal power cycles: large single-family homes in developed nations and small rural communities in the developing world. As a result, the design point for this system is 12.5 kW of power. Also, The power output of this system is at least an order of magnitude smaller than typical solar-thermal applications.

Residential use of this system in developed nations would be for single-family purposes. Table 2 shows typical power use of a few household appliances. These appliances may operate simultaneously and create a load of 8.5 to 10.5 kW [68]. The system power level is designed to provide peak load. When peak load is not required, the excess energy is collected in the thermal energy storage unit.

The application of this system in developing countries fits within the scope of

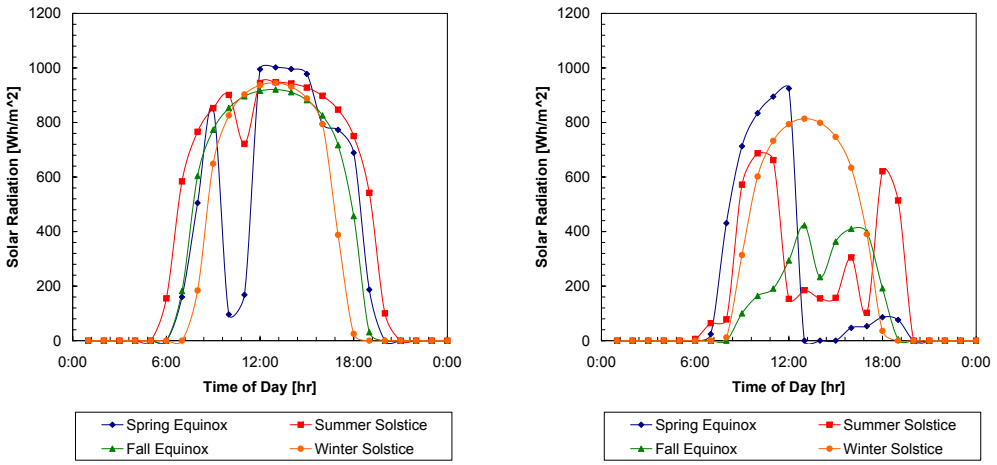

(a) (b)

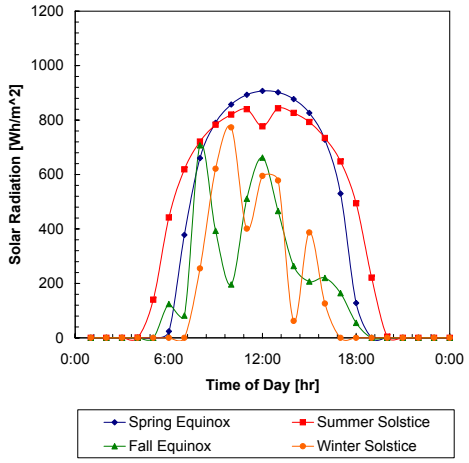

(c)

Figure 8: METSTAT direct solar radiation calculated solar radiation vs. time (a) Tucson, Arizona (b) Atlanta, Georgia (c) Bangor, Maine [53]

Table 2: Power Use of Household Appliances [68]

Appliance	Power Consumption [kW]
Coffee Maker	0.900-1.200
Refrigerator	0.725
Hair Dryer	1.2-1.875
Toaster Oven	1.225
Computer	0.270
Water Heater (40 gallons)	4.5-5.5
Total	8.8-10.8

micro-gird technologies. Micro-grid technologies typically use small-scale solar technologies, small-scale wind devices, diesel engines, fuel cells, and micro-turbines to produce electricity. The micro-grids can be connected to the grid or operate in a "stand alone" mode. A review of micro-grid technologies was completed by Jiayi in 2008 [29]. For a small, rural community, electricity provided through one or two meso-scale solar thermal units connected in a micro-grid configuration would power pumps, lights, etc. Five to nine deep well pumps for portable water or irrigation could be powered using just one 12.5 kW meso-scale, solar thermal power system.

Also, it is important to note that the fluctuations in demand caused by the use of common household electronic devices are on the same order of magnitude as the total, meso-scale system power output. This inherent characteristic of meso-scale systems can be offset by utilizing an impulse turbine. An impulse turbine is of interest in this situation because it has flatter efficiency vs. load curves, schematically represented in Figure 9, resulting in reduced load sensitivity and a wider range of near-optimal operating conditions when compared with alternative work extraction devices.

The impulse turbine is also useful when there are fluctuations in the incoming solar radiation. For example, on the 2005 summer solstice in Atlanta, Georgia (Figure 8(b)) a drop in the incoming radiation occurred around 4 in the afternoon. The impulse turbine would be able to compensate for this small fluctuation.

Additionally, a solar thermal system must use thermal storage techniques because

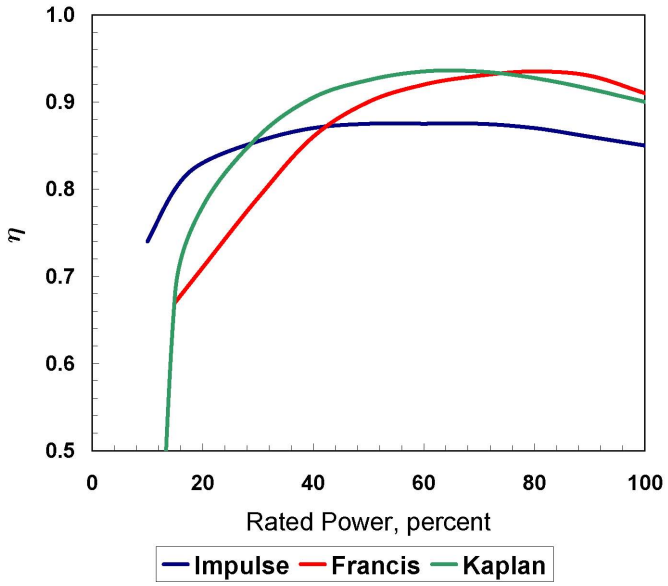

Figure 9: Efficiency vs. Power for different turbine designs [78]

of the unpredictability of the heat availability. Obviously, "on-demand" power cannot be supplied at night or during periods of long lapse in sunlight such as the afternoon of the 2005 spring equinox in Atlanta (Figure 8(b)). Thermal energy storage technologies include sensible heat storage, latent heat storage and thermochemical heat storage [21]. The 24-hour power challenge associated with solar technologies is a large drawback and often prevents widespread adoption of these technologies. The scope of this project does not address the 24-hour power challenges associate with the meso-scale power generation; however, it is important to note that this challenge exists.

1.2.3 Cost Competitiveness

For a solar-thermal power system to be viable at the meso-scale, it must offer cost competitive electricity supply. For large-scale power plants, the thermodynamic system efficiency of the plant is as high as possible to counter the expense of components necessary to produce mega-Watts of power. At the meso-scale, the cost-to-efficiency

ratio must be a low as possible. Since cost and efficiency have an inverse relationship, the system design point is a trade off between the two parameters, neither of which are at their respective maxima.

For this meso-scale system, pressure and temperature constraints are placed on the system to reduce the component costs. As a result, the efficiency of the system may not be as high as a conventional power plant but the cost of power production may still be cost competitive with large scale systems. To further reduce costs, the systems under consideration are the simplest thermodynamic implementations of the cycles considered in this study, and do not contain additional heat exchangers, pumps, or turbine; thus, with fewer components, the capital cycle cost decreases.

1.3 Research Objectives

Specifically, this study aims to critically assess the following objectives regarding meso-scale solar-thermal power generation that arise from the conventional scale understanding of thermodynamic power cycle design:

1. To thermodynamically characterize potential power generating cycles for use in a meso-scale system operating under meso-scale dependent constraints
2. To construct a representative cost model for meso-scale solar-thermal power systems
3. To perform a comparative analysis of meso-scale power cycles utilizing thermoeconometric principles to establish commercial viability of solar-thermal power systems based on cost-to-efficiency trade offs
4. To establish guidelines for the selection of site-suitable design constraints for a meso-scale power system

1.4 Organization of Thesis

To address the research objectives of this study, thorough dissemination of previous works is included in Chapter 2. Key material for the initial cycle evaluation of the organic Rankine cycles in relation to the Kalina and Rankine cycle base models is presented in Chapter 3. Chapter 4 provides a detailed evaluation of ammonia-water power cycles with the inclusion of the solar source stream characterization. In Chapter 5, thermodynamic performance and a detailed meso-scale cost model are integrated to form the thermoeconometric parameterization for evaluation of the cost effectiveness of the meso-scale power cycles.

CHAPTER 2

REVIEW OF SALIENT BACKGROUND INFORMATION

It is necessary and prudent, in order to avoid duplicating work, that previous papers considering the cycles in question be thoroughly reviewed. The rest of this section is devoted to such a task, specifically, a detailed look into the previously completed thermodynamic cycle analyses.

2.1 Organic Rankine Cycles

Research on organic Rankine cycles (ORC) has increased over the past few years accompanying the push for affordable, clean energy systems. The standard ORC includes a condenser to reject waste heat, pump to increase the working fluid pressure, evaporator unit for heating and boiling the working fluids, and a turbine for work extraction. A simplified, standard version of the ORC is represented in the schematic in Figure 10. The ORC differs from the standard Rankine cycle only because of the fluid selection. Therefore, a comprehensive discussion of a standard Rankine cycle is not presented in this work and readers are referred to a general thermodynamics textbook for additional discussion on the Rankine cycle [8]. A standard Rankine cycle with water as the working fluid is used as a baseline for comparison.

2.1.1 Applications of ORCs

For low temperature heat sources coupled with low pressure operating points, Rankine cycles utilizing organic working fluids offer higher efficiencies compared to applications with water as the working fluid. Recently, studies have been conducted to evaluate appropriate organic working fluids for various system parameters such as low-grade heat sources associated with geothermal power generation [60], solid

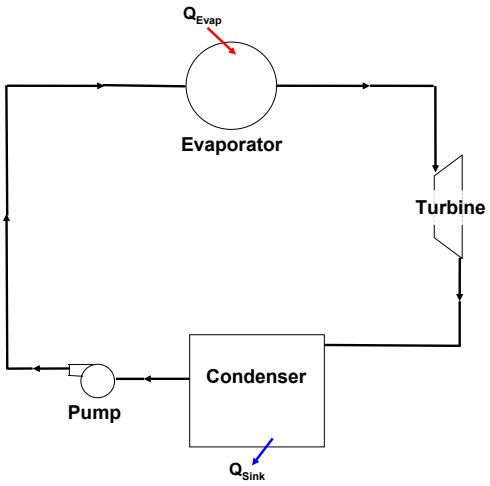

Figure 10: Standard Rankine Cycle and Organic Rankine Cycle Diagram

biomass power-heat cogeneration systems [14], and industrial exhaust gas recovery systems [77].

2.1.2 Working Fluid Selection

Important definition of power cycles comes with the thermodynamic characteristics of the fluids through the slope of the saturation curve on a T-s diagram. Fluids with two distinct T-s diagram shapes, a bell shape and an overhang, are examined in this study [60]. Water and ammonia have a bell shaped T-s diagram and the organic fluids have an overhang shape as shown in Figure 11. Fluids with an overhanging T-s diagram are advantageous because ORC fluids may be expanded directly from the saturated vapor line and still achieve single phase gaseous flow at the turbine exhaust. The water and ammonia-water cycles cannot expand from the saturated vapor line because the turbine exhaust would enter the two-phase region. Studies examining the optimal fluid for an ORC have been completed and a review of a selected number of papers is presented in this work.

Lee *et al.* [36] examined ozone-safe organic fluids using the Iwai-Margerum-Lu Equation of State (EOS). The basic Rankine cycle in this study does not consider

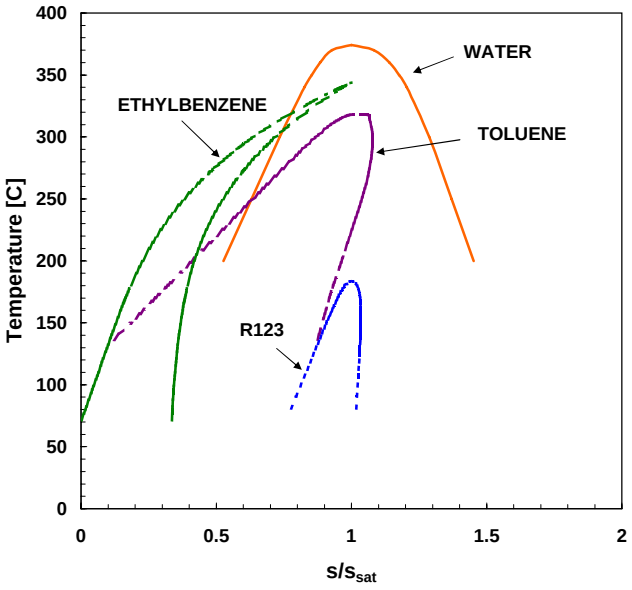

Figure 11: T-s Diagrams for Cycle Fluids

superheat because the fluids of interest have over-hang T-s diagrams. The conclusions of this study show that R123, also known as HCFC-123 or 1,1-dicholoro-2, 2,2-triflouroethane, is the fluid of choice. It is important to note that this fluid is a hydrocholorflorocarbon. Many HCFCs have damaging effects on the environment. A study completed by DuPont in 2001 under the US Environmental Protection Agency showed few ill effects the human safety or the environment and R123 is commercially available from Dupont© Suva 123 [70].

In 2005, Saleh *et al.* [60] studied 31 pure fluids for use in sub- or super-critical ORCs coupled with geothermal heat sources. The geothermal power plants operate at a maximum pressure of 2 MPa between a source temperature of 100°C and a sink of 30°C. The fluid properties were modeled using the BACKONE Equation of state for polar and non-polar pure fluids [60]. The results from this study indicate that R601 and n-hexane have the highest first law cycle efficiencies at 12.9% and 13% respectively. The geothermal heat source temperatures are well below the limits achievable with standard concentrated solar collection techniques.

Mago [44] tested multiple organic fluids at 1.5 MPa maximum process pressure and 25°C minimum process temperature over the turbine temperature range of 27-225°C. The study compared fluids through first- and second-law efficiencies. From a first-law standpoint, an ORC with R113, trichlorotrifluoroethane, has the best thermal efficiency; however, R113 is banned from use by the Montreal Protocol. Therefore, R123, the second most efficient fluid from this study, is again confirmed as promising ORC fluid.

In 2007, Drescher [14] surveyed 700 organic fluids for use in biomass power and heat plants. This study showed that the alkylbenzene family illustrated the highest efficiencies at a turbine pressure of 2 MPa and turbine temperature of 300°C. Therefore, this study explores the suitability of ethylbenzene and toluene, members of the alkylbenzene family, as the working fluid in the solar-thermal ORC power cycles considered in this study.

2.1.3 ORC Property Modeling Techniques

Water is modeled using thermodynamic correlations from Harr [24]. R123 and toluene are modeled via the Roth-Tillner EOS [67]. In accordance with Drescher [14], ethylbenzene properties were modeled with standard liquid thermodynamic relations, basic thermodynamic relations for phase change processes, and the Peng-Robinson cubic EOS is used for modeling the gaseous fluid properties. The necessary property data for ethylbenzene needed to evaluate the Peng-Robinson EOS were referenced from the Design Institute for Physical Properties (DIPPR) Project 801 [6].

2.2 Ammonia-Water Cycles

Binary fluid power cycles are advantageous because they offer better slope matching between the source and working fluid compared to a pure fluid (Figure 12). The gliding temperature profile for a binary fluid is a result of varying specific heat in the

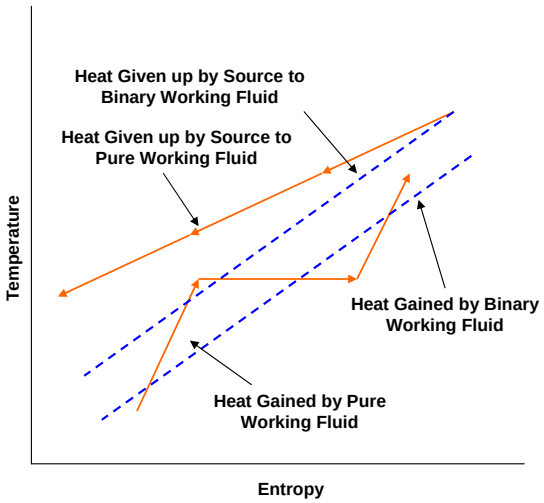

Figure 12: Heat transfer between source and working fluid [21]

fluid and equates to less irreversibilty in the heat transfer process. In the heating process, this is an advantage but it becomes a disadvantage for condensation processes. The binary fluid cycles under consideration are the Maloney-Robertson cycle and the Kalina cycle. Both cycles use ammonia-water as the working fluid.

2.2.1 Maloney-Robertson Cycle

Maloney and Robertson [45] published an ammonia-water cycle used for power generation with a maximum operating temperature of 148 °C (300 °F) and a maximum pressure of 1.7 MPa (248 psia) in 1953. The purpose of the study completed by Maloney and Robertson was to determine if absorption-type power cycle offer higher thermal efficiencies than steam power cycles. This cycle operates between two pressures, the absorber pressure and the turbine pressure, and utilizes seven basic components: a pump, a turbine, a flash preheater, a boiler, a superheater, a throttling valve, and an absorber. Each stream has an ammonia concentration of either the vapor concentration, X_V, the basic concentration, X_B, or the dilute concentration, X_D where $X_V > X_B > X_D$.

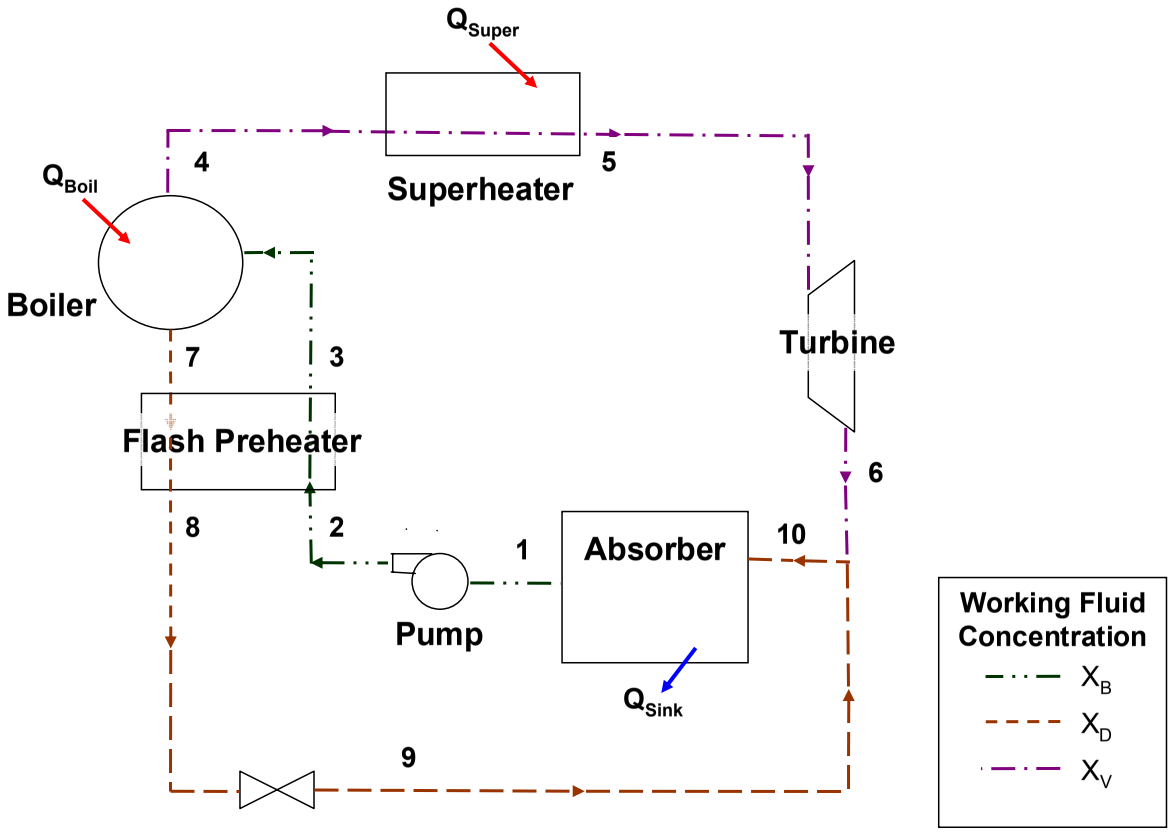

Figure 13: Maloney-Robertson Cycle Diagram [45]

A schematic of the Maloney-Robertson cycle is found in Figure 13. The basic stream at concentration X_B leaves the absorber and is pumped to the turbine pressure. Then the basic stream undergoes a heat exchange with the weak stream leaving the boiler. Heat is added to the cycle in the boiler unit to create a vapor stream with concentration X_V that is superheated and expanded through the work-extracting turbine. The turbine exhaust gas is mixed with the weak stream and then heat is rejected to allow the weak solution to absorb the vapor solution to create stream with basic concentration.

In the technical report prepared by Maloney and Robertson, trends from five iterations of the theoretical models are analyzed and a comparison to the Rankine cycle was prepared. The authors chose to define an absorber temperature and impose a restriction on the turbine exhaust outlet quality. With these constraints in mind, the results of this case study are discussed. The first case examines the effects of increasing the temperature of the boiler for a set vapor concentration on the cycle efficiency. Their results show that increasing the temperature increases the cycle efficiency up to a temperature of 193 °C (380 °F). After this point, there is little increase in efficiency because the turbine exhaust temperature increases which equates to less work output. The second case explores the effect of ammonia concentration in the turbine stream. Their results conclude that decreasing the ammonia in the stream increases the cycle efficiency. Their study is limited to a maximum concentration of 0.4 because of the quality limits on the turbine exhaust. The next three cases have relatively simple results. The third case includes the effects of inefficiencies in the turbine on the overall cycle efficiency. Including a turbine efficiency allows for expansion to a lower pressure given the same quality limits on the turbine exhaust stream. The binary fluid does not show a smaller decrease in efficiency compared to the steam cycle when accounting for turbine efficiency. The fourth case examines the removal of the analyzer which acts as a control system to keep the vapor concentration in equilibrium with

the basic stream. After the removal of this component, the working fluid stream is in equilibrium with the weak stream and no change in efficiency is reported. Finally, adding superheat to the ammonia-water based cycle does not increase efficiency but actually decreases efficiency. The increase in expansion from a higher temperature is not greater than the increase in heat necessary for the superheat process; and thus, the efficiency decreases. Furthermore, Maloney and Robertson conclude that the Rankine cycle outperforms the ammonia-water cycle when both cycles are under identical operating constraints. The authors suggest that a more volatile solution, such as lithium bromide, as the working fluid that may offer efficiency gains over the standard steam cycle.

2.2.2 Kalina Cycle

In 1984, Kalina patented the "exergy cycle" that became known as the Kalina cycle [32]. Like the Maloney-Robertson cycle, the Kalina cycle uses an ammonia-water based working fluid. The Kalina cycle uses an additional mixing process that results in 4 different ammonia concentrations in the cycles where $X_V < X_B < X_{WF} < X_V$ in terms of ammonia concentration and X_{WF} is the working fluid concentration. Explicit control over the ammonia stream concentration at the turbine is accomplished by decoupling the flash separation process pressure and the maximum cycle pressure. The Kalina cycle was proposed as a bottoming cycle for a gas turbine [32].

In Figure 14, the working fluid with basic concentration, X_B, leaves the absorber at State 1 and is pumped to the intermediate pressure. The fluid passes through heat exchangers to reach the flash tank temperature. The basic fluid enters the isothermal, isobaric flash tank where a flash distillation process results in an ammonia rich solution, X_V, at State 7 and a dilute ammonia solution, X_D, at State 19. The ammonia rich solution is combined with the basic solution to form the concentration of the working fluid. From State 8, the working fluid must pass through the intermediate

pressure condenser (IPC) to return to liquid. The liquid that is at the working fluid concentration is pumped to the turbine pressure and is heated in the IPC, recuperator, preheater, boiler and superheater to reach the turbine temperature. The fluid is expanded through the turbine to produce work, then heat is extracted from the exhaust gas for the flash preheating and recuperation processes. The cooled working fluid from the recuperator is mixed with the cooled and depressurized weak solution from the flash tank to return the concentration to the basic level. Heat is removed in the absorber to return the fluid back to liquid. The rejected heat from the absorber may be used as a heat source if additional heat is required for the basic solution at State 4 to reach the flash tank temperature.

The real innovation in the Kalina cycle is the introduction of the "thermal compressor". The thermal compressor refers to the multi-pressure mixing, separation, and heating processes that occur between the exhaust stream outlet (Figure 14: State 16) and the inlet to the second pump (Figure 14: State 9).

Implementation of a thermal compressor is only possible with the use of a binary fluid. Figures 15(a) and 15(b) are T-s diagrams for 60% ammonia and 90% ammonia. Note from these figures that a lower ammonia concentration leads to a higher condensation temperature, a higher critical temperature, a higher critical pressure, and more heat input at a constant pressure. The thermal compressor takes advantage of the higher condensation temperature for a lower concentration, of the smaller heat input for a higher ammonia concentration, and of the expansion to a low turbine exhasut pressure for a higher concentration. In order to achieve these results, strategic mixing of variable ammonia concentration streams is necessary.

In the Kalina cycle, a high concentration is desired in the heat input stages because less heat is required for a higher concentration fluid than a lower concentration at a constant pressure. The disadvantage of the high concentration fluid in the working fluid stream is that it must be condensed at temperatures far below that of a standard

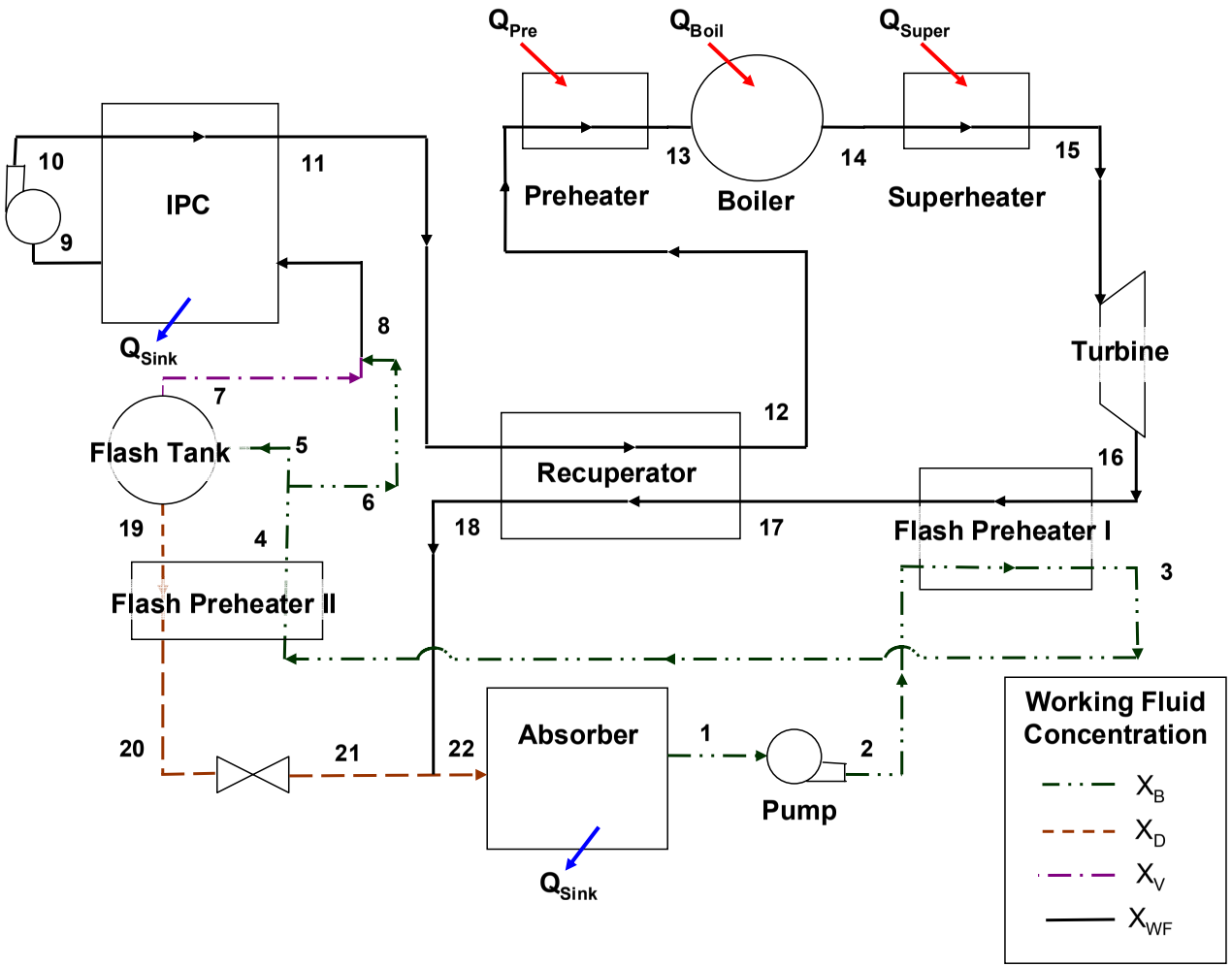

Figure 14: Kalina Cycle Diagram modeled from Rogdakis [58]

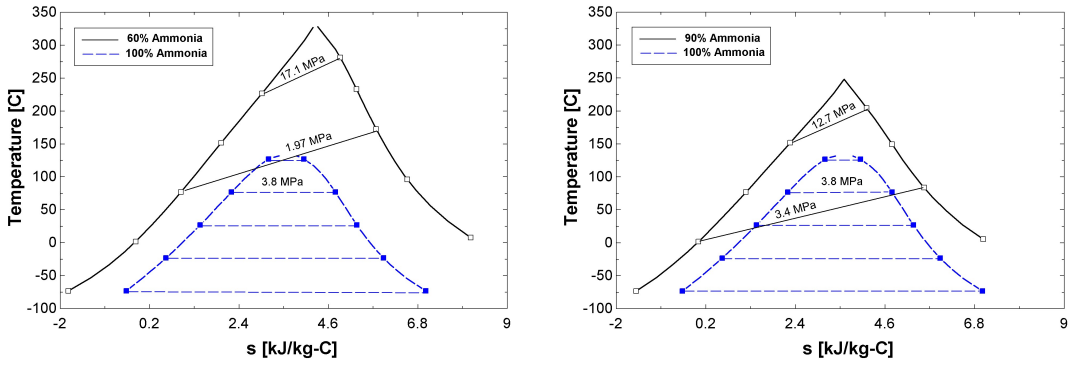

(a) (b)

Figure 15: T-s diagram for Pure Ammonia vs (a) 60% Ammonia-Water (b) 90% Ammonia-Water

heat sink unless expansion is limited. The implementation of mixing the turbine exhaust at a concentration of X_{WF} with the weak solution, X_W, to create a stream with an intermediate concentration X_B allows expansion to a low pressure in the turbine and an increase in the condensation temperature. An additional mixing state between the basic and vapor streams is employed as means to increase the stream ammonia concentration before the boiling process.

The stream concentrations are controlled through use of the intermediate pressure flash tank. The flash tank provides the vapor and weak solutions used in the mixing processes. The flash tank pressure is such that the sink stream is able to condense the stream with working fluid concentration. The flash tank temperature cannot exceed the temperature achievable through the heat extraction processes in the thermal compressor.

2.2.3 Applications

Over the past two decades, the Kalina cycle has been utilized for refrigeration processes [75, 74, 59] as well low-temperature bottoming cycles [31, 17, 62, 63, 25, 58] and geothermal power production [13, 49, 50, 7, 39]. Rogdakis and Antonopoulos [59] explored the use of the Kalina cycle coupled with an absorption refrigeration cycle.

Ammonia-water mixtures have suitable thermodynamic properties for refrigeration and power cycles; therefore, only one working fluid is needed. Multiple distillation processes act as the mass transfer mechanisms between the power and absorption cycles. Vijayaraghavan and Goswami [75] have made recent advances in ammonia-water combine cycle research. In contrast to implementing two cycles with a single working fluid, the Kalina cycle is also used as a separate bottoming cycle. Rogdakis [58] conducted a parametric study on the thermodynamics of the Kalina cycle utilizing turbine exhaust gas for the heat input to the cycle. It was found that the efficiency of the Kalina bottoming cycle ranges from 42.6% to 46.6% under optimal operating conditions of $X_D = 34\%$, $X_B = 42\%$, $X_{WF} = 70\%$, $X_V = 96.7\%$, an absorber pressure of 170 kPa, an intermediate pressure of 470 kPa, a turbine pressure of 11 MPa, and a superheat temperature of 510°C. The combined efficiency of the plant is greatly improved because not only is the amount of heat rejected reduced, but the amount of power output is increased. In contrast to the power advantages seen with the combined refrigeration-absorption cycles and bottoming cycles, the geothermal cycles utilize the Kalina cycle because the low temperature conditions couple with the binary working fluid. Numerical simulations of geothermal power plants show that the Kalina cycle exhibits a 2% to 2.50% first-law efficiency gain over the standard Rankine cycle [62]. Today, Iceland has the only operational Kalina geothermal power plant which produces 2.1 MW of power by utilizing the artesian geothermal wells just south of Hsavk [39, 38, 49, 50]. In a comparison between the operational Kalina cycle and ORC, the Kalina cycle an increase of 2.3% over the ORC [13].

In 1996, Ibrahim and Klein [27] examined the Maloney-Robertson cycle for purposes of theoretical comparison with the Kalina cycle [45]. The researchers compare these two cycles in terms of maximum power output verses heat exchanger NTU, the number of transfer units, which by definition is a dimensionless number relating the overall heat transfer rate to the heat capacity rate of a heat exchanger. The research

by Ibrahim and Klein [27] indicates that the Maloney-Robertson cycle is best suited for power systems with heat exchangers with NTU values less than 5 because the power output of the Maloney-Robertson cycle is greater than that of the Kalina cycle. As the NTU value increases, the Kalina cycle power output increases to a point where the Kalina cycle produces 90% of the maximum power whereas the Maloney-Robertson produces only 70% of the maximum power. As the design point for micro- and meso- scale heat exchangers is still an area of active research, both cycles are considered to remove bias in the study and provide full domain characterization.

2.2.4 Ammonia-Water Property Modeling Techniques

The ammonia-water mixture data [26] tabulated by Ibrahim and Klein are well accepted and are utilized for the Maloney-Robertson Cycle and the Kalina cycle models. Perturbed Chain Statistical Associating Fluid Theory(PC-SAFT) was explored as an alternative modeling technique for the ammonia-water mixtures [47, 23]. However, PC-SAFT was not valid over a larger temperature range, did not have a higher upper temperature limit, and did not dramatically increase the state property accuracy as compared to the Ibrahim and Klein data. Also, the Peng-Robinson EOS coupled with the WATAM model developed by Exergy, the company started by A. Kalina, offers data accurate over the temperature range 283K to 866K. However, the WATAM database is proprietary [18].

2.3 Summary

A review of the power cycle literature helped to characterize the meso-scale power system. In addition, the pertinent literature on ORC resulted in the selection of R123, toluene and ethylbenzene as fluids of priority in this study for ORCs. It was established that the ORCs and ammonia-water cycles of interest have not been studied for the end use of meso-scale solar-thermal power generation applications. Detailed analyses will follow in the subsequent chapters.

CHAPTER 3

ORGANIC RANKINE CYCLES PERFORMANCE EVALUATION

This chapter will analyze three ORCs, identified in Section 2.3, utilizing traditional power cycle analysis techniques. The application of ORC power cycle to meso-scale solar-thermal power generation has not been widely studied, with no reported studies at the power level identified in this work; thus, this chapter aims to provide insight into the anticipated performance of the cycles. In addition, as part of the investigation, two baseline cycles, Rankine and Kalina, will be utilized to assess the relative performance of the ORC cycles considered. Specific attention to the ammonia-water binary fluid cycles will be provided in Chapter 4.

3.1 Model Development

The detailed system consists of the collector, the heat exchange between the collector and the evaporator unit, the thermodynamic cycle and the generator as represented in Figure 16. In order to closely approximate a real system, collection efficiency, heat exchanger losses, cycle component efficiencies, and generator efficiencies are all assessed.

3.1.1 Effectiveness Heat Exchanger Modeling Technique

The effectiveness modeling technique is one of two widely-used models for heat exchangers. Heat exchanger modeling assumes that all of the heat leaving the hot stream is transferred to the cold stream. The effectiveness of a heat exchanger is

$$\epsilon = \frac{q}{q_{max}} \tag{1}$$

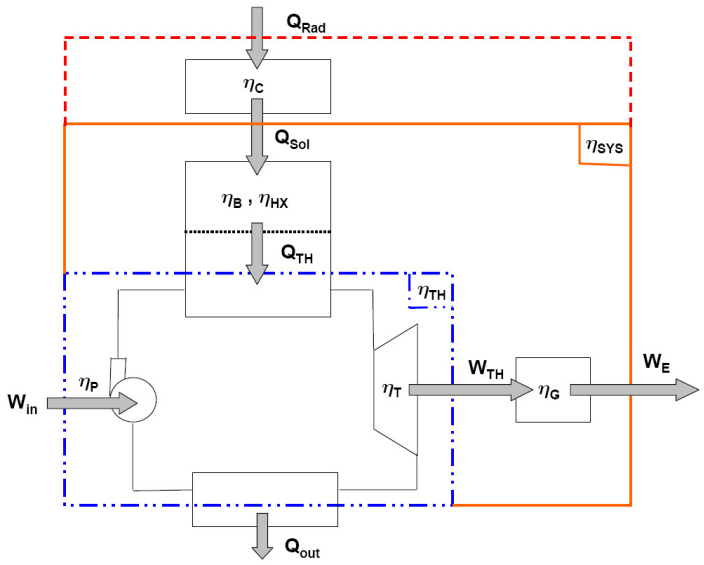

Figure 16: Schematic of the System of Interest

The maximum heat transfer is determined by assuming that the heat exchanger is counterflow and has infinite length. If the hot fluid has a higher specific heat value, then the cold stream will experience the greatest temperature change and the maximum heat transfer equals $q_{max} = C_c\,(T_{h,i} - T_{c,i})$. On the contrary, if the specific heat of the cold stream is greater than that of the hot stream, then the hot stream will experience the greatest temperature change and the maximum heat transfer is represented as $q_{max} = C_h\,(T_{h,i} - T_{c,i})$. Therefore, the maximum heat transfer is

$$q_{max} = C_{min}\,(T_{h,i} - T_{c,i}) \tag{2}$$

where C_{min} is equal to the smaller of C_h or C_c. An effectiveness of 1 indicates that the hot stream outlet temperature converge to the cold stream outlet temperature and heat transfer ceases.

3.1.2 ORCs

For the purpose of this study, the Rankine cycle and ORCs include a pump, a turbine, a recuperator, a preheater, a boiler, and a superheater. A schematic

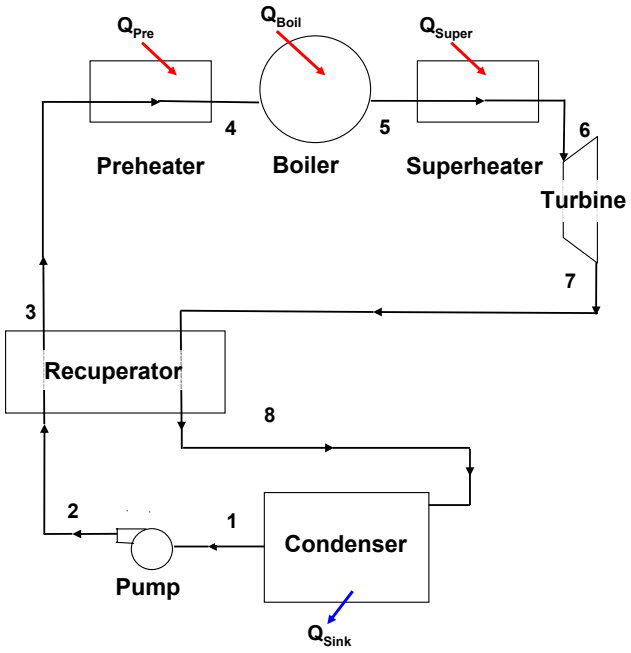

Figure 17: Organic Rankine Cycle Diagram

representative of the cycle is shown in Figure 17. The only additional component in the ORC cycle from that discussed in Section 2.1 is the addition of the recuperator. The recuperator is used as a heat recovery component to decrease source heat input, which increases efficiency. The recuperator extracts heat from the turbine exhaust and transfers it to the fluid prior to entering the preheater via a heat exchanger with two unmixed streams; one at the turbine pressure and one at the condenser pressure. The recuperation process should not be confused with regeneration or reheat processes. Regeneration refers to the process of extracting some of the exhaust stream to an open or closed feed water heater that operates at an intermediate pressure and reheat processes involve multi-stage turbine expansion stages with additional heating between each successive turbine.

The thermodynamic modeling of the ORCs is completed on a first-law basis. Thermodynamic properties at a given state are defined by two independent intensive

Table 3: ORC State Definition

State	Independent Properties	Outlet Component	Inlet Component
1	T,P	Condenser	Pump
2s	s,P	Pump	Recuperator
2	h,P	Pump	Recuperator
3	h,P	Recuperator	Preheater
4	P, Qu	Preheater	Boiler
5	P, Qu	Boiler	Superheater
6	P,T	Superheater	Turbine
7s	s,P	Turbine	Recuperator
7	h,P	Turbine	recuperator
8	h,P	Recuperator	Condenser

properties for a single-component working fluid. Table 3 lists the independent properties used to define each state in the ORC. Additional explanation of each of the states follows.

Heat is removed from the working fluid in the condenser which causes it to condense from a superheated vapor to a saturated liquid at State 1 in Figure 17. The saturated liquid is pumped to turbine pressure. The universal thermodynamic pump modeling technique described below can be found in any standard thermodynamic textbook [8]. First, the pump is modeled as an isentropic process to determine the ideal pump work then a real world estimate of the pump work is accounted for through the assessment of a component efficiency. The pump process is represented mathematically using the following equations:

$$w_{p,s} = h_{out,s} - h_{in} \tag{3}$$

$$w_{p,act} = \frac{w_{p,s}}{\eta_p} \tag{4}$$

$$h_{out} = h_{in} + w_{p,act} \tag{5}$$

After leaving the pump, the fluid enters the recuperator where heat extracted from the exhaust stream is used to heat the fluid before entering the preheater. The enthalpies at cold and hot stream outlets, respectively (Figure 17: States 3 & 8, respectively), are determined through an enthalpy balance on the heat exchange. The effectiveness modeling approach is utilized and the implementation is discussed in Section 3.3. The fluid then enters the evaporator unit which consists of the preheater, the boiler, and the superheater. All required heat inputs for the evaporator come from the external solar collector. From a thermodynamics modeling stand point, the stream entering the preheater comes from the recuperator and exits at the saturation temperature as a saturated liquid. The phase change process occurs in the boiler and the fluid exits as saturated vapor. The final stage in the evaporator is the superheat process where the working fluid is heated before expansion through the turbine.

The turbine is used to convert the high pressure flow into a low pressure flow while extracting the work due to pressure change. The turbine is modeled as an isentropic expansion process to determine the ideal work output. Through accounting for efficiency, the actual pump work is determined. The following mathematical expressions represent the standard modeling technique for a turbine:

$$w_{t,s} = h_{in} - h_{out,s} \tag{6}$$

$$w_{t,act} = w_{t,s}\eta_t \tag{7}$$

$$h_{out} = h_{in} - w_{t,act} \tag{8}$$

The net specific work and mass flow rate of a system define the maximum power output. For this study, the net power output is defined and the mass flow rate is determined for the system. The net power for the ORCs is

$$\dot{W}_{net} = \dot{m}_{cycle} \left(w_{t,act} - w_{p,act} \right) \tag{9}$$

3.1.2.1 Fluid Modeling Implementation

The cycles are modeled in Engineer Equation Solver (EES) Academic Professional Version 8.8125. EES has an extensive built in property database. The EES function calls using the EOS defined in Section 2.1.2 are used for the ORCs with R123, toluene, and water as the working fluids. There is not a defined property data set for ethylbenzene. In accordance with Drescher [14], the Peng-Robinson cubic EOS is used for modeling the properties of the gaseous states and the incompressible liquid relationships for enthalpy and entropy are used for modeling the properties at States 1,2, and 3. The mathematical representations of the incompressible liquid relationships are

$$\Delta h = C_p \Delta T \tag{10}$$

$$\Delta s = C_P \ln \left(\frac{T_{out}}{T_{in}} \right) \tag{11}$$

State 4 in the ORC cycle is found using the saturation enthalpy data and basic thermodynamic relations for phase change processes. The temperature is constant for a phase change process of a pure fluid, the saturation enthalpy, h_{FG} is the difference between the enthalpy at a quality of 0 and the enthalpy at a quality of 1, and the saturation entropy is $s_{FG} = \frac{h_{fg}}{T_{sat}}$.

States 5, 6, 7 and 8 are all vapor phases and the Peng Robinson implementation is used to determine the fluid properties. The necessary fluid properties to complete the Peng-Robinson EOS referenced from DIPPR [6] listed as follows: a) specific heat capacity for an ideal gas, b) the specific heat capacity for a liquid, c) the accentric factor, d) temperature-dependent density data, e) the molar mass, f) the critical

pressure, and g) the critical temperature.

The Peng-Robinson fundamental EOS defines pressure as a function of temperature in the following manner[61]:

$$P = \frac{RT}{V-b} - \frac{a\,(T)}{V(V+b)+b(V-b)} \tag{12}$$

where T_{CR} and P_{CR} are the critical temperature and pressure, respectively, with $b = 0.0778\dfrac{RT_{CR}}{P_{CR}}$ and $a(T) = 0.45724\dfrac{R^2T_{CR}^2}{P_{CR}}\,\alpha(T)$.
Temperature dependence is accounted for through

$$\alpha(T) = 1 + \kappa\left(1 - \sqrt{\frac{T}{T_{CR}}}\right) \tag{13}$$

with $\kappa = 0.37464 + 1.5422\omega - 0.26992\omega^2$ and ω defined as the accentric factor. The compressibility ratio, Z, is defined as

$$0 = Z^3 + (-1+B)Z^2 + (A - 3B^2 - 2B)Z - (AB - B^2 - B^3) \tag{14}$$

where $A = \dfrac{a(T)P}{R^2T^2}$ and $B = \dfrac{Pb}{RT}$. The EES Peng-Robinson call is utilized to define the compressibility ratio, Z, and the constants A and B in Equation 14. The enthalpy and entropy departure functions are defined as

$$H(T,P) - H^{IG}(T,P) = RT(Z-1) + \frac{T(\frac{da}{dT}) - a}{2\sqrt{2}b}\ln\left[\frac{Z + (1+\sqrt{2})B}{Z + (1-\sqrt{2})B}\right] \tag{15}$$

with $\dfrac{da}{dT}$ defined as the derivative of $a(T)$ with respect to temperature. Therefore, the change in enthalpy is

$$H(T_2,P_2) - H(T_1,P_1) = \int_{T_1}^{T_2} C_P dT + \left[H(T,P) - H^{IG}(T,P)\right]_{T_{R2},P_{R2}} \tag{16}$$

$$- \left[H(T,P) - H^{IG}(T,P)\right]_{T_{R1},P_{R1}} \tag{17}$$

where T_R and P_R are the reduced temperature and pressure, respectively.

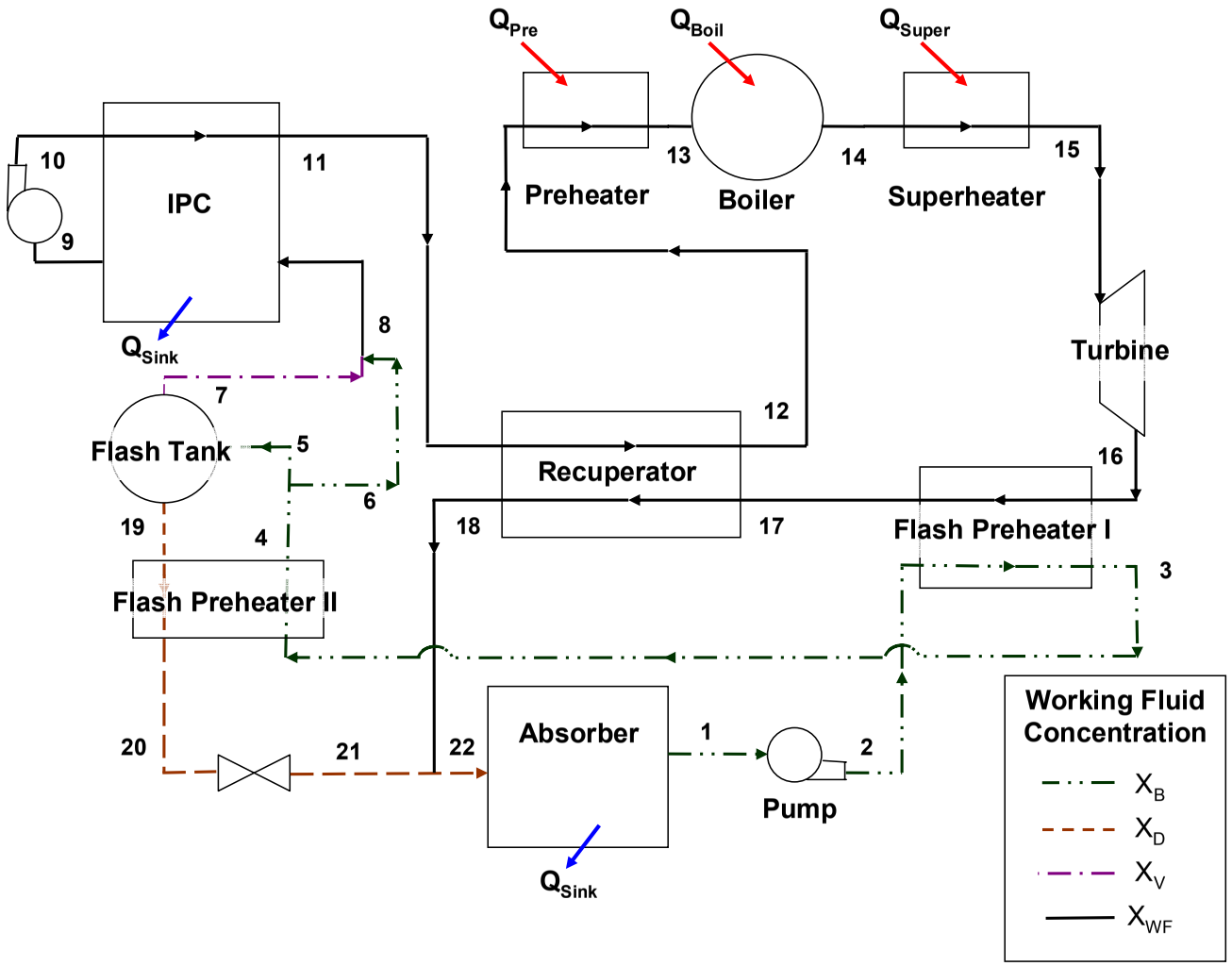

Figure 18: Kalina Diagram I

3.1.3 Kalina Model I

The Kalina cycle is thermodynamically complex because of the vapor-liquid equilibrium with a binary fluid and the varying ammonia concentration in different streams throughout the cycle. The explanation of the process flow for the Kalina cycle as shown in Figure 18 is found in Section 2.2.2. A detailed explanation of the mass flow in each stream and the thermodynamic relationships necessary to characterize the Kalina cycle follow.

The relative mass flow rates at each state in the Kalina cycle can be related back to the working fluid flow rate and the concentration of the various flows. First, the mass flow rate through the turbine is defined as $\dot{m}_{WF}$. By performing mass and species balances at the mixing and separation states along the cycle path, relative flow rates as a function of the total mass flow rate through the turbine are developed.

The mass flow leaving the flash tank has a value of $\dot{m}_D = g\dot{m}_{WF}$. The constant g is found through the second mixing state (Figure 18: States 18, 21, and 22). The mass balance at this point is

$$\dot{m}_D + \dot{m}_{WF} = \dot{m}_B \tag{18}$$

The species balance at the same location is

$$\dot{m}_D^{NH3} + \dot{m}_{WF}^{NH3} = \dot{m}_B^{NH3} \tag{19}$$

Substituting the flow of ammonia in terms of concentration and total mass flow, $m_i^{NH3} = m_i X_i$, into Equation 19 yields

$$\dot{m}_D X_D + \dot{m}_{WF} X_{WF} = \dot{m}_B X_B \tag{20}$$

Equation 18 can be substituted into Equation 20 to solve for the ratio of working fluid flow rate to dilute stream flow rate in the following manner

$$g = \frac{\dot{m}_{WF}}{\dot{m}_D} = \frac{X_{WF} - X_B}{X_B - X_D} \tag{21}$$

Equation 21 only characterizes the ratio of the working fluid flow to the dilute stream flow. A characterization of the working fluid flow to the basic flow and vapor flow are also needed. The basic, vapor and dilute flows are all components that interact with the flash tank. A mass balance on the flash tank leads to the relationship of the basic and vapor streams relative to the working fluid stream flow rate. The mass balance on the flash tank is

$$\dot{m}_B = \dot{m}_V + \dot{m}_D \tag{22}$$

The species balance on the flash tank is

$$X_D \dot{m}_D + X_V \dot{m}_V = X_B \dot{m}_B \tag{23}$$

Substituting the mass balance into the species balance yields the ratio of the flow rate of the dilute stream to the basic stream as follows

$$\frac{\dot{m}_D}{\dot{m}_B} = \frac{X_V - X_B}{X_V - X_B} \tag{24}$$

Then Equation 21 can be substituted into Equation 24 to relate the basic stream flow rate to the working fluid flow rate as follows

$$f = \frac{\dot{m}_B}{\dot{m}_{WF}} = g\frac{X_V - X_B}{X_V - X_B} \tag{25}$$

where $f\,\dot{m}_{WF}$ equals to the flow entering the flash tank (Figure 18: State 5).

Tracking the relative flow rates through the system based on the Equations 21 to 25 fully defines the cycle system flow rates. Figure 19 shows the flows around the flash tank. The flow rate entering the condenser at State 22 is $(1 + g)\dot{m}_{WF}$ after

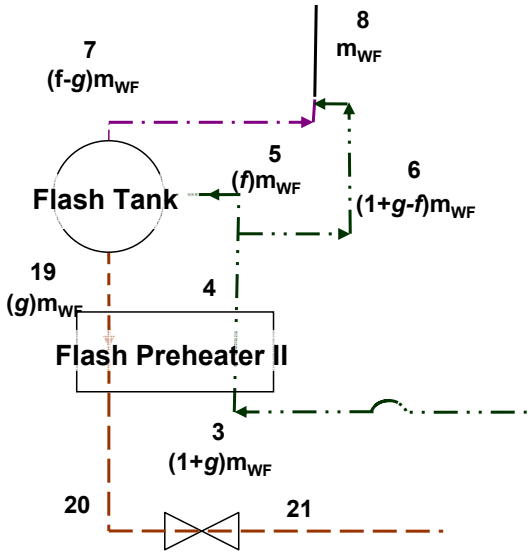

Figure 19: Mass Flow rates relative to concentrations for the Kalina Cycle

Mixing State II. Then the separation process at State 4 results in a flow leaving at State 6 as $(1+g-f)\dot{m}_{WF}$ and the flow entering the flash tank as defined by Equation 25 as $f\dot{m}_{WF}$. Then the flow leaving the flash tank as vapor is $(f-g)\dot{m}_{WF}$. The exit to Mixing State I is simply $\dot{m}_{WF}$.

After establishing the relative mass flow rates in the streams, the thermodynamic modeling is addressed. For a binary fluid, three independent properties will define the properties at a given state. The heat exchange source and sink streams are currently modeled as simple heat inputs. Likewise, the pressure drops within the heat echange devices due to friction effects are neglected. Table 4 lists the three independent properties that define each state.

The Kalina cycle has two pumps that are modeled in identical manners to the pumps in the ORCs using Equations 3 through 5. The turbine is also modeled through the implementation of a turbine efficiency following Equations 6 to 8 as used in the ORC simulations. The flash preheaters and recuperator are modeled

Table 4: Kalina I State Definition following Rogdakis

State	Independent Properties	Outlet Component	Inlet Component
1	T,P,X	Condenser	Pump I
2s	s,P,X	Pump I	Flash Preheat I
2	h,P,X	Pump	Flash Preheater I
3	h,P,X	Flash Preheater I	Flash Preheater II
4	T,P,X	Flash Preheater II	Flash Preheater III
5	h,P,X	Mass Separation	Flash Tank
6	h,P,X	Flash Preheater II	Mass Separation
7	T,P,Qu	Flash Tank	Mixing State I
8	h,P,X	Mixing State I	IPC (cold)
9	P,X,Qu	IPC(cold)	Pump II
10s	P,s,X	Pump II	IPC (hot)
10	P,h,X	Pump II	IPC (hot)
11	P,X,Qu	IPC (hot)	Recuperator
12	T,P,X	Recuperator	Preheater
13	P,X,Qu	Preheater	Boiler
14	P,X,Qu	Boiler	Superheater
15	T,P,X	Superheater	Turbine
16s	P,s,X	Turbine	Flash Preheater I (hot)
16	P,h,X	Turbine	Flash Preheater I (hot)
17	P,h,X	Flash Preheater I (hot)	Recuperator (hot)
18	T,P,X	Recuperator	Mixing State II
19	T,P,Qu	Flash Tank	Flash Preheater II
20	T,P,X	Flash Preheater II	Valve
21	P,h,X	Valve	Mixing State II
22	P,h,X	Mixing State II	Condenser Inlet

using the effectiveness modeling technique allowing heat exchange with the respective hot streams. The effectiveness modeling implementation outputs are stream outlet temperatures. The mixing and separation states employ a standard enthalpy balance to determine outlet conditions. Per Kalina and Rogdakis, the flash tank is modeled as an isothermal, isobaric process. Volumetric expansion forces the basic ammonia solution entering the flash tank to separate into an stream of ammonia rich saturated vapor (State 7) and a stream of ammonia weak saturated liquid (State 20). Per Rogdakis, the only heat input from an external source is in the preheater, boiler and superheater. All other heat requirements can be extracted from the exhaust streams and from the reutilization of the sink streams. A total enthalpy balance on the heat rejection streams confirms that there is enough heat in the stream to support the "thermal compressor".

The flow rate through the turbine, $\dot{m}_{WF}$, must be large enough to provide the net power output. Therefore, the flow rate in the turbine is related to the desired thermal output through the following relationship:

$$\dot{W}_{net} = \dot{m}_{WF} \left(w_{t,act} - w_{p1,act} - w_{p2,act} \right) \tag{26}$$

3.2 Design Specifications

General design parameters are assigned as an initial examination of the potential power cycles. An upper-bound constraint of 500 °C is imposed on the maximum operating temperature in the cycles. Although this limit is consistent with the temperature levels considered achievable with high levels of concentration [21], the authors recognize that there exist significant challenges in realizing this temperature with conventional collector technologies. However, in the interest of a full domain characterization and absence of data related to meso-scale collection techniques, a more conservative upper bound on temperature was not imposed. Innovations in

Table 5: Critical States for ORC Fluids

Fluid	T_{CR} [°C]	P_{CR} [MPa]
Water [a]	374	22.06
R123 [b]	186.7	3.668
Toluene [b]	318.6	4.126
Ethylbenzene [c]	344.05	3.606

[a] EES call using Harr data [24]
[b] EES call using Roth-Tillner EOS [67]
[c] DIPPR database [6]

solar collection, controls, boiler design and thermal storage are future research goals encompassed in this project and are not addressed within the scope of this thesis.

The incoming solar radiation is assessed at $Q'' = 1000\frac{W}{m^2}$. This radiation level is often used in solar design [21]. The author acknowledges that the concentration is site specific, as seen in Figure 8, but accounting for time dependent and site specific solar radiation conditions is beyond the scope of this project. The calculated collection area is

$$A = \frac{\dot{Q}_{HX}}{Q''\eta_{Concentrator}} \tag{27}$$

where $\eta_{Concentrator}$ is the efficiency of the concentration technology and $\dot{Q}_{HX}$ is the amount of heat needed to complete the heat exchanger process. The concentrator efficiency is taken to be 60% [21]. $\dot{Q}_{HX}$ accounts for imperfect heat transfer in real world heat exchange processes by the introduction the loss parameters, K, through

$$\dot{Q}_{HX} = \frac{\dot{Q}_{pre}}{(1-K_{HX})} + \frac{\dot{Q}_{Boil}}{(1-K_{Boil})} + \frac{\dot{Q}_{Super}}{(1-K_{HX})} \tag{28}$$

Supercritical cycles are not considered in this study. Supercritical cycles run above the critical temperature-pressure combination listed in Table 5. For all ORCs considered in this chapter, the condenser pressure is set to 100 kPa and a maximum cycle pressure of 4 MPa is assessed.

The quality of the turbine exhaust at 100 kPa must meet or exceed 100% vapor and cannot enter the two-phase flow regime. Most turbines can support a limited amount of condensate but the turbine wears faster because of cavitation effects on the blades. This conservative result is imposed on the turbine outlet condition due to the lack of comprehensive performance data and wear models for meso-scale impulse turbines.

Conservative component efficiencies and effectivenesses are listed in Table 6. For all cycles considered, the designed power output from the turbine is 14.7 kW calculated from the generator efficiency of 80% and the target residential power output of 12.5 kW. The respective power, heat, and flow rates were calculated in order to satisfy this power level..

Heat exchangers that interact with the cycle working fluid are modeled as counterflow heat exchangers with an effectiveness of 80%. Existing boiler technologies have not been developed for the cycle operating points in this study. Based on the recent preponderance of research into microchannel enhanced heat transfer, as reviewed by Thome [65, 66] and Kandlikar [33], future boiler technologies at this scale will incorporate microchannel techniques to achieve high heat transfer.

A loss parameter, K, accounting for heat loss to the environment is assessed on the source heat exchangers. Typically, boiler efficiencies are not thermal efficiencies but rather assessed based on the annual fuel utilization efficiency (AFUE). The Energy Star standard for the AFUE is 85% [71]. The steady state thermal efficiency is often much higher than this but a conservative loss parameter equal to the AFUE value is assessed. Additionally, a loss parameter of 20% is assessed on the preheater and superheater.

The Kalina cycle parameters follow from the optimization completed by Rogdakis[58] and are included in Table 7. The isobaric, isothermal distillation process in the flash tank defines saturated vapor concentration and saturated liquid dilute concentration.

Table 6: Assessed Component Efficiencies for Effectiveness Modeling

η_G	0.85	ϵ_{HX}	0.8
η_P	0.7	K_B	0.15
η_T	0.85	K_{HX}	0.2

Table 7: Simulation Parameters for the Kalina Cycle

Absorber Outlet Temperature	20.3 °C
Flash Tank Temperature	66.1 °C
Flash Tank Pressure	470 kPa
X_{WF}	70% ammonia
X_B	42% ammonia

This cycle operating at the specified parameters provides a bench mark for ammonia-water cycle performance.

3.3 Numerical Validation and Implementation

3.3.1 Numerical Validation of Ethylbenzene Modeling

In order to ensure that the methodology used to model the ethylbenzene ORC is accurate, the validity of the Peng-Robinson first-law calculations is verified through a comparison of the toluene ORC. Two models for the toluene ORC were created: one using the Roth-Tillner EOS that is built into EES as the "toluene" function call and the other calling the EES code written by the author that utilizes the Peng-Robinson EOS. Over the design space, maximum difference in the efficiency calculations via the two methods was 3.15%. The efficiency percent difference, defined as $\frac{(\eta_{EES}-\eta_{PR})}{\eta_{EES}}$, at sample pressures over the design space temperatures for toluene is shown in Figure 20. At low pressures, the Peng-Robinson efficiency calculation is always higher than the EES calculation. However, as the pressure increases, the Peng-Robinson calculations under estimate the efficiency. Since systems with maximum operating conditions at low temperature, high pressure combinations yield lower efficiencies than high-temperature, high-pressure systems, the conclusions of this study relative to ethylbenzene are not affected.

Table 8: Ethylbenzene Specific Heat Variations with Pressure [30]

Temperature $[K]$	C_P at 2 MPa $\left[\frac{kJ}{kg-K}\right]$	C_P at 20 MPa $\left[\frac{kJ}{kg-K}\right]$	Percent Difference [%]
350	1.933	1.905	1.45
375	2.025	1.987	1.88
400	2.117	2.069	2.27
425	2.208	2.151	2.58
450	2.298	2.233	2.83
475	2.386	2.315	2.98
500	2.474	2.397	3.11
525	2.561	2.479	3.20

The specific heat capacity data for liquids as reported in the DIPPR database ends at a temperature of 400K. The DIPPR dataset references Johnson *et al.* [30] as the source of specific heat data at 375 K and 400 K. The paper by Johnson contains additional liquid specific heat data at elevated pressures of 20 to 200 bar ranging in temperature from 350 K to 550 K. Less than 3.5% variation occurs in the specific heat at a constant temperature with an increase of order of magnitude in pressure as demonstrated in (Table 8). To cover the operating temperatures explored in this study for ethylbenzene, the specific heat data for ethylbenzene at 20 bar is coupled with the specific heat values from the DIPPR database to evaluate the liquid specific heat capacity of ethylbenzene over the range of 185K to 525K.

The Clapeyron Equation is used to estimate the enthalpy of vaporization at temperatures beyond 487 K for the ethylbenzene modeling because the data from the DIPPR does not go beyond this temperature. The Clapeyron Equation relates the slope of the saturation curve on a P-T diagram to the specific volume of the saturated liquid and saturated vapor at the specified temperature. The relationship is as follows

$$\left(\frac{dP}{dT}\right)_{SAT} = \frac{h_{fg}}{Tv_{fg}} \tag{29}$$

In order to estimate the change in pressure with temperature, a small neighborhood of ± 2 K degrees is take on either side of the temperature of interest and a linear

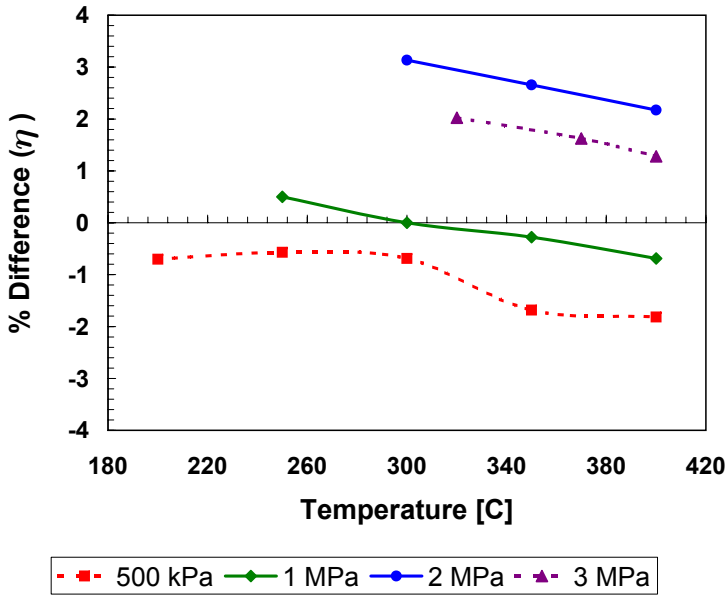

Figure 20: Percent Difference in Efficiency using the EES function call and the Peng-Robinson EOS

estimation assuming a constant slope is calculated. The upper temperature is T^+ and the lower limit is T^-. Therefore, $\frac{dP}{dT}$ is estimated as

$$\left(\frac{dP}{dT}\right)_{SAT} \cong \left(\frac{\Delta P}{\Delta T}\right)_{SAT,T} = \frac{P_{SAT,T^-} + P_{SAT,T^+}}{T^- + T^+} \tag{30}$$

Likewise, the specific volume data for the vapor phase are calculated using the Peng-Robinson EOS and the liquid volume is found from the density in the DIPPR database.

3.3.2 Numerical Validation of the Kalina Model

The Kalina cycle model is validated through comparison with the simulation performed by Rogdakis [58]. The simulation by Rogdakis takes into account multiple reheat and expansion stages, a maximum pressure of 11 MPa, and a maximum temperature of 510°C. With these additional components implemented, there is only a

2.7% difference in the efficiency calculations of the cycle models. The authors recognize that there is an extrapolation of the ammonia-water data set presented by Ibrahim and Klein [26] to achieve results beyond 326°C. A detailed discussion of the extrapolation of the ammonia-water data is provided in Section 4.4.

3.3.3 Effectiveness Iteration Loop

The effectiveness heat exchanger modeling technique is used for the heat exchangers that do not interact with the source and sink. Figure 21 illustrates the procedure implemented for the effectiveness models. The inputs to the loop are the hot and cold side inlet temperatures, pressures, and flow rates as well as the desired effectivenesses of the heat exchangers. A check to make sure that the hot stream inlet is greater than the cold stream inlet is performed to be sure that heat exchange can occur. The first iteration sets the cold stream inlet to equal the cold stream outlet temperature. An enthalpy balance on the cold stream indicates the heat needed from the hot stream to accomplish the temperature change in the cold stream. Then an enthalpy balance between the hot and cold stream is calculated and used to determine the hot stream outlet temperature. The average temperature of each of the streams is used to determine the specific heat of each stream. Then the minimum specific heat value is used to determine the maximum heat transfer rate as indicated in Equation 2. Equation 1 is used to calculate the effectiveness of this heat exchange process. The cold stream outlet temperature is increased until the calculated effectiveness converges to the specified effectiveness from the program input variables.

3.3.4 Turbine Exhaust Quality Iteration Loop

An iteration loop on the superheat temperature required to satisfy the constraint of turbine exhaust quality imposed on all cycles was implemented in the EES cycle models and a flow chart is shown in Figure 22. The inputs to this loop are the turbine high side pressure, turbine low side pressure, and turbine efficiency. The iteration

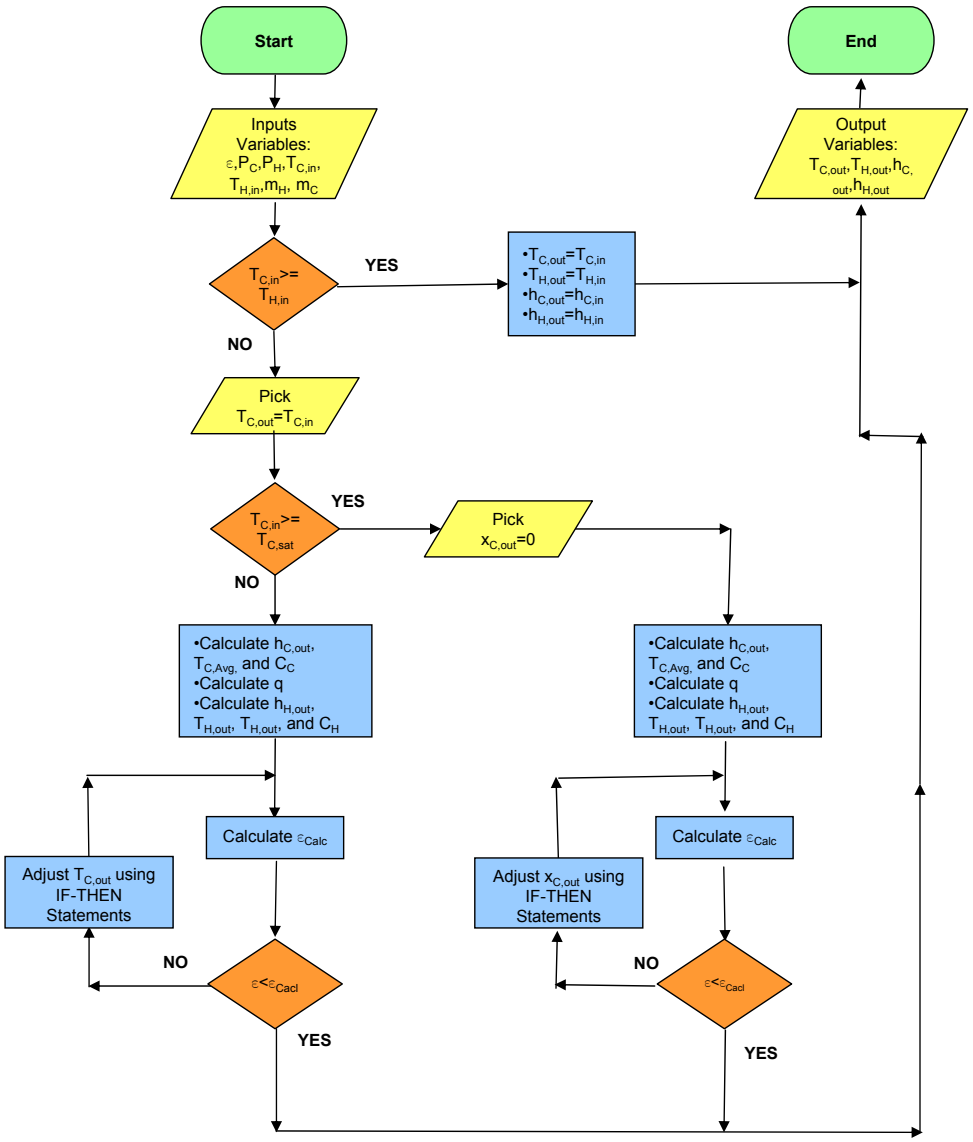

Figure 21: Flow Chart for the Effectiveness Heat Exchanger Implementation

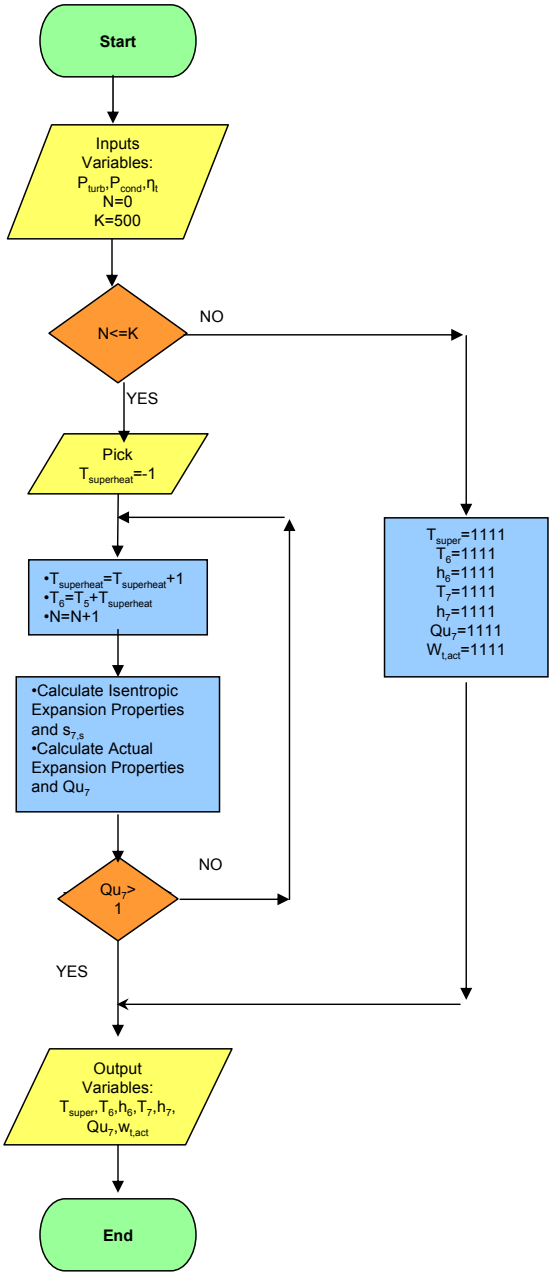

Figure 22: Flow Chart for determining the Superheat necessary in the Rankine cycle, R123 ORC, and Toluene ORC

process begins by assessing a superheat of 0 K. Fluid properties for isentropic and actual expansion processes are calculated using Equations 6 to 8. From the enthalpy and pressure at the turbine outlet, the quality is assessed. If the quality is greater than 1, then the condition is met and the loop is exited. If the quality constraint is not satified, the superheat is increased by 1 K and the loop continues until the condition is satisfied. The outputs from this loop are the amount of superheat, the temperatures at the turbine inlet and exit, the enthalpy at the turbine exit, the specific turbine work, and the turbine exhaust quality.

The quality loop for the ammonia-water based cycles (Figure 23) calculates the isentropic work, actual work and exhaust quality in the same thermodynamic manner as the quality loop for ORCs. However, the working fluid ammonia concentration must be added as an input variable because three independent intensive properties are required to define the properties of a binary fluid. Since the EES ammonia-water call encompasses all 8 state definitions, additional outputs from the procedure are included to avoid redundant calculations in the main program. The quality loop converges on the minimum temperature required for single phase vapor flow leaving the turbine just as the ORC loop.

3.4 Results

The cycle simulations in EES were completed numerically by varying the turbine temperature and pressure to determine the first-law system efficiency and the required solar collection area. The first law is defined as

$$\eta = \frac{\dot{W}_{Net}}{\dot{Q}_{In}} \tag{31}$$

where $\dot{W}_{Net}$ is the net system power in kW and $\dot{Q}_{In}$ is the heat rate into the system in kW. The solar collection area is defined by Equations 27 and 28.

The turbine inlet temperature was varied in increments of 20°C and over the ranges

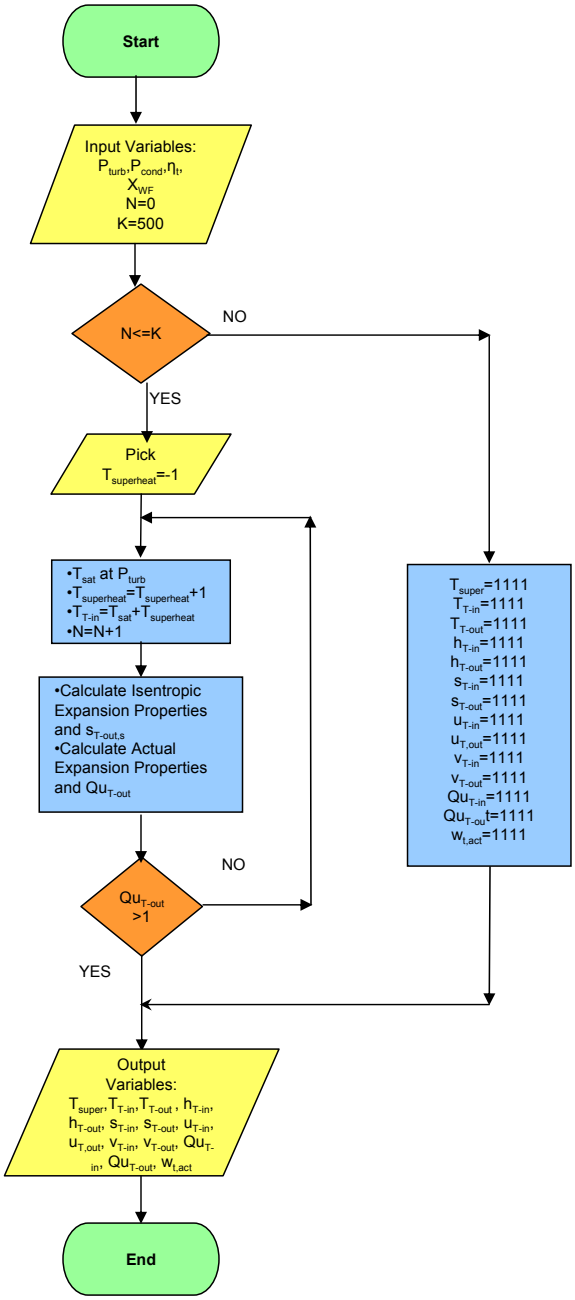

Figure 23: Maloney-Robertson Quality Iteration Loop

Table 9: Definition of the Design Space

Cycle	Fluid	Temperature [°C]	Pressure [MPa] [MPa]
Rankine	Water	279-500	0.5-2.3
Kalina	Ammonia-Water	183-500	0.5-4
ORC	R123	100-252	0.5-3.668
ORC	Toluene	179-427	0.5-4
ORC	Ethylbenzene	184-500	0.5-3.606

Table 10: Maximum Efficiency and Minimum Collection Area for Initial Cycles Analysis

Cycle	η [%]	Collector Area $[m^2]$	Pressure [MPa]	Temperature [°C]
Rankine Cycle	21.47	82.39	2.3	500
R123 ORC	24.42	3.5	74.77	240
Toluene ORC	25.59	4.0	71.3	420
Ethylbenzene ORC	27.16	67.49	3.6	500
Kalina Cycle	27.18	64.99	4.0	500

listed in Table 9. The temperature and pressure spaces for each fluid individually are defined through several criteria. The maximum operating pressure corresponds to the smaller of either the critical pressure or 4 MPa. Water is a special case because the saturation temperature of water at pressures above 2.323 MPa are greater than 500 °C. The minimum cycle temperature is the smaller of either the minimum turbine inlet temperature that does not violate the imposed turbine exhaust constraint, the minimum temperature that does not violate the Carnot efficiency, or 100 °C. The maximum cycle temperature is defined by the smaller of either the maximum temperature supported by the available property data or 500 °C.

Representative samples of the thermal efficiency and collector area across the design space at turbine pressures of 0.5 MPa, 1 MPa, 1.5 MPa, 2 MPa, 2.5 MPa, 3 MPa, 3.5 MPa, and 4 MPa are plotted in Figures 24 and 25, respectively. Figure 26 collapses this characteristic data set by extracting the maximum efficiency and minimum collector area for each of the fluids over the temperature range of interest. The maximum efficiency and minimum collection area are tabulated in Table 10.

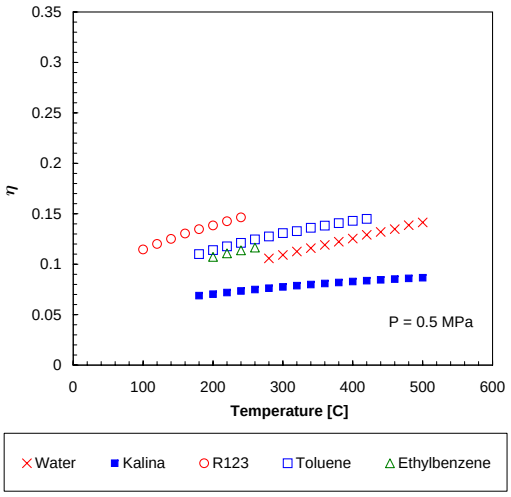

(a)

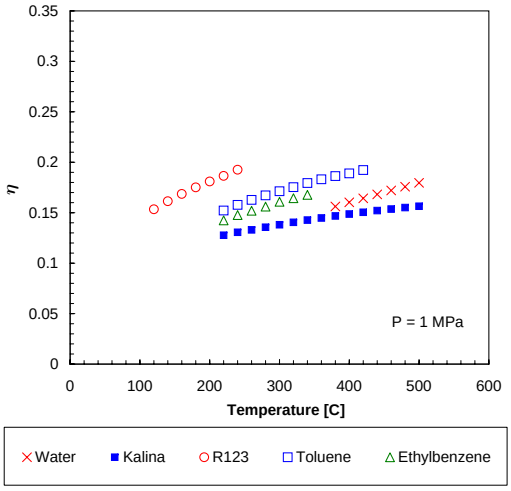

(b)

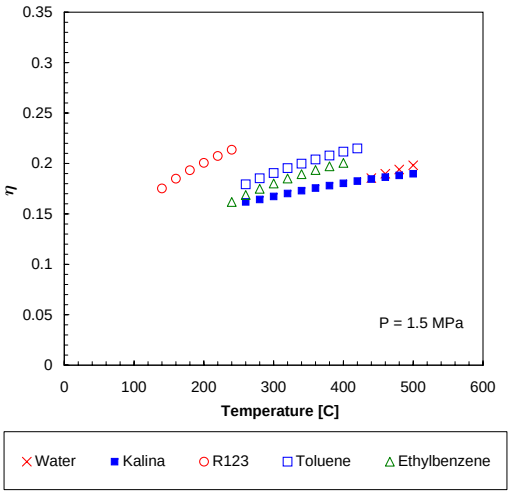

(c)

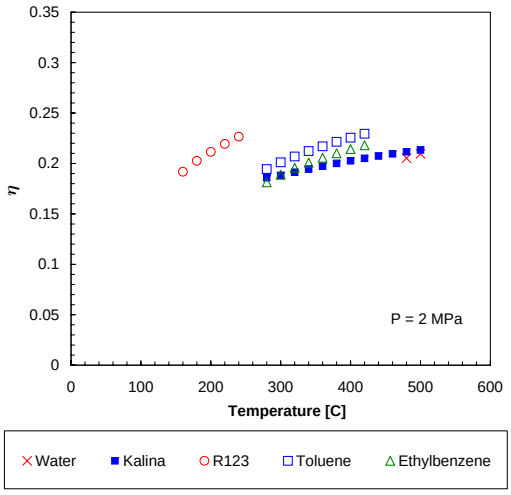

(d)

Figure 24: Cycle System Efficiency vs Turbine Temperature at Turbine Pressures of (a)500 kPa (b) 1MPa (c) 1.5 MPa (d) 2 MPa

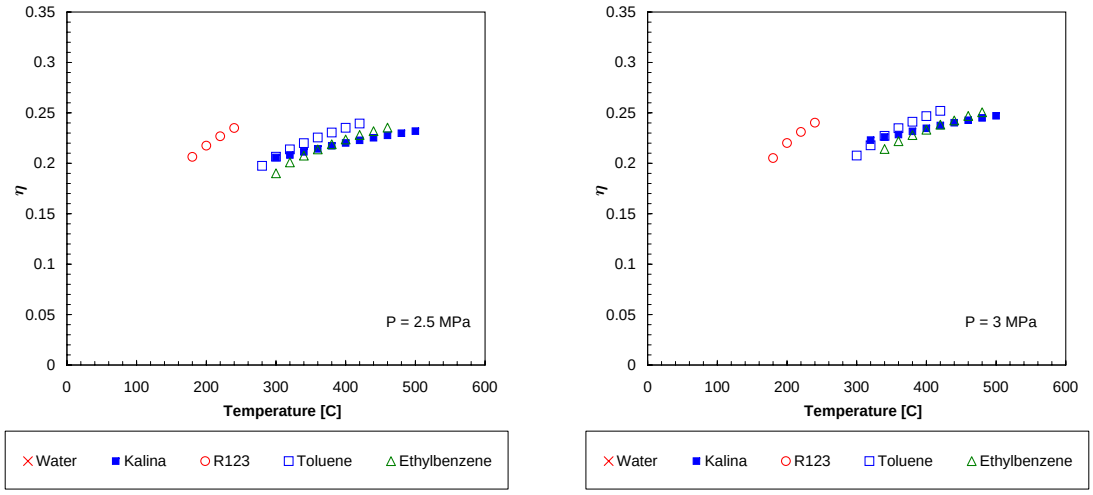

(e)

(f)

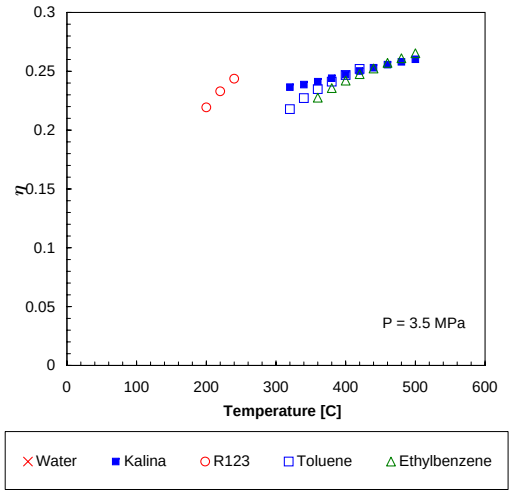

(g)

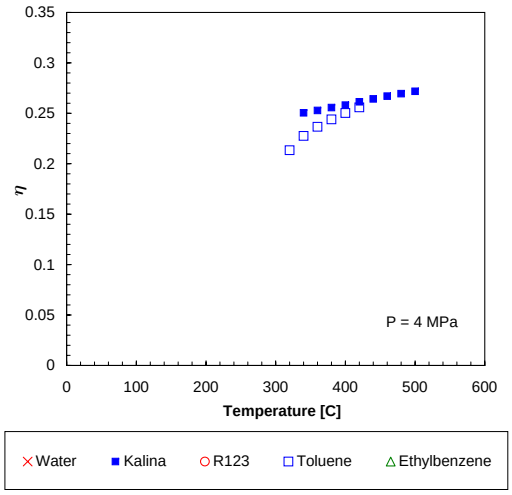

(h)

Figure 24: Cycle System Efficiency vs Turbine Temperature at Turbine Pressures of (e) 2.5 MPa (f) 3 MPa (g) 3.5 MPa (h) 4 MPa

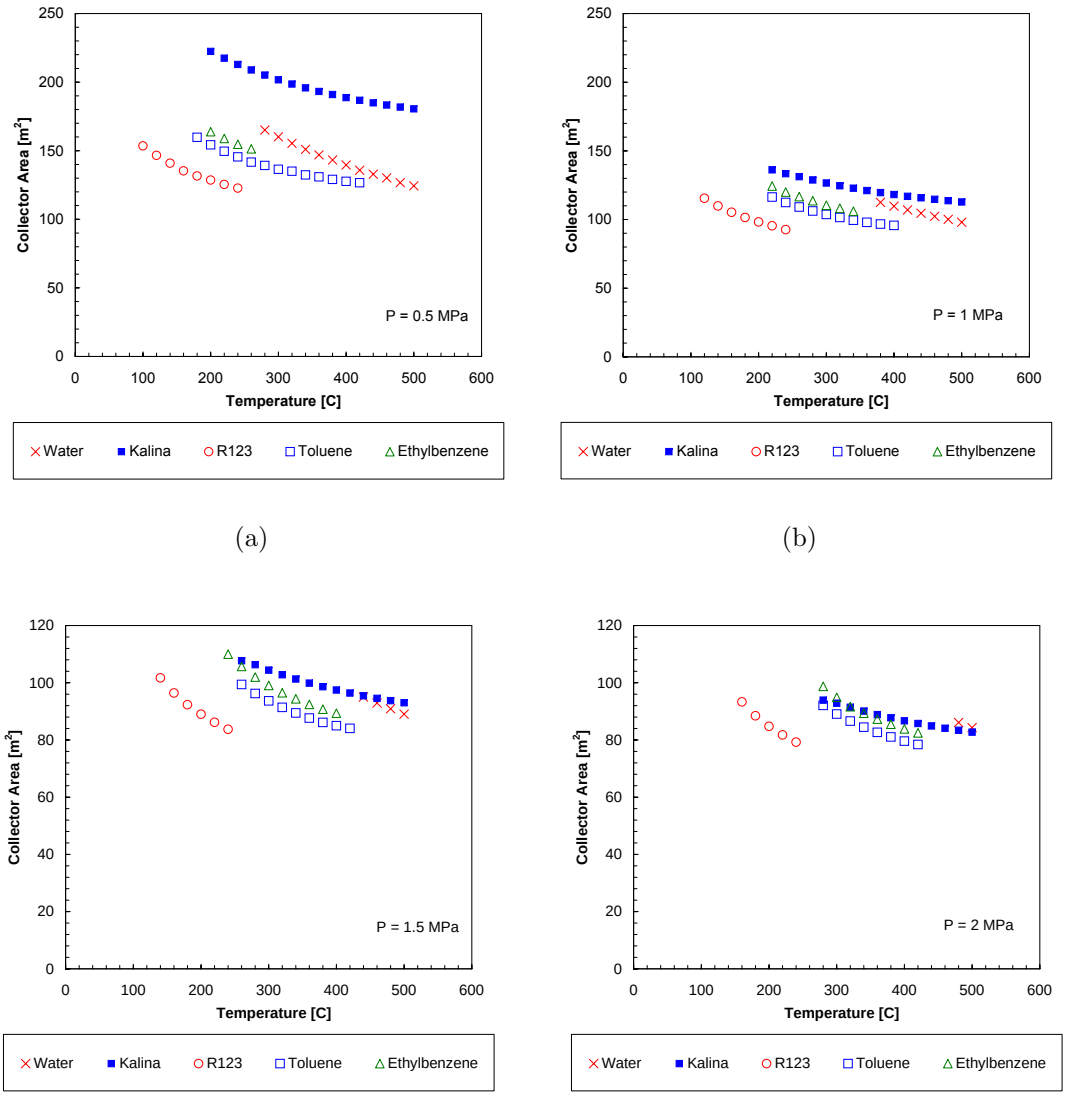

Figure 25: Collection Area vs Turbine Temperature at Turbine Pressures of (a)500 kPa (b) 1MPa (c) 1.5 MPa (d) 2 MPa

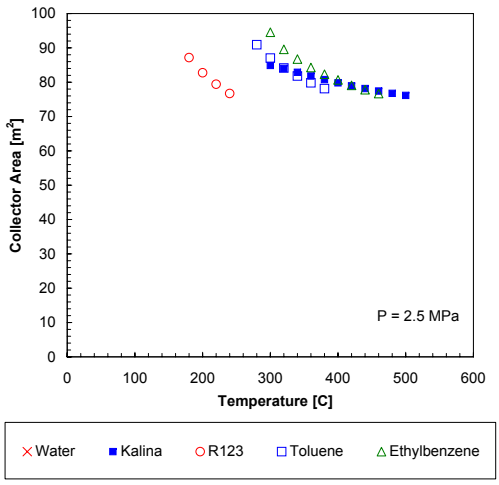

(e)

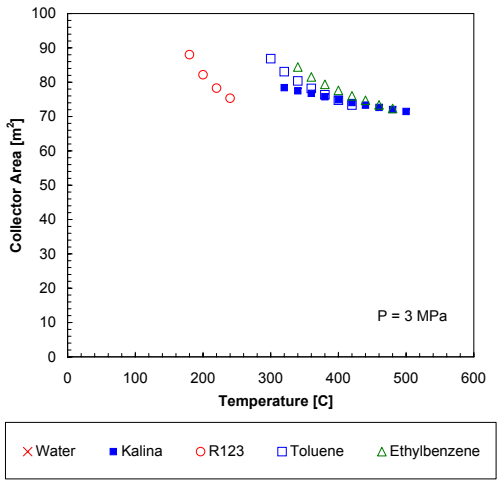

(f)

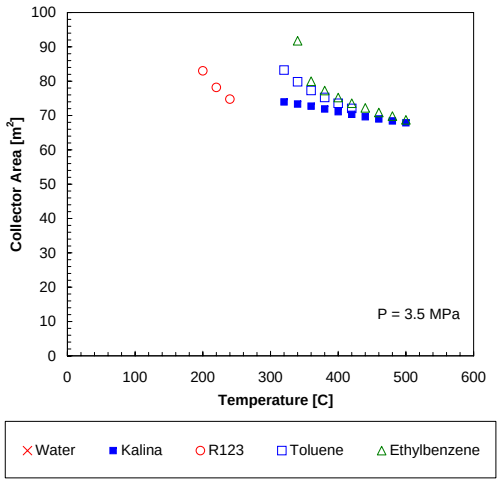

(g)

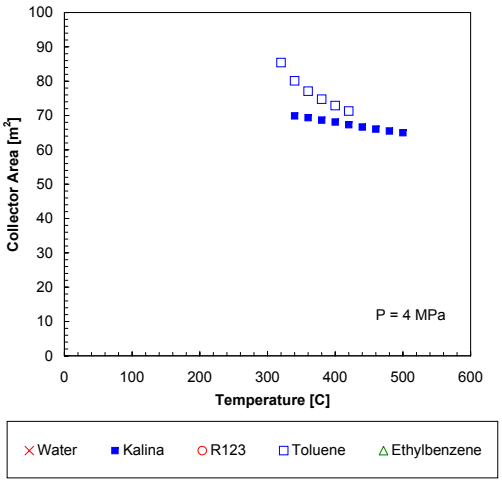

(h)

Figure 25: Collection Area vs Turbine Temperature at Turbine Pressures of (e) 2.5 MPa (f) 3 MPa (g) 3.5 MPa (h) 4 MPa

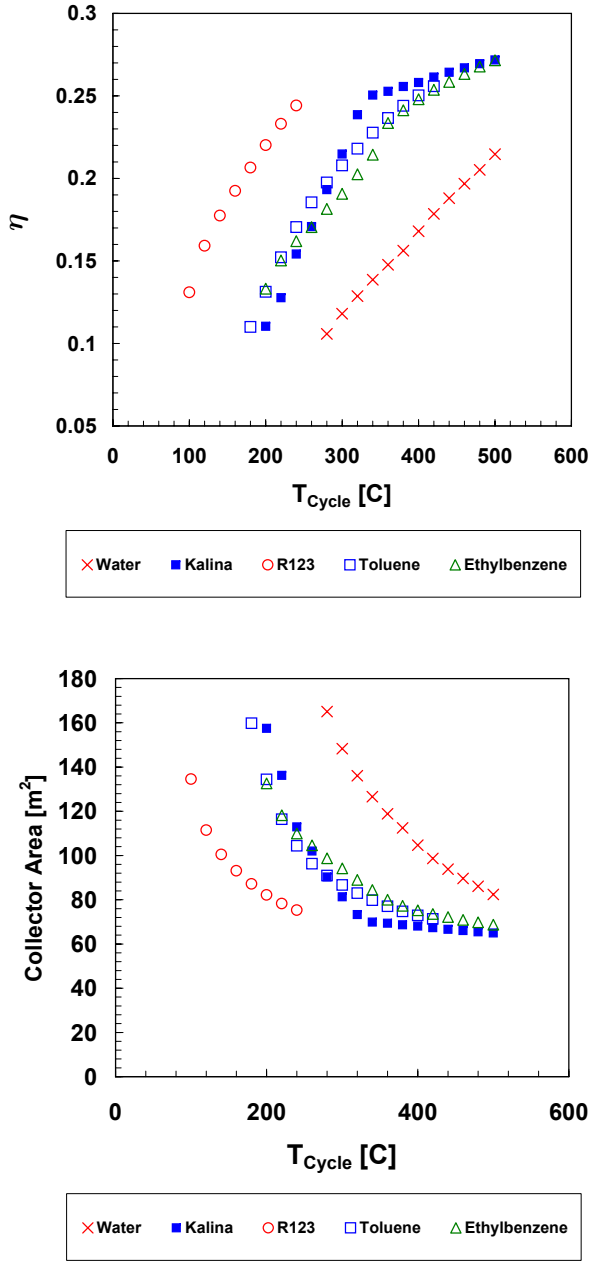

Figure 26: (a) Maximum Efficiency vs. Maximum Turbine Temperature (b) Minimum Collector Area vs. Maximum Turbine Temperature

Table 11: ORC Operating Conditions without Superheating

Fluid	Temperature [°C]	Pressure [MPa]
R123	160-220	2.2-3.5
Toluene	300-340	2.7-4.0
Ethylbenzene	300-360	2.4-3.5

3.5 Discussion

The general trend that ORCs outperform other cycle at low temperatures and pressure is confirmed. Interestingly, the Kalina cycle begins to outperform the ORCs for a pressure of 2 MPa and a temperature of 280°C. As the pressure increases beyond 3.5 MPa, R123 and ethylbenzne approach supercritical cycles. At pressures above 2 MPa, the Rankine cycle is no longer considered because the turbine inlet temperature must exceed 500°C to meet the exhaust quality constraint.

The ORCs do not require superheating in order to meet the turbine exhaust standard because of the fluid properties. Eliminating the superheat process eliminates a component and decreases the collection area. Superheating the working fluid before expansion at the turbine increases the enthalpy change corresponding to expansion but also increases the amount of heat, which directly translates to a larger collection area, needed for the cycle. As a result, the superheat process was eliminated and the pressure and temperature ranges for the ORCs are listed in Table 11.

As expected, the maximum efficiency and minimum collector area for a particular fluid occurs at the maximum cycle pressure corresponding to the temperature of interest. However, the ORCs differ slightly from this trend when the maximum cycle temperature and pressure are in the range of the saturation points. In Figure 27 the cycle efficiency versus pressure is shown for the R123 ORC at various maximum cycle temperatures. For a constant temperature process, the last data point corresponds to expansion from the saturation point. From Figure 27 it is evident that a local maximum exists over the pressure domain and beyond this point increasing

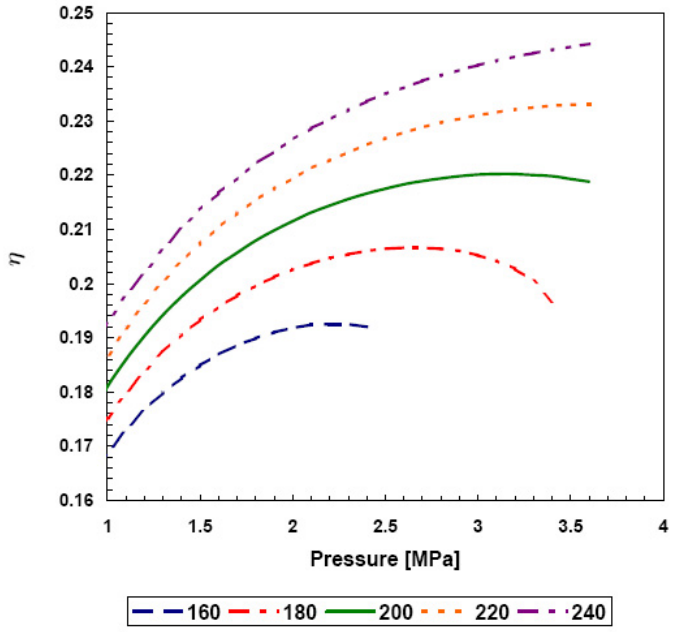

Figure 27: Cycle Efficiency vs. Maximum Cycle Pressure for R123

pressure decreases the efficiency. The efficiency decreases because the additional heat input is greater than the additional work output for the increase in pressure. As a result, expanding from the saturation point does not correspond with maximum cycle efficiency.

Beginning at 2.5 MPa, the advantageous effects of the binary ammonia-water solution begin to become apparent. The Kalina cycle has the smallest collection area yet it does not have the highest efficiency. The Kalina collection area is 2.62% smaller than the toluene ORC but the efficiency is 1.98% lower. Likewise, this trend is evident in Figure 26 where the Kalina cycle has the lowest collection area at a cycle temperature of 280°C but it does not have the highest efficiency until the maximum temperature reaches 300°C. In a binary fluid, the amount of heat to traverse the saturation dome decreases with increasing pressure as with a single component fluid; however, this process for a binary fluid is not isothermal and the saturation temperature on the fluid side of the saturation curve is lower than the saturation temperature

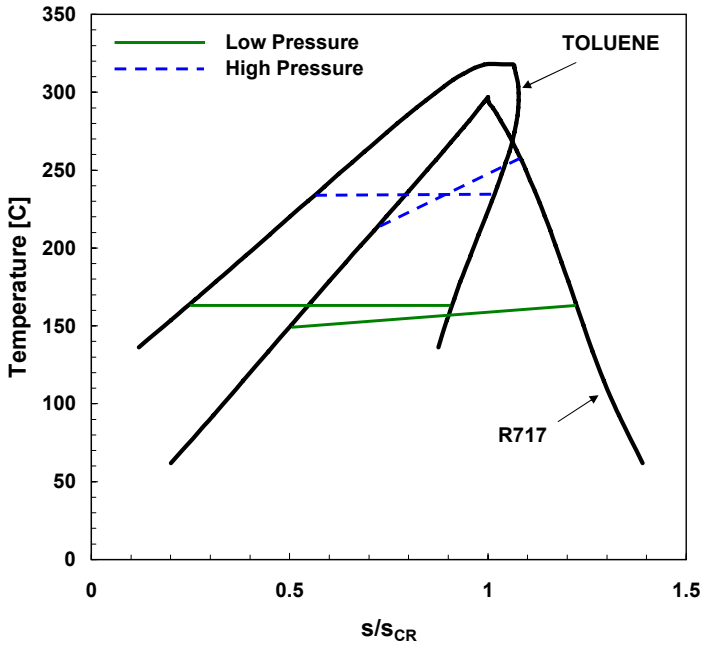

Figure 28: T-s Diagram for Ammonia-water and Toluene

on the gaseous side of the saturation curve at a constant pressure.

Figure 28 is a T-s diagram of 70% ammonia-water and toluene, and it is referenced to explain the varying specific heat that is advantageous in the Kalina cycle. At low pressures, the latent heat of vaporization for the ammonia-water mixture exceeds or is approximately equal to that of a pure fluid; therefore, there is not a large benefit from the varying specific heat of a binary mixture. However, as pressure increases, the varying specific heat for ammonia-water mixtures allows for significantly less heat input. As a result, less heat is required in the superheat stages and the collector area decreases for the Kalina cycle. However, the efficiency of the Kalina cycle is still lower than the ORCs because the ORCs are approaching supercritical but the Kalina cycle is not (P_{CR} for 70% ammonia fliud is 49 MPa [26]).

The elbow apparent in the Kalina cycle in Figure 26 exists because of the maximum pressure constraint on the cycles. The linear trend with a larger slope for turbine

temperatures of 200°C to 340°C exists because at temperatures below 340°C, an increase in turbine pressure and an increase in turbine temperature are both required to meet the turbine exhaust quality constraint. If just the pressure is increased while the temperature is held constant, the ammonia-water mixture may not completely vaporize in the boiler. At 340°C, the 70% ammonia water solution can be expanded from 4 MPa to 100 kPa without violating the quality constraint. At temperatures greater than 340°C, the only mechanism contributing to an increase in efficiency and a decrease in collection area is the increase in temperature due to the pressure constraint that holds the maximum turbine pressure to 4 MPa.

CHAPTER 4

AMMONIA-WATER CYCLES PERFORMANCE EVALUATION

This chapter presents a detailed treatment of the performance evaluation of the binary-fluid cycles considered in this study, including two Kalina cycles implementations and the Maloney-Robertson cycle, due to the promising potential of the Kalina cycle as characterized in the previous chapter. Specifically, this study adopts the closest approach temperature (CAT) methodology in order to describe the heat source and heat sink characterization, leading to more realistic models of the actual implementation characteristics of the proposed solar-thermal meso-scale power systems. Consistent with the overall goal of this research effort of establishing improved guidelines for power cycle selection at the meso-scale, this chapter will also present a detailed comparative analysis of the anticipated thermodynamic performance of the binary-fluid cycles against the baseline Rankine cycle and the ORCs, established in Chapters 2 and 3.

4.1 Model Development

The inclusion of the source and sink streams in this set of models allows for an improved characterization of cycle feasibility. The source stream is considered the stream leaving the collector that performs the heat exchange with the superheater, boiler, and preheater. The CAT between the source inlet and the turbine temperature establishes the maximum operating temperature, and thus pressure, of the cycle. Additionally, the inclusion of CAT between the condenser or absorber outlet and the sink stream characterizes the temperature needed for heat rejection. If the sink

temperature is too low or a higher turbine temperature is needed to meet the quality constraints on the turbine, the cycle is no longer feasible.

The two parameters considered in this study that affect the source temperature are the concentrator type and the method of heat transfer. A dual loop concept is introduced where a parabolic trough concentrator heats a thermal oil to a temperature of 350 °C. Dowtherm A and Dowtherm Q are two proprietary thermal oils made by DowChemical that will not breakdown in this temperature range. Source temperatures that exceed 350 °C require the use of a parabolic dish concentrator. A direct steam generation technique is proposed for these operating points. Figure 29 illustrates the difference in the heat transfer process between the dual loop and DSG system implementations.

4.1.1 Implementation of Closest Approach Temperature Modeling

CAT modeling is defined by assigning a temperature difference between the hot and cold streams in a heat exchanger (Figure 30(a)). It is understood that heat transfer is one directional, hot to cold. If the temperatures of the two streams converge, the heat transfer will cease (Figure 30(b)). The energy balance on the hot and cold streams, respectively, are

$$\dot{Q} = \dot{m}_h \left(h_{h,in} - h_{h,out}\right) = \dot{m}_h C_{P,h} \left(T_{h,in} - T_{h,out}\right) \tag{32}$$

$$\dot{Q} = \dot{m}_c \left(h_{c,out} - h_{c,in}\right) = \dot{m}_h C_{P,c} \left(T_{c,out} - T_{c,in}\right) \tag{33}$$

Once the enthalpy balance is established, the CAT between the hot and cold streams is checked. The pinch points for a counterflow heat exchanger are defined as

$$\Delta T_1 = T_{h,in} - T_{c,out} \tag{34}$$

$$\Delta T_2 = T_{h,out} - T_{c,in} \tag{35}$$

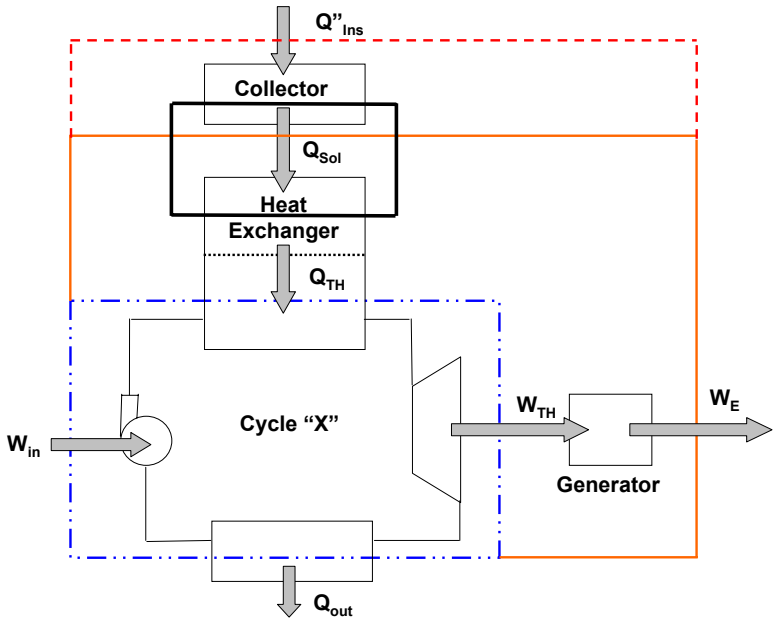

(a)

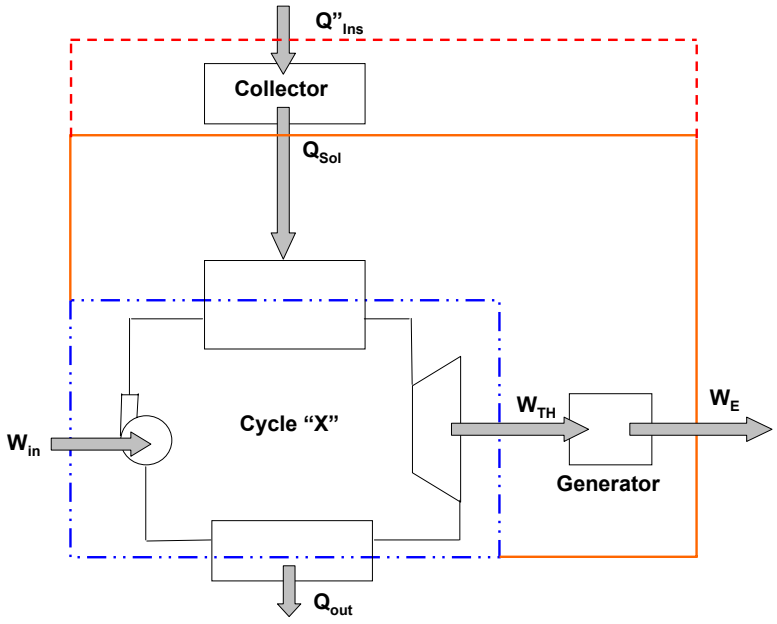

(b)

Figure 29: System Configuration for (a) Dual Loop Heat Transfer or (b) DSG

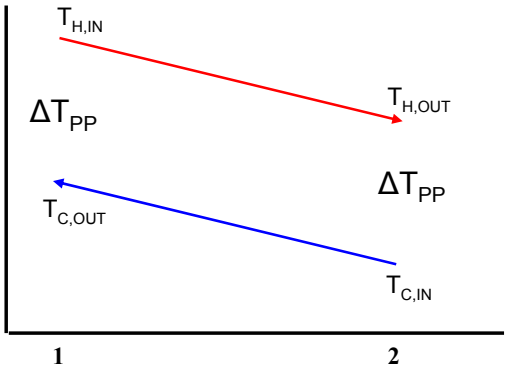

(a)

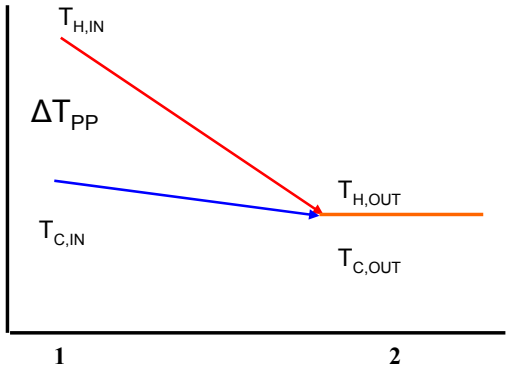

(b)

Figure 30: Pinch Point Differences for (a) Counter Flow Heat Exchanger (b) Parallel Heat Exchanger with ΔT_{CAT}=0 K

4.1.2 Organic Rankine Cycles

The basic cycle modeling of the ORCs is identical to the effectiveness analysis presented in Section 3.1.2 with the exception of the heat exchangers. The heat exchangers are modeled using the closest approach temperature method as described in Section 4.1.1. Additionally, the source and sink streams are characterized through the implementation of the CAT technique and the characterization of the respective fluids.

4.1.3 Kalina Cycle Models I and II

The Kalina cycle as described in Section 3.1.3 is modeled using the CAT technique for the heat exchangers. The limits imposed on this cycle through the CAT model when considering more rigorous characterization of the source and sink temperatures available to the cycle do not allow for the extraction of sufficient heat from the exhaust and dilute streams to run the thermal compressor under the conditions stated by Rogdakis. Figure 31 represents the schematic of the Kalina cycle with the addition of the Flash Preheater III that provides additional heat from the source. Also, the IPC in this cycle exchanges heat with both the sink and the working fluid. CATs are imposed on the hot working fluid stream, the cold working fluid stream, and the sink stream inlets and outlets, respectively. The addition of this component leads to increased cost and increased collection area. Therefore, an alternative configuration of the Kalina cycle was explored and a schematic is represented in Figure 32.

In the second version of the Kalina cycle, two of the flash preheaters have been removed. Also, the IPC does not exchange additional heat with the working fluid stream to avoid CAT violations. The flash tank remains an isobaric, isothermal component, efficiencies are assessed on the pumps and turbine, and all of the heat exchangers are modeled using the CAT methodology. The independent properties used to model each state are listed in Table 13.

Table 12: Kalina I State Definition

State	Independent Properties	Outlet Component	Inlet Component
1	T,P,Qu	Condenser	Pump I
2s	s,P,X	Pump I	Flash Preheat I
2	h,P,X	Pump	Flash Preheater I
3	h,P,X	Flash Preheater I	Flash Preheater II
4	h,P,X	Flash Preheater II	Flash Preheater III
5	h,P,X	Flash Preheater III	Mass Separation
6	h,P,X	Mass Separation	Flash Tank
7	h,P,X	Flash Preheater III	Mixing State I
8	T,P,Qu	Flash Tank	Mixing State I
9	h,P,X	Mixing State I	IPC (cold)
10	T,P,Qu	IPC(cold)	Pump II
11s	P,s,X	Pump II	IPC (hot)
11	P,h,X	Pump II	IPC (hot)
12	P,X,h	IPC (hot)	Recuperator
13	P,s,h	Recuperator	Preheater
14	P,X,Qu	Preheater	Boiler
15	P,X,Qu	Boiler	Superheater
16	T,P,X	Superheater	Turbine
17s	P,s,X	Turbine	Flash Preheater I (hot)
17	P,h,X	Turbine	Flash Preheater I (hot)
18	P,h,X	Flash Preheater I (hot)	Recuperator (hot)
19	P,h,X	Recuperator	Mixing State II
20	T,P,Qu	Flash Tank	Flash Preheater II
21	P,h,X	Flash Preheater II	Valve
22	P,h,X	Valve	Mixing State II
23	P,h,X	Mixing State II	Condenser Inlet

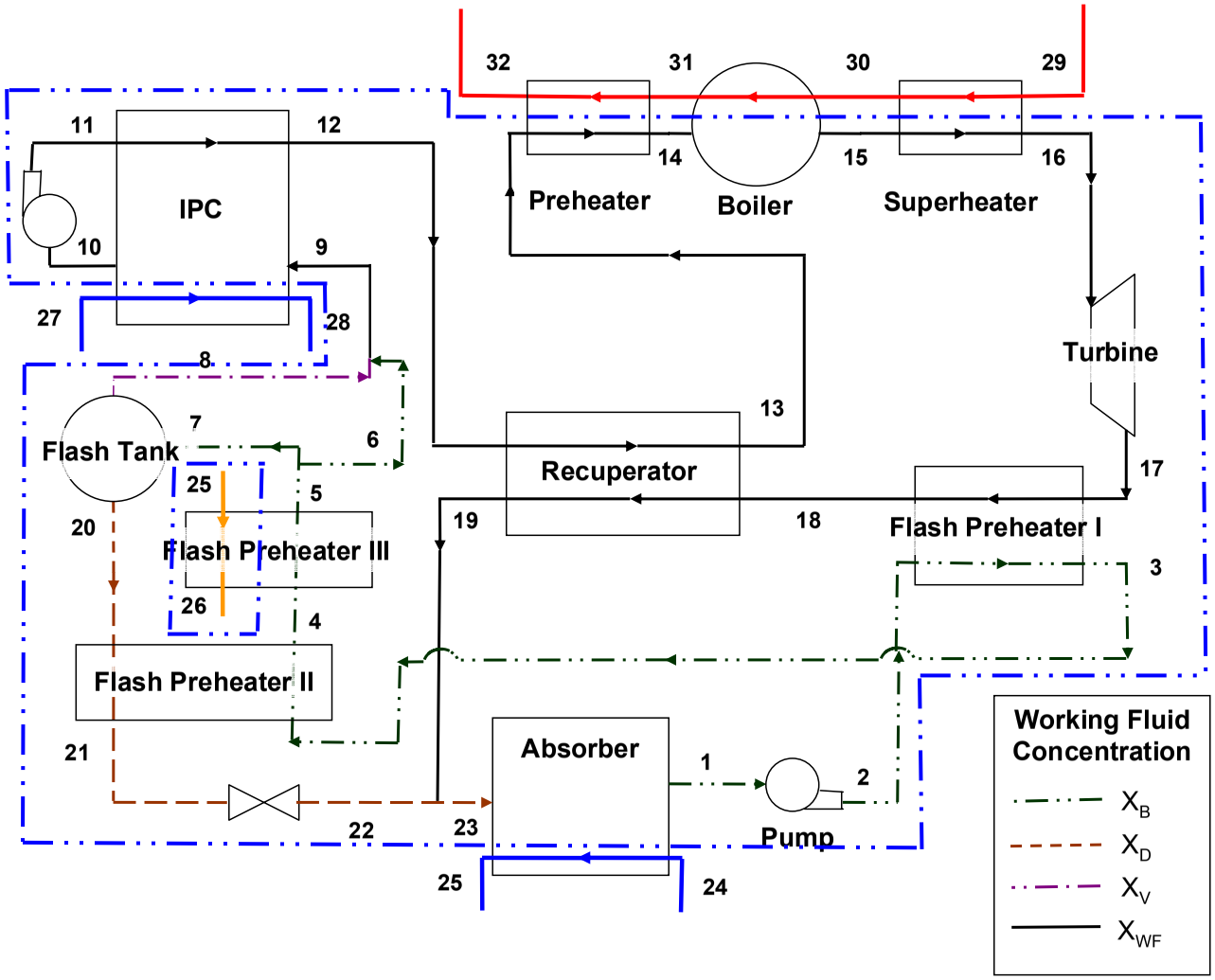

Figure 31: Kalina Diagram I

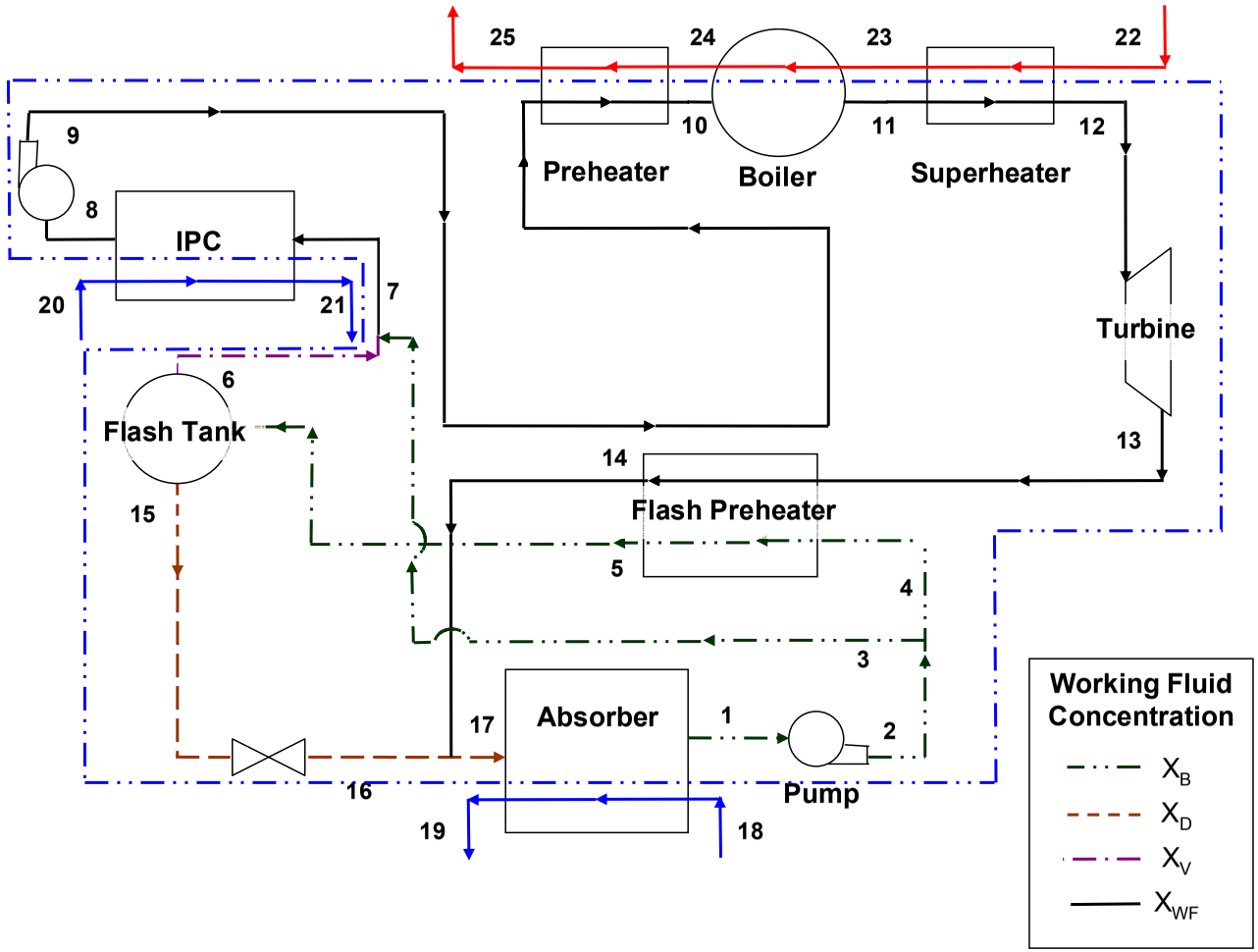

Figure 32: Kalina Diagram II

Table 13: Kalina II State Definition

State	Independent Properties	Outlet Component	Inlet Component
1	T,P,Qu	Condenser	Pump I
2s	s,P,X	Pump I	Mass Separation
2	h,P,X	Pump	Mass Separation
3	-	Mass Separation	Mixing State I
4	-	Mass Separation	Flash Preheater (cold)
5	h,P,X	Flash Preheater (cold)	Flash Tank
6	T,P,Qu	Flash Tank (Vapor)	Mixing State I
7	h,P,X	Mixing State I	IPC
8	P,X,Qu	IPC	Pump II
9s	P,s,X	Pump II	Preheater
9	P,h,X	Pump II	Preheater
10	P,X,Qu	Preheater	Boiler
11	P,X,Qu	Boiler	Superheater
12	T,P,X	Superheater	Turbine
13s	P,s,X	Turbine	Flash Preheater (hot)
13	P,h,X	Turbine	Flash Preheater (hot)
14	P,h,X	Flash Preheater (hot)	Mixing State II
15	T,P,Qu	Flash Tank (Dilute)	Valve
16	P,h,X	Valve	Mixing State II
17	P,h,X	Mixing State II	Condenser

4.2 Maloney-Robertson Cycle

The promising results from the initial assessment of the Kalina cycle leads to the implementation of a thermodynamic cycle simulation of the Maloney-Robertson cycle. This section conveys the technique to determine the mass flow rate of ammonia in each stream in the system normalized to the concentration of ammonia in the working fluid. Also, a detailed thermodynamics description of the cycle is provided. An optimization of the Maloney-Robertson cycle boiler conditions is presented in Section 4.4.4.

4.2.1 Model Development

The schematic for the Maloney Robertson cycle used for simulation purpose is depicted in Figure 33 and a detailed cycle description can be found in Section 2.2.1. The Maloney-Robertson cycle differs from the Kalina cycle because the Maloney-Robertson cycle does not employ a thermal compressor. Removing the mixing of the basic and vapor streams results in a high ammonia concentration in the fluid that is expanded in the turbine.

4.2.2 Species Balance

For the Maloney-Robertson cycle, the mixing state coupled with the boiler allow for a relationship between mass flow rates and species balances. The mixing state (Figure 34(a)) defines the mass in the basic stream in terms of the mass of the dilute stream and the vapor stream as

$$\dot{m}_B = \dot{m}_V + \dot{m}_D \tag{36}$$

Then the mass balance of ammonia at the boiler (Figure 34(b)) is used to determine the mass flow rate in the dilute stream as a function of the mass flow rate of the vapor stream. The total mass balance of ammonia in the boiler is

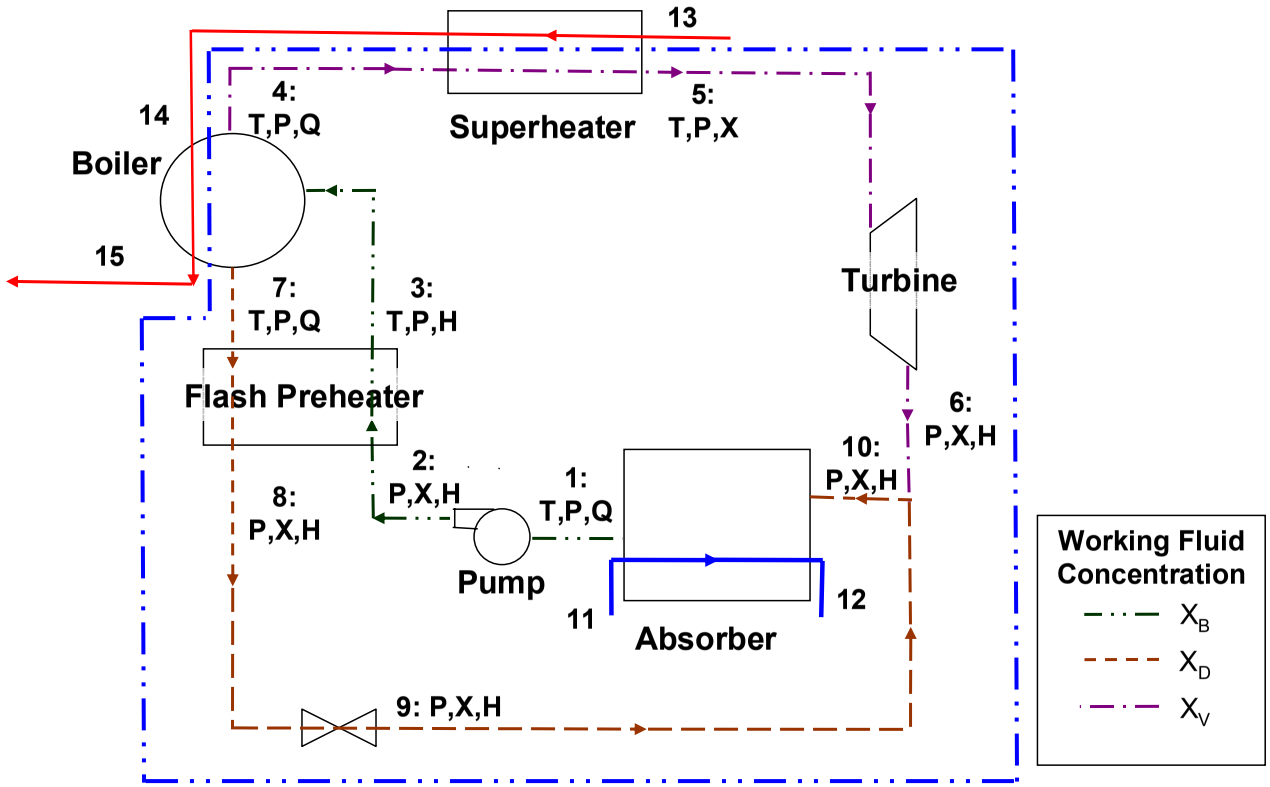

Figure 33: Maloney-Robertson Cycle Diagram

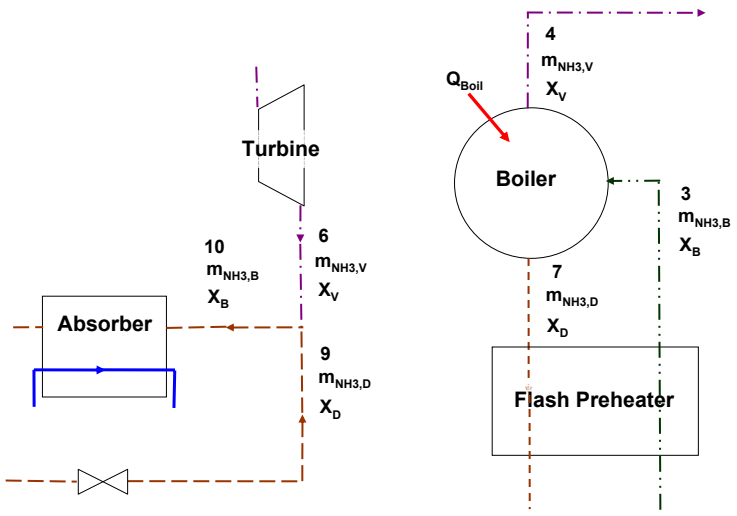

(a) (b)

Figure 34: Maloney-Robertson Cycle (a)Mass and Species Balance at the Mixing State (b) Mass and Species Balance on the Boiler

$$\dot{m}_V^{NH3} + \dot{m}_D^{NH3} = \dot{m}_B^{NH3} \tag{37}$$

The mass of ammonia can be related to the total mass by the mass fraction equation, $\dot{m}_i^{NH3} = \dot{m}_i X_i$, where i is a single fluid. Using the mass fraction relationship to rewrite Equation 37 yields the species balance

$$\dot{m}_V X_V + \dot{m}_D X_D = \dot{m}_B X_B \tag{38}$$

Next, substitute Equation 36 into 38 yields a mass balance that is only a function of the working fluid mass and the dilute stream mass

$$\dot{m}_V X_V + \dot{m}_D X_D = (\dot{m}_V + \dot{m}_D) X_B \tag{39}$$

Combining like terms and simplifying yields

$$\dot{m}_V \left(X_V - X_B\right) = \dot{m}_D \left(X_B - X_D\right) \tag{40}$$

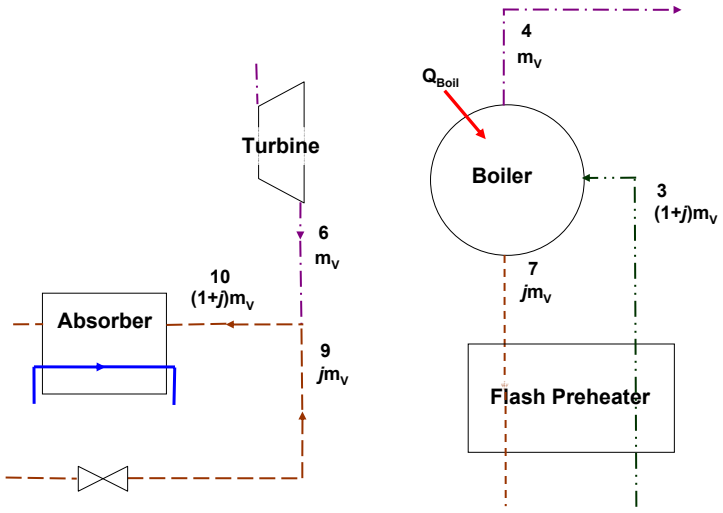

(a) (b)

Figure 35: Maloney-Robertson Cycle (a)Relative Mass Flow Rates at the Mixing State (b) Relative Mass Flow Rates at the Boiler

For simplicity sake in coding and representing the relative mass fraction of flow at the dilute exit in the boiler, the constant j is introduced and defined as

$$j = \frac{\dot{m}_D}{\dot{m}_V} = \frac{(X_V - X_B)}{(X_B - X_D)} \tag{41}$$

From Equation 41 and mixing of the vapor stream and the dilute stream, the flow rate in the basic stream is $(1 + j)\dot{m}_V$ at State 10 in Figure 33.

$$\frac{dm_D}{dt} = \frac{d}{dt}(m_V g)\,\frac{dm_D}{dt} = \frac{dm_V}{dt}g + m_V\frac{dg}{dt}\dot{m_D} = g\dot{m_V} \tag{42}$$

The overall flow in each stream in the Maloney-Robertson cycle is represented in Figure 35. The mass flow rate of the vapor stream, $\dot{m_V}$ is defined by the work output at the turbine through

$$\dot{W}_{turb} = \dot{m}_V\,(w_{t,act} - w_{p,act}) \tag{43}$$

Table 14: Maloney Robertson State Definition

State	Independent Properties	Outlet Component	Inlet Component
1	T,P,Qu	Condenser	Pump I
2s	s,P,X	Pump I	Flash Preheater (cold)
2	h,P,X	Pump	Flash Preheater (cold)
3	h,P,X	Flash Preheater (cold)	Boiler
4	T,P,Qu	Boiler (Vapor)	Superheater
5	T,P,X	Superheater	Turbine
6s	P,s,X	Turbine	Mixing State
6	P,h,X	Turbine	Mixing State
7	T,P,Qu	Boiler (Dilute)	Flash Preheater (hot)
8	P,h,X	Flash Preheater (hot)	Valve
9	P,h,X	Valve	Mixing State
10	P,h,X	Mixing State	Condenser

4.2.3 Thermodynamic Modeling

The thermodynamic steady-state component models implemented for the Maloney-Robertson cycle follow closely with the Kalina cycle. Table 14 presents the property combinations used to determine state properties. The pump and turbine are modeled using Equations 3 to 5 and 6 to 8, respectively. Additionally, an enthalpy balance on all components is met. However, there are three main differences between the Maloney-Robertson cycle and the Kalina. The first distinction is that the Maloney-Robertson cycle does not employ the two-pressure thermal compressor. As a result, maximum pressure in the Maloney-Robertson cycle is limited because of the low critical pressure for the high ammonia concentration in the vapor stream. Secondly, the Maloney-Robertson cycle does not use an isothermal flash process. The boiler unit couples as a heat input device and a separation unit. Finally, the Maloney-Robertson cycle does not use exhaust gas recuperation.

4.3 Target Design Specifications Revisions

Table 15 lists the modified design specifications associated with the CAT models. The generator, turbine, and pump component efficiencies assessed in Chapter 3 are not changed. The original turbine exhaust quality assumption is still applicable to the CAT models and the iteration loops from Section 3.3.4 are utilized. An efficiency associated with the concentration technique is assessed. The efficiency of a PTC with north-south orientation is 60% and that of a parabolic dish is 65%[21]. The author acknowledges that the collection efficiency changes according to the amount of direct versus diffuse radiation incident on the concentrator and the ambient temperature; however, the characterization of such fluctuations is beyond the scope of this project.

The CAT for source and sink temperatures were incorporated in these enhanced models. For temperatures at or below 350 °C, the source stream is modeled as Dowtherm A or Dowtherm Q in a dual-loop configuration (Figure 4.1). To achieve source stream temperatures in the range of 350 °C to 500 °C, the use of a parabolic dish collection system that achieves the high concentration ratios necessary to maintain such high temperatures is assumed [21]. DSG technologies are assumed for this model (Figure 4.1). The minimum flow rate of the source and sink streams, respectively, are characterized to met the CAT constraints. A CAT, $T_{CAT,ss}$=10 °C, was assessed between all source-cycle and sink-cycle interactions. The closest approach temperature assessed within the cycle is $T_{CAT,cyc}$=5 °C.

The loss parameters assessed in Chapter 3 to calculate the collection area using Equations 27 and 28 are also amended. The boiler and heat exchanger loss values are assessed equal values that are dramatically decreased to only a 3% loss. Detailed discussion of this change is in Section 4.4.1. Additionally, the heat exchanger loss assumption is only used for the dual-loop configuration when a PTC concentration is specified.

The operating parameters of the Kalina cycles have been amended due to the

Table 15: Assessed Component Efficiencies for CAT Modeling

η_G	0.85	$K_{HX,PTC}$	0.03
η_P	0.7	η_{PTC}	0.6
η_T	0.85	η_{PD}	0.65
$\Delta T_{CAT,cyc}$	5 K	$\Delta T_{CAT,ss}$	10 K

Table 16: Simulation Parameters for the Kalina Cycle II [32]

Absorber Outlet Quality	Saturated Liquid
Absorber Pressure	100 kPa
Flash Tank Temperature	75 °C
Flash Tank Pressure	300 kPa
X_{WF}	42.6% ammonia

CAT violations and are listed in Table 16. Decreasing the low-side system pressure to 100 kPa caused violation of the CATs on the sink streams using the Rogdakis operating constraints on these cycles. New operating parameters are assessed that reflect the design point in Kalina's 1984 patent for a system with a maximum operating temperature of 350 °C and a minimum operating temperature of 35 °C. The isobaric, isothermal flash tank is still employed. An optimization is performed to define the operating parameters of the Maloney-Robertson cycle and the procedure is presented in Section 4.4.4.

4.4 Numerical Validation and Implementation

4.4.1 Adjustment of the Heat Exchanger Loss Parameter

In order to assess the validity of the heat exchanger loss parameter, a simple conduction analysis on a shell & tube heat exchanger from McMaster-Carr is presented. The model assumptions are as follows:

1. Neglect Radiation losses
2. Neglect Contact Resistance
3. Heat exchanger is sitting in air at 25 °C

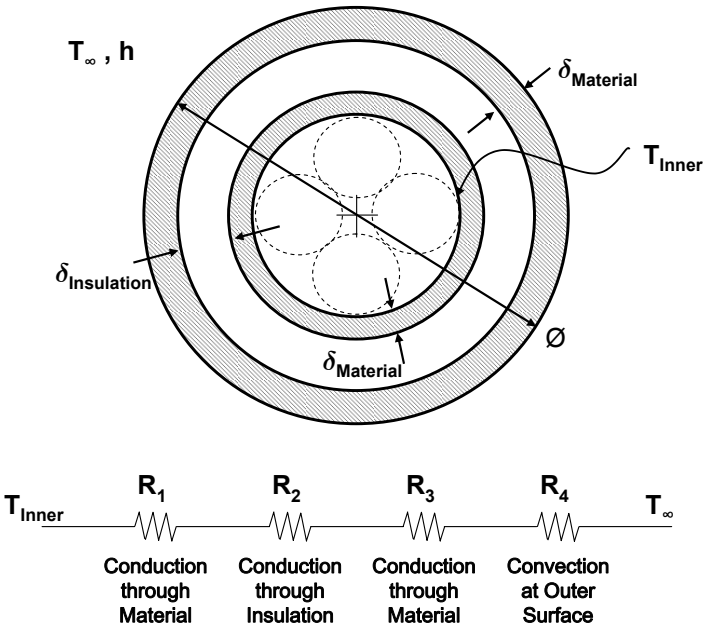

Figure 36: Conduction Analysis on Heat Exchanger

4. Natural convection on the outer shell surface

5. Inner shell temperature of 500 °C, which corresponds to the maximum source temperature in this study

6. Outer shell temperature is 125 °C above ambient temperature

With these assumptions, a simple heat transfer analysis using thermal resistance networks is conducted to determine the amount of heat lost through the shell. McMaster-Carr Shell & Tube heat exchanger with an outer diameter of 0.1143 m (4.5 in), tube diameter of 19.05 mm (0.75 in) and a length of 0.276225 m (10.875 in) that has a cooling capacity of 70337 W (240,000 BTU/hr) is used for this analysis. The shell thickness and insulation thickness are assumed dimensions of:

1. Inner and Outer shell wall thickness = 6.35 mm (0.25 in)

2. Insulation thickness = 2.54 mm (0.1 in), 6.35 mm (0.25 in), or 12.7 mm (0.5 in)

3. Urethane insulation material with $k_{mat} = 0.24 \frac{W}{m-K}$ [28]

The one dimensional conduction model of the heat exchanger is shown in Figure 36 and consists of conduction resistance through the inner wall,R_1, insulation, R_2, and outer well, R_3, as well as natural convection at the outer surface, R_4. The standard cylindrical resistance for conduction is

$$R_{conduction} = \frac{\ln \frac{r_o}{r_i}}{2\pi L k_{mat}} \tag{44}$$

where r_o is the outer radius, r_i is the inner radius, L is the length of the cylinder, and k_{mat} is the thermal conductivity of the material through which conduction is occurring. The resistance resulting from a convective load on the outside of a cylinder is

$$R_{convection} = \frac{1}{h\pi DL} \tag{45}$$

where h is the convection coefficient, r is the outer radius where convection is occurring, and L is the length of the cylinder. The convection coefficient is related to the Nusselt number by $Nu = \frac{hD}{k}$. The Nusselt number is determined from the Churchill and Chu correlation [28]:

$$Nu_D = \left(0.6 + \frac{(0.387 Ra_D)^{\frac{1}{6}}}{\left(1 + \left(\frac{0.559}{Pr}\right)^{\frac{9}{16}}\right)^{\frac{9}{16}}} \right)^2 \tag{46}$$

where Ra is the Rayleigh number and Pr is the Prandtl number. The Rayleigh number is

$$Ra = \frac{g\beta \left(T_s - T_\infty\right) D^3}{\nu\alpha} \tag{47}$$

where g is the gravitational constant, β is the thermal expansion coefficient, ν is the kinematic viscosity, and α is the thermal diffusivity.

Table 17: Maximum Efficiency and Minimum Collection Area for Initial Cycles Analysis

Material	Insulation Thickness	Percentage Heat Loss
Brass	2.54 mm (0.1 in)	1.443%
	6.35 mm (0.25 in)	1.015%
	12.7 mm (0.5 in)	0.657%
Stainless Steel	2.54 mm (0.1 in)	1.426%
	6.35 mm (0.25 in)	1.006%
	12.7 mm (0.5 in)	0.687%

The properties of air used in Equations 46 and 47 are taken from the EES function call for air. Additionally, the thermal conductivity of the heat exchanger materials, brass and stainless steel, are property calls in EES.

The amount of heat lost divided by the total heat transfer of the system provides an estimate of the loss to the environment. The results of this stimulation are shown in Table 17. The average heat loss is highly dependent on the amount of insulation. However, even when just 0.1 in of insulation surrounds the heat exchanger, approximately 1.5% of the heat is lost. Therefore, the assumption of 3% heat loss is reasonable for this simulation.

4.4.2 Numerical Validation of Ammonia-Water Models

The temperature limit on the data in the publication by Ibrahim and Klein is 600 K [26]. The data limit on the ammonia-water cycles is 500°C and the Ibrahim and Klein data are extrapolated to this temperature. Table 18 provides justification that the Ibrahim and Klein data available in EES is not a gross over-estimate of the properties of ammonia-water mixtures at high temperatures and high pressures. This table relates the difference in the change in enthalpy between two states. The entropy data are not included because the state entropy is not provided in the literature.

The validation with Maloney-Robertson cycle modeling was achieved through comparison with the data provided in the 1953 report [45]. A slightly modified cycle

Table 18: Evaluation of Error in NH3-H2O Property Models using an Extrapolation Approach

Paper	State	T [°C]	P [MPa]	X [% Ammonia]	h from Literature [kJ/kg]	h from EES [kJ/kg]	% Difference
Kalina 84[31]	15	532.2	8.273	0.5	3037.47	3076	
Kalina 84[31]	16	482.32	6.032	0.5	2916.14	2946	
Change in Enthalpy	15 to 16				121.33	130	7.15
Kalina 84[31]	17	420.69	3.964	0.5	2768.88	2792	
Change in Enthalpy	16 to 17				147.26	154	4.58
Kalina 84[31]	18	353.89	2.482	0.5	2613	2632	
Change in Enthalpy	17 to 18				155.8	160	2.64
Kouremous and Rogdakis 90[35]	9	510	11	0.7	3520	2825	
Kouremous and Rogdakis 90[35]	10	338.6	2.74	0.7	3066	2389	
Change in Enthalpy	9 to 10				454	436	3.96

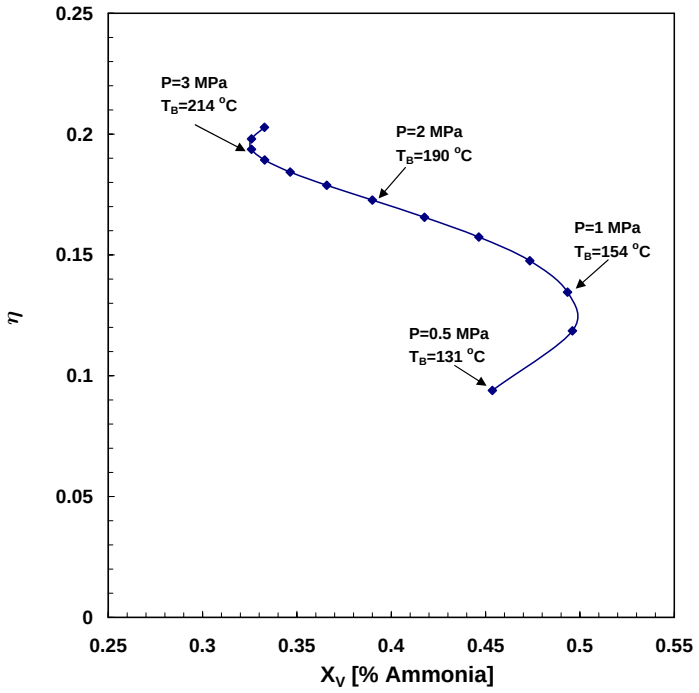

Figure 37: Efficiency vs Vapor Concentration

simulation using the temperatures, pressures, and concentrations presented in Maloney and Robertson study resulted in less than 6% difference in the efficiency. It is noted that the ammonia-water property data presented by Ibrahim and Klein were published in 1993; therefore, the fluid property data used in this study are more accurate than the property data used by Maloney and Robertson. Thus, the improved property data can account for the difference in the enthalpy at the states.

Additionally, Maloney and Robertson note that the efficiency of the cycle decreases with increasing ammonia concentration[45]. This trend is illustrated in Figure 37 for the optimized cycle. The trend of efficiency vs boiler concentration has curved portions at the extremes because the temperature of the boiler decreases and as a result the concentration decreases. This creates a local minimum and maximum in terms of vapor concentration. If the temperature is constant at the boiler, the vapor ammonia concentration has an increasing trend with increasing pressure.

Kalina II is verified through comparison of the EES model and the 1984 patent. There is only a 0.5% difference in the efficiency of the two models. The revised Kalina I model is not presented in literature so there is not a form of justification for the validity of this model through the use of past literature.

Four checks are coded in the CAT thermodynamic models. The first check ensures that the energy coming into the system equals the energy leaving; thus, the steady state energy accumulation in the system is 0. Next, the models are validated through the inclusion of a check confirming that the total entropy generation and the exergy destruction in the system are greater than 0. The component entropy and exergy calculations are verified through two separate calculations. The entropy and exergy destructions are calculated via the entropy and exergy open system equations, respectively. If the entropy and exergy equations are correct, the exergy generation terms found from the exergy equation will equal $\dot{I}_{gen} = T_o \dot{S}_{gen}$ where the entropy generation is found from the entropy equation. Finally, the first law efficiency was verified by using the two exergy forms

$$\begin{aligned} \eta_I &= \frac{\dot{W}_{NET}}{Q_{IN}} \\ &= \left(1 - \frac{T_{L,Eff}}{T_{H,eff}}\right) - \frac{T_{L,eff}\dot{S}_{gen}}{\dot{Q}_{in}} \\ &= \frac{\left(1 - \frac{T_{L,Eff}}{T_{H,eff}}\right)}{\left(1 - \frac{T_{L,eff}\dot{I}_{Dest}}{T_o \dot{W}}\right)} \end{aligned} \tag{48}$$

4.4.3 Implementation of Closest Approach Temperature

Two implementations of the CAT technique are utilized in this study. The first implementation is for heat exchangers residing within the cycle that do not interact with the source and sink streams. The second implementation is used for the source and sink stream iterations.

For heat exchange processes within the cycle, the flow rate in the hot and cold streams cannot be changed. Taking the recuperator as an example, only the exit temperatures of the hot and cold streams can be manipulated to satisfy the specified pinch point. To implement this heat exchanger technique for the recuperator, the pinch point between the hot stream outlet and the cold stream inlet is imposed. After evaluating the energy balance on the heat exchanger, the temperature of the cold stream outlet is defined. If the temperature differences between the hot stream inlet and the cold stream outlet is satisfied, then no further iteration is required. However, if the pinch point is violated, then the pinch point between the hot stream outlet and cold stream inlet is increased until the pinch point between the hot stream inlet and cold stream outlet is satisfied.

Heat exchangers interacting with the source and sink do not have a specified stream flow rate. The sink stream is a simple application where the minimum sink flow rate is found to satisfy the CAT. The source stream is more complicated since it interacts with multiple components. The temperatures of the inlet and outlet of the source stream are defined by the CAT between the superheater outlet and preheater inlet. Using the enthalpy balance, the temperatures across the source stream are found as well as the minimum flow rate required to maintain the CAT. The source stream flow rate has to be such that the CAT on the boiler is preserved. If the boiler CAT is not met, the flow rate is increased and the temperature difference at the sink stream preheater outlet is increased.

4.4.4 Maloney-Robertson Cycle Optimization

As far as the author can tell, optimization of the Maloney-Robertson cycle has not been presented in the literature. As a result, an optimization of the boiler temperature for maximum efficiency over the pressure ranges of 500 kPa to 3 MPa is presented. This optimization optimizes the first law efficiency because the boiler constraints

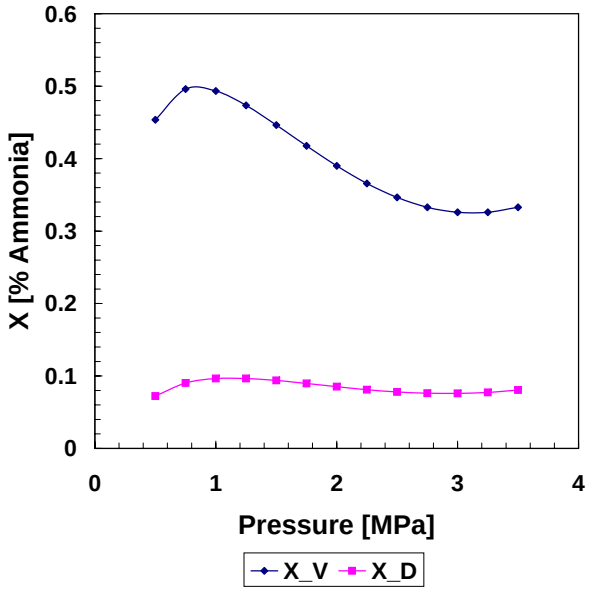

Figure 38: Maloney-Robertson Vapor and Dilute Concentration Variation vs Pressure

define the ammonia concentrations in the weak and vapor solutions.

The ammonia concentrations in the Maloney-Robertson cycle can either be explicitly stated or implicitly defined as a function of quality, temperature and pressure. In this study, the concentrations are implicitly defined to allow the ammonia concentration of the dilute and vapor streams to vary with cycle pressure and boiler temperature. Figure 38 represents the change of ammonia concentration in these streams as cycle pressure changes. The basic stream concentration is defined as saturated liquid at the absorber temperature and pressure; therefore, it has a constant ammonia concentration of 32.22% for th imposed constant absorber constraints and is not dependent on turbine pressure and boiler temperature.

Figure 40 represents the effects of boiler temperature on system efficiency when all other aspects of the cycle are held constant. An optimization approach is taken to determine the relationship between the boiler temperature, the boiler pressure, and the cycle efficiency. An underlying assumption on this system is that $X_D <$

$X_B < X_V$; therefore, a certain range of boiler temperatures exists for a given pressure where these constraints are met. The lowest temperature in this range corresponds to $X_D = X_B$ while the high temperature is where $X_B = X_D$. EES code following the structure of the flow charts in Figure 39 determines the appropriate temperature ranges on the boiler given the boiler pressure. Utilizing the temperature constraints as the bounds on the cycle, the turbine pressure on the cycle is varied between 0.5 MPa to 2.5 MPa in increments of 0.5 MPa, noting that impossible solutions such as cycle efficiency greater than Carnot efficiency or CAT violations within the cycle are disregarded. A parametric evaluation of the cycle efficiency at a constant pressure is performed. Next extrema seeking for the maximum efficiency at a given pressure yields the boiler temperature corresponding to the maximum efficiency as shown in Figure 41. A least square regression polynomial curve was fit to the data to translate the boiler temperature and pressure relationship into an equation that is coded into the Maloney-Robertson EES cycle model.

4.5 Results

The cycle simulations in EES were completed numerically by varying the source temperature and pressure to determine the first-law system efficiency and the required solar collection area. The source temperature was varied in increments of 25°C from 100°C to 500°C. The maximum pressure limit is coupled to the source temperature through the pinch point difference. Furthermore, the maximum cycle temperature is constrained so that a single-phase gaseous exhaust stream exits the turbine. In order to simulate real-world operating conditions, typical mechanical efficiency of 85%, 80%, and 70% were assumed for the generator, turbines, and pumps, respectively. Likewise, the sink stream is assumed to be water at 15°C.

Representative samples of the thermal efficiency across the design space at source temperatures of 250 °C, 275 °C, 300 °C, 325 °C, and 350 °C are plotted in Figure 42.

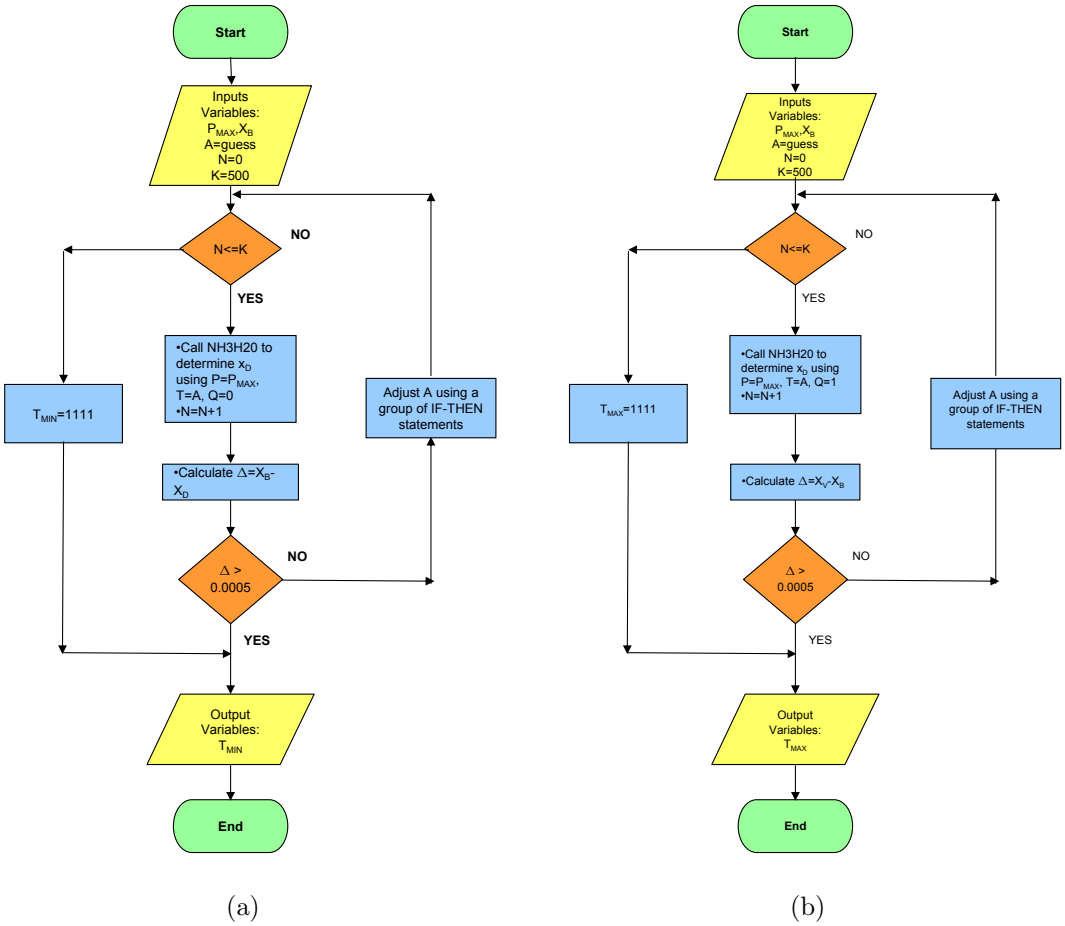

(a) (b)

Figure 39: Boiler Temperature Iteration Loops (a)Minimum Boiler Temperature (b)Maximum Boiler Temperature

Table 19: Maximum Efficiency and Minimum Collection Area for Enhanced Cycle Models

Cycle	η [%]	Collector Area $[m^2]$	Pressure [MPa]	Temperature [°C]
Rankine Cycle	24.53	92.18	4.4	500
R123 ORC	20.61	122.6	3.1	200
Toluene ORC	22.53	112.1	3.6	325
Ethylbenzene ORC	24.09	104.8	3.5	350
Maloney-Robertson Cycle	24.28	93.13	5.4	450
Kalina Cycle	27.81	81.32	8.3	500

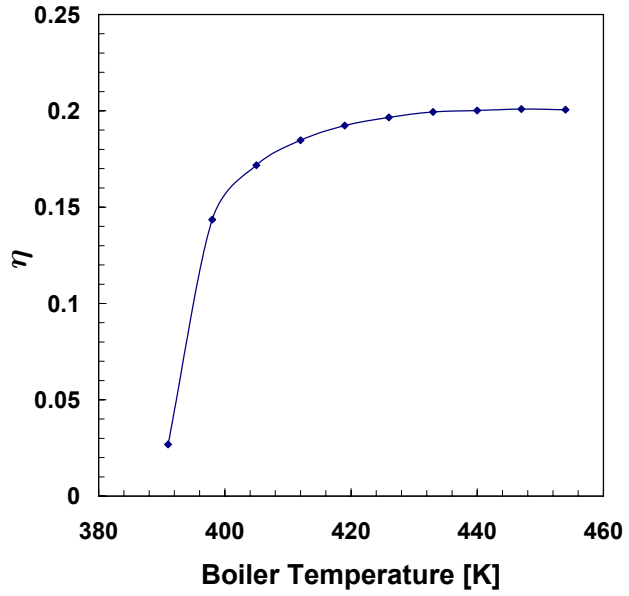

Figure 40: Efficiency vs Boiler Temperature for Cycle Pressure of 1.5 MPa

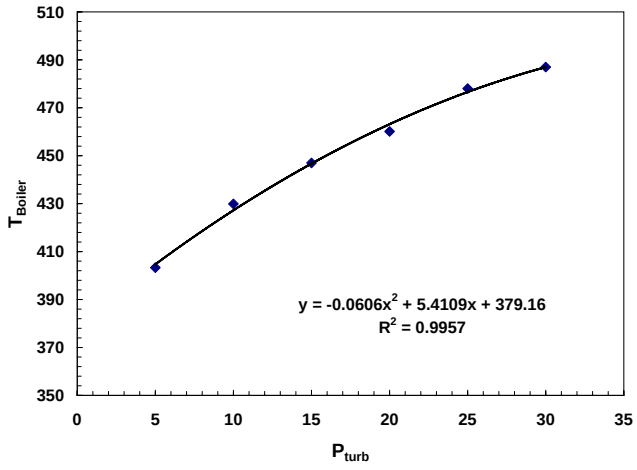

Figure 41: Boiler Temperature Optimization of the Maloney-Robertson Cycle

Table 19 specifically calls attention to temperature and pressure relating to the maximum efficiency and minimum collection area for the CAT cycle models.

The collector area required to satisfy the thermal heat input was evaluated at each point in the simulation space. Due to the simple coupling of the cycle efficiency and the collector, in which the collector area decreases with increasing efficiency, the corresponding collector area plots are not presented. Figures 43(a) and 43(b) show the maximum efficiency and minimum collection area, respectively, for each of the fluid over the source temperature range of interest.

4.6 Discussion

After imposing the sink closest approach constraint, the optimization by Rogdakis is no longer valid at the cycle parameters defined in Section 4.3. The assumed sink temperature must be lower than the liquid saturation temperature of the ammonia water for the pressure specified. Figure 44 shows the liquid saturation temperature for various concentrations of ammonia-water solutions at pressures of 100 kPa, 300 kPa, and 470 kPa. The sink temperature of 15°C and a CAT of 10°C indicates that the saturation temperature cannot be lower than 25°C. At a pressure of 100 kPa, the concentration of ammonia cannot exceed 28%. The optimization by Rogdakis with a basic fluid solution of 42% ammonia at a pressure of 100 kPa condenses fully at 8.4°C and would require a sink stream temperature of -2.4°C assuming a CAT of 10°C. Likewise, the saturation temperature of a 70% ammonia solution at 470 kPa is 14.6°C and the sink stream would need to be at 4.6°C after assessing a 10 degree CAT. The low sink temperatures necessary for condensation of the basic and working fluid stream using the Rogdakis concentrations is not practical for a residential application. As a result, the Kalina parameters as indicated in Table 16 are used for the CAT modeling.

At low source temperatures, the R123 ORC is the only cycle that produces power

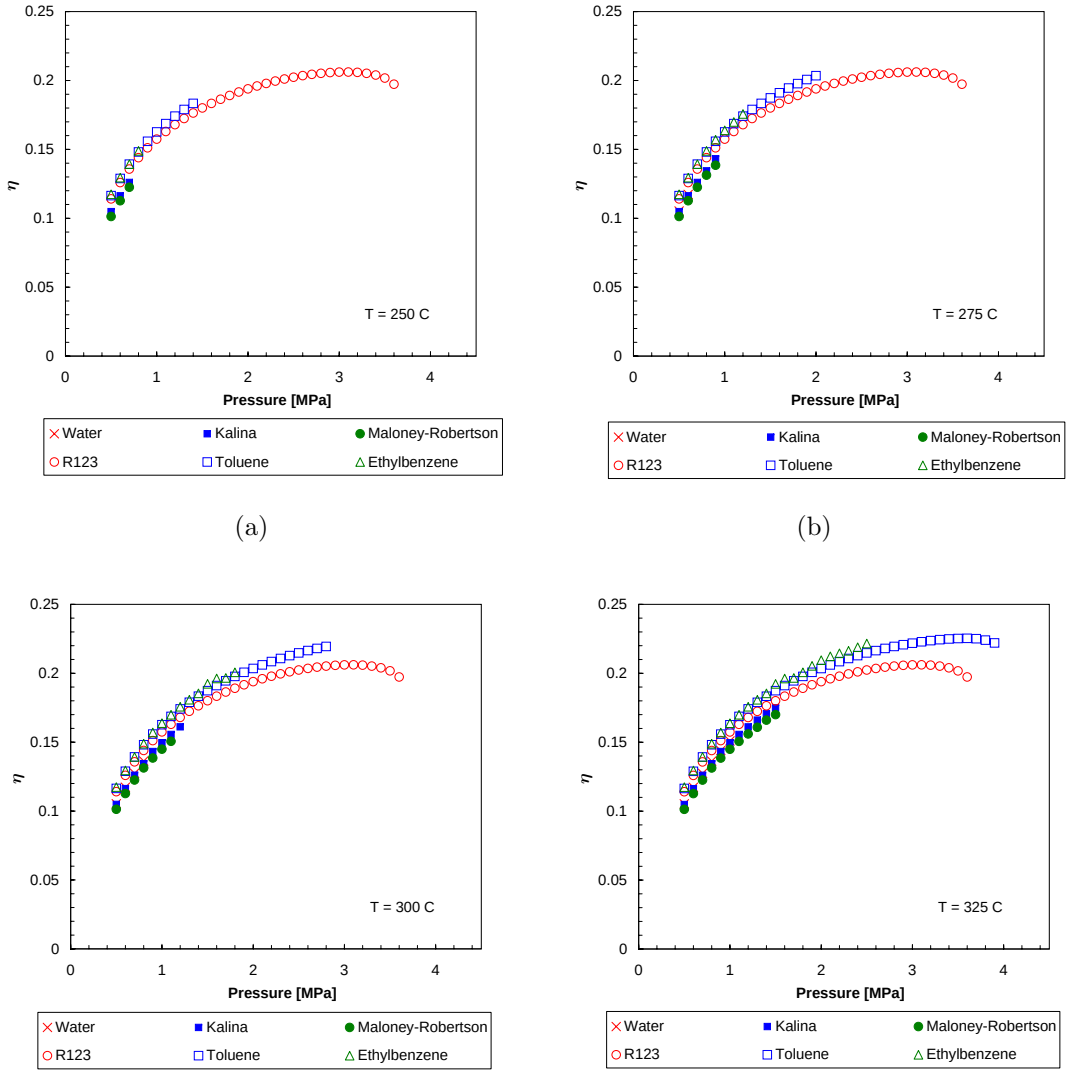

Figure 42: Cycle System Efficiency vs Source Temperature at (a) 250°C (b) 275°C (c) 300°C (d) 325°C

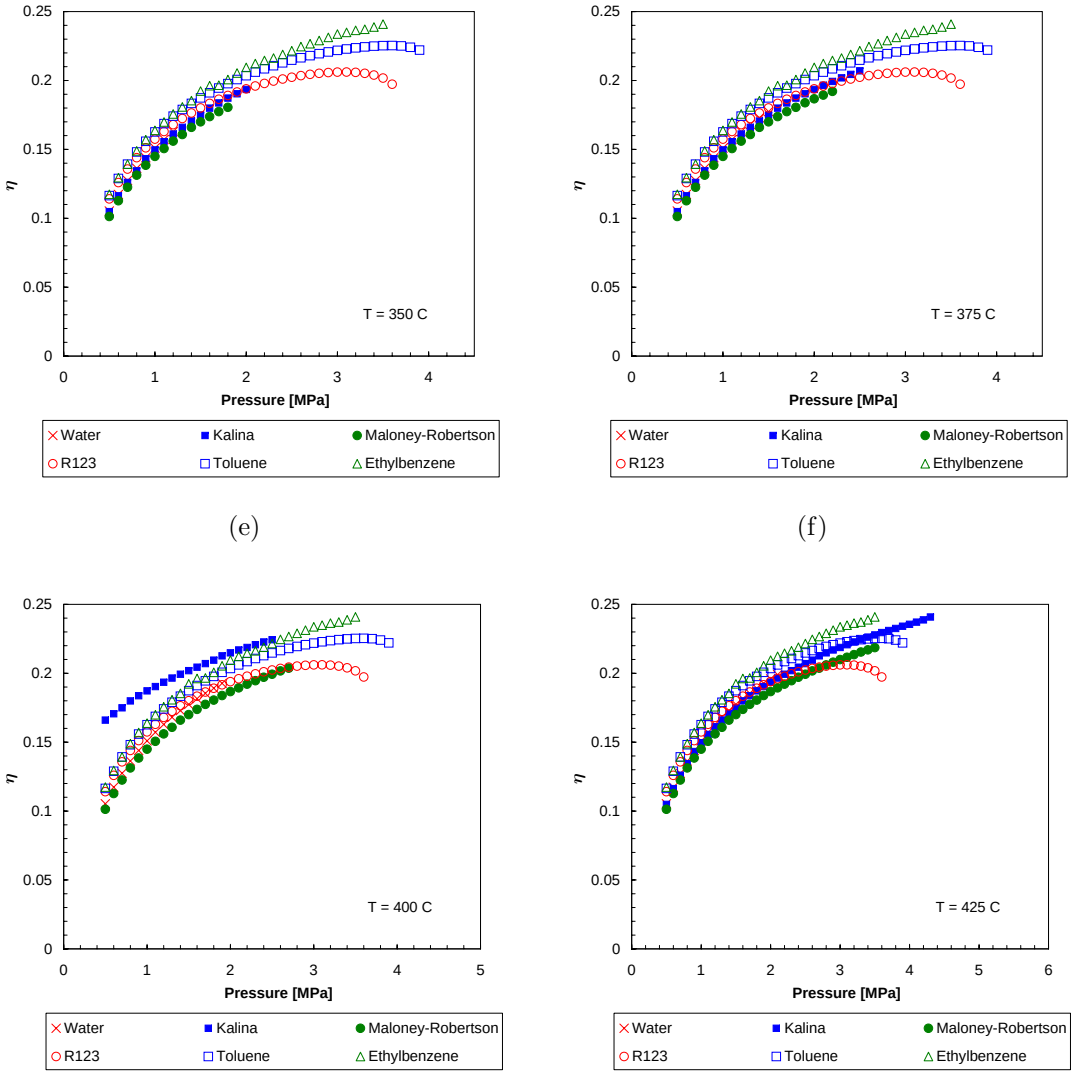

Figure 42: Cycle System Efficiency vs Source Temperature at (e) 350°C (f) 375°C (g) 400°C (h) 425°C

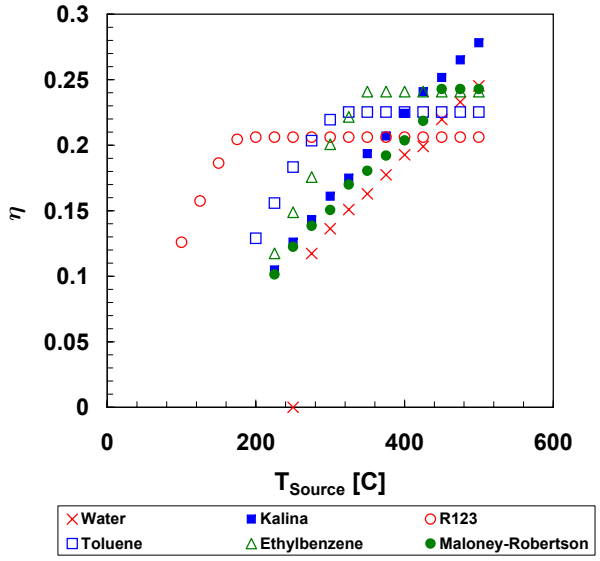

(a)

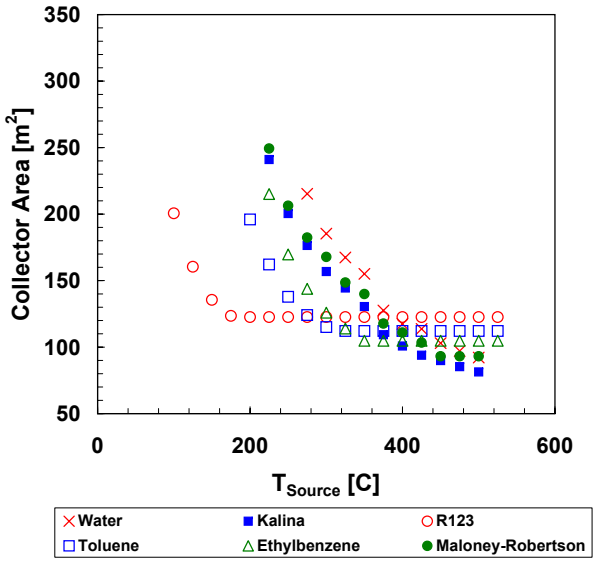

(b)

Figure 43: (a) Maximum Efficiency vs. Source Temperature (b) Minimum Collection Area vs. Source Temperature

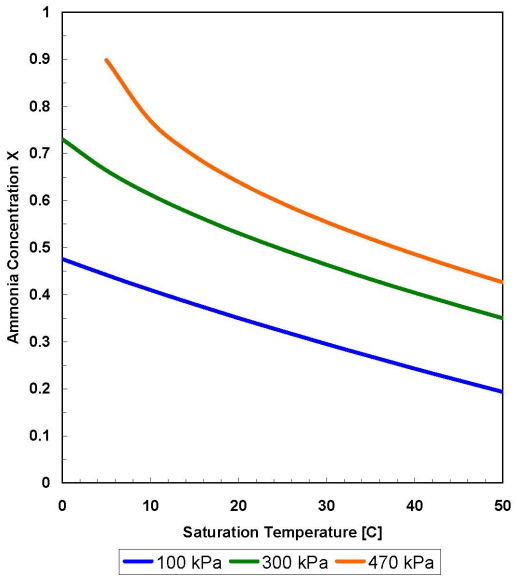

Figure 44: Saturation Temperature of Ammonia-Water Mixtures

(Ref: Figure 43(a) and 43(b)). The elbows apparent in Figures 43(a) and 43(b) for the ORCs occur because increasing the source temperature beyond these points does not increase the cycle efficiency due to the nature of the superheat iteration loop. The superheat is not increased because the iteration loop finds the minimum superheat required to satisfy the turbine exhaust constraint, regardless of the input temperature. The higher source temperature simply increases the difference in the source temperature and the turbine inlet temperature.

At high source temperatures and high pressure, the ammonia-water cycles show promise. The the Kalina cycle maximum efficiency at 500 °C and 8.3 MPa is 13.3% higher than the ethylbenzene ORC at its highest point of 350 °C and 3.5 MPa. The Maloney Robertson maximum cycle efficiency at 450 °C and 5.4 MPa is 0.77% higher than the maximum ethylbenzene point.

It is also noted that these results indicate a lower maximum efficiency for all of the cycles in comparison with the work in Chapter 3 at comparable turbine temperatures and pressures. The limits on the source stream temperature constrain the maximum

operating temperature of the cycle, and as a result, the quality constraint at the turbine outlet is not met. Therefore, the maximum cycle temperature and pressure remain low and the cycle efficiency is lower. The Kalina cycle has comparable maximum efficiency the pressure is at 8.3 MPa and not 4 MPa. The need for higher pressure for comparable efficiency results from the lower ammonia concentration in the working fluid stream for the second simulation.

The choice of a CAT of 10 °C is simply a design specification that can be adjusted to meet the specific requirements of the system based on the site selection. The area of the exchanger is calculated from $\dot{Q} = UA\Delta T_{LMTD}$ where U is the overall heat transfer coefficient, A is the heat exchanger area, and ΔT_{LMTD} is the log mean temperature difference. If the CAT is increased, the log mean temperature increases and the heat exchanger area decreases assuming that the overall heat transfer coefficient and heat rate are constant. Changing the CAT to match the site is part of the optimization of the heat exchanger component design that is not addresses in this thesis.

The second-law efficiency can be defined using Carnot efficiency or the rate of exergy recovered to the rate of exergy supplied to a system. For the purposes of this study, the second-law efficiency is a ratio of the amount of work produced to the maximum amount of work possible and is defined as

$$\eta_{II} = \frac{\eta_{TH}}{\eta_{TH,rev}} \tag{49}$$

The Carnot efficiency is an indication of the maximum amount of reversible work that can be extracted when a heat engine is placed between a source and a sink. Therefore, the ratio of the actual efficiency of the system to the Carnot efficiency characterizes the system performance relative to the best possible performance achievable. The second law analysis shows expected results. The ORCS are operating at high second law efficiencies as shown in Figure 45(a) and the fluid characteristics of the ORC fluids leads to better utilization of low energy source heat. The slope of the second

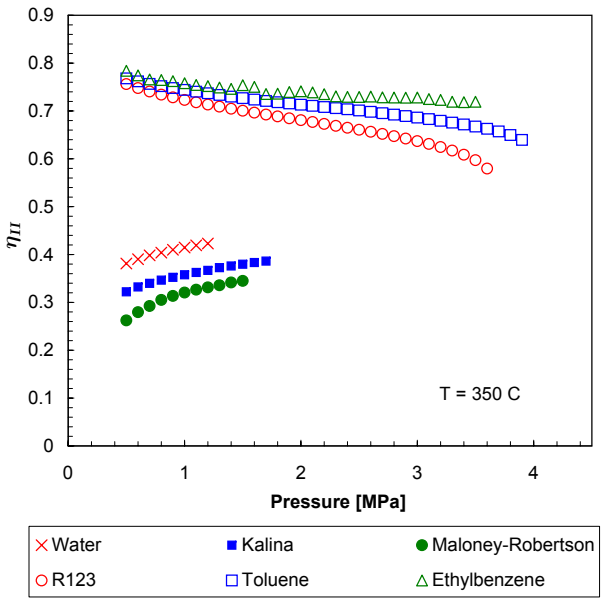

(a)

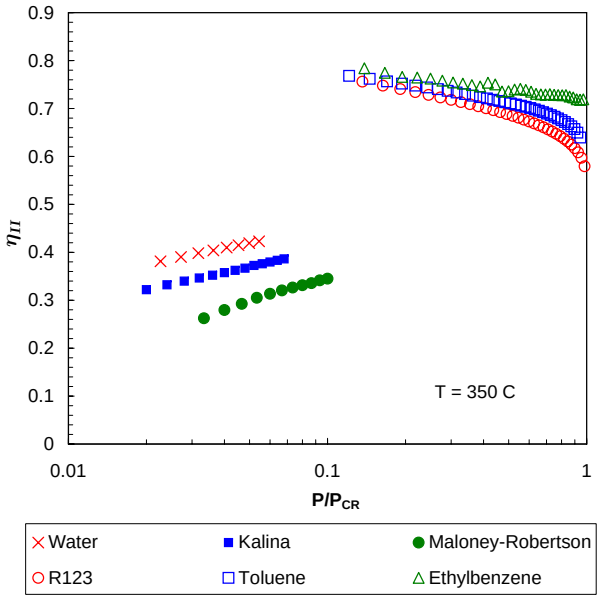

(b)

Figure 45: Second Law efficiency at 350 °C for cycles vs (a)Turbine Maximum Pressure (b) Critical Pressure Ratio

law efficiency curve for the ORCs is decreasing whereas the Rankine and ammonia-water cycles have an increasing slope. For the Rankine and ammonia-water cycles, the efficiency of the system increases faster than increase in Carnot efficiency due to the higher operating temperature resulting in an increasing second law efficiency with increasing pressure(Figure 45(b)). The ORCs are reaching the critical point where an increase in the source temperature does not contribute to a large change in enthalpy during the expansion process. The Rankine and ammonia-water cycles are at less than 10 % of their critical pressure; however, from a first law perspective, the ammonia-water cycles show promising results.

CHAPTER 5

THERMOECONOMETRIC CYCLE EVALUATION

Without sound economic justification, there would be no foundation for continued development of a meso-scale solar-thermal power system. As such, the engineering models previously described are parlayed into a thermoeconomic model.

Alternative energy technologies such as solar and wind power have not been economically feasible in the past. Table 20 shows the relative costs of power production using various energy sources according to the EIA [12]. It is important to note the cost for coal power production utilizing new emission cleaning technologies as a basis of comparison.

5.1 Cost Model

From an economics stand point, an overall evaluation of large scale power generation systems has been readily explored by Bejan, Tsatsaronis and Moran [4]. Bejan, Tsatsaronis and Moran note that exergy analysis can lead to a better understanding of where the system inefficiencies occur; therefore, economic costing based in exergy analysis offers a different perspective on the efficiency and places to improve

Table 20: Cost for Power Producing Technologies [12]

Technology	Size MW	Base Cost $(2007)/kW	Fixed OM $(2007)/kW
Integrated-Coal Gasification Combined Cycle	500	2223	38.67
Fuel Cells	10	4640	5.65
Distributed Generation -Base	2	1305	16.03
Geothermal	50	1630	164.64
Wind	50	1797	30.30
Solar Thermal	100	4693	56.78
PV	5	5750	11.638

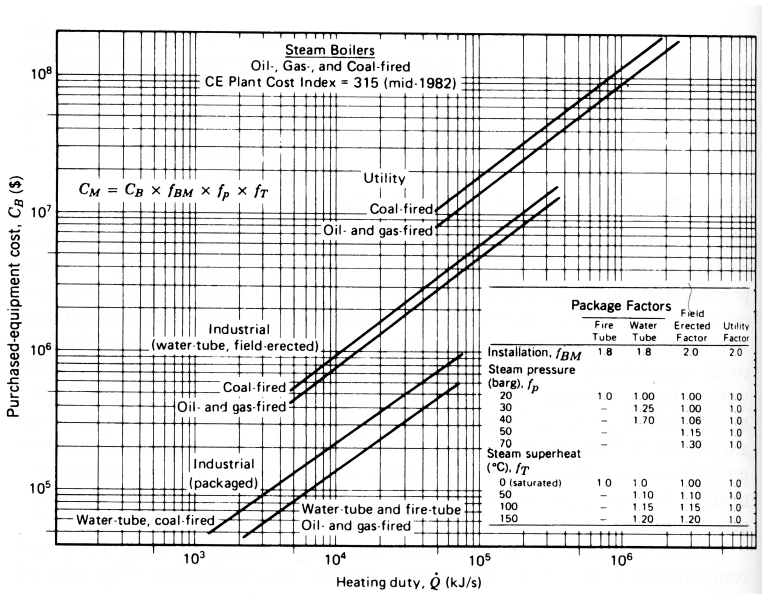

Figure 46: Conventional scale costing for power cycle components [4]

the power generation. Also, the difference between thermodynamic optimization and true system optimization based on parameters such as size, cost, and reliability is stressed.

O'Gallagher presents a simplified economic evaluation technique with emphasis on concentrating solar energy systems [55]. In general, the technique minimizes a ratio of a thermodynamic system evaluation parameter (such as first- or second- law efficiency) to cost where both the evaluation parameter and cost are defined relative to one system variable which parallels the thermoeconomic evaluation presented in this study.

The thermoeconomic models and costing data detailed by Bejan, Tsatsaronis and Moran are not valid at the meso-scale because the capital outlay for the systems will be orders of magnitude lower (Figure 46). Conventional scale parabolic trough collectors (PTCs) large scale solar thermal power systems, for example PS10, cost approximately $200 per square meter and these structures have up to 650 kW of thermal output [52, 43]. The thermal output for the large-scale systems is an order

of magnitude larger than the requirements for this system, and therefore, the costing data is not relevant at the meso-scale.

The meso-scale system cost, C, depends on the cost of the concentrators, the trackers, the turbines, the pumps, and the heat exchangers. The cost of piping, controls, and fluids are not considered. General costing data was collected on commercially available parts that closest fit the applications of this study. The following equations are an overview of the cost related to each cycle:

$$\begin{aligned} C_{Rankine} =& C_P + C_{Cond} + K_{ST}\left(C_{Boil} + C_{Super} + C_{Rec}\right) \\ &+ K_{Pre}C_{Pre} + C_T + C_{Coll} \end{aligned} \tag{50a}$$

$$C_{ORC} = C_P + C_{Cond} + K_{ST}\left(C_{Boil} + C_{Rec}\right) + K_{Pre}C_{Pre} + C_T + C_{Coll} \tag{50b}$$

$$C_{MR} = C_P + C_{Abs} + K_{ST}\left(C_{Boil} + C_{Super} + C_{rec}\right) + C_T + C_{Coll} \tag{50c}$$

$$\begin{aligned} C_{KalinaI} =& C_{P1} + C_{P2} + C_{Abs} + K_{ST}\left(C_{FPI} + C_{FPII} + C_{FPIII}\right) \\ &+ K_{ST,P_{Turb}}\left(C_{Boil} + C_{Super} + C_{Rec} + C_{IPC}\right) + K_{Pre}C_{Pre} \\ &+ C_T + C_{Coll} + C_{FT} \end{aligned} \tag{50d}$$

$$\begin{aligned} C_{KalinaII} =& C_{P1} + C_{P2} + C_{Abs} + K_{ST,P_{FT}}\left(C_{FPI}\right) \\ &+ K_{ST,P_{Turb}}\left(C_{Boil} + C_{Super} + C_{Rec} + C_{IPC}\right) + K_{Pre}C_{Pre} \\ &+ C_T + C_{Coll} + C_{FT} \end{aligned} \tag{50e}$$

A two component collector cost, C_{Coll}, is proposed that accounts for estimated costs for tracking structures and the parabolic trough collectors on a dollar per square meter basis, $C''_{Tracker}$ and $C''_{Reflector}$, respectively. The area of the collector is found using Equations 27 and 28 under the assumptions of Chapter 4 found in Table 15. The collector cost is

$$C_{Collector} = \left(C''_{Tracker} + C''_{Reflector}\right) A \tag{51}$$

Per Goswami [21], parabolic trough collectors are used to heat fluids to a temperature between 150 °C and 350 °C. Additionally, concentrated dish collectors have an operating range of 200 °C to 700 °C. This study considers parabolic trough collection for the source temperature ranges 100 °C to 350 °C and parabolic dish collectors with DSG for 350 °C to 500 °C. Equation 51 relates the two-component collector cost model. The reflector cost was estimated from a price point of $C''_{Concentrator} = \frac{\$33}{m^2}$ for a parabolic trough collector manufactured by Naugatuck Glass or a cost of $C''_{Concentrator} = \frac{\$44}{m^2}$ from the DSG project at the Plataforma Solar de Almeria [15]. WattSun PV two-axis tracking systems cost $C''_{Tracker} = \frac{\$32}{m^2}$ based off of the 18.6 square meter structure. The PV system includes the support structure and is a commercially available data point for solar tracking systems[76]. Assuming a two-axis tracking for systems with parabolic trough collection techniques offers higher collection efficiency [3] and provides a conservative estimate on the collector cost if future design work illustrates one-axis tracking is sufficient. Parabolic dish collection techniques employ two-axis tracking. The total cost of the collector per square meter is $65 for the dual-loop PTC designs and $76 for DSG parabolic dish collection.

The heat exchanger, boiler, and appropriate collector efficiency are assessed as indicated in Section 4.3. The tracker and reflector costing data on a per area cost multiplied by the area (Equation 27) defines the total collector cost.

The cost model must also account for the power cycle components. The chemical interactions between the component materials and working fluid constrain the component selection process. In general, brass can be used for water, R123, toluene, and ethylbenzene while stainless steel is necessary for the ammonia-water mixtures[22]. The shell and tube heat exchangers and the pump are commercially available in both brass and stainless steel. The other components are not available in different

Table 21: Assessed Pump Costs

Pump	Material	Flow Rate [lpm]	P_{Max} [MPa]	Cost [$]
Pump #1	Brass	18.18	8	720
Pump #2	Brass	113.652	8	3488
Pump #3	Stainless Steel	18.18	8	1899
Pump #4	Stainless Steel	113.652	8	6512

Table 22: Shell and Tube Heat Exchanger Costs from McMaster [46]

	Heat Rate [kW]	Cost (Brass) [$ (2009)]	Cost (Stainless Steel) [$]
HX #1	70.34	442.10	1062
HX #2	79.34	493.5	1272
HX #3	96.71	539.7	1485
HX #4	153.9	879.4	2020
HX #5	205.1	1071	2174
HX #6	395.6	1295	2914
HX #7	468.9	1606	3418
HX #8	703.4	2393	4540
HX #9	805.9	2957	5155

materials.

The pump costs are determined based on the material selection and the volumetric flow rate in the system. The volumetric flow rate is found through $\dot{V} = \frac{\dot{m}}{\rho}$. Table 21 indicates the pricing structure used for the pump costs per a sales associate at a Cat Pump Distributor. The pump costs is a simple step function. An intermediate step may be added but the general trend of higher flow rate equating to higher cost is accounted for sufficiently.

The heat exchange units are estimated through standard heat exchanger pricing from McMaster-Carr Supply Company [46] and Grainger Industrial Supply Company [22]. The costing parameters from McMaster Carr for brass and stainless steel shell and tube heat exchangers and from Grainger for a R-22 to water heat exchanger are listed in Tables 22 and 23, respectively. Shell-and-tube heat exchanger are used to estimate the cost of the heat exchanger processes between liquid and gas flows

Table 23: Refrigerant to Water Heat Exchanger Costs from Grainger [22]

	Heat Rate [kW]	Cost (Brass) [$ (2009)]	Cost (Stainless Steel) [$]
HX #1	1.785	304	1272
HX #2	3.517	346	1272
HX #3	8.792	498	1485
HX #4	17.58	580	2020
HX #5	26.38	720	2174
HX #6	35.17	849	2914
HX #7	59.79	1788	3418

in the boiler, superheater, and recuperator for all cycles as well as the IPC and flash preheaters used in the Kalina cycles. A R22-to-water heat exchanger is used to estimate the cost of the preheater for all cycles since it is a liquid-to-liquid heat exchange.

The heat exchangers also have a rated maximum pressure. The shell and tube heat exchangers are rated to 1 MPa and the R22-to-water heat exchanger is rated to 3 MPa. Pressure dependence in the cost model is assessed through the assumption of three cost profiles that vary with pressure. Scaling values of 10 at 4 MPa for the shell & tube heat exchanger pressure model and 3 at 4 MPa for the R22-to-water heat exchanger are assessed and used in Equation 50. Linear, polynomial and power series variations illustrated in Figures 47(a) and 47(b) are fit to the specified parameters and the mathematical equations for K values follows:

$$K_{ST,Lin} = P_{HX} \tag{52}$$

$$K_{ST,Poly} = 0.08\overline{3}P_{HX}^2 + 0.91\overline{6} \tag{53}$$

$$K_{ST,Power} = 4.316627P_{HX}^{0.5} - 3.31\overline{6} \tag{54}$$

$$K_{Pre,Lin} = P_{HX} - 2 \tag{55}$$

$$K_{Pre,Poly} = 0.071429P_{HX}^2 + 0.35743 \tag{56}$$

$$K_{Pre,Power} = 5.04876P_{HX}^{0.5} - 7.744563 \tag{57}$$

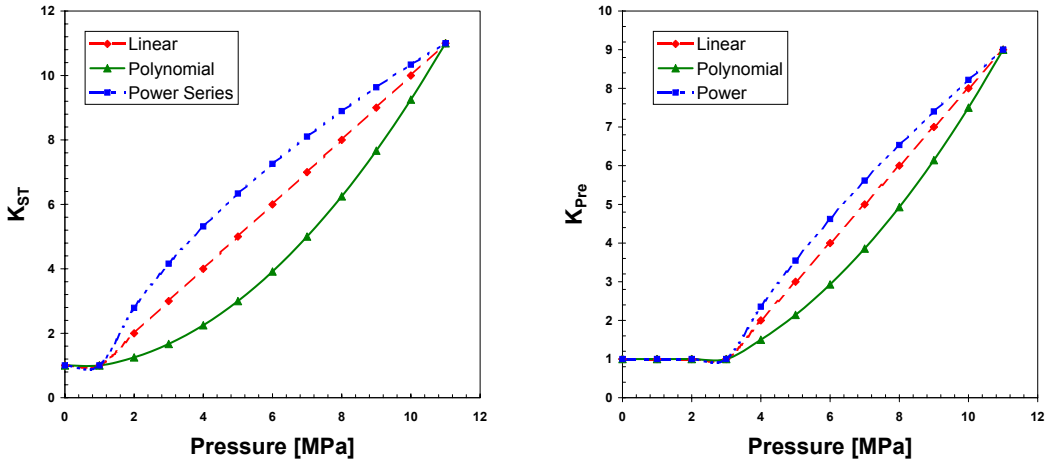

(a) (b)

Figure 47: Pressure Dependence for (a) Shell & Tube Heat Exchanger (Evaporator) (b) R22 Heat Exchanger (Recuperator)

The impulse turbine is a component that is not commercially available at power levels suitable for meso-scale applications. The turbine cost is estimated from a standard car turbo-changer. The turbine wheel is not commercially available by itself therefore the total cost of the unit is used. A Garrett GT1241 turbocharger costs around $650 and has a maximum pressure ratio of 3 to 1[19, 51]. Therefore, multiple stages are used to determine the equivalent number of turbochargers needed to achieve the expansion from the maximum cycle pressure to atmospheric pressure.

Costing data for the flash tank is not available at this time as this is a specialized small scale application. Therefore, the cost of the flash tank is assigned to be the maximum cost of any of the components that come in contact with the working fluid (ie. the collector and tracker costs are not included). Likewise, the boiler is considered to be a shell-and-tube heat exchanger since the boiler will closely resemble a counter flow heat exchanger between the working fluid and a thermal oil that is heated in the solar collector for temperatures less than 350 °C. The evaporator unit cost, including the preheater, boiler and superheater, is not defined for a DSG system so the cost approximations for these components were not altered.

5.2 Thermoeconomic Results

The cost of the cycles is presented in Table 24. The cost presented is for the pressure and material dependent model as it is the most conservative evaluation. The cost-to-efficiency ratio, Z, is used as the thermoeconomic analysis parameter and is defined as

$$Z\left(T,P\right)=\frac{C\left(T,P\right)}{\eta_{sys}\left(T,P\right)} \tag{58}$$

The thermoeconomic results for this study are presented in Figures 48, 49, and 50. Figure 48 assumes all of the cycles have components with the same materials and the ammonia-water cycles are not penalized for the increased cost of stainless steel components. Figure 49 accounts for the use of stainless steel components for the ammonia-water cycles. Figure 50 account for the power series pressure dependent cost model for the heat exchanger costs. Table 25 shows the minimum Z value for each cycle for each cost model.

5.3 Discussion

In the general assessment of cost, component pricing at the meso-scale are approximated based on commercially available components. These estimations may not always be a fair representation of the component cost at this scale. For example, the cost of heat exchangers requiring heat transfer at levels below the specified heat rates in Tables 22 and 23 are assigned the cost associated with the smallest heat exchanger commercially available. If a superheater only requires 10 kW of heat to be transferred, a cost of $442.10 is assessed for a brass shell and tube heat exchanger with a heat rating of 70.34 kW. As a result, the actual cost of the superheater, or other components assigned cost in this fashion, may be lower.

The efficiency of the Kalina I cycle is slightly higher than that of the Kalina II cycle under the CAT constraints. However, Kalina I has an additional flash preheater

Table 24: Tabulated Cycle Costs using Material and Pressure Dependent Costing Model

(a) Collector Cost

Cycle	Concentrator Type	Concentrator Efficiency [%]	$C_{Collector}$ [$]
Rankine Cycle	PTC	60	10,062
R123 ORC	PTC	60	8,792
Toluene ORC	PTC	60	9,411
Ethylbenzene ORC	PTC	60	8,523
Maloney-Robertson Cycle	PTC	60	11,130
Kalina Cycle	PTC	60	10,952

(b) Conversion Plant Cost

Cycle	Coversion Efficiency [%]	C_{Plant} [$]	Temperature [°C]	Pressure [MPa]
Rankine Cycle	16.289	3,833	350	1.2
R123 ORC	18.638	6,460	150	1.7
Toluene ORC	17.412	4,059	250	1.2
Ethylbenzene ORC	19.23	4,827	300	1.5
Maloney-Robertson Cycle	14.49	7,484	300	1
Kalina Cycle	14.49	13,806	300	1

(c) Total Plant Cost

Cycle	Overal Efficiency [%]	C_{Total} [$]	Cost per kW $[\frac{\$}{kW}]$
Rankine Cycle	9.772	13,894	1111.52
R123 ORC	11.18	15,252	1220.16
Toluene ORC	10.45	13,470	1077.60
Ethylbenzene ORC	11.54	13,350	1068
Maloney-Robertson Cycle	8.693	18,795	1503.6
Kalina Cycle	8.798	24,758	1980.64

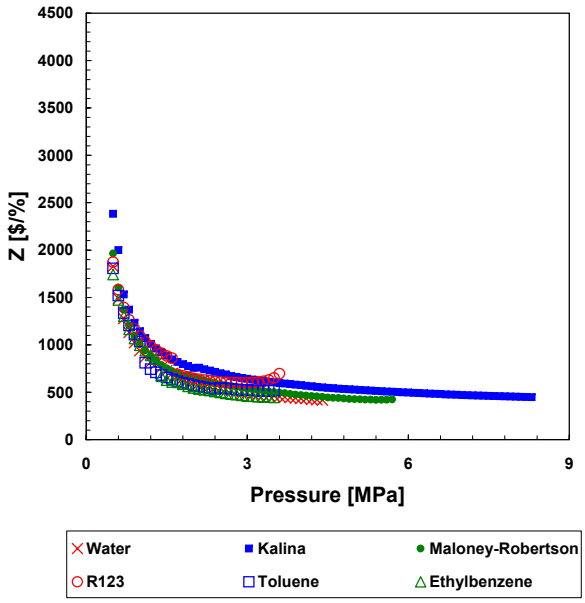

(a)

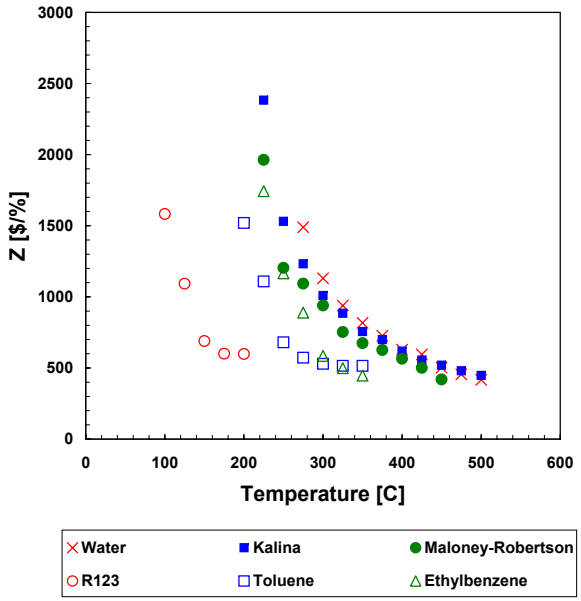

(b)

Figure 48: Cost assuming no Material Cost Penalty: (a) Minimum Z vs. Turbine Pressure (b) Minimum Z vs. Maximum Source Temperature

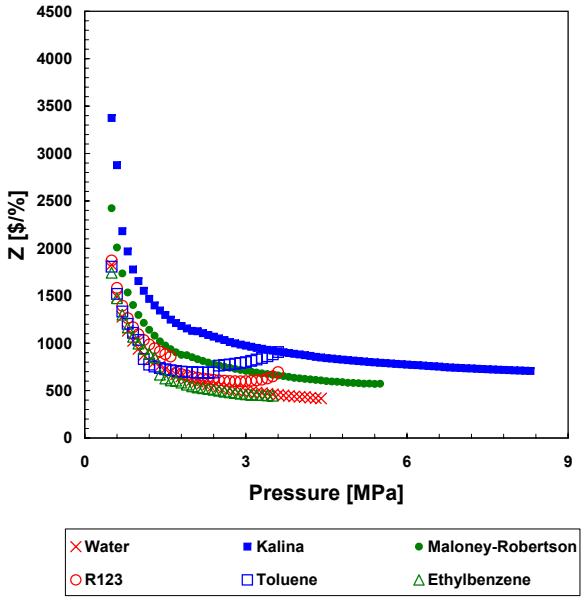

(a)

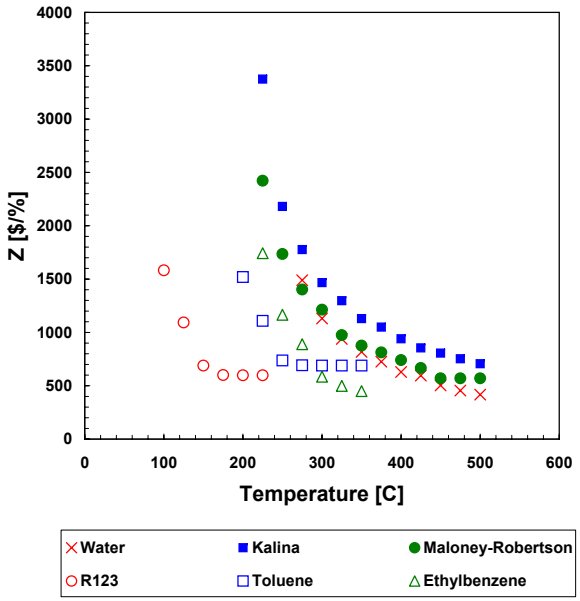

(b)

Figure 49: Cost assuming Material Cost Penalty: (a) Minimum Z vs. Turbine Pressure (b) Minimum Z vs. Maximum Source Temperature

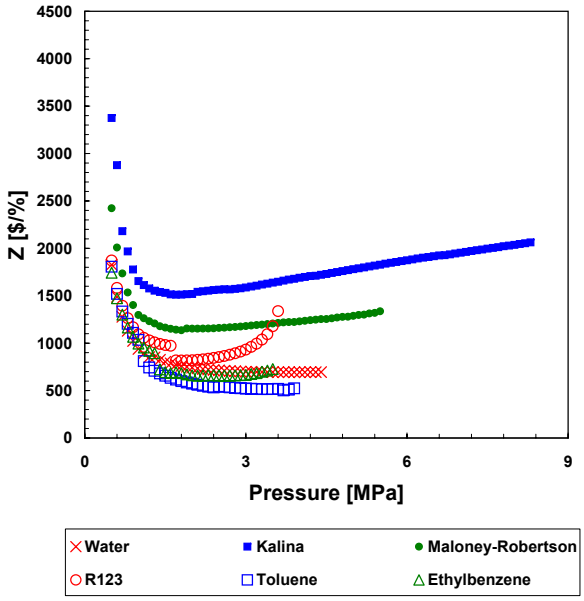

(a)

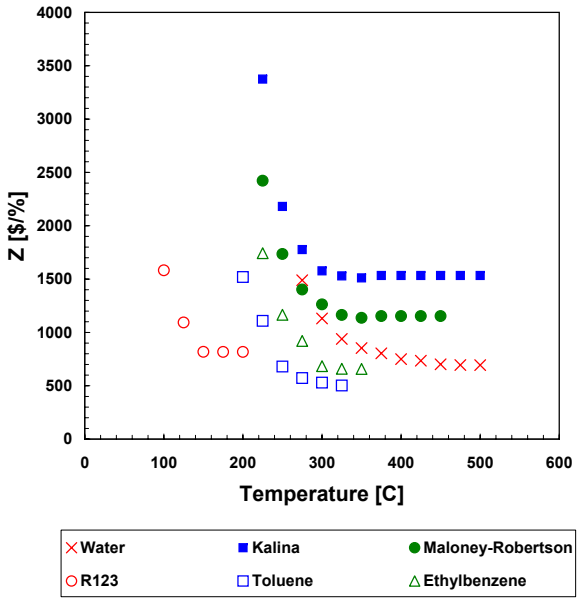

(b)

Figure 50: Cost assuming Material and Pressure Cost Penalties: (a) Minimum Z vs. Turbine Pressure (b) Minimum Z vs. Maximum Source Temperature

Table 25: Tabulated Minimum Cost-to-Efficiency Ratio, Z , over the Design Space

(a) Material and Pressure Independent Cost Model

Cycle	Z $[\frac{\$}{\%}]$	Pressure [MPa]	Temperature [°C]
Rankine Cycle	416.97	4.4	500
R123 ORC	598.44	2.9	200
Toluene ORC	515.44	3.4	325
Ethylbenzene ORC	446.45	3.5	350
Maloney-Robertson Cycle	419.52	5.6	450
Kalina Cycle	447.57	8.3	500

(b) Material Dependent and Pressure Independent Cost Model

Cycle	Z $[\frac{\$}{\%}]$	Pressure [MPa]	Temperature [°C]
Rankine Cycle	416.97	4.4	500
R123 ORC	598.44	2.9	200
Toluene ORC	689.04	2.3	325
Ethylbenzene ORC	449.95	3.4	350
Maloney-Robertson Cycle	570.17	5.4	450
Kalina Cycle	706.65	8.3	500

(c) Material and Pressure Dependent Cost Model

Cycle	Z $[\frac{\$}{\%}]$	Pressure [MPa]	Temperature [°C]
Rankine Cycle	693.33	4	500
R123 ORC	817.26	1.8	200
Toluene ORC	502.41	3.7	325
Ethylbenzene ORC	657.7	2.6	350
Maloney-Robertson Cycle	1153.2	2.1	425
Kalina Cycle	1510.71	1.7	350

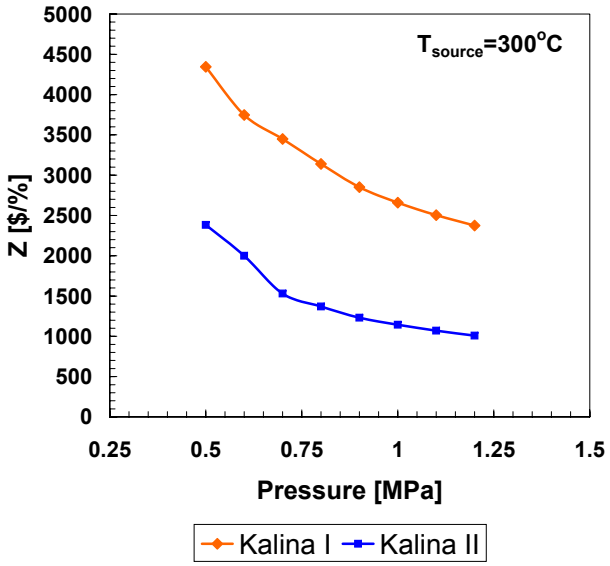

Figure 51: Comparison of Cost-to-Efficiency Ratio vs Turbine Pressure for Kalina I vs Kalina II

and an additional heat exchange stage in the IPC. As a result, the cost of the Kalina II cycle is than Kalina I. The increased cost on the Kalina I cycle overpowers the gain in efficiency; as a result the Kalina II has a 45% to 57% lower cost-to-efficiency ratio at a source temperature of 300 °C (Figure 51).

The cost per kW for this solar-thermal system ranges from $1,068 per kW to $1,980 per kW (Figure 24(c)). Operation and maintenance costs, control costs, and land-use costs are not included in this cost model. With the inclusion of those expenses, this system cost will be cost comparable with other power production technologies as listed in Table 20.

Additionally, the cost of components plays a large role in the cost-to-efficiency ratio. This effect is apparent with the R123 ORCs in any of the cost-to-efficiency ratio plots (Figures 48 to 50). There is a jump in the R123 cost-to-efficiency ratio at 1.6 MPa. This jump is a result of changing pump cost due to a lower flow rate. The five fold decrease in pump cost is amplified when the cost is divided by the efficiency. This cost step is also apparent in the toluene ORC at 1.2 MPa and the ethylbenzene

ORC at 1.3 MPa.

Figure 48 presents data from simulations that do not penalize the ammonia-water cycles for high pressures or materials. When this is the case, the ammonia-water cycles are competitive with the ORCs on a cost-to-efficiency basis and Z always decreases with increasing temperature. When cost is not a function of pressure but the material considerations are represented (Figure 49), the cost-to-efficiency ratio of the ammonia-water cycles increases significantly. From 100 °C to 350 °C, the ORCs have the lowest cost-to-efficiency ratio and increasing the temperature beyond 350 °C is not advantageous. When parabolic dish collection is used (source temperatures reach 350 °C to 500 °C), the Maloney-Robertson cycle has a higher cost effectiveness than the Kalina and Rankine cycles until a temperature of 425 °C. Over the range of 425 °C to 500 °C, the Rankine cycle outperforms the Kalina cycle. Additionally, the ORCs and Rankine cycle outperform the ammonia-water cycles until 4.5 MPa when the ORCs have exceeder their critical points and the Rankine cycle cannot extract enough heat from the source to meet the turbine exhaust quality requirement.

The addition of the pressure dependent cost model dramatically impacts the selection guidelines for the preferred operating cycle in both the temperature based and pressure based design spaces. A worse case scenario is assessed through the utilization of the power series pressure dependent cost representation. When the pressure influences are accounted for in cost, the power series always has a higher cost-to-efficiency value (Figure 52).

The pressure dependent cost model illustrates that R123 is still the preferred cycle at temperatures ranging from 100 to 200 °C and the ORCs are favorable at temperatures below 300 °C. Conversely, the Rankine cycle now has a lower cost-to-efficiency ratio at temperatures above 300 °C compared to the ammonia-water cycles. The ammonia-water cycles are heavily penalized for the high cycle pressures necessary. When the pressure based design is considered, the Rankine cycle and ORCs always

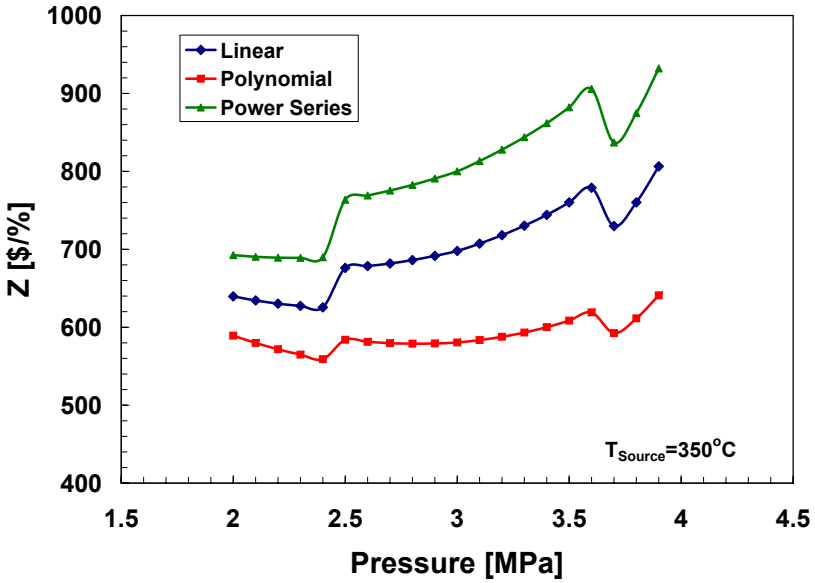

Figure 52: Z vs Turbine Pressure for Three Heat Exchanger Pressure Dependent Cost Models (Equations 52 to 57)

have a lower cost-to-efficiency ratio under to pressure dependent cost constraint. The increase in efficiency seen in the ammonia-water cycles due to the removal of the pressure constraint, as seen in the Chapter 4 results, is not substantial enough to justify the increased component costs. At a pressure between 1 MPa and 3.2 MPa, the toluene and ethylbenzene ORCs have the highest cost effectiveness. At pressures beyond 3.2 MPa, the Rankine cycle has the minimum thermoeconomic metric.

The goal of any project is to have the minimum cost with the maximum efficiency. For the thermodynamic cycles of interest, an increase in the turbine pressure and the source temperature results in an increase in the cost and efficiency. Therefore, the minimal cost and maximum efficiency have an inverse relationship. The Rankine cycle has the highest efficiency at a source temperature of 500 °C and a turbine pressure of 4.4 MPa but a minimum cost at a source temperature of 350 °C and a turbine pressure of 1.2 MPa. The most cost-effective operating point for the Rankine cycle is at 500 °C and a pressure of 4.0 MPa. All of the cycles follow a similar trend where the minimum

cost-to-efficiency ratio is not at the source temperature-turbine pressure combination that corresponds to either the maximum efficiency or minimum cost. Therefore, the cost-to-efficiency ratio provides guidelines for the cycle operating turbine pressure and source temperature that account for a balance between the most efficient cycle and the lowest capital cost.

CHAPTER 6

CONCLUSIONS AND FUTURE WORK

This Chapter will present conclusions from the study that have been drawn based on the foregoing thermodynamic and thermodynamic evaluation of the performance and relative performance of the cycles of interest at meso-scale solar thermal power generation systems. In addition, this chapter will include a brief discussion on potential avenues for continuation of this study.

6.1 Conclusions

The thermodynamic design space for a 12.5 kW distributed solar thermal power generation system has been characterized in this study through a full-domain parametric evaluation of six selected power cycles; three organic Rankine cycles considering R123, and a standard Rankine cycle as a baseline.

The main constraints imposed on the cycles limited the maximum source temperature to 500°C, limited the turbine exhaust quality to single-phase flow, and did not allow for over expansion of the working fluid below atmospheric pressure. In addition to these design-point operating constraints, a set of standard component efficiencies was assumed based on established guidelines. On the basis of the results of the parametric evaluation of the six cycles considered, the study draws the following conclusions:

1. Guidelines for temperature based and pressure based collection sites should be based on a model that incorporates CAT constraints with the source and sink streams

2. An R123 ORC cycle implementation is the most cost effective power cycle for solar thermal systems with maximum cycle temperatures in the range of 100°C to 240°C, providing the highest efficiency and minimum required collection area.
3. For temperatures greater than 240 °C and less than 350 °C, the toluene and ethylbenzene ORCs outperform the other cycles on a first-law bases.
4. The Kalina cycle has the highest first-law efficiency over the source temperature operating range of 375 °C to 500 °C. However, when considering cycle cost and overall feasibility, including thermodynamic and economic performance, the Kalina cycle has poor performance on a cost-to-efficiency basis.
5. From a thermoeconomics standpoint, R123 ORC has the lowest cost effectiveness at source temperatures of 100 °C to 280 °C.
6. For source operating temperatures between 240 °C and 375 °C, the toluene and ethylbenzene ORCs have the best performance from a cost-to-efficiency ratio regardless of the material and pressure penalties assessed.
7. Under the costing model that penalizes for pressure and material, the standard Rankine cycle has a competitive cost-to-efficiency ratio at maximum turbine pressures below 4.4 MPa and the lowest cost-to-efficiency ratio for source temperatures of 350 °C to 500 °C

In addition to the specific conclusions drawn above, further contributions from this study include:

1. A comprehensive literature review of Kalina power cycles, concluding that 14 possible implementations of the cycle have been studied and reported on.
2. The identification and establishment of the Maloney-Robertson binary-fluid power cycle as an alternative for meso-scale solar-thermal power generation
3. A new methodology for optimization of the Maloney-Robertson boiler temperature for maximum first-law cycle efficiency

6.2 Contributions from Study

The following contributory, peer-review conference and journal publications have been generated from this work:

1. "Thermodynamic Design and Comparative Analysis of Rankine, ORC, and Kalina Cycles for Low-Cost, Meso-Scale Power Generation Systems" published in the conference proceedings of and presented at the ASME Energy Sustainability 2008 in Jacksonville, Florida on August 11, 2008
2. "Thermodynamic Design and Comparative Analysis of Rankine, ORC, and Kalina Cycles for Low-Cost, Meso-Scale Power Generation Systems" submitted for publication in the *ASME Journal of Energy Resources Technologies* Special Publication tentatively titled "Sustainable Sources of Energy"
3. "Analysis of Solar-Thermal Power Cycles For Distributed Power Generation" to be presented at the ASME Energy Sustainability Conference 2009 in San Francisco, California on July 21, 2009

6.3 Future Work

Upon the completion of this study, the author acknowledges areas for innovation in relation to meso-scale solar-thermal power generation. Implementation of transient power cycle modeling and system control optimization will further the temperature- and pressure based cycle design space by capturing the fluctuations of the heat source. Recent work in this area was completed by Lu *et al.* [42, 41], Colonna [10] and van Putten [73]. Additional research and development relating to meso-scale solar-thermal power components will lead to a more accurate representation of true cycle cost. Components of particular interest are the solar reflectors, the solar tracker, the impulse turbine, and the boiler. These components have a large impact on system cost as well as system performance.

APPENDIX A

EFFECTIVENESS MODELING CODES

The cycle simulations in Chapter 3 follow the effectiveness modeling codes using the EES programming language. The Rankine, R123, and toluene ORCs all come from one set of code and simply require the user to change the fluid name. The ORC code is currently set up for water. Replacing 'water' in all of the code line with either 'R123' or 'toluene' will change the fluid and use the EES function calls for these fluids. The ethylbenzene ORC code uses the EES Peng-Robinson Builtin function but also has additional coding to determine the enthalpy and entropy at a state. The Maloney-Robinson and Kalina codes access the EES ammonia-water fluid call 'NH3H2O'.

A.1 Rankine, R123 ORC, and Toluene ORC Code

```
Procedure HX_eff(epsilon, T_h_in,T_c_in,m_c,m_h,
P_c,P_h:T_C_out,h_c_out,T_h_out,h_h_out)
N=0
K=1000

Fluid$='water'

IF T_c_in>T_h_in THEN
T_c_out=T_c_in
T_h_out=T_h_in
h_c_in=enthalpy(water,T=T_c_in,P=P_c)
h_h_in=enthalpy(water,T=T_h_in,P=P_h)
h_h_out=h_h_in
h_c_out=h_c_in
GOTO 100
ENDIF

error=1
T_c_out=T_c_in
T_C_sat=T_sat(Fluid$,P=P_c)
T_h_sat=T_sat(Fluid$,P=P_h)

REPEAT

IF N<K THEN
N=N+1

IF error>0.3 THEN
T_c_out=T_c_out+1[K]
ELSE
```

```
IF (error>.01) AND (error<0.3) AND (T_c_out<T_C_sat) THEN
T_c_out=T_c_out+.1[K]
ENDIF
ENDIF

IF (T_c_out>=T_c_sat) THEN
GOTO 11
ENDIF

h_c_out=enthalpy(Fluid$,T=T_c_out,P=P_c)
T_c_avg=(T_c_in+T_c_out)/2
q_c=m_c*(h_c_out-enthalpy(Fluid$,T=T_c_in,P=P_c))
C_c=m_c*Cp(Fluid$,T=T_c_avg,P=P_c)

h_h_out=((enthalpy(Fluid$,T=T_h_in,P=P_h))*m_h-q_c)/m_h
T_h_out=Temperature(Fluid$,h=h_h_out,P=P_h)
T_h_avg=(T_h_out+T_h_in)/2
C_h=m_h*(Cp(Fluid$,T=T_h_avg,P=P_h))
q_max=IF(C_c,C_h,C_c,C_C,C_h)*(T_h_in-T_c_in)
epsilon_calc=q_c/q_max

Error=(epsilon-epsilon_calc)

UNTIL(error<0.01)
GOTO 100
ELSE
T_c_out="T_c_out"111
GOTO 100
ENDIF

//This loop is for two phase flow out in the recuperator
11: x_c_out=0.0
T_c_out=T_sat(Fluid$,P=P_c)
REPEAT
IF N<K THEN
N=N+1

IF Error>0.005 THEN
x_c_out=x_c_out+.01
ENDIF

h_c_out=enthalpy(Fluid$,x=x_c_out,T=T_c_out)
T_c_avg=(T_c_in+T_c_out)/2
q_c=m_c*(h_c_out-enthalpy(Fluid$,T=T_c_in,P=P_c))
C_c=m_c*Cp(Fluid$,T=T_c_avg,P=P_c)

h_h_out=((enthalpy(Fluid$,T=T_h_in,P=P_h))
*m_h-q_c)/m_h
T_h_out=Temperature(Fluid$,h=h_h_out,P=P_h)
T_h_avg=(T_h_out+T_h_in)/2
C_h=m_h*(Cp(Fluid$,T=T_h_avg,P=P_h))
q_max=IF(C_c,C_h,C_c,C_C,C_h)*(T_h_in-T_c_in)
epsilon_calc=q_c/q_max
Error=(epsilon-epsilon_calc)

UNTIL (error<0.01)

ELSE
T_c_out=111
ENDIF

100: dummy=1

END

Procedure q_coll(P,h_pre_out,h_boil_out,h_super_out:
 q_pre,q_boil,q_super)
```

```
h_g=enthalpy(water,P=P,x=0)
"h_f=enthalpy(water,P=P,x=1)" "Note: state 4 is defined
 by h_f"
IF (h_g>h_pre_out) THEN
q_pre=h_g-h_pre_out
q_boil=h_boil_out-h_g
ELSE
q_pre=0
q_boil=h_boil_out-h_pre_out
ENDIF
q_super=h_super_out-h_boil_out
END
"Rankine Cycle with Preheat and Superheat
Variables that must be defined:
1.Turbine Inlet Pressure
2. Turbine Inlet Temperature
3. Turbine Work out OR System Mass Flow rate
4. Turbine outlet Pressure
5. Pump Efficiency
6. Turbine Efficiency
7. Medium Temperature and Pressure for exergy Analysis
 and start up conditions
8. Quality of the steam leaving the boiler"
P[5]=1200 [kPa]
T[5]=(400+273.15) [K]
W_out=14.7 [kW]
P[6]= 100 [kPa]
P[5]=P[4]
P[5]=P[3]
P[5]=P[2]
P[1]=P[6]
P[7]=P[6]
eta_p=.7
eta_t=.8
eta_HX=.8
eta_B=.85
P_med=101.3 [kPa]
T_med=(22.5+273.15) [K]
h_med=enthalpy(air,T=T_med)
s_med=entropy(air,T=T_med,P=P_med)
b_0=h_med-T_med*s_med
x[4]=1
"State 5:Superheat Exit,Turbine Inlet"
h[5]=enthalpy(water,P=P[5],T=T[5])
s[5]=entropy(water,P=P[5],T=T[5])
ex[5]=(h[5]-T_med*s[5])-b_0
rho[5]=density(water,T=T[5],P=P[5])
x[5]=quality(water,T=T[5],P=P[5])
"State 6:Turbine outlet,Preheater hot stream inlet"
s_6s=s[5]
T_6s=Temperature(water,P=P[6],s=s_6s)
h_6s=Enthalpy(water,T=T_6s,P=P[6])
w_t_s=h[5]-h_6s
w_t_act=w_t_s*eta_t
h[6]=h[5]-w_t_act
T[6]=Temperature(water, h=h[6],P=P[6])
s[6]=Entropy(water,T=T[6],P=P[6])
ex[6]=(h[6]-T_med*s[6])-b_0
```

```
rho[6]=density(water,T=T[6],P=P[6])
x[6]=quality(water,T=T[6],P=P[6])
"W_Turbine=m_dot*w_t_act"

"State 1: Condenser outlet, Pump inlet"
T[1]=T_sat(water,P=P[1])
h[1]=enthalpy(water,T=T[1],P=P[1])
s[1]=entropy(water,T=T[1],P=P[1])
ex[1]=(h[1]-T_med*s[1])-b_0
rho[1]=density(water,P=P[1],T=T[1])
x[1]=quality(water,T=T[1],P=P[1])

"State 2: Pump Exit and Preheater Inlet"
s_2s=s[1]
T_2s=Temperature(water,s=s_2s,P=P[2])
h_2s=Enthalpy(water,T=T_2s,P=P[2])
w_p_s=h_2s-h[1]
w_p_act=w_p_s/eta_p
h[2]=w_p_act+h[1]
T[2]=Temperature(water, h=h[2],P=P[2])
s[2]=Entropy(water,T=T[2],P=P[2])
ex[2]=(h[2]-T_med*s[2])-b_0
rho[2]=density(water,T=T[2],P=P[2])
x[2]=quality(water,T=T[2],P=P[2])
"W_Pump=m_dot*w_p_act"

"Define the mass flow rate and work terms"
w_net=w_t_act-w_p_act
m_dot=W_out/w_net

"State 4: Boiler Exit, Superheater Inlet"
T_sat=T_sat(Water,P=P[4])
T[4]=T_sat
h[4]=enthalpy(water,P=P[4],x=x[4])
s[4]=entropy(water,P=P[4],x=x[4])
ex[4]=(h[4]-T_med*s[4])-b_0
rho[4]=density(water,P=P[4],h=h[4])

"States 3 and 7"
Call HX_eff(eta_HX, T[6],T[2],m_dot,m_dot,P[2],P[6]:
T[3],h[3],T[7],h[7])

"h[3]=enthalpy(water,T=T[3],P=P[3])"
s[3]=entropy(water,T=T[3],h=h[3])
ex[3]=(h[3]-T_med*s[3])-b_0
rho[3]=density(water,P=P[3],h=h[3])
x[3]=quality(water,P=P[3],h=h[3])

"h[7]=enthalpy(water,T=T[7],P=P[7])"
s[7]=entropy(water,T=T[3],h=h[3])
ex[7]=(h[7]-T_med*s[7])-b_0
rho[7]=density(water,P=P[7],T=T[7])
x[7]=quality(water,P=P[7],T=T[7])

q_pre_c=h[3]-h[2]
Q_pre_cold=m_dot*q_pre_c
h_3_sat=enthalpy(water,P=P[3], x=0)

Call q_coll(P[3],h[3],h[4],h[5]:q_pre,q_boil,q_super)

Q_dot_Pre=m_dot*q_pre
Q_dot_Boiler=m_dot*q_boil
Q_dot_Super=m_dot*q_super
```

```
Q_dot_Solar=Q_dot_super/eta_HX+Q_dot_boiler/eta_B
+Q_dot_pre/eta_HX
{q_out_con=h[7]-h[1]
Q_BC=m_dot*q_out_con}
eta_sys=w_net/(q_pre+q_boil+q_super)

Check=(h[4]-h[3])-q_pre
Check_2=(h[6]-h[3])-q_pre-q_boil-q_super

eta_carnot=(1-T[1]/T[5])

eta_check=w_net/(h[6]-h[3])
Quality=IF(x[6],1,1111,1,0)
STOP=IF(T[3],111,0,111,0)
```

A.2 Ethylbenzene ORC Code

```
Procedure HXtrial(epsilon, h_h_in,h_c_in,T_h_in,T_c_in,
m_c,m_h,P_c,P_h,s_c_in,s_h_in,h_c_sat,h_h_sat:
T_C_out,h_c_out, s_c_out,T_h_out,h_h_out,s_h_out,chi_c)

T_c_sat=Interpolate('T sat','P','T',P=P_c)
h_g=(h_c_sat-(interpolate('h fg','T','h fg',T=T_c_sat)))
"h_g is the saturation point on the cold side x=0)"
T_h_sat=Interpolate('T sat','P','T',P=P_h)
h_f=(h_h_sat+(interpolate('h fg','T','h fg',T=T_h_sat)))

//c_c_est=m_c*(Interpolate('Cp kJ/kg-k', 'T','Cp',T=T_c_in))

//Assume cold stream has minimum heat capacity
//Find the max heat
//Pick T_c_out
T_c_out=T_c_in+1[K]
10: T_avg=(T_c_out+T_c_in)/2
c_c_est=Interpolate('Cp kJ/kg-k', 'T','Cp',T=T_avg)
v_c_in=1/(Interpolate('density','T','rho',T=T_c_in))
v_c_out=1/(Interpolate('density','T','rho',T=T_c_out))
h_c_out_calc=h_c_in+c_c_est*(T_c_out-T_c_in)+
p_c*(v_c_out-v_c_in)
q_max=m_c*c_c_est*(T_h_in-T_c_in)
q_act=q_max*epsilon
h_c_out=h_c_in+q_act/m_c

error=abs(h_c_out-h_c_out_calc)

IF Error>1 THEN
T_c_out=T_c_out+0.5[K]
GOTO 10
ENDIF

IF (h_g<h_c_out) AND (h_c_sat>h_c_out) THEN
T_c_out="T_c_sat"111 "T_c_out"  "Put in more coding if
needed!"
ELSE
IF (h_g>h_c_out) AND (h_c_sat>h_c_out) THEN
T_c_out=T_c_out
ELSE
T_c_out=111
ENDIF
ENDIF

C_c=m_c*c_c_est
```

```
h_h_out=h_h_in-q_act/m_h

T_h_out=T_h_in
11: T_h_avg=(T_h_out+T_h_in)/2
c_h_est=Interpolate('CpIG kJ/kg-k', 'T','Cp',T=T_h_avg)
v_h_in=1/(Interpolate('density','T','rho',T=T_h_in))
v_h_out=1/(Interpolate('density','T','rho',T=T_h_out))
h_h_out_calc=h_h_in+c_h_est*(T_h_out-T_h_in)+
p_h*(v_h_out-v_h_in)

error=abs(h_h_out_calc-h_h_out)

IF Error>1 THEN
T_h_out=T_h_out-0.5[K]
GOTO 11
ENDIF

IF (h_f>h_h_out) AND (h_h_sat<h_h_out) THEN
T_h_out=T_h_sat"111" "T_c_out"  "Put in more coding
 if needed!"
ELSE
IF (h_f<h_h_out) AND (h_h_sat<h_h_out) THEN
T_h_out=T_h_out
ELSE
T_h_out=111
ENDIF
ENDIF

C_h=m_h*c_h_est

IF c_c<c_h THEN
GOTO 99
ELSE

T_h_out=T_h_in
100: T_avg=(T_h_out+T_h_in)/2
c_h_est=Interpolate('CpIG kJ/kg-k', 'T','Cp',T=T_avg)
v_h_in=1/(Interpolate('density','T','rho',T=T_h_in))
v_h_out=1/(Interpolate('density','T','rho',T=T_h_out))
h_h_out_calc=h_h_in+c_h_est*(T_h_out-T_h_in)
+p_h*(v_h_out-v_h_in)
q_max=m_h*c_h_est*(T_h_in-T_c_in)
q_act=q_max*epsilon
h_h_out=h_h_in-q_act/m_h

error=abs(h_h_out-h_h_out_calc)

IF Error>1 THEN
T_h_out=T_h_out-0.5[K]
GOTO 100
ENDIF

IF (h_f>h_h_out) AND (h_h_sat<h_h_out) THEN
T_h_out=T_h_sat"11111" "T_c_out"  "Put in more coding
if needed!"
ELSE
IF (h_f<h_h_out) AND (h_h_sat<h_h_out) THEN
T_h_out=T_h_out
ELSE
T_h_out=111
ENDIF
ENDIF

C_h=m_h*c_h_est

h_c_out=h_c_in+q_act/m_c

T_c_out=T_c_in
101: T_avg=(T_c_out+T_c_in)/2
```

```
c_c_est=Interpolate('Cp kJ/kg-k', 'T','Cp',T=T_avg)
v_c_in=1/(Interpolate('density','T','rho',T=T_c_in))
v_c_out=1/(Interpolate('density','T','rho',T=T_c_out))
h_c_out_calc=h_c_in+c_c_est*(T_c_out-T_c_in)
+P_c*(v_c_out-v_c_in)

error=abs(h_c_out_calc-h_c_out)

IF Error>1 THEN
T_c_out=T_c_out+0.5[K]
GOTO 101
ENDIF

IF (h_g<h_c_out) AND (h_c_sat>h_c_out) THEN
T_c_out=T_c_sat
ELSE
IF (h_g>h_c_out) AND (h_c_sat>h_c_out) THEN
T_c_out=T_c_out
ELSE
T_c_out=111
ENDIF
ENDIF

C_c=m_c*c_c_est

ENDIF


99:
T_c_avgs=(T_c_in+T_c_out)/2
C_c_s=Interpolate('Cp kJ/kg-K', 'T', 'Cp',T=T_c_avgs)
T_h_avgs=(T_h_in+T_h_out)/2
C_h_s=Interpolate('CpIG kJ/kg-K', 'T','Cp',T=T_h_avgs)

h_fg_c=Interpolate('h fg','T','h fg',T=T_c_sat)
Chi_c_cal=(h_c_out-h_g)/h_fg_c
Chi_c=If(Chi_c_cal,0,0,1,1)*Chi_c_cal
s_fg_c=Interpolate('s fg','T','s fg',T=T_c_sat)

s_c_out=C_c_s*ln(T_c_out/T_c_in)+s_c_in+chi_c*s_fg_c

h_fg_h=Interpolate('h fg','T','h fg',T=T_h_sat)
Chi_h_cal=(h_h_out-h_h_sat)/h_fg_h
Chi_h=If(Chi_h_cal,1,1,1,0)*Chi_h_cal
s_fg_h=Interpolate('s fg','T','s fg',T=T_h_sat)
s_h_out=C_h_s*ln(T_h_out/T_h_in)+s_h_in+chi_h*s_fg_h

200: dummy=0

END

"Heat Exchanger Check examines the direction of heat
exchange in the recuperator"
Function HXCheck(q_pre)
If q_pre<0 then
A:=1111
else
A:=0
endif

HXCheck:=A

end

"Temperature Iteration for T6 ideal based on entropy"
Function Ideal(T, T_cr, T[5], P[6], P[5], P_cr, omega,
R_u, M, C_5, s[5], s_5_dep)

N:=0
```

```
K=500

REPEAT

IF N<K THEN
C_6_ideal:=Interpolate('CpIG kJ/kg-K', 'T', 'Cp', T=T)
"{Lookup table} DIPPR DATA, specific heat for liquid
in kJ/kg-K"
C_6_Mideal:=Interpolate('CpIG kJ/kmol-K', 'T', 'Cp', T=T)
"{Lookup table} DIPPR DATA, specific heat for liquid
in kJ/kmol-K"
T_r:=T /T_cr
P_r:=P[6]/P_cr
CALL AB_PR(T_r, P_r, omega: A, B)
Z:=Z_G_PR(A,B)

s_IG:=((C_6_Mideal+C_5)/2)*ln(T/T[5])-R_u*ln(P[6]/P[5])
s_dep:=S_DEP_PR(T_r,omega,Z,B)*R_u
s_ideal:=s[5]+(s_IG-(s_dep-s_5_dep))/M

e:=s[5]-s_ideal
S:=e*e
D:=0.00075^2

IF (e>0.15[kJ/kg-K]) THEN
T:=T+10 [K]
N:=N+1
ELSE
     IF (e<=0.15[kJ/kg-K]) AND (e>0.075[kJ/kg-K]) THEN
     T:=T+1 [K]
     N:=N+1
     ELSE
          IF (0.075 [kJ/kg-K]>=e) AND (e>0.0005[kJ/kg-K]) THEN
          T:=T+0.1 [K]
          N:=N+1
          ELSE
               IF (e<-0.15[kJ/kg-K]) THEN
               T:=T-10 [K]
               N:=N+1
               ELSE
                    IF (-0.15[kJ/kg-K]<=e) AND (e<-0.075
                     [kJ/kg-K]) THEN
                    T:=T-1 [K]
                    N:=N+1
                    ELSE
                         IF (-0.075[kJ/kg-K]<=e) AND
                          (e<-0.0005[kJ/kg-K]) THEN
                         T:=T-0.1 [K]
                         N:=N+1
                         ENDIF
                    ENDIF
               ENDIF
          ENDIF
     ENDIF
ENDIF
UNTIL (S<D)    "(e*e)<(0.0020*0.0020)"

ELSE
T=T
ENDIF

Ideal=T

END

"Temperature Iteration for T6 actual based on enthalpy"
Function Temp(T, T_cr, T[5], P[6], P[5], P_cr, omega,
R_u, M, C[5], h[6], h[5], h_5_dep)
```

```
N:=0
K=300

REPEAT

If N<K THEN
C[6]:=Interpolate('CpIG kJ/kg-K', 'T', 'Cp', T=T)
"{Lookup table} DIPPR DATA, specific heat for
liquid in kJ/kg-K"  "This is an approximation
that can be iterated on"
C_6:=Interpolate('CpIG kJ/kmol-K', 'T', 'Cp', T=T)
"{Lookup table} DIPPR DATA, specific heat for
 liquid in kJ/kmol-K"

P_r:=P[6]/P_cr
T_r:=T/T_cr
CALL AB_PR(T_r, P_r, omega: A, B)
Z:=Z_G_PR(A,B)

h_IG:=((C[6]+C[5])/2)*(T-T[5])
h_dep:=H_DEP_PR(T_r, omega, Z, B)*R_u*T_cr/M
h_check:=h[5]+(h_IG-(h_dep-h_5_dep))
e:=h[6]-h_check
S:= e^2
D:=2

IF (e>50[kJ/kg]) THEN
T:=T+20 [K]
N:=N+1
ELSE
     IF (50[kJ/kg]>=e) AND (e>25[kJ/kg]) THEN
     T:=T+10[K]
     N:=N+1
     ELSE
          IF (25[kJ/kg]>=e) AND (e >1[kJ/kg]) THEN
          T:=T+0.5[K]
          N:=N+1
          ELSE
               IF (e<-50[kJ/kg]) THEN
               T:=T-20[K]
               N:=N+1
               ELSE
                    IF (-50[kJ/kg]<=e) AND
                     (e<-25[kJ/kg]) THEN
                    T:=T-10[K]
                    N:=N+1
                    ELSE
                         IF (-25[kJ/kg]<=e) AND
                          (e<-1[kJ/kg]) THEN
                         T:=T-0.5[K]
                         N:=N+1
                         ENDIF
                    ENDIF
               ENDIF
          ENDIF
     ENDIF
ENDIF
UNTIL (S<D)

ELSE
T= T
ENDIF

Temp=T

END
```

```
Procedure q_coll(h_sat,h_pre_out,h_boil_out,h_super_out:
 q_pre,q_boil,q_super)
h_g=h_sat
"h_f=enthalpy(water,P=P,x=1)" "Note: state 4 is
defined by h_f"

IF (h_g>h_pre_out) THEN
q_pre=h_g-h_pre_out
q_boil=h_boil_out-h_g
ELSE
q_pre=0
q_boil=h_boil_out-h_pre_out
ENDIF
q_super=h_super_out-h_boil_out

END

"Rankine Cycle with Preheat and Superheat
Variables that must be defined:
1.Turbine Inlet Pressure
2. Turbine Inlet Temperature
3. Turbine Work out OR System Mass Flow rate
4. Turbine outlet Pressure
5. Pump Efficiency
6. Turbine Efficiency
7. Medium Temperature and Pressure for exergy Analysis
 and start up conditions
8. Quality of the steam leaving the boiler"

"Reference Temp and Pressure for Energy (First Law)
Analysis"
T_ref="220.3 [K]" T[1]
P_ref=P[1]"14.55 [kPa]"
u_ref=0
rho_ref=(Interpolate('density','T','rho',T=T_ref))
v_ref=1/rho_ref
h_ref=P_ref*v_ref
s_ref=0 "This is 0 when the reference state and state
 1 are equal"

"Surrounding Medium Temp and Pressure for Exergy
(Second Law) Analysis"
P_med=100 [kPa]
T_med=(25+273) [K]

"Turbine Pressure, Turbine Temp, Turbine Power output,
 and Condenser Pressure.  Turbine and Pump Efficiencies"
P[5]=500 [kPa]
T[5]=(360+273.15)" 570" [K]
W_out=14.7 [kW]
P[6]= 100 "24.3"[kPa]
eta_p=.7"1"
eta_t=.8
eta_B=.85
eta_HX=.8
epsilon_rec=0.8"1"

"Working Fluid Properties for Peng-Robinson EOS"
T_cr=617.2 [K]  "DIPPR DATABASE: Critical Temp for
the specific fluid."
P_cr= 3.60600E+03[kPa]  "DIPPR DATABASE: Critical
Pressure for the specific fluid."
omega=0.302604 "DIPPR DATABASE: Accentric Factor for
the specific fluid."
```

```
R_u=8.314472 "[kJ/kmol-K]"
M=106.167  "[kg/kmol]" "DIPPR DATABASE: Molecular Weight"

P[4]=P[5]
P[3]=P[5]
P[2] =P[5]
P[1]=P[6]
P[7]=P[6]

"Boiler"
T_sat=Interpolate('T sat', 'P', 'T', P=P[5]) "{Lookup
 table} DIPPR DATA: Saturation Temp at given Pressure"
C_sat=Interpolate('Cp kJ/kg-K', 'T', 'Cp', T=T_sat) "{Lookup
 table} DIPPR DATA, specific heat for liquid in kJ/kg-K"
rho_sat=Interpolate('density', 'T', 'rho', T=T_sat) "{Lookup
 table} DIPPR DATA, density in kg/m^3"
C_ref=interpolate('Cp kJ/kg-K','T','Cp',T=T_ref) "The IG is
 a better approximation of CP at this point for this
 fluid for high temps?"
u_sat=(C_sat+C[1])/2*(T_sat-T[1])+u_1
h_sat=u_sat+(1/rho_sat)*(P[3])
s_sat=(C_sat+C[1])/2*ln(T_sat/T[1])+s[1]

T[4]=T_sat "{Lookup table} DIPPR DATA: Saturation
 Temp at given Pressure"
"q_boil=(-4.3339*10^(-8))*T[4]^4+(5.9467*10^(-5))*T[4]^3
-0.030207*T[4]^2+6.1544*T[4]+16.174" "Curve
Fit for DIPPR data for ETHYLBENZENE!"
q_boil_int=Interpolate('h fg','T', 'h fg', T=T[4])
q_boil=IF(T_sat,487,q_boil_int,q_boil_int,h_fg_calc)
h[4]=h_sat+q_boil
"s_boil=(5.4835*10^(-12))*T[4]^4-(5.3372*10^(-8))*T[4]^3
+(6.64*10^(-5))*T[4]^2-0.032439*T[4]+6.4801"
"Curve Fit for DIPPR data"
s_boil=q_boil/T_sat "Interpolate('s fg','T', 's fg',
 T=T[4])"
s[4]=s_sat+s_boil

"State 4 departure enthalpy and entropy"
C[4]=Interpolate('CpIG kJ/kg-K', 'T', 'Cp', T=T[4])
"{Lookup table} DIPPR DATA, specific heat for
liquid in kJ/kg-K"
T_r_4=T[4]/T_cr "Peng-Robinson EOS: EES Call needs
 reduced T"
P_r_4=P[4]/P_cr "Peng-Robinson EOS: EES Call needs
 reduced P"
CALL AB_PR(T_r_4, P_r_4, omega: A[4], B[4])
"Peng-Robinson EOS: EES Call for A and B"
Z[4]=Z_G_PR(A[4],B[4]) "Peng-Robinson EOS: EES
 Call for Z"
h_4_dep=H_DEP_PR(T_r_4, omega, Z[4], B[4])*R_u*T_cr/M
  "Peng-Robinson EOS: EES Call for h_departure"
s_4_dep=S_DEP_PR(T_r_4,omega,Z[4],B[4])*R_u "Peng-Robinson
 EOS: EES Call for s_departure"
v_4=Z[4]*(R_u/M)*T[4]/P[4]

"State 5 departure enthalpy and entropy"
C[5]=Interpolate('CpIG kJ/kg-K', 'T', 'Cp', T=T[5])
"{Lookup table} DIPPR DATA, specific heat for
liquid in kJ/kg-K"
C_5=Interpolate('CpIG kJ/kmol-K', 'T', 'Cp', T=T[5])
```

```
"{Lookup table} DIPPR DATA, specific heat for
liquid in kJ/kmol-K"
T_r_5=T[5]/T_cr
P_r_5=P[5]/P_cr
CALL AB_PR(T_r_5, P_r_5, omega: A[5], B[5])
Z[5]=Z_G_PR(A[5],B[5])

h_45_IG=(C[5]+C[4])/2*(T[5]-T[4])        "PR EOS:
enthalpy of the fluid modeled as an IG"
h_5_dep=H_DEP_PR(T_r_5, omega, Z[5], B[5])*T_cr*R_u/M
"PR EOS: departure enthalpy"
h[5]=(h_45_IG-(h_5_dep-h_4_dep))+h[4] "PR EOS: enthalpy
is the difference between the entropy of the fluid
as an IG and the departure functions"

s_45_IG=(C_5+C[4]*M)/2*ln(T[5]/T[4])-R_u*ln(P[5]/P[4])
"PR EOS: entropy of the fluid modeled as an IG"
s_5_dep=S_DEP_PR(T_r_5,omega,Z[5],B[5])*R_u "PR EOS:
departure entropy"
s[5]=(s_45_IG-(s_5_dep-s_4_dep))/M+s[4] "PR EOS: entropy
 is the difference between the entropy of the fluid
 as an IG and the departure functions"

"State 6: Turbine Exhaust"
T_6_ideal=Ideal(500[K], T_cr, T[5], P[6], P[5], P_cr, omega,
R_u, M, C_5, s[5], s_5_dep) "ITERATIONS BEGIN HERE"

C_6_ideal=Interpolate('CpIG kJ/kg-K', 'T', 'Cp',
 T=T_6_ideal)
C_6_Mideal=Interpolate('CpIG kJ/kmol-K', 'T', 'Cp',
 T=T_6_ideal)
T_r_6i=T_6_ideal/T_cr
P_r_6=P[6]/P_cr
CALL AB_PR(T_r_6i, P_r_6, omega: A_6i, B_6i)
Z_6_ideal=Z_G_PR(A_6i,B_6i)

s_6_IGi=((C_6_Mideal+C_5)/2)*ln(T_6_ideal/T[5])
-R_u*ln(P[6]/P[5])
s_6_depi=S_DEP_PR(T_r_6i,omega,Z_6_ideal,B_6i)*R_u
s_6_ideal=s[5]+(s_6_IGi-(s_6_depi-s_5_dep))/M

h_6_IGi=((C_6_ideal+C[5])/2)*(T_6_ideal-T[5])
h_6_depi=H_DEP_PR(T_r_6i, omega, Z_6_ideal, B_6i)*R_u*T_cr/M
h_6_ideal=h[5]+(h_6_IGi-(h_6_depi-h_5_dep))
w_t_ideal=h[5]-h_6_ideal
w_t_act=w_t_ideal*eta_t
h[6]=h[5]-w_t_act

T[6]=Temp(T_6_ideal, T_cr, T[5], P[6], P[5], P_cr, omega,
R_u, M, C[5], h[6], h[5], h_5_dep)    "ITERATIONS
BEGIN HERE INCORPORATING THE LOOKUP TABLES!"

C[6]=Interpolate('CpIG kJ/kg-K', 'T', 'Cp', T=T[6])
C_6=Interpolate('CpIG kJ/kmol-K', 'T', 'Cp', T=T[6])

T_r_6=T[6]/T_cr
CALL AB_PR(T_r_6, P_r_6, omega: A[6], B[6])
Z[6]=Z_G_PR(A[6],B[6])

h_6_IG=("("C[6]"+C[5])/2")*(T[6]-T[5])
h_6_dep=H_DEP_PR(T_r_6, omega, Z[6], B[6])*R_u*T_cr/M
h_6_check=h[5]+(h_6_IG-(h_6_dep-h_5_dep))

s_6_IG=((C_6+C_5)/2)*ln(T[6]/T[5])-R_u*ln(P[6]/P[5])
```

```
s_6_dep=S_DEP_PR(T_r_6,omega,Z[6],B[6])*R_u
s[6]=s[5]+(s_6_IG-(s_6_dep-s_5_dep))/M

"State 1: Condenser outlet, Pump inlet"
C[1]=Interpolate('Cp kJ/kg-K', 'T', 'Cp', T=T[1])
T[1]=Interpolate('T sat', 'P', 'T', P=P[1])
u_1=C[1]*(T[1]-T_ref)+u_ref
rho_1=Interpolate('density', 'T', 'rho', T=T[1])  "{Lookup
 table} DIPPR DATA: density in kg/m^3 "
h[1]=u_1+1/rho_1*(P[1]-P_ref)+h_ref
s[1]=C[1]*ln(T[1]/T_ref)+s_ref

"State 2: Pump outlet, Preheater Inlet"
T_2s=T[1]
rho_2=Interpolate('density', 'T', 'rho', T=T_2s)  "{Lookup
table} DIPPR DATA: density in kg/m^3"
Delta_h_2s=1/rho_2*(P[2]-P[1])   "Since we are modeling
this as a negligable change in Temperature, there is
no change in internal energy and the enthalpy is only
a function of pressure and specific volume"
w_ps=Delta_h_2s
w_pact=w_ps/eta_p
h[2]=w_pact+h[1]
C[2]=C[1] "This is an assumption that is valid for water.
If the fluid changes, this may not be applicable and
should be checked for accuracy"
T[2]=(h[2]-h[1])/C[2]+T[1]
u_2=C[2]*(T[2]-T[1])-w_pact+u_1
s[2]=C[2]*ln(T[2]/T[1])+s[1]
h_2check=u_2+1/rho_2*(P[2]-P[1])

"States 3 and 7"
Call HXtrial(epsilon_rec, h[6],h[2],T[6],T[2],m_dot,m_dot,
P[2],P[6],s[2],s[6],h[4],h[1]:T[3],h[3], s[3],T[7],
h[7],s[7],chi_3)
"Work and Heat Terms"
{q_additional=h_sat-h[3]        "This is the additional heat
required to reach the saturation point since the turbine
exhaust gas does not yield enough heat to reach this limit"
q_super=h[5]-h[4]
q_condenser=h[7]-h[1]
q_sol=(q_additional+q_boil)"/epsilon_B"+q_super"/epsilon_HX"}

w_net=w_t_act-w_pact
m_dot=W_out/w_net

"Q_preheater=q_preheat*m_dot"
"Heat and Work Terms"
Call q_coll(h_sat,h[3],h[4],h[5]:q_pre,q_boiler,q_super)

Q_dot_Pre=m_dot*q_pre
Q_dot_Boiler=m_dot*q_boiler
Q_dot_Super=m_dot*q_super
Q_dot_Solar=Q_dot_super/eta_HX+Q_dot_boiler/eta_B
+Q_dot_pre/eta_HX
{q_out_con=h[7]-h[1]
Q_BC=m_dot*q_out_con}
eta_sys=w_net/(q_pre+q_boiler+q_super)

eta_carnot=(1-T[1]/T[5])
```

```
STOP=IF(T[3],111,0,11111,0)
Quilaity=IF(T[6],T[7],1111,1,0)
Eff=IF(eta_sys,eta_carnot,0,1,1111)

"Clayperon Equation"
T_L=T_sat-2[K]
T_U=T_sat+2[K]
P_L=Interpolate('T sat','P','T',T=T_L)
P_U=Interpolate('T sat','P','T',T=T_U)
dPdt=(P_U-P_L)/(T_U-T_L)
h_fg_calc=dPdT*T_sat*(v_4-1/rho_sat)
```

A.3 Kalina I Effectiveness Model

```
Procedure HX_eff(epsilon, h_h_in,h_c_in,T_h_in,T_c_in,
m_c,m_h,P_c,P_h,x_c,x_h:T_C_out,T_h_out)
N=0
K=1000

IF T_c_in>T_h_in THEN
T_c_out=T_c_in
T_h_out=T_h_in
GOTO 100
ENDIF

T_c=T_c_in+1[K]

REPEAT

IF N<K THEN
N=N+1
Call NH3H2O(123, T_c,P_c,x_c:T_c_out,P_c_out,x_c_out,
h_c_out,s_c_out,u_c_out,v_C_out,chi_c_out)
q_c=m_c*(h_c_out-h_c_in)
C_c=m_c*(h_c_out-h_c_in)/(T_c_out-T_c_in)

h_h=(h_h_in*m_h-q_c)/m_h
Call NH3H2O(234, P_h,X_h,h_h: T_h_out,P_h_out,x_h_out,
h_h_out,s_h_out,u_h_out,v_h_out,chi_h_out)
C_h=m_h*(h_h_in-h_h_out)/(T_h_in-T_h_out)
q_max=IF(C_c,C_h,C_c,C_C,C_h)*(T_h_in-T_c_in)
epsilon_calc=q_c/q_max

Error=epsilon-epsilon_calc

IF error>0.2 THEN
T_c=T_c_out+.1[K]
ELSE
IF (error>.001) AND (error<0.3) THEN
T_C=T_c_out+.01[K]
ENDIF
ENDIF

UNTIL(error<0.001)

ELSE
T_c=111
ENDIF

100: dummy=1

END

Procedure q_coll(h_pre_out,h_sat,h_boil_out,h_super_out:
 q_pre,q_boil,q_super)

IF (h_sat>h_pre_out) THEN
```

```
q_pre=h_sat-h_pre_out
q_boil=h_boil_out-h_sat
ELSE
q_pre=0
q_boil=h_boil_out-h_pre_out
ENDIF
q_super=h_super_out-h_boil_out

END

"Kalina Cycle with EES Ammonia-Water Properties"
"The state Temperature, Pressure and ammonia composition
 are taken from Kalina 1984"
T_absorber=5 [C] "Absorber outlet"
P_abs=1.0 [bar] "absorber outlet"
P_int=4.7 [bar]  "intermediate pressure"
T_FT=66.1[C]  "Flash tank temperature"
"T_11in=T[8]"  "!!! This condition allows two phase
flow in the recuperator, Doesn't match Rogdakis'
model"

T_turbine=280[C]
P_tur=10 [bar]

eta_p1="1".7
eta_p2="1".7
eta_t="1".8
epsilon_HX=.8"1"
eta_HX=.8
eta_B=.85

W_net=14.7 [kW]
"m_dot=1 [kg/sec]"

X_WF=0.7
X_B=0.42"X[1]"

T_tur=ConvertTemp('C','K',T_turbine)
T_abs=ConvertTemp('C','K',T_absorber)
T_flash=ConvertTemp('C','K',T_FT)

//With the temperature and pressure of the flash tank
 set, the concentrations of the fluid entering and
 leaving the FT are found.
"State 7 Properties"
"Flash Tank Vapor outlet"
Call NH3H2O(128, T_flash, P_int, 1: T[7], P[7], X[7],
h[7],s[7],u[7],v[7],chi[7])
X_V=X[7]

"State 19 Properties"
"Dilute Stream Leaving the FT"
"The dilute solution leaving the flash tank is also at
the same temperature, pressure and dilute concentration."
Call NH3H2O(128, T_flash,  P_int, -0.001: T[19], P[19],
X[19], h[19], s[19], u[19], v[19],chi[19])
X_D=X[19]

"State 1 Properties"
"!!! This was changed from 128 to 123"
Call NH3H2O(123, T_abs, P_abs, X_B: T[1], P[1], X[1],
h[1], s[1], u[1], v[1], chi[1])

f=g*(X_V-X_D)/(X_V-X_B)
g=(X_WF-X_B)/(X_B-X_D)
```

```
"The normalized mass balance"
m[1]=(1+g)*m_dot
m[2]=(1+g)*m_dot
m[3]=(1+g)*m_dot
m[4]=(1+g)*m_dot
m[5]=f*m_dot
m[6]=(1+g-f)*m_dot
m[7]=(f-g)*m_dot
m[8]=m_dot
m[9]=m_dot
m[10]=m_dot
m[11]=m_dot
m[12]=m_dot
m[13]=m_dot
m[14]=m_dot
m[15]=m_dot
m[16]=m_dot
m[17]=m_dot
m[18]=m_dot
m[19]=g*m_dot
m[20]=g*m_dot
m[21]=g*m_dot
m[22]=(1+g)*m_dot

"State 2 Properties"
"Across a pump, the entropy is constant"
Call NH3H2O(235,P_int,x_B,s[1]:T_2s, P_2s, X_2s, h_2s,
s_2s,u_2s,v_2s,chi_2s)
w_p1s=h_2s-h[1]
"w_p1s=v[1]*(P_int-P[1])*(100 [kPa/bar])"   "vdP work
for an isentropic pump."
w_p1act=w_p1s/eta_p1
h_2actinput=w_p1act+h[1]
Call NH3H2O(234, P_int, X_B, h_2actinput: T[2], P[2],
X[2], h[2],s[2], u[2], v[2], chi[2])
W_dot_pump1=w_p1act*m[1]

"State 15 Properties"
"Superheat"
Call NH3H2O(123, T_tur, P_tur, X_WF: T[15], P[15],
X[15], h[15], s[15], u[15], v[15], chi[15])

"State 16 Properties"
"Turbine"
"We model the turbine as an isentropic process"
Call NH3H2O(235, P_abs, x[15],s[15]: T_16s, P_16s,
X_16s, h_16s,s_16s,u_16s,v_16s,chi_16s)
w_ts=h[15]-h_16s
"w_ts_calc=v[15]*(P_tur-P_abs)*(100 [kPa/bar])"
w_tact=w_ts*eta_t
h_16input=h[15]-w_tact
Call NH3H2O(234, P_abs, X_WF, h_16input: T[16], P[16],
X[16], h[16], s[16], u[16], v[16], chi[16])
W_dot_turbine=w_tact*m_dot

"State 9 Properties"
"Intermediate Pressure Condenser: Condensing Stream"
Call NH3H2O(238, P_int, x_WF, 0: T[9], P[9], x[9],
h[9], s[9], u[9], v[9], chi[9])
```

```
"State 10 Properties"
"Intermediate pump"
"The pump will have be treated as isentropic to begin with"
Call NH3H2O(235,P_tur,x[9],s[9]:T_10s, P_10s, X_10s,
h_10s,s_10s,u_10s,v_10s,chi_10s)
w_p2s=h_10s-h[9]
w_p2act=w_p2s/eta_p2
h_10actinput=(w_p2act+h[9])
Call NH3H2O(234, P_tur, x_WF, h_10actinput: T[10], P[10],
x[10], h[10], s[10], u[10], v[10], chi[10])
W_dot_pump2=w_p2act*m[9]

//Adding the work term completes this analysis
W_net=m_dot*(w_tact-w_p2act-w_p1act)

"State 13 Properties"
"PreHeater"
Call NH3H2O(238, P_tur, x_WF, 0: T[13], P[13], x[13],
h[13],s[13], u[13], v[13], chi[13])

"State 14 Properties"
"Boiler"
"The constraint on the boiler that it all turns to
vapor.  Q must be 1"
Call NH3H2O(238, P_tur, x_WF, 1.0: T[14], P[14], x[14],
h[14], s[14], u[14], v[14], chi[14])

"State 3 Properties"
"Flash Preheating: Cold Stream. The heat input comes
from the turbine exhaust"
Call HX_eff(epsilon_HX, h[16],h[2],T[16],T[2],m[2],m[16],
P[2],P[16],x[2],x[16]:T_3,T_17)
Call NH3H2O(123, T_3, P_int ,x_B: T[3], P[3], x[3], h[3],
s[3], u[3], v[3], chi[3])
Call NH3H2O(123, T_17, P[16] ,x_WF: T[17], P[17], x[17],
h[17],s[17], u[17], v[17], chi[17])
{q_23=(h[3]*m[3]-h[2]*m[2])
C_c_FP1=m[3]*(h[3]-h[2])/(T[3]-T[2])}

"State 17 is now defined"
"State 17 is determined by the heat from process 2-3 that
 is needed "
{h_17input=(h[16]*m[16]-q_23)/m[17]
Call NH3H2O(234, P_abs, x_WF,h_17input: T[17], P[17], x[17],
h[17], s[17], u[17], v[17], chi[17])
C_h_FP1=m[17]*(h[17]-h[16])/(T[17]-T[16])
q_max_FP1=IF(C_c_FP1,C_h_FP1,C_c_FP1,C_C_FP1,C_h_FP1)
*(T[16]-T[2])
epsilon_FP1=q_23/q_max_FP1}

"States 4 and 20"
Call HX_eff(epsilon_HX, h[19],h[3],T[19],T[3],m[3],
m[19],P[3],P[19],x[3],x[19]:T_4,T_20)
Call NH3H2O(123, T_4, P_int ,x_B: T[4], P[4], x[4],
h[4],s[4], u[4], v[4], chi[4])
Call NH3H2O(123, T_20, P[19] ,x_D: T[20], P[20], x[20],
h[20],s[20], u[20], v[20], chi[20])

{Call NH3H2O(123, T_flashint2, P_int ,x_B: T[4], P[4],
x[4], h[4],s[4], u[4], v[4], chi[4])
q_34=(h[4]*m[4]-h[3]*m[3])
C_c_FP2=m[4]*(h[4]-h[3])/(T[4]-T[3])
```

```
h_20input=(h[19]*m[19]-q_34)/m[20]
Call NH3H2O(234, P_int, x_D,h_20input: T[20], P[20],
x[20], h[20], s[20], u[20], v[20], chi[20])
C_h_FP2=m[20]*(h[20]-h[19])/(T[20]-T[19])
q_max_FP2=IF(C_c_FP2,C_h_FP2,C_c_FP2,C_C_FP2,C_h_FP2)
*(T[19]-T[3])
epsilon_FP2=q_34/q_max_FP2}

"States 5 and 6 Properties"
"The intensive properties at 3 are equal to the intensive
properties at 4 and 5.  The flow rates change."
T[5]=T[4]
P[5]=P[4]
X[5]=X[4]
h[5]=h[4]
s[5]=s[4]
u[5]=u[4]
v[5]=v[4]
chi[5]=chi[4]
T[6]=T[4]
P[6]=P[4]
X[6]=X[4]
h[6]=h[4]
s[6]=s[4]
u[6]=u[4]
v[6]=v[4]
chi[6]=chi[4]

"Check Enthalpy Balance on the FT"
Q_in_FT=-(m[5]*h[5]-m[7]*h[7]-m[19]*h[19])
CHECK=Q_in_FT+m[5]*h[5]-m[7]*h[7]-m[19]*h[19]

"State 8 Properties"
"The mixing occurs at this state.  The temperature and
pressure are constant but the other properties change"
h_8input=(h[7]*m[7]+h[6]*m[6])/m[8]
Call NH3H2O(234, P_int, x_WF, h_8input: T[8], P[8],
X[8], h[8], s[8], u[8], v[8], chi[8])
q_89=(h[8]-h[9])*m[8]
C_c_IPC=m[8]*(h[8]-h[9])/(T[8]-T[9])
Q_rej_IPc=q_89-q_1011

"State 11 Properties"
"The IPC outlet"
"Call HX_eff(epsilon_HX, h[19],h[3],T[19],T[3],m[3],m[19],
P[3],P[19],x[3],x[19]:T_4,T_20)"
Call NH3H2O(238,P_tur,x_WF,-0.001: T[11], P[11], X[11],
h[11], s[11], u[11], v[11], chi[11])
"Call NH3H2O(123,T_11in,P_tur,x_WF:T[11], P[11], X[11],
h[11], s[11], u[11], v[11], chi[11])"
c_h_IPC=m[11]*(h[11]-h[10])/(T[11]-T[10])
q_max_IPC=IF(C_c_IPC,C_h_IPC,C_c_IPC,C_C_IPC,C_h_IPC)
*(T[8]-T[10])
q_1011=m[11]*(h[11]-h[10])
"epsilon_IPC=q_1011/q_max_IPC"

"State 18: Recuperator Outlet"
//Pick T[18]?

Call HX_eff(epsilon_HX, h[17],h[11],T[17],T[11],m[11],
m[17],P[11],P[17],x[11],x[17]:T_12out,T_18)
```

```
T_12=IF(T_12out,T[11],T_12out,T[11],T[11])
Call NH3H2O(123,T_12,P_tur,x_WF:T[12], P[12], X[12],
h[12], s[12], u[12], v[12], chi[12])
Call NH3H2O(123,T_18,P_abs,x_WF:T[18], P[18], X[18],
h[18], s[18], u[18], v[18], chi[18])

{T_18in=T[17]-0[K]
Call NH3H2O(123, T_18in, P_abs, X_WF: T[18], P[18], X[18],
h[18], s[18], u[18], v[18], chi[18])
Q_1718=m[18]*(h[17]-h[18])
C_h_REC=m[17]*(h[17]-h[18])/(T[17]-T[18])

"State 12"
h_12*m[12]=h[11]*m[11]+Q_1718
Call NH3H2O(234, P[11],x[11],h_12:T[12], P[12], X[12],
h[12], s[12], u[12], v[12], chi[12])
C_c_REC=m[11]*(h[12]-h[11])/(T[12]-T[11])
q_max_REC=IF(C_c_REC,C_h_REC,C_c_REC,C_C_REC,C_h_REC)
*(T[17]-T[11])
epsilon_REC=Q_1718/q_max_REC}

"State 21"
//Throttling Vlave
h_21=h[20]
Call NH3H2O(234, P_abs, x_D,h_21: T[21], P[21], x[21],
h[21], s[21], u[21], v[21], chi[21])

"State 22"
//Mixing State
h_22*m[22]=m[18]*h[18]+m[21]*h[21]
Call NH3H2O(234, P_abs, x_B,h_22: T[22], P[22], x[22],
h[22], s[22], u[22], v[22], chi[22])

Call q_coll(h[12],h[13],h[14],h[15]:q_pre,q_boiler,
q_super)

q_check=q_pre+q_boiler+q_super

Q_dot_pre=m[12]*q_pre
Q_dot_boiler=m[13]*q_boiler
Q_dot_super=m[14]*q_super
Q_dot_solar=Q_dot_pre/eta_HX+Q_dot_Boiler/eta_B
+Q_dot_Super/eta_HX
Q_dot_in=Q_dot_pre+Q_dot_boiler+Q_dot_super
w_out_tot=w_tact
eta_sys=W_net/Q_dot_in
eta_sys_2=W_net/(Q_dot_in+Q_in_FT)
T_min=IF(T[1],T[9],T[1],T[1],T[9])
eta_carnot=(1-T_min/T[15])

"Q_out from absorber"
Q_out_abs=m[22]*(h[22]-h[1])
Check_HEATOUT=IF(Q_out_abs,Q_rej_IPC,11111,1,0)
STOP=IF(eta_sys,Eta_carnot,0,111,1111)
Quality=IF(chi[16],1,1111,1,0)
```

APPENDIX B

CAT MODELING CODES

The CAT modeling codes using the EES programming language are used in Chapter 4. The Rankine, R123, and toluene ORCs all come from one set of code and simply require the user to change the fluid name in the variable Fluid$ to access the EES fluid calls. The ethylbenzene ORC code uses the EES Peng-Robinson Builtin function just as the effectiveness modeling. It implements the CAT coding opposed to the effectivness coding for heat exchangers. The Maloney-Robinson and Kalina codes access the EES ammonia-water fluid call 'NH3H2O'.

B.1 Rankine, R123 ORC, and Toluene ORC Code

```
Procedure Qual2(P_t,P_c,eta_t: T_super, h[6], w_t_act,h[7],Qu[7],
 T[7], T[6])
$COMMON Fluid$, T_PP, T[1]
N=0
K=10000
T_super=-0.99 [K] "Start at -1 so that the properties calculate
correspond to the T_super that is reported"
Qu[7]=0
T[7]=T_PP

REPEAT
IF (N<K) THEN
T_super=T_super+1[K]
N=N+1

T_satur=Temperature(Fluid$,P=P_t,x=1)
T[6]=T_satur+T_super
h[6]=Enthalpy(Fluid$,P=P_t,T=T[6])
s[6]=entropy(Fluid$,h=h[6],P=P_t)
h_7s=Enthalpy(fluid$,P=P_c,s=s[6])
w_t_s=h[6]-h_7s
w_t_act=w_t_s*eta_t
h[7]=h[6]-w_t_act
T[7]=Temperature(Fluid$,h=h[7],P=P_c)
Qu[7]=Quality(fluid$,h=h[7],P=P_c)
h_check=enthalpy(Fluid$,P=P_c,x=1)
UNTIL ((Qu[7]>2))

ELSE
T_super=T_super"1111"
h[6]=h[6]"1111"
w_t_act=w_t_act"1111"
Qu[7]=Qu[7]"1111"
```

```
T[7]=T[7] "1111"
T[6]=T[6]" 1111"
ENDIF

END

Procedure HX_TPP(P_c,T_c_in,h_c_in,P_h,T_h_in,h_h_in,T_PP:T_c_out,
h_c_out,T_h_out,h_h_out)
$COMMON Fluid$
T_h_out=T_c_in+T_PP
N=0

10: dummy=N+1
IF T_h_out>=T_h_in THEN
T_h_out=T_h_in
h_h_out=h_h_in
T_c_out=T_c_in
h_c_out=h_c_in
ELSE
h_h_out=enthalpy(Fluid$,T=T_h_out,P=P_h)
q=h_h_in-h_h_out
h_c_out=h_c_in+q
T_c_out=Temperature(Fluid$,P=P_c,h=h_c_out)
DELTA=T_h_in-T_c_out

IF DELTA<T_PP THEN
T_h_out=T_h_out+1[C]
GOTO 10
ENDIF
ENDIF

END

Function Pump(M,rho_in,rho_out,m_dot)
rho=(rho_in+rho_out)/2
gpm=(m_dot/rho)*Convert('m^3/s','gal/min')

IF (M=1) AND (gpm<4) THEN
Pump=720
ELSE
IF (M=1) AND (gpm>=4) AND (gpm<25) THEN
Pump=3488
     ELSE
     IF (M=2) AND (gpm<4) THEN
     Pump=1899
          ELSE
          IF (M=2) AND (gpm>-4) AND (gpm<25) THEN
          Pump=6512
ELSE
Pump=1000000
        ENDIF
     ENDIF
ENDIF
ENDIF


END

Function ST(M,kW)
N=0

IF kW<=0 THEN
ST=0
N=10000
GOTO 10
ENDIF

IF M=1 THEN
ST=Interpolate('S&T Brass','kW','Price','kW'=kW)
```

```
ELSE
ST=Interpolate('S&T SS', 'kW','Price','kW'=kW)
ENDIF

10: end=N

END

Procedure q_coll(P,h_pre_in,h_pre_out,h_boil_out,h_super_out: q_pre,
q_boil,q_super)
$Common Fluid$
h_f=enthalpy(fluid$,P=P,x=0)
h_g=enthalpy(Fluid$,P=P,x=1)

IF (h_f>=h_pre_in) THEN
q_pre=h_pre_out-h_pre_in
q_boil=h_boil_out-h_pre_out
{ELSE
IF (h_g>=h_pre_in) AND (h_f<=h_pre_in) THEN
q_pre=h_pre_out-h_pre_in
q_boil=h_boil_out-h_pre_out}
ELSE
q_pre=0
q_boil=h_boil_out-h_pre_out
ENDIF
{ENDIF}
q_super=h_super_out-h_boil_out

END

Function Turb(P_in,P_out,P_R)
N=0

REPEAT
P=P_in/P_R
N=N+1
UNTIL (P<=P_in)

Turb=N*632.90 [$]

END

Procedure P_dep(P_turb:A_1a,A_1b,A_2a,A_2b, A_3a,A_3b)

"Shell and Tube"
IF P_turb<1000[kPa] THEN
A_1a=1
A_2a=1
A_3a=1
ELSE
A_1a=1*P_turb/1000 "Linear"
A_2a=0.08333333*(P_turb/1000)^2+0.9166666667 "Polynomial"
A_3a= 4.316627*(P_turb/1000)^0.5-3.3166667 "Power Series"
ENDIF


"R22/Recuperator"
IF P_turb<3000 [kPa] THEN
A_1b=1
A_2b=1
A_3b=1
ELSE
A_1b=1*P_turb/1000-2 "linear"
A_2b=0.071428575*(P_turb/1000)^2+0.35742857 "Polynomial"
A_3b=5.04867559792*(P_turb/1000)^(0.5)-7.74456264654 "Power"
ENDIF


END
```

```
"!!!User Defined Parameters"
//Operating Pressures
P_turb=1200 [KPa]
P_cond=100 [kPa]
Fluid$='Water'

//Sink and Source Temperatures
T_source=ConvertTemp('C','K',350) "The source inlet temperature"
T_sink=ConvertTemp('C','K',15) "The Sink inlet temperature"
T_o=ConvertTemp('C','K',25)
P_o=101.35 [kPa]
b_o=enthalpy(Air,T=T_o)-T_o*(entropy(Air,T=T_o,P=P_o))
Fluid2$='Dowtherm_Q'  "Source Fluid"
T_PP_Source=10 [K]
Fluid3$='Water'  "Sink Fluid"
T_PP_Sink= 10 [K]
P_sink=101.35 [kPa]

//Closest Approach/Pinch Point Temperatures
T_PPhi=10 [K]  "Pinch Point/Closest Approach Temperature on the
hot stream(source) inlet (T[11] and T[6])"
T_PPho=10[K] "Pinch Point/Closest Approach Temperature on the
hot stream(source) outlet (T[14] and T[3])"
T_ppci=10 [K] "Pinch Point/Closest Approach Temperature on the
cold stream(sink) inlet (T[9] and T[1])"
T_PPco=10[K] "Pinch Point/Closest Approach Temperature on the
cold stream(sink) outlet (T[10] and T[8])"
T_PP=5 [K] "Pinch Point/Closest Approach Temperature of the
Recuperator"
T_subcool=0 [K] "Subcool liquid leaving the condenser"

//Net work out of the system
W_dot_net=14.7 [kW] "Convert('W','kW')*25 [W]"

eta_B=0.97"1"
eta_HX=0.97"1"

//Component Efficiencies
eta_T=0.85
eta_P=0.7

//Material Selection: 1=Brass, 2=Stainless Steel
Material=1
C_FPcoll=C_PTC "[$/m^2]"
C_PTC=33" 44" [$/m^2]
eta_Coll=.6" 0.65"
Q_dot_rad=1 [kW/m^2]

//State 4: Saturated Liquid
P[4]=P[3]
T[4]=T_sat(fluid$,P=P[4])
h[4]=enthalpy(fluid$,T=T[4], x=Qu[4])
s[4]=entropy(fluid$,h=h[4],P=P[4])
Qu[4]=0
ex[4]=h[4]-T_o*s[4]-b_o

//State 5: Saturated Vapor
T[5]=T_sat(fluid$,P=P[5])
h[5]=enthalpy(fluid$,T=T[4],x=Qu[5])
s[5]=entropy(fluid$,T=T[5],x=Qu[5])
P[5]=P_turb
Qu[5]=1
```

```
ex[5]=h[5]-T_o*s[5]-b_o

//Procedure call for States 6 and 7
//!Qual is defined in a self installed library file
Call Qual2(P_turb, P_cond, eta_t: T_super, h[6],w_t_act,
h[7],Qu[7],T[7],T[6])

//State 6: Superheater Vapor Outlet
P[6]=P[5]
s[6]=entropy(fluid$,T=T[6],P=P[6])
Qu[6]=Quality(fluid$,T=T[6],P=P[6])
rho[6]=density(fluid$,T=T[6],P=P[6])
ex[6]=h[6]-T_o*s[6]-b_o

//State 7:Turbine Outlet
P[7]=P_cond
s[7]=Entropy(fluid$,T=T[7],P=P[7])
rho[7]=density(fluid$,T=T[7],P=P[7])
ex[7]=h[7]-T_o*s[7]-b_o
Qual_check=Quality(fluid$,T=T[7],P=P[7])

//State 1: condenser Outlet
P[1]=P_cond
T[1]=(T_sat(fluid$,P=P[1]))+T_subcool
h[1]=enthalpy(fluid$,x=Qu[1],P=P[1])
s[1]=entropy(fluid$,h=h[1],P=P[1])
rho[1]=density(fluid$,P=P[1],h=h[1])
Qu[1]=0 "IF(T[1],T_sat(fluid$,P=P[1]),1,0,1)*(Quality(fluid$,
T=T[1],P=P[1]))!!!!"
ex[1]=h[1]-T_o*s[1]-b_o

//State 2: Pump Outlet
P[2]=P_turb
s_2s=s[1]
T_2s=Temperature(fluid$,s=s_2s,P=P[2])
h_2s=Enthalpy(fluid$,T=T_2s,P=P[2])
w_p_s=h_2s-h[1]
w_p_act=w_p_s/eta_p
h[2]=w_p_act+h[1]
T[2]=Temperature(fluid$, h=h[2],P=P[2])
s[2]=Entropy(fluid$,T=T[2],P=P[2])
rho[2]=density(fluid$,T=T[2],P=P[2])
Qu[2]=quality(fluid$,T=T[2],P=P[2])
ex[2]=h[2]-T_o*s[2]-b_o

//Recuperator
Call HX_TPP(P[2],T[2],h[2],P[7],T[7],h[7],T_PP:T[3],h[3],
T[8],h[8])
//h[3]=h[2]
//h[7]=h[8]
//T[3]=T[2]
//T[7]=T[8]


//State 3: recuperator outlet
//h[3]=h[2]+q_HX
P[3]=P[2]
//T[3]=Temperature(fluid$,h=h[3],P=P[3])
Qu[3]=Quality(fluid$,h=h[3],P=P[3])
s[3]=entropy(fluid$,h=h[3],P=P[3])
```

```
ex[3]=h[3]-T_o*s[3]-b_o

//State 8: Superheater Outlet
P[8]=P[7]
s[8]=entropy(fluid$,P=P[8],h=h[8])
Qu[8]=quality(fluid$,P=P[8],h=h[8])
q_HX=h[7]-h[8]
ex[8]=h[8]-T_o*s[8]-b_o

//Source Heat Exchanger Stream
T[11]=T_source
T[14]=T[3]+T_PP_Source
h[11]=h[12]+DELTA_H_1112/m_dot_source
s[11]=s[12]+DELTA_S_1112/m_dot_source
ex[11]=h[11]-T_o*s[11]-b_o
Cp_Avg=(c_(Fluid2$,T=T[14])+c_(Fluid2$,T=T[11]))/2

"State: Source superheater outlet"
T[12]=T[11]-((q_super)*m_dot_cycle)/(m_dot_Source*Cp_Avg) "Solves
for T[12]"
h[12]=h[13]+DELTA_H_1213/m_dot_source
s[12]=s[13]+DELTA_S_1213/m_dot_source
DELTA_H_1112=Cp_Avg*m_dot_Source*(T[11]-T[12])
DELTA_S_1112=IF(T[11]-T[12],0.5,0.0001,0.0001,
Cp_Avg*m_dot_source*ln(T[11]/T[12]))
T_eff_super_H=DELTA_H_1112/DELTA_S_1112
ex[12]=h[12]-T_o*s[12]-b_o

"State: Source Boiler outlet"
T[13]=T[12]-(m_dot_cycle*(q_boil))/(m_dot_Source*Cp_Avg) "Solves
 for T[13]"
h[13]=h[14]+DELTA_H_1314/m_dot_source
s[13]=s[14]+DELTA_S_1314/m_dot_source
ex[13]=h[13]-T_o*s[13]-b_o
DELTA_h_1213=Cp_avg*m_dot_source*(T[12]-T[13])
DELTA_S_1213=Cp_Avg*m_dot_source*ln(T[12]/T[13])
T_eff_Boiler_H=DELTA_H_1213/DELTA_S_1213

"State 14: Source Preheater Outlet"
T[14]=T[13]-(m_dot_cycle*(q_pre))/(m_dot_Source*Cp_AVG) "Solves
for T[14]"
h[14]=0
s[14]=0
h_14=h[13]-DELTA_H_1314/m_dot_source
s_14=s[13]-DELTA_S_1314/m_dot_source
ex[14]=h[14]-T_o*s[14]-b_o
DELTA_h_1314=IF(q_pre,1,0,0,Cp_avg*m_dot_source*(T[13]-T[14]))
DELTA_S_1314=IF(q_pre,1,0,0,Cp_avg*m_dot_Source*(T[13]/T[14]))
T_eff_pre_H=DELTA_H_1314/DELTA_S_1314

//Sink Heat Exchanger Stream
T[9]=T_Sink
P[9]=P_sink
h[9]=enthalpy(Fluid3$,T=T[9],P=P_sink)
s[9]=entropy(Fluid3$,T=T[9],P=P_sink)
ex[9]=h[9]-T_o*s[9]-b_o
T[10]=T[8]-T_PP_Sink
P[10]=P_sink
h[10]=enthalpy(Fluid3$,T=T[10],P=P_sink)
s[10]=entropy(Fluid3$,T=T[10],P=P_sink)
ex[10]=h[10]-T_o*s[10]-b_o
```

```
Cp_Sink=(Cp(Fluid3$,T=T[9],P=P_Sink)+Cp(Fluid3$,T=T[10],
P=P_Sink))/2
m_dot_cycle*(h[8]-h[1])=Cp_Sink*m_dot_Sink*(T[10]-T[9])
Q=m_dot_cycle*(h[1]-h[8])
Q_2=Cp_Sink*m_dot_Sink*(T[10]-T[9])

//Heat and Work Terms
Call q_coll(P[3],h[3],h[4],h[5],h[6]:q_pre,q_boil,q_super)

Check_1=(h[4]-h[3])-q_pre
Check_2=(h[5]-h[4])-q_boil
Check_3=(h[6]-h[5])-q_super
Check_4=(h[6]-h[3])-q_pre-q_boil-q_super

Q_dot_rec=m_dot_cycle*(h[3]-h[2])
Q_dot_Pre=m_dot_cycle*q_pre
Q_dot_Boiler=m_dot_cycle*q_boil
Q_dot_Super=m_dot_cycle*q_super
Q_dot_Solar=Q_dot_super/eta_HX+Q_dot_boiler/eta_B+Q_dot_pre/eta_HX
Q_dot_sink=m_dot_cycle*(h[8]-h[1])

w_out=w_t_act-w_p_act
W_dot_net=m_dot_cycle*w_out "Solves for m_dot_cycle"
eta_cyc=w_out/(q_pre+q_boil+q_super)

E_dot_AR=q_dot_Pre+Q_dot_Boiler+Q_dot_Super-Q_dot_sink-W_dot_net
 "Energy Accumulation Rate"

//Carnot Efficiency
eta_Carnot=(1-T[1]/T[6])

//STOP1 checks to see if the source temperature is hotter than the
temperature at state 6.  If [6] is greater, then the analysis
is invalid
STOP1=IF(T_source,(T[6]+T_PPhi),1111,1,0)
//STOP2 checks to see if the turbine outlet temperature is hotter
than the recuperator hot stream outlet temperature.  If T[8] is
greater then the analysis is invalid
STOP2=IF(T[8],T[7],0,1,1111)
//STOP3 checks to see if the preheater inlet temperature is hotter
 than the recuperator cold stream outlet temperature.  If T[3]
 is greater then the analysis is invalid
STOP3=IF(T[3],T[4],0,1,1111)
//Stop 4 checks to see if the sink inlet temperature is less than
 the condenser oultet temperature.  If T_sink is greater, then
 the analysis is invalid
STOP4=IF(T_sink,(T[1]-T_ppci),0,1,1111)
//Stop 5 checks to see that the efficiency is less than carnot
STOP5=IF(eta_carnot,eta_cyc,1111,1,0)

C_P=Pump(Material,rho[1] ,rho[2],m_dot_cycle)
C_B=ST(Material, Q_dot_Boiler)
C_pre=IF(q_pre,0,0,0,1)*Interpolate('R22HX','kW','Price',
'kW'=Q_dot_Pre)
C_super=ST(Material, Q_dot_Super)
C_turb=Turb(P[6],P[7],3) "3 is the pressure ratio on the
Garrett Turbine"
Area=Q_dot_solar/(eta_Coll*Q_dot_rad)
C_Coll=IF(T_source, 140, C_FPcoll,C_PTC,C_PTC)*Area
C_Tracker=31.88[$/m^2]*Area
```

```
C_rec=ST(Material,Q_dot_rec)
C_cond=ST(Material,Q_dot_sink)

C_COL=C_coll+C_tracker
C_other=C_p+C_turb+C_cond+A_3b*C_rec+(C_B+C_pre+C_super)*A_3a
eff_multi=eta_cyc*eta_coll

Call P_dep(P_turb:A_1a,A_1b,A_2a,A_2b,A_3a,A_3b)

C_not=C_P+C_turb+C_coll+C_tracker+C_cond+C_rec+(C_B+C_pre+C_super)
C_tot_1=C_P+C_turb+C_coll+C_tracker+C_cond+A_1b*C_rec
+(C_B+C_pre+C_super)*A_1a
C_tot_2=C_P+C_turb+C_coll+C_tracker+C_cond+A_2b*C_rec
+(C_B+C_pre+C_super)*A_2a
C_tot_3=C_P+C_turb+C_coll+C_tracker+C_cond+A_3b*C_rec
+(C_B+C_pre+C_super)*A_3a

Z_not=C_not/eta_cyc
Z_1=C_tot_1/eta_cyc
Z_2=C_tot_2/eta_cyc
Z_3=C_tot_3/eta_cyc

//Entropy Analysis and Exergy Analysis
//All of the work producing devices will be adiabatic
//The entropy generation within the system should be positive
since this is not a reversible system (pump and turbine
efficiencies)
S_dot_gen_pump=m_dot_cycle*(s[2]-s[1])
S_dot_gen_turbine=m_dot_cycle*(s[7]-s[6])
I_dot_calc_pump=m_dot_cycle*(ex[1]-ex[2])+m_dot_cycle*w_p_act
I_dot_mult_pump=S_dot_gen_pump*T_o
I_dot_calc_turb=m_dot_cycle*(ex[6]-ex[7])-m_dot_cycle*w_t_act
I_dot_mult_turb=S_dot_gen_turbine*T_o
eta_II_pump=((h[2]-h[1])/(ex[2]-ex[1]))^(-1)
eta_II_turb=(h[6]-h[7])/(ex[6]-ex[7])

//For the HXers, T_eff must be calculated and is equal to
delta(h)/delta(s)
//Preheater
T_eff_pre=(h[4]-h[3])/(s[4]-s[3])
S_dot_gen_Pre=-Q_dot_pre/T_eff_pre+m_dot_cycle*(s[4]-s[3])
I_dot_gen_Pre=T_o*S_dot_gen_Pre
//I_dot_gen_pre_2=(m_dot_cycle*(s[4]-s[3])
+m_dot_source*(s[13]-s[14]))*T_o
I_dot_calc_gen_Pre=-m_dot_cycle*(ex[3]-ex[4])
-Q_dot_pre*(1-T_o/T_eff_pre)
eta_II_Pre=1+T_o/T_eff_pre_H-T_o/T_eff_pre

//Boiler
T_eff_boiler=(h[5]-h[4])/(s[5]-s[4])
S_dot_gen_boiler=-Q_dot_boiler/T_eff_boiler
+m_dot_cycle*(s[5]-s[4])
I_dot_gen_boiler=T_o*S_dot_gen_boiler
I_dot_calc_gen_Boiler=-Q_dot_boiler*(1-T_o/T_eff_Boiler)
+m_dot_cycle*(ex[5]-ex[4])
eta_II_Boiler=1+T_o/T_eff_Boiler_H-T_o/T_eff_Boiler

//Superheater
T_eff_super=(h[6]-h[5])/(s[6]-s[5])
S_dot_gen_super=-Q_dot_super/T_eff_super
+m_dot_cycle*(s[6]-s[5])
```

```
I_dot_gen_super=T_o*S_dot_gen_super
I_dot_calc_gen_Super=-Q_dot_Super*(1-T_o/T_eff_Super)
-m_dot_cycle*(ex[5]-ex[6])
eta_II_Super=1+T_o/T_eff_Super_H-T_o/T_eff_Super

//Overall for the recuperator, it can be said that no heat
is leaving the recuperator so then just a simple entropy
balance can be used or each stream can be broken up
S_dot_gen_recup=m_dot_cycle*(s[3]+s[8]-s[2]-s[7])
I_dot_calc_rec=m_dot_cycle*(ex[2]+ex[7]-ex[3]-ex[8])
I_dot_mult_rec=S_dot_gen_recup*T_o

//Condenser
T_eff_cond=(h[1]-h[8])/(s[1]-s[8])
S_dot_gen_cond=Q_dot_sink/T_eff_cond+m_dot_cycle*(s[1]-s[8])
I_dot_multi_cond=T_o*S_dot_gen_cond
I_dot_calc_cond=Q_dot_sink*(1-T_o/T_eff_cond)
-m_dot_cycle*(ex[8]-ex[1])

S_dot_gen=s_dot_gen_pump+S_dot_gen_turbine+S_dot_gen_Pre
+S_dot_gen_Boiler+S_dot_gen_Super+S_dot_gen_recup
+S_dot_gen_cond

(Q_dot_pre+Q_dot_Boiler+Q_dot_Super)/T_eff_H=Q_dot_pre/T_eff_pre
+Q_dot_boiler/T_eff_boiler+Q_dot_super/T_eff_Super
T_eff_L=T_eff_Cond
eta_Check=(1-T_eff_L/T_eff_H)/(1+(T_eff_L*T_o*S_dot_gen)
/(T_o*W_dot_net))

eta_2=eta_cyc/eta_carnot

}
```

B.2 Ethylbenzene Cycle Code

```
Procedure HX_TPP(P_c,T_c_in,h_c_in,x_c,P_h,T_h_in,h_h_in,
x_h,T_PP:T_h_out,T_c_out)
N=0
T_Hout=T_C_In+T_PP

10: N=N+1
IF T_Hout>=T_H_in THEN
T_H_out=T_h_in
T_c_out=T_c_in
h_H_out=h_h_in
h_C_out=h_h_in
ELSE
Call NH3H2O(123,T_Hout,P_H,x_H:T_h_out,P_h_out,x_h_out,
h_h_out,s_h_out,u_h_out,v_h_out,chi_h_out)
h_cout=h_c_in+(h_h_in-h_h_out)
Call NH3H2O(234,P_c,x_c,h_cout:T_c_out,P_c_out,x_c_out,
h_c_out,s_c_out,u_c_out,v_c_out,chi_c_out)
DELTA=T_H_in-T_c_out

IF DELTA<T_PP THEN
T_hout=T_hout+1[K]
GOTO 10
ENDIF

T_PP_cohi=T_h_in-T_c_out
T_PP_ciho=T_h_out-T_c_in

ENDIF
END
```

```
Procedure HX_TPP2(P_c,T_c_in,h_c_in,x_c,m_c,P_h,T_h_in,
h_h_in,x_h,m_h,T_PP:T_h_out,T_c_out)
N=0
T_Hout=T_C_In+T_PP

10: N=N+1
IF T_Hout>=T_H_in THEN
T_H_out=T_h_in
T_c_out=T_c_in
h_H_out=h_h_in
h_C_out=h_h_in
ELSE
Call NH3H2O(123,T_Hout,P_H,x_H:T_h_out,P_h_out,x_h_out,
h_h_out,s_h_out,u_h_out,v_h_out,chi_h_out)
h_cout=(m_c*h_c_in+m_h*(h_h_in-h_h_out))/m_c
Call NH3H2O(234,P_c,x_c,h_cout:T_c_out,P_c_out,x_c_out,
h_c_out,s_c_out,u_c_out,v_c_out,chi_c_out)
DELTA=T_H_in-T_c_out

IF DELTA<T_PP THEN
T_hout=T_hout+1[K]
GOTO 10
ENDIF

T_PP_cohi=T_h_in-T_c_out
T_PP_ciho=T_h_out-T_c_in

ENDIF
END


Procedure q_coll(h_pre_out,h_sat,h_boil_out,h_super_out:
 q_pre,q_boil,q_super)

IF (h_sat>h_pre_out) THEN
q_pre=h_sat-h_pre_out
q_boil=h_boil_out-h_sat
ELSE
q_pre=0
q_boil=h_boil_out-h_pre_out
ENDIF
q_super=h_super_out-h_boil_out

END


Function Pump(M,rho_in,rho_out,m_dot)
rho=(rho_in+rho_out)/2
gpm=(m_dot/rho)*Convert('m^3/s','gal/min')

IF (M=1) AND (gpm<4) THEN
Pump=720
ELSE
IF (M=1) AND (gpm>=4) AND (gpm<25) THEN
Pump=3488
     ELSE
     IF (M=2) AND (gpm<4) THEN
     Pump=1899
          ELSE
          IF (M=2) AND (gpm>-4) AND (gpm<25) THEN
          Pump=6512
ELSE
Pump=1000000
          ENDIF
     ENDIF
ENDIF
ENDIF
```

```
END

Function ST(M,kW)
N=0

IF kW<=0 THEN
ST=0
N=10000
GOTO 10
ENDIF

IF M=1 THEN
ST=Interpolate('S&T Brass','kW','Price','kW'=kW)
ELSE
ST=Interpolate('S&T SS', 'kW','Price','kW'=kW)
ENDIF

10: end=N

END

Function Turb(P_in,P_out,P_R)
N=0

REPEAT
P=P_in/P_R
N=N+1
UNTIL (P<=P_in)

Turb=N*632.90 [$]

END

Procedure P_dep(P_t,P_FTbar:A_1a,A_1b,A_2a,A_2b, A_3a,
A_3b,A_1c,A_2c,A_3c)
P_turb=Convert('bar','kPa')*P_t
P_FT=Convert('bar','kPa')*P_FTbar

"Shell and Tube"
IF P_turb<1000[kPa] THEN
A_1a=1
A_2a=1
A_3a=1
ELSE
A_1a=1*P_turb/1000 "Linear"
A_2a=0.08333333*(P_turb/1000)^2+0.9166666667 "Polynomial"
A_3a= 4.316627*(P_turb/1000)^0.5-3.3166667 "Power Series"
ENDIF

"R22/Recuperator"
IF P_turb<3000 [kPa] THEN
A_1b=1
A_2b=1
A_3b=1
ELSE
A_1b=1*P_turb/1000-2 "linear"
A_2b=0.071428575*(P_turb/1000)^2+0.35742857 "Polynomial"
A_3b=5.04867559792*(P_turb/1000)^(0.5)
-7.74456264654 "Power"
ENDIF

{
"Shell and Tube"
IF P_turb<1000[kPa] THEN
A_1a=1
A_2a=1
A_3a=1
ELSE
```

```
A_1a=3*P_turb/1000-2 "Linear"
A_2a=0.6*(P_turb/1000)^2+0.4 "Polynomial"
A_3a= 9*(P_turb/1000)^0.5-8 "Power Series"
ENDIF

"R22/Recuperator"
IF P_turb<3000 [kPa] THEN
A_1b=1
A_2b=1
A_3b=1
ELSE
A_1b=2*P_turb/1000-5 "linear"
A_2b=0.2857*(P_turb/1000)^2-1.5714 "Polynomial"
A_3b=7.4641*(P_turb/1000)^(0.5)-11.9282 "Power"
ENDIF
}

"Shell and Tube: P_FT"
IF P_FT<1000[kPa] THEN
A_1c=1
A_2c=1
A_3c=1
ELSE
A_1c=1*P_FT/1000 "Linear"
A_2c=0.08333333*(P_FT/1000)^2+0.9166666667 "Polynomial"
A_3c= 4.316627*(P_FT/1000)^0.5-3.3166667 "Power Series"
ENDIF

END

//Define Cycle Parameters
//Define the turbine and absorber pressures
P_turb=10 [bar]
P_abs=1.0 [bar]

//Define the ammonia Concentration in the working fluid
X_WF=0.426

//Define the Flash Tank Parameters
P_FT=3 [bar]
T_FT=ConvertTemp('C','K',75)

//Define the sink and source temperatures
T_Sink1=ConvertTemp('C','K',25)
T_sink2=ConvertTemp('C','K',25)
T_Source=ConvertTemp('C','K',325)

//Define the medium
T_o=ConvertTemp('C','K',25)
P_o=Convert('kPa','bar')*101.35[kPa]
b_o=enthalpy(air,T=T_o)-T_o*entropy(air,T=T_o,P=P_o)

//Define the net work output from the turbine
W_dot_net="763.4 "14.7 [kW]

//Define the component efficiencies
eta_t=0.85
eta_p1=.7
eta_p2=.7
eta_HX="1"0.97
eta_B="1"0.97

//Material Selection: 1=Brass, 2=Stainless Steel
Material=2
C_FPcoll=C_PTC "[$/m^2]"
C_PTC=33"44" [$/m^2]
```

```
eta_Coll=.6" 0.65"
Q_dot_rad=1 [kW/m^2]

//Define the Pinch Point/Closest Approach Temperatures
//Pinch Points used in cycle calculations
T_PP=5 [K]
T_PPABSho=10 [K] "The pinch point between the hot stream
 outlet T[1] and the cold stream inlet T[??] of the absorber"
T_PPpreci=10 [K] "The pinch point between the cold strem inlet
 at T[13] and the source stream outlet at T[32] of the Preheater"
T_FP3ho=10 [K] "The pinch point between the hot stream outlet
T[26] and the cold stream inlet T[3] of the Flash Preheater II"
T_IPChi=10[K] "The pinch point between the hot stream inlet
T[9] and the cold stream outlet T[28] of the IPC"
T_IPCho=10 [K] "The pinck point between the hot stream outlet
 T[10] and the cold stream inlet T[27] on the IPC"
T_PPsource=10 [K] "The pinch point between the source T[29]
 and the max cycle temp"
//T_PPFP3=5 [K] "The pinch point beteen T[25] and T[5]"}
//Determine the basic concentration from the parameters at
 the absorber (state 1)
T_1=T_sink1+T_PPABSho
P_1=P_abs
Call NH3H2O(128,T_1,P_1,0:T[1],P[1],x[1],h[1],s[1],u[1],
v[1],Qu[1])
x_B=x[1]
ex[1]=h[1]-T_o*s[1]-b_o
//Determine the pump work (process 1 to 2)
Call NH3H2O(235, P_FT, x_B, s[1] : T_2s, P_2s, x_2s, h_2s,
s_2s, u_2s, v_2s, Qu_2s)
w_p1s=h_2s-h[1]   "v[1]*(P_FT-P[1])*(100 [kPa/bar])
vdP work for an isentropic pump."
w_p1act=w_p1s/eta_p1
h_2actinput=w_p1act+h[1]
Call NH3H2O(234, P_FT, x_B, h_2actinput: T[2], P[2], x[2],
 h[2],s[2], u[2], v[2], Qu[2])
ex[2]=h[2]-T_o*s[2]-b_o
//Determine the WF concentration from the condensation
 parameters for state 8
Call NH3H2O(238, P_FT,x_WF,0:T[8], P[8], x[8], h[8],s[8],
 u[8], v[8], Qu[8])
ex[8]=h[8]-T_o*s[8]-b_o
//Determine the pump work (process 8 to 9)
Call NH3H2O(235, P_turb, x_WF, s[8] : T_9s, P_9s, x_9s,
 h_9s,s_9s, u_9s, v_9s, Qu_9s)
w_p2s=h_9s-h[8]   "v[1]*(P_FT-P[1])*(100 [kPa/bar])
vdP work for an isentropic pump."
w_p2act=w_p2s/eta_p2
h_9actinput=w_p2act+h[8]
Call NH3H2O(234, P_FT, x_WF, h_9actinput: T[9], P[9], x[9],
 h[9],s[9], u[9], v[9], Qu[9])
ex[9]=h[9]-T_o*s[9]-b_o
//Determine the preheater input heat (process 9 to 10)
Call NH3H2O(238, P_turb,x_WF,0:T[10],P[10],x[10],h[10],
```

```
s[10],u[10],v[10],Qu[10])
ex[10]=h[10]-T_o*s[10]-b_o

//Detemine the evaporator input heat (process 10 to 11)
Call NH3H2O(238, P_turb,x_WF,1:T[11],P[11],x[11],h[11],
s[11],u[11],v[11],Qu[11])
ex[11]=h[11]-T_o*s[11]-b_o

//Determine the superheat input heat
//Determine the turbine specific work (process 12 to 13)
Call QualKal(P_turb, P_abs, eta_t,x_WF: T_super,h_12,w_t_act,
h[13],Qu[13] ,T[13],T_12,s[13],u[13],v[13],P[13])
x[13]=x_WF
Call NH3H2O(123,T_12, P_turb,x_WF:T[12],P[12],x[12],h[12],
s[12],u[12],v[12],Qu[12])
ex[12]=h[12]-T_o*s[12]-b_o
ex[13]=h[13]-T_o*s[13]-b_o

//w_net=w_t_act-w_p1act-w_p2act
//m_dot_WF=W_dot_net/w_net
W_dot_net=m_dot_WF*w_t_act-w_p1act*m_dot_WF*(1+g)-w_p2act*m_dot_WF

//Determine the vapor and dilute concentrations and the inlet
 conditions to the Flash Tank (states 6,7 and 8)
Call NH3H2O(128,T_FT,P_FT,1:T[6],P[6],x[6],h[6],s[6],u[6],v[6],Qu[6])
x[6]=x_V
ex[6]=h[6]-T_o*s[6]-b_o
Call NH3H2O(128,T_FT,P_FT,0:T[15],P[15],x[15],h[15],s[15],
u[15],v[15],Qu[15])
x[15]=x_D
ex[15]=h[15]-T_o*s[15]-b_o
//Call NH3H2O(123,T_FT,P_FT,x_B:T[6],P[6],x[6],h[6],s[6],
u[6],v[6],Qu[6])

//The intensive properties at 2 are equal to the intensive
 properties at 3 and 4.  The flow rates change.
T[3]=T[2]
P[3]=P[2]
x[3]=x[2]
h[3]=h[2]
s[3]=s[2]
u[3]=u[2]
v[3]=v[2]
Qu[3]=Qu[2]
ex[3]=ex[2]
T[4]=T[2]
P[4]=P[2]
x[4]=x[2]
h[4]=h[2]
s[4]=s[2]
u[4]=u[2]
v[4]=v[2]
Qu[4]=Qu[2]
ex[4]=ex[2]

//Define the mass balance terms
f=g*(X_V-X_D)/(X_V-X_B)
g=(X_WF-X_B)/(X_B-X_D)

"The normalized mass balance"
m[1]=m_dot_WF*(1+g)
m[2]=m_dot_WF*(1+g)
```

```
m[3]=m_dot_WF*(1+g-f)
m[4]=f*(m_dot_WF)
m[5]=f*(m_dot_WF)
m[6]=(f-g)*m_dot_WF
m[7]=m_dot_WF
m[8]=m_dot_WF
m[9]=m_dot_WF
m[10]=m_dot_WF
m[11]=m_dot_WF
m[12]=m_dot_WF
m[13]=m_dot_WF
m[14]=m_dot_WF
m[15]=g*m_dot_WF
m[16]=g*m_dot_WF
m[17]=m_dot_WF*(1+g)
m_dot_B=m[1]
m_dot_D=m[15]
m_dot_V=m[6]

//Flash Preheater
//Since the FT temperature is defined (state 5), the inlet
 to the cold side (state 4) and the turbine hot side inlet,
 a simple entahlpy balance yields state 14
Call NH3H2O(123, T_FT,P_FT,X_B:T[5],P[5],x[5],h[5],s[5],
 u[5],v[5],Qu[5])
ex[5]=h[5]-T_o*s[5]-b_o
h_14*m[14]+h[5]*m[5]=h[4]*m[4]+h[13]*m[13]
Call NH3H2O(234,P_abs,x_WF,h_14:T[14],P[14],x[14],h[14],
s[14],u[14],v[14],Qu[14])
ex[14]=h[14]-T_o*s[14]-b_o

//Mixing at State 7
h_7*m[7]=m[6]*h[6]+m[3]*h[3]
Call NH3H2O(234,P_FT,x_WF,h_7:T[7],P[7],x[7],h[7],s[7],
u[7],v[7],Qu[7])
ex[7]=h[7]-T_o*s[7]-b_o

//Throttling Valve
Call NH3H2O(234,P_abs,x_D,h[15]:T[16],P[16],x[16],h[16],
s[16],u[16],v[16],Qu[16])
ex[16]=h[16]-T_o*s[16]-b_o

//Mixing at State 17
h_17*m[17]=h[16]*m[16]+h[14]*m[14]
Call NH3H2O(234,P_abs,x_B,h_17:T[17],P[17],x[17],h[17],
s[17],u[17],v[17],Qu[17])
ex[17]=h[17]-T_o*s[17]-b_o

Call q_coll(h[9],h[10],h[11],h[12]:q_pre,q_boiler,q_super)
Q_dot_pre=m[11]*q_pre
Q_dot_boiler=m[12]*q_boiler
Q_dot_super=m[13]*q_super
Q_dot_Sink_1=m[1]*(h[17]-h[1])
Q_dot_Sink_2=m[8]*(h[7]-h[8])
Q_dot_in=Q_dot_pre+Q_dot_boiler+Q_dot_super
Q_dot_rec=m[13]*(h[13]-h[14])
Q_dot_FP1=m[4]*(h[5]-h[4])
Q_dot_IPC=m[7]*(h[7]-h[8])

eta_sys=W_dot_net/(m[11]*(h[12]-h[9]))
```

```
FT_CHECK=-m[5]*h[5]+m[6]*h[6]+m[15]*h[15]
STOP_1=IF(FT_CHECK,0.001,0,0,11111)
STOP_2=IF(T[12],T_source-T_PP,0,0,1111)

Q_dot_solar=Q_dot_pre/eta_HX+Q_dot_Boiler/eta_B
+Q_dot_Super/eta_HX
E_dot_AR=Q_dot_in-Q_dot_sink_1-W_dot_net-Q_dot_sink_2
Q_mixing=-m[6]*h[6]+m[7]*h[7]-m[3]*h[3]

eta_Carnot=1-(T[1]/T[12])
eta_sys_2=eta_sys/eta_carnot

eta_sys_93=0.93*eta_sys

//STOP1: Checks to make sure that the absorber inlet
[23] is greater than the absorber outlet T[1]
STOP_3=IF(T[17],T[1],1311,1,0)
//STOP2: Checks to make sure that the hot stream sink
inlet of the IPC T[27] is colder than the IPC cold
stream outlet T[10]
//STOP_4=IF(T[10],(T_source+T_IPCho),1111,1,0)
//STOP3: Checks to make sure that the source inlet T[29]
is greater than the superheater outlet T[16]
//STOP_5=IF(T[29],(T[16]+T_PPsource),1111,1,0)
//STOP4: Checks to make sure that the superheater
temperature does not exceed 600 K, the limit on the
data set
//STOP_6=IF(600,T[16],1111,1,0)
//STOP5: carnot
//STOP_7=IF(eta_carnot,eta_sys,1111,1,0)


//Quality Checks
Qual_1=IF(x_D,x_B,0,1,1111)
Qual_2=IF(x_B,x_WF,0,1,1111)
Qual_3=IF(x_WF,x_V,0,1,1111)

//Price Calcs

C_P1=Pump(Material,1/v[1], 1/v[2],m[1])
C_P2=Pump(Material,1/v[10], 1/v[11],m[10])
C_B=ST(Material, Q_dot_Boiler)
C_pre=IF(q_pre,0,0,0,1)*Interpolate('R22HX','kW','Price',
'kW'=Q_dot_Pre)
C_super=ST(Material, Q_dot_Super)
C_rec=ST(Material,Q_dot_Rec)
C_FP1=ST(Material, Q_dot_FP1)
//C_FP2=ST(Material,Q_dot_FP2)
//C_FP3=ST(Material,Q_dot_FP3)
C_sink1=ST(Material,Q_dot_sink_1)
C_sink2=ST(Material,Q_dot_sink_2)
C_IPC=ST(Material,Q_dot_IPC)
C_FT=Max(C_sink1,C_sink2,C_super,C_B,C_Pre)

C_turb=Turb(P[6],P[7],3) "3 is the pressure ratio on the
 Garrett Turbine"
Area=Q_dot_solar/(eta_Coll*Q_dot_rad)
C_Coll=IF(T_source, 140, C_FPcoll,C_PTC,C_PTC)*Area
C_Tracker=31.88[$/m^2]*Area

Call P_dep(P_turb,P_FT:A_1a,A_1b,A_2a,A_2b, A_3a,A_3b,
A_1c,A_2c,A_3c)
```

```
C_COL=C_coll+C_tracker
C_other=C_P1+C_P2+C_turb+C_sink1+C_FT+A_3b*C_pre
+(C_B+C_rec+C_super+C_sink2)*A_3a+(C_FP1+C_IPC)*A_3c
eff_multi=eta_sys*eta_coll

C_not=C_P1+C_P2+C_turb+C_coll+C_tracker+C_sink1+C_FT
+C_pre+(C_B+C_rec+C_super+C_sink2)+(C_FP1+C_IPC)
C_tot_1=C_P1+C_P2+C_turb+C_coll+C_tracker+C_sink1+C_FT
+A_1b*C_pre+(C_B+C_rec+C_super+C_sink2)*A_1a+(C_FP1+C_IPC)*A_1c
C_tot_2=C_P1+C_P2+C_turb+C_coll+C_tracker+C_sink1+C_FT
+A_2b*C_pre+(C_B+C_rec+C_super+C_sink2)*A_2a+(C_FP1+C_IPC)*A_2c
C_tot_3=C_P1+C_P2+C_turb+C_coll+C_tracker+C_sink1+C_FT
+A_3b*C_pre+(C_B+C_rec+C_super+C_sink2)*A_3a+(C_FP1+C_IPC)*A_3c

Z_not=C_not/eta_sys
Z_1=C_tot_1/eta_sys
Z_2=C_tot_2/eta_sys
Z_3=C_tot_3/eta_sys

//Entropy Analysis
//Pump 1
S_dot_gen_pump1=m[2]*(s[2]-s[1])
I_dot_pump1=m[1]*ex[1]-m[2]*ex[2]+w_p1act*m[2]
I_dot_pump_multi=T_o*S_dot_gen_pump1

//Flash Preheater 1
S_dot_gen_FP1="0"m[5]*s[5]+m[14]*s[14]-m[4]*s[4]
-m[13]*s[13]
I_dot_FP1="0"m[4]*ex[4]-m[5]*ex[5]+m[13]*ex[13]
-m[14]*ex[14]
I_dot_FP1_multi=S_dot_gen_FP1*T_o

//Flash Tank
S_dot_gen_FT=m[15]*s[15]+m[6]*s[6]-m[5]*s[5]
I_dot_FT=m[5]*ex[5]-m[6]*ex[6]-m[15]*ex[15]
I_dot_FT_multi=S_dot_gen_FT*T_o

//Mixing 1
S_dot_gen_mixing1=m[7]*s[7]-m[6]*s[6]-m[3]*s[3]
I_dot_Mixing1=ex[3]*m[3]-ex[7]*m[7]+m[6]*ex[6]
I_dot_Mixing1_multi=S_dot_gen_mixing1*T_o

//IPC
T_eff_IPC=(h[8]-h[7])/(s[8]-s[7])
S_dot_gen_IPC=Q_dot_sink_2/T_eff_IPC+m[8]*s[8]-m[7]*s[7]
I_dot_IPC=-Q_dot_sink_2*(1-T_o/T_eff_IPC)-m[8]*ex[8]
+m[7]*ex[7]
I_dot_IPC_calc=T_o*S_dot_gen_IPC

//Pump 2
S_dot_gen_pump2=m[8]*(s[9]-s[8])
I_dot_pump2=m[8]*ex[8]-m[9]*ex[9]+w_p2act*m[8]
I_dot_pump2_multi=T_o*S_dot_gen_pump2

//Preheater
T_eff_Pre=(h[9]-h[10])/(s[9]-s[10])
S_dot_gen_Pre=-Q_dot_pre/T_eff_Pre+m[10]*s[10]-m[9]*s[9]
I_dot_Pre=Q_dot_pre*(1-T_o/T_eff_Pre)-m[10]*ex[10]
+m[9]*ex[9]
I_dot_Pre_multi=T_o*S_dot_gen_pre

//Boiler
T_eff_Boiler=(h[11]-h[10])/(s[11]-s[10])
S_dot_gen_Boiler=-Q_dot_boiler/T_eff_Boiler+m[11]*s[11]
```

```
-m[10]*s[10]
I_dot_Boiler=Q_dot_boiler*(1-T_o/T_eff_Boiler)+m[10]*ex[10]
-m[11]*ex[11]
I_dot_Boiler_Multi=S_dot_Gen_Boiler*T_o

//Superheater
T_eff_Super=(h[12]-h[11])/(s[12]-s[11])
S_dot_gen_Super=-Q_dot_super/T_eff_super+m[12]*s[12]
-m[11]*s[11]
I_dot_super=Q_dot_super*(1-T_o/T_eff_super)+m[11]*ex[11]
-m[12]*ex[12]
I_dot_super_multi=T_o*S_dot_gen_super

//Turbine
S_dot_gen_turbine=m[13]*s[13]-m[12]*s[12]
I_dot_turbine=-w_t_act*m[13]+m[12]*ex[12]-m[13]*ex[13]
I_dot_turb_Multi=T_o*S_dot_gen_turbine

//Throtling Valve
S_dot_gen_valve=m[15]*(s[16]-s[15])
I_dot_valve=m[15]*(ex[15]-ex[16])
I_dot_valve_multi=S_dot_gen_valve*T_o

//Mixing 2
S_dot_gen_mixing2=m[17]*s[17]-m[14]*s[14]-m[16]*s[16]
I_dot_mixing2=m[14]*ex[14]+m[16]*ex[16]-m[17]*ex[17]
I_dot_mixing2_multi=T_o*S_dot_Gen_mixing2

//Absorber
T_eff_abs=(h[17]-h[1])/(s[17]-s[1])
S_dot_gen_abs=Q_dot_sink_1/T_eff_abs+m[1]*s[1]-m[17]*s[17]
I_dot_abs=-Q_dot_sink_1*(1-T_o/T_eff_abs)+m[17]*ex[17]-m[1]*ex[1]
I_dot_abs_multi=T_o*S_dot_gen_abs

S_dot_gen=S_dot_gen_pump1+S_dot_gen_FP1+S_dot_gen_FT
+S_dot_gen_Mixing1+S_dot_gen_IPC+S_dot_gen_pump2
+S_dot_gen_pre+S_dot_gen_Boiler+S_dot_gen_super
+S_dot_gen_turbine+S_dot_gen_valve+S_dot_gen_mixing2
+S_dot_gen_abs

I_dot=I_dot_pump1+I_dot_FP1+I_dot_FT+I_dot_Mixing1+I_dot_IPC
+I_dot_pump2+I_dot_pre+I_dot_Boiler+I_dot_super
+I_dot_turbine+I_dot_valve+I_dot_mixing2+I_dot_abs

I_dot_multi=T_o*S_dot_gen

(Q_dot_pre+Q_dot_Boiler+Q_dot_Super)/T_eff_H=
Q_dot_pre/T_eff_pre+Q_dot_boiler/T_eff_boiler
+Q_dot_super/T_eff_Super
(Q_dot_sink_1+Q_dot_sink_2)/T_eff_L=Q_dot_sink_1/T_eff_abs
+Q_dot_sink_2/T_eff_IPC

eta_Check=(1-T_eff_L/T_eff_H)/(1+(T_eff_L*T_o*S_dot_gen)
/(T_o*W_dot_net))

eta_check_2=(1-T_eff_L/T_eff_H)-(T_eff_L*S_dot_gen)/(Q_dot_in)
```

B.3 Maloney-Robertson Cycle Code

```
Procedure HX_TPP2(P_c,T_c_in,h_c_in,x_c,m_c,P_h,T_h_in,h_h_in,
x_h,m_h,T_PP:T_h_out,T_c_out)
N=0
T_Hout=T_C_In+T_PP
```

```
10: N=N+1
IF T_Hout>=T_H_in THEN
T_H_out=T_h_in
T_c_out=T_c_in
h_H_out=h_h_in
h_C_out=h_h_in
ELSE
Call NH3H2O(123,T_Hout,P_H,x_H:T_h_out,P_h_out,x_h_out,h_h_out,
s_h_out,u_h_out,v_h_out,chi_h_out)
h_cout=(m_c*h_c_in+m_h*(h_h_in-h_h_out))/m_c
Call NH3H2O(234,P_c,x_c,h_cout:T_c_out,P_c_out,x_c_out,h_c_out,
s_c_out,u_c_out,v_c_out,chi_c_out)
DELTA=T_H_in-T_c_out

IF DELTA<T_PP THEN
T_hout=T_hout+1[K]
GOTO 10
ENDIF

T_PP_cohi=T_h_in-T_c_out
T_PP_ciho=T_h_out-T_c_in

ENDIF
END

Function Pump(M,rho_in,rho_out,m_dot)
rho=(rho_in+rho_out)/2
gpm=(m_dot/rho)*Convert('m^3/s','gal/min')

IF (M=1) AND (gpm<4) THEN
Pump=720
ELSE
IF (M=1) AND (gpm>=4) AND (gpm<25) THEN
Pump=3488
     ELSE
     IF (M=2) AND (gpm<4) THEN
     Pump=1899
          ELSE
          IF (M=2) AND (gpm>-4) AND (gpm<25) THEN
          Pump=6512
ELSE
Pump=1000000
          ENDIF
     ENDIF
ENDIF
ENDIF

END


Function ST(M,kW)
N=0

IF kW<=0 THEN
ST=0
N=10000
GOTO 10
ENDIF

IF M=1 THEN
ST=Interpolate('S&T Brass','kW','Price','kW'=kW)
ELSE
ST=Interpolate('S&T SS', 'kW','Price','kW'=kW)
ENDIF

10: end=N

END
```

```
Function Turb(P_in,P_out,P_R)
N=0

REPEAT
P=P_in/P_R
N=N+1
UNTIL (P<=P_in)

Turb=N*632.90 [$]

END


Procedure P_dep(P_t:A_1a,A_2a,A_3a)
P_turb=Convert('bar','kPa')*P_t

"Shell and Tube"
IF P_turb<1000[kPa] THEN
A_1a=1
A_2a=1
A_3a=1
ELSE
A_1a=1*P_turb/1000 "Linear"
A_2a=0.08333333*(P_turb/1000)^2+0.9166666667 "Polynomial"
A_3a= 4.316627*(P_turb/1000)^0.5-3.3166667 "Power Series"
ENDIF

"R22/Recuperator"
IF P_turb<3000 [kPa] THEN
A_1b=1
A_2b=1
A_3b=1
ELSE
A_1b=1*P_turb/1000-2 "linear"
A_2b=0.071428575*(P_turb/1000)^2+0.35742857 "Polynomial"
A_3b=5.04867559792*(P_turb/1000)^(0.5)-7.74456264654 "Power"
ENDIF

{
"Shell and Tube"
P_turb=Convert('bar','kPa')*P_t
IF P_turb<1000[kPa] THEN
A_1a=1
A_2a=1
A_3a=1
ELSE
A_1a=3*P_turb/1000-2 "Linear"
A_2a=0.6*(P_turb/1000)^2+0.4 "Polynomial"
A_3a= 9*(P_turb/1000)^0.5-8 "Power Series"
ENDIF

"R22/Recuperator"
P_t=Convert('bar','kPa')*P_turb
IF P_t<1000 [kPa] THEN
A_1b=1
A_2b=1
A_3b=1
ELSE
A_1b=2*P_t-5 "linear"
A_2b=0.2857*(P_t/1000)^2-1.5714 "Polynomial"
A_3b=7.4641*(P_t/1000)^(0.5)-11.9282 "Power"
ENDIF
}
{
"Shell and Tube: P_FT"
```

```
IF P_FT<3000 [kPa] THEN
A_1c=1
A_2c=1
A_3c=1
ELSE
A_1c=2*P_FT/1000-5 "linear"
A_2c=0.2857*(P_FT/1000)^2-1.5714 "Polynomial"
A_3c=7.4641*(P_FT/1000)^(0.5)-11.9282 "Power"
ENDIF}

END

"User Defined Variables"
eta_p=.7
eta_t=.85

P_abs=1 [bar]
P_turb=10 [bar]
T_source=ConvertTemp('C','K',425)
T_sink=(15+273.15) [K]
T_FT=(-0.0606*P_turb^2+5.4109*P_turb + 379.16) "This must be
within the range found from file FT Min/mas in Cycle/MR"
W_dot_net=14.7 [kW]

T_o=ConvertTemp('C','K',25)
P_o=Convert('kPa','bar')*101.35 [KPa]
b_o=enthalpy(air,T=T_o)-T_o*entropy(air,T=t_o,P=P_o)

Fluid2$='Dowtherm_Q'  "Source Fluid"
T_PP_Source=10 [K]
Fluid3$='Water'  "Sink Fluid"
T_PP_Sink= 10 [K]
P_sink=Convert('kPa','bar')*101.35 [kPa]

T_PPpre=10[K] "Pinch point on the preheater"
T_PPFT=10 [K]  "Sets the Difference between T[15] and T[3] on
the Flash Tank"
T_PPsuper=10 [K] "This is an imposed Pinch Point that is checked
 to make sure that T[13] is greater than T[5]"
T_PPabs=10[K]  "This is the pinch point used to calculate the
minimum flow rate for the sink stream (between States 12 and 10"
T_PPabsout=10[K] "This is the pinch point between the source
(state 11) and the abs outlet (state 1) and is used to
determine T_abs"
T_PPpci=5[K]
T_PPpco=5[K]
"!! I do not have subcooling as an option for the absorber outlet"

eta_B="1"0.97
eta_HX="1"0.97


//Material Selection: 1=Brass, 2=Stainless Steel
Material=2
C_FPcoll=C_PTC "[$/m^2]"
C_PTC=33" 44" [$/m^2]
eta_Coll=0.6" 0.65"
Q_dot_rad=1 [kW/m^2]

//States 5 and 6
//turbine Inlet and Exit
P[5]=P[6]
P[5]=P_turb
X[5]=X[6]
X[5]=X_WF
```

```
Call QualNH3(P_turb, P_abs, eta_t,x_WF: T_super,h[5],w_tact,h[6],
Qu[6],T[6],T[5],s[6],u[6],v[6],Qu[5],s[5],u[5],v[5])
ex[5]=h[5]-T_o*s[5]-b_o
ex[6]=h[6]-T_o*s[6]-b_o

//State 4
//Flash Tank Vapor Stream Outlet/Superheater Inlet
Call NH3H2O(128, T_FT, P_turb, 1: T[4], P[4], x[4], h[4],s[4],
u[4],v[4],Qu[4])
x[4]=x_WF
ex[4]=h[4]-T_o*s[4]-b_o

//State 7
//Flash Tank Dilute Stream Outlet
Call NH3H2O(128, T_FT,P_turb,0: T[7],P[7],x[7],h[7],s[7],
u[7],v[7],Qu[7])
X[7]=X_D
ex[7]=h[7]-T_o*s[7]-b_o

//State 1
//Absorber Outlet
T_abs=T_sink+T_PPabsout
Call NH3H2O(128, T_abs,P_abs,0: T[1],P[1],x[1],h[1],s[1],
u[1],v[1],Qu[1])
X[1]=X_B
ex[1]=h[1]-T_o*s[1]-b_o

//State 2
//Pump Outlet
Call NH3H2O(235, P_turb, x_B,s[1]: T_2s, P_2s, x_2s, h_2s,s_2s,
 u_2s, v_2s, Qu_2s)
w_p_s=h_2s-h[1] "v[1]*(P_turb-P[1])*(100 [kPa/bar])  vdP work for
 an isentropic pump."
w_pact=w_p_s/eta_p
h_2_act=w_pact+h[1]
Call NH3H2O(234, P_turb, x_B, h_2_act: T[2], P[2], x[2], h[2],s[2],
 u[2], v[2], Qu[2])
ex[2]=h[2]-T_o*s[2]-b_o

//Now State 8 is found through the imposed temperature constraint
Call HX_TPP2(P[2],T[2],h[2],x[2],m[2],P[7],T[7],h[7],x[7],
m[7],T_PPpre:
T_h_out,T_c_out)
//h[7]*m[7]+h[2]*m[2]=h_3*m[3]+h[8]*m[8]
Call NH3H2O(123, T_h_out, P_turb, x_D: T[8], P[8], x[8], h[8],s[8],
u[8], v[8], Qu[8])
ex[8]=h[8]-T_o*s[8]-b_o

//A mass balance must be completed to perform the heat balance to
find state 3"=
g=(X_B-X_D)/(X_WF-X_B)  "m_dot_WF/m_D"
W_dot_net=m_dot_WF*w_tact-(m_dot_WF/g+m_dot_WF)*w_pact
m_dot_WF=m[4]
m[4]=m[5]
m[5]=m[6]
m_dot_WF/g=m[7] "M_D"
m[7]=m[8]
m[8]=m[9]
m[7]+m[6]=m[10]
m[10]=m[1]
m[1]=m[2]
```

```
m[2]=m[3]

//State 3
//Heat Exchanger Outlet
Call NH3H2O(123,T_c_out, P_turb, x_B: T[3], P[3], x[3], h[3],s[3],
u[3], v[3], Qu[3])
ex[3]=h[3]-T_o*s[3]-b_o

//Throttling Valve
//State 9
Call NH3H2O(234,  P_abs, x_D,h[8]: T[9], P[9], x[9], h[9],s[9],
 u[9], v[9], Qu[9])
ex[9]=h[9]-T_o*s[9]-b_o

//Mixing State
//State 10
m[9]*h[9]+m[6]*h[6]=m[10]*h_10
Call NH3H2O(234,  P_abs, x_B,h_10: T[10], P[10], x[10], h[10],s[10],
 u[10], v[10], Qu[10])
ex[10]=h[10]-T_o*s[10]-b_o

//Heat and Work Terms
q_boil=h[4]+h[7]-h[3]
q_super=h[5]-h[4]

Q_dot_rec=m[3]*(h[3]-h[2])
Q_dot_Boiler=m[4]*h[4]+m[7]*h[7]-m[3]*h[3]
Q_dot_Super=m[5]*q_super
Q_dot_Solar=Q_dot_super/eta_HX+Q_dot_boiler/eta_B

Q_dot_Sink=m[1]*(h[10]-h[1])

eta_cyc=W_dot_net/(Q_dot_boiler+Q_dot_Super)

E_dot_AR=Q_dot_Boiler+Q_dot_Super-Q_dot_sink-W_dot_net
"Energy Accumulation Rate"

eta_carnot=1-T[1]/T[5]

eta_cyc_II=eta_cyc/eta_carnot

//Source Stream Calculations
T[13]=T_source
T_source_avg=(T[15]+T[13])/2
Cp_source=C_(Fluid2$,T_source_avg)

T[15]=T[7]+T_PP_source
m[15]=m_dot_source
m[14]=m[15]
m[13]=m[14]
h[15]=0 [kJ/kg] "Take this to be the reference point"
s[15]=0 [kJ/kg-K]
ex[15]=h[15]-T_o*s[15]-b_o
T[14]=Q_dot_boiler/(m_dot_source*Cp_source)+T[15]
DELTA_H_1415=Q_dot_boiler
DELTA_S_1415=Cp_source*ln(T[14]/T[15])
h[14]=h[15]+DELTA_H_1415/m_dot_source
s[14]=s[15]+DELTA_S_1415
ex[14]=h[14]-T_o*s[14]-b_o

Q_dot_super=Cp_source*m_dot_source*(T[13]-T[14])
DELTA_H_1314=Q_dot_super
h[13]=h[14]+DELTA_H_1314/m_dot_source
DELTA_S_1314=Cp_sink*(ln(T[13]/T[14]))
```

```
s[13]=s[14]+DELTA_S_1314
ex[13]=h[13]-T_o*s[13]-b_o

//Sink Stream Calculations
m[11]=m_dot_sink
m[11]=m[12]
T[11]=T_sink
T[12]=T[10]-T_PP_Sink
Cp_sink=Cp(air,T=t_sink)
Q_dot_sink=m_dot_sink*Cp_sink*(T[12]-T[11])
h[11]=enthalpy(air,T=T[11])
h[12]=enthalpy(air,T=T[12])
s[11]=entropy(air,T=T[11],P=P_sink)
s[12]=entropy(air,T=T[12],P=P_sink)
ex[11]=h[11]-T_o*s[11]-b_o
ex[12]=h[12]-T_o*s[12]-b_o

//Definition of the STOP functions
//STOP1 Checks that the temperautre at the source (T[13]) is
greater than the temperature at the superheater outlet (T[5])
STOP1=IF(T[5],(T_source-T_PPsuper),0,1,1111)
//STOP2 Checks to see that the superheat temperature is in the
range of the data set (max is 600 K)
STOP2=IF(600,T[5],1111,1,0)
// STOP3 Checks that T[10] is not less than T[1]
STOP3=IF(T[10],T[1],1111,1,0)
//STOP4 Checks to see that the FT temperature is less than the
superheat temperature
STOP4=IF(T[5],T_FT, 1111,1,0)
//STOP5 Checks that the temperature at 8 is greater than the
temperature at 2
STOP5=IF(T[8],(T[2]+T_PPpci),1111,1,0)
//STOP6 Checks that the temperature at 7 is greater than the
temperature at 3
STOP6=IF(T[7],(T[3]+T_PPpco),1111,1,0)
//Stop7 checks to make sure that the efficeicny if not greater
than carnot
STOP7=IF(eta_cyc,eta_Carnot,0,1,1111)

C_P=Pump(Material,1/v[1], 1/v[2],m_dot_WF) "Cost of the pump"
C_turb=Turb(P[6],P[7],3) "3 is the pressure ratio on the Garrett
 Turbine"
Area=Q_dot_solar/(eta_Coll*Q_dot_rad) "Area of the collector
accounting for efficiencies"
C_Coll=IF(T_source, 140, C_FPcoll,C_PTC,C_PTC)*Area "Cost of the
 collector"
C_Tracker=31.88[$/m^2]*Area "Cost of the tracker"
C_abs=ST(Material,Q_dot_sink) "Cost of the absorber"
C_B=ST(Material, Q_dot_Boiler) "Cost of the Boiler"
C_super=ST(Material, Q_dot_Super) "Cost of the Superheater"
C_rec=ST(Material,Q_dot_rec) "Cost of the recuperator/Preheater"

Call P_dep(P_turb:A_1a,A_2a, A_3a)


C_COL=C_coll+C_tracker
C_other=C_P+C_turb+C_abs+(C_B+C_rec+C_super)*A_3a
eff_multi=eta_cyc*eta_coll
```

```
C_not=C_P+C_turb+C_coll+C_tracker+C_abs+(C_B+C_rec+C_super)
C_tot_1=C_P+C_turb+C_coll+C_tracker+C_abs
+(C_B+C_rec+C_super)*A_1a
C_tot_2=C_P+C_turb+C_coll+C_tracker+C_abs
+(C_B+C_rec+C_super)*A_2a
C_tot_3=C_P+C_turb+C_coll+C_tracker+C_abs
+(C_B+C_rec+C_super)*A_3a

Z_not=C_not/eta_cyc
Z_1=C_tot_1/eta_cyc
Z_2=C_tot_2/eta_cyc
Z_3=C_tot_3/eta_cyc


//Entropy Analysis
//All of the work producing devices will be adiabatic
//The entropy generation within the system should be positive
 since this is not a reversible system (pump and turbine
 efficiencies)
//Pump
S_dot_gen_pump=m[2]*(s[2]-s[1])
I_dot_pump=m[1]*ex[1]-m[2]*ex[2]+m[2]*w_pact
I_dot_pump_multi=T_o*S_dot_gen_pump

//Preheater/Recuperator
//There is no heat crossing the boundary so Q_dot=0
S_dot_gen_Pre=m[3]*(s[3]-s[2])+m[8]*(s[8]-s[7])
I_dot_pre=m[2]*ex[2]+m[7]*ex[7]-m[3]*ex[3]-m[8]*ex[8]
I_dot_pre_multi=S_dot_gen_pre*T_o

//Valve
S_dot_gen_valve=m[9]*(s[9]-s[8])
I_dot_valve=m[8]*ex[8]-m[9]*ex[9]
I_dot_valve_multi=S_dot_gen_valve*T_o

//Boiler
T_eff_Boiler=(m[4]*h[4]+m[7]*h[7]-m[3]*h[3])/(+m[4]*s[4]
+m[7]*s[7]-m[3]*s[3])
S_dot_gen_Boiler=-Q_dot_boiler/T_eff_Boiler+m[4]*(s[4])
+m[7]*s[7]-m[3]*s[3]
I_dot_boiler_multi=S_dot_gen_boiler*T_o
I_dot_boiler=Q_dot_boiler*(1-T_o/T_eff_Boiler)+ex[3]*m[3]
-ex[4]*m[4]-ex[7]*m[7]

//Superheater
T_eff_Super=(h[5]-h[4])/(s[5]-s[4])
S_dot_gen_Super=-Q_dot_super/T_eff_super+m[5]*(s[5]-s[4])
I_dot_super=Q_dot_super*(1-T_o/T_eff_super)+m[4]*ex[4]
-m[5]*ex[5]
I_dot_super_multi=S_dot_gen_super*T_o

//Turbine
S_dot_gen_turbine=m[5]*(s[6]-s[5])
I_dot_turbine=m[5]*ex[5]-m[6]*ex[6]-w_tact*m[6]
I_dot_turbine_multi=S_dot_gen_turbine*T_o

//Absorber
T_eff_abs=(h[10]-h[1])/(s[10]-s[1])
S_dot_gen_abs=Q_dot_sink/T_eff_abs+m[1]*(s[1]-s[10])
I_dot_abs=-Q_dot_sink*(1-T_o/T_eff_abs)+m[10]*ex[10]
-m[1]*ex[1]
I_dot_abs_multi=S_dot_gen_abs*T_o
```

```
//Mixing
S_dot_gen_mixing=-m[9]*s[9]+s[10]*m[10]-m[6]*s[6]
I_dot_mixing=m[9]*ex[9]+m[6]*ex[6]-m[10]*ex[10]
I_dot_mixing_multi=S_dot_gen_mixing*T_o

S_dot_gen=S_dot_gen_pump+S_dot_gen_Pre+S_dot_gen_Boiler
+s_Dot_gen_super+S_dot_gen_abs+S_dot_gen_turbine
+S_dot_gen_Mixing

T_eff_L=T_eff_abs
(Q_dot_boiler+Q_dot_super)/T_eff_H=Q_dot_Boiler/T_eff_Boiler
+Q_dot_Super/T_eff_Super
eta_Check=(1-T_eff_L/T_eff_H)/(1+(T_eff_L*T_o*S_dot_gen)
/(T_o*W_dot_net))
```

B.4 Kalina I CAT Code

```
Procedure HX_TPP(P_c,T_c_in,h_c_in,x_c,P_h,T_h_in,h_h_in,
x_h,T_PP:T_h_out,T_c_out)
N=0
T_Hout=T_C_In+T_PP

10: N=N+1
IF T_Hout>=T_H_in THEN
T_H_out=T_h_in
T_c_out=T_c_in
h_H_out=h_h_in
h_C_out=h_h_in
ELSE
Call NH3H2O(123,T_Hout,P_H,x_H:T_h_out,P_h_out,x_h_out,
h_h_out,s_h_out,u_h_out,v_h_out,chi_h_out)
h_cout=h_c_in+(h_h_in-h_h_out)
Call NH3H2O(234,P_c,x_c,h_cout:T_c_out,P_c_out,x_c_out,
h_c_out,s_c_out,u_c_out,v_c_out,chi_c_out)
DELTA=T_H_in-T_c_out

IF DELTA<T_PP THEN
T_hout=T_hout+1[K]
GOTO 10
ENDIF

T_PP_cohi=T_h_in-T_c_out
T_PP_ciho=T_h_out-T_c_in

ENDIF
END

Procedure HX_TPP2(P_c,T_c_in,h_c_in,x_c,m_c,P_h,T_h_in,
h_h_in,x_h,m_h,T_PP:T_h_out,T_c_out)
N=0
$COMMON T_FT
T_Cout2=T_H_In-T_PP
T_Cout=IF(T_Cout2,T_FT,T_Cout2,T_FT,T_FT)

10: N=N+1
IF T_Cout<=T_C_in THEN
T_H_out=T_h_in
T_c_out=T_c_in
h_H_out=h_h_in
h_C_out=h_h_in
ELSE
Call NH3H2O(123,T_cout, P_c,x_c:T_c_out,P_c_out,x_c_out,
h_c_out,s_c_out,u_c_out,v_c_out,chi_c_out)
q_c=m_c*(h_c_out-h_c_in)
```

```
h_hout=h_h_in-q_c/m_h
Call NH3H2O(234,P_H,x_H,h_hout:T_h_out,P_h_out,x_h_out,
h_h_out,s_h_out,u_h_out,v_h_out,chi_h_out)
DELTA=T_h_out-T_c_in

IF DELTA<T_PP THEN
T_cout=T_cout-0.5[K]
GOTO 10
ENDIF

q_h=m_h*(h_h_in-h_h_out)

T_PP_cohi=T_h_in-T_c_out
T_PP_ciho=T_h_out-T_c_in

ENDIF
END


Procedure q_coll(h_pre_out,h_sat,h_boil_out,h_super_out:
 q_pre,q_boil,q_super)

IF (h_sat>h_pre_out) THEN
q_pre=h_sat-h_pre_out
q_boil=h_boil_out-h_sat
ELSE
q_pre=0
q_boil=h_boil_out-h_pre_out
ENDIF
q_super=h_super_out-h_boil_out

END


Function Pump(M,rho_in,rho_out,m_dot)
rho=(rho_in+rho_out)/2
gpm=(m_dot/rho)*Convert('m^3/s','gal/min')

IF (M=1) AND (gpm<4) THEN
Pump=720
ELSE
IF (M=1) AND (gpm>=4) AND (gpm<25) THEN
Pump=3488
     ELSE
     IF (M=2) AND (gpm<4) THEN
     Pump=1899
          ELSE
          IF (M=2) AND (gpm>-4) AND (gpm<25) THEN
          Pump=6512
ELSE
Pump=1000000
         ENDIF
     ENDIF
ENDIF
ENDIF

END


Function ST(M,kW)
N=0

IF kW<=0 THEN
ST=0
N=10000
GOTO 10
ENDIF

IF M=1 THEN
ST=Interpolate('S&T Brass','kW','Price','kW'=kW)
```

```
ELSE
ST=Interpolate('S&T SS', 'kW','Price','kW'=kW)
ENDIF

10: end=N

END

Function Turb(P_in,P_out,P_R)
N=0

REPEAT
P=P_in/P_R
N=N+1
UNTIL (P<=P_in)

Turb=N*632.90 [$]

END

Procedure P_dep(P_t,P_FTbar:A_1a,A_1b,A_2a,A_2b, A_3a,
A_3b,A_1c,A_2c,A_3c)
P_turb=Convert('bar','kPa')*P_t
P_FT=Convert('bar','kPa')*P_FTbar

IF P_turb<1000[kPa] THEN
A_1a=1
A_2a=1
A_3a=1
ELSE
A_1a=1*P_turb/1000 "Linear"
A_2a=0.08333333*(P_turb/1000)^2+0.9166666667 "Polynomial"
A_3a= 4.316627*(P_turb/1000)^0.5-3.3166667 "Power Series"
ENDIF

"R22/Recuperator"
IF P_turb<3000 [kPa] THEN
A_1b=1
A_2b=1
A_3b=1
ELSE
A_1b=1*P_turb/1000-2 "linear"
A_2b=0.071428575*(P_turb/1000)^2+0.35742857 "Polynomial"
A_3b=5.04867559792*(P_turb/1000)^(0.5)-7.74456264654 "Power"
ENDIF

"Shell and Tube: P_FT"
IF P_FT<1000[kPa] THEN
A_1c=1
A_2c=1
A_3c=1
ELSE
A_1c=1*P_FT/1000 "Linear"
A_2c=0.08333333*(P_FT/1000)^2+0.9166666667 "Polynomial"
A_3c= 4.316627*(P_FT/1000)^0.5-3.3166667 "Power Series"
ENDIF

END

//Define Cycle Parameters
//Define the turbine and absorber pressures
//P_turb=6 [bar]
P_abs=1.0 [bar]

//Define the ammonia Concentration in the working fluid
X_WF=0.426
```

```
//Define the Flash Tank Parameters
P_FT=3 [bar]
T_FT=342.5 [K]"ConvertTemp('C','K',66.1)"

//Define the sink and source temperatures
T_Sink1=ConvertTemp('C','K',25)
T_sink2=ConvertTemp('C','K',25)
T_Source=ConvertTemp('C','K',350)

//Define the net work output from the turbine
W_dot_net=14.7 [kW]

//Define the component efficiencies
eta_t=.8
eta_p1=.7
eta_p2=.7
eta_HX=0.8
eta_B=0.85


//Define the medium
T_o=ConvertTemp('C','K',25)
P_o=Convert('kPa','bar')*101.35[kPa]
b_o=enthalpy(air,T=T_o)-T_o*entropy(air,T=T_o,P=P_o)

//Material Selection: 1=Brass, 2=Stainless Steel
Material=2
C_FPcoll=C_PTC "[$/m^2]"
C_PTC=33 [$/m^2]
eta_Coll=.6
Q_dot_rad=1 [kW/m^2]


//Define the Pinch Point/Closest Approach Temperatures
//Pinch Points used in cycle calculations
T_PP=5 [K]
T_PPABSho=10 [K] "The pinch point between the hot stream
outlet T[1] and the cold stream inlet T[24] of the absorber"

T_PPpreci=10 [K] "The pinch point between the cold strem inlet
 at T[13] and the source stream outlet at T[32] of the
  Preheater"
T_FP3ho=10 [K] "The pinch point between the hot stream outlet
 T[26] and the cold stream inlet T[3] of the Flash Preheater II"
T_IPChi=10[K] "The pinch point between the hot stream inlet
T[9] and the cold stream outlet T[28] of the IPC"
T_IPCho=10 [K] "The pinck point between the hot stream outlet
 T[10] and the cold stream inlet T[27] on the IPC"
T_PPsource=10 [K] "The pinch point between the source T[29]
and the max cycle temp"

//Determine the basic concentration from the parameters at
the absorber (state 1)
T_1=T_sink1+T_PPABSho
P_1=P_abs
Call NH3H2O(128,T_1,P_1,0:T[1],P[1],x[1],h[1],s[1],u[1],v[1],Qu[1])
x_B=x[1]

//Determine the pump work (process 1 to 2)
Call NH3H2O(235, P_FT, x_B, s[1] : T_2s, P_2s, x_2s, h_2s,
s_2s, u_2s, v_2s, Qu_2s)
w_p1s=h_2s-h[1]   "v[1]*(P_FT-P[1])*(100 [kPa/bar])
```

```
vdP work for an isentropic pump."
w_p1act=w_p1s/eta_p1
h_2actinput=w_p1act+h[1]
Call NH3H2O(234, P_FT, x_B, h_2actinput: T[2], P[2], x[2],
 h[2],s[2], u[2], v[2], Qu[2])

//Determine the vapor and dilute concentrations and the inlet
 conditions to the Flash Tank (states 6,7 and 8)
Call NH3H2O(128,T_FT,P_FT,1:T[8],P[8],x[8],h[8],s[8],u[8],v[8],Qu[8])
x[8]=x_V
Call NH3H2O(128,T_FT,P_FT,0:T[20],P[20],x[20],h[20],s[20],
u[20],v[20],Qu[20])
x[20]=x_D
Call NH3H2O(123,T_FT,P_FT,x_B:T[6],P[6],x[6],h[6],s[6],
u[6],v[6],Qu[6])
//Note: Due to the way the mass flows are defined, the enthalpy
 balance on the FT is correct

//The intensive properties at 5 are equal to the intensive
 properties at 6 and 7.  The flow rates change.
T[6]=T[5]
P[6]=P[5]
x[6]=x[5]
h[6]=h[5]
s[6]=s[5]
u[6]=u[5]
v[6]=v[5]
Qu[6]=Qu[5]
T[7]=T[5]
P[7]=P[5]
x[7]=x[5]
h[7]=h[5]
s[7]=s[5]
u[7]=u[5]
v[7]=v[5]
Qu[7]=Qu[5]

//Define the mass balance terms
f=g*(X_V-X_D)/(X_V-X_B)
g=(X_WF-X_B)/(X_B-X_D)

"The normalized mass balance"
m[1]=m_dot_WF*(1+g)
m[2]=m_dot_WF*(1+g)
m[3]=(1+g)*m_dot_WF
m[4]=m_dot_WF*(1+g)
m[5]=m_dot_WF*(1+g)
m[6]=m_dot_WF*(1+g-f)
m[7]=f*m_dot_WF
m[8]=(m_dot_WF)*(f-g)
m[9]=m_dot_WF
m[10]=m_dot_WF
m[11]=m_dot_WF
m[12]=m_dot_WF
m[13]=m_dot_WF
m[14]=m_dot_WF
m[15]=m_dot_WF
m[16]=m_dot_WF
m[17]=m_dot_WF
m[18]=m_dot_WF
```

```
m[19]=m_dot_WF
m[20]=g*m_dot_WF
m[21]=g*m_dot_WF
m[22]=g*m_dot_WF
m[23]=m_dot_WF*(1+g)
m_dot_B=m[1]
m_dot_D=m[20]
m_dot_V=m[8]

//Starting at the boiler, it is known that the entrance to the
 boiler must be at P_turb and Qu=0 and the outlet at P_turb
 with Qu=1
Call NH3H2O(238,P_turb,x_WF,0:T_boil_sat,P_boil_sat,x_boil_sat,
h_boil_sat,s_boil_sat,u_boil_sat,v_boil_sat,Qu_boil_sat)
x_14=IF(T_boil_sat,T[13],Qu[13],0,0)
Call NH3H2O(238,P_turb,x_WF,x_14:T[14],P[14],x[14],h[14],s[14],
u[14],v[14],Qu[14])

Call NH3H2O(238,P_turb,x_WF,1:T[15],P[15],x[15],h[15],s[15],
u[15],v[15],Qu[15])

//The superheating and the turbine expansion processes are
determined in the procedure (included as a library file)
QualKal
Call QualKal(P_turb, P_abs, eta_t,x_WF: T_super,h_16,w_t_act,
h[17],Qu[17] ,T[17],T_16,s[17],u[17],v[17],P[17])
x[17]=x_WF
Call NH3H2O(123,T_16, P_turb,x_WF:T[16],P[16],x[16],h[16],
s[16],u[16],v[16],Qu[16])

//Flash Preheater 1: Define the properties at state 3 so that
 then state 18 can be determined
Call HX_TPP2(P[2],T[2],h[2],x[2],m[2],P[17],T[17],h[17],
x[17],m[17],T_PP:T_18, T_3)
//T_3=IF(T_3i,T_FT,T_3i,T_3i,T_FT)
Call NH3H2O(123, T_3,P_FT,x_B:T[3],P[3],x[3],h[3],s[3],
u[3],v[3],Qu[3])
Call NH3H2O(123,T_18, P_abs,x_WF:T[18],P[18],x[18],h[18],
s[18],u[18],v[18],Qu[18])

//m_dot_WF=0.03027 [kg/sec]

//Flash Preheater 2
Call HX_TPP2(P[3],T[3],h[3],x[3],m[3],P[20],T[20],h[20],
x[20],m[20],T_PP:T_21, T_4i) "!!!!"
Call NH3H2O(123,T_21, P_FT,x_D:T[21],P[21],x[21],h[21],
s[21],u[21],v[21],Qu[21])
T_4=IF(T_4i,T_FT,T_4i,T_FT,T_FT)
Call NH3H2O(123,T_4, P_FT,x_B:T[4],P[4],x[4],h[4],s[4],
u[4],v[4],Qu[4])

//The Valve is an adiabatic process (constant enthalpy)
Call NH3H2O(234, P_abs,x_D,h[21]:T[22],P[22],x[22],h[22],
s[22],u[22],v[22],Qu[22])

//Define the mixing process at state 9
m[9]*h_9=m[6]*h[6]+m[8]*h[8]
Call NH3H2O(234, P_FT,x_WF,h_9:T[9],P[9],x[9],h[9],s[9],
u[9],v[9],Qu[9])

//Pump 2: State 10 can also be determined because it must
 be at saturation for this low pressure as well a
 state 11
```

```
Call NH3H2O(238, P_FT,x_WF,0:T[10],P[10],x[10],h[10],
s[10],u[10],v[10],Qu[10])

//The pump will have be treated as isentropic to begin
Call NH3H2O(235, P_turb, x_WF, s[10]: T_11s, P_11s, x_11s,
 h_11s, s_11s, u_11s, v_11s, Qu_11s)
w_p2s=h_11s-h[10] "v[10]*(P_turb-P[10])*(100 [kPa/bar])
 Isentropic pump work"
w_p2act=w_p2s/eta_p2
h_11actinput=(w_p2act*m[11]+h[10]*m[10])/m[11]
Call NH3H2O(234, P_turb, x_WF, h_11actinput: T[11], P[11],
 x[11], h[11], s[11], u[11], v[11], Qu[11])

//IPC heat exchange
Call HX_TPP(P[11],T[11],h[11],x[11],P[9],T[9],h[9],x[9],
T_PP:T_int, T_12)
Call NH3H2O(123, T_12, P_turb, x_WF: T[12], P[12], x[12],
 h[12], s[12], u[12], v[12], Qu[12])
Call NH3H2O(123, T_int,P_FT,x_WF:T|star,P|star,x|star,
h|star,s|star,u|star,v|star,Qu|star)

//Recuperator: Define state 19 so that the Pinch point is
met and the recuperator cold stream outlet can be defined
(state 13)
Call HX_TPP(P[12],T[12],h[12],x[12],P[18],T[18],h[18],x[18],
T_PP:T_19, T_13"i")
//T_13=IF(T_13i,T[14],T_13i,T_13i,T[14])
Call NH3H2O(123, T_19, P_abs, x_WF: T[19], P[19], x[19],
h[19], s[19], u[19], v[19], Qu[19])
Call NH3H2O(123, T_13, P_turb, x_WF: T[13], P[13], x[13],
 h[13], s[13], u[13], v[13], Qu[13])

//Define the mixing state before the absorber (absorber
 inlet at state 23)
h[19]*m[19]+h[22]*m[22]=h_23*m[23]
Call NH3H2O(234, P_abs, x_B, h_23: T[23], P[23], x[23],
h[23], s[23], u[23], v[23], Qu[23])

//Define Heat and work terms
W_dot_net=m[16]*(h[16]-h[17])-m[2]*(h[2]-h[1])
-m[10]*(h[11]-h[10]) "this defined m_dot_WF"

Call q_coll(h[13],h[14],h[15],h[16]:q_pre,q_boiler,q_super)

q_check=m[11]*(h[12]-h[11])-Q_dot_IPC
q_check_2=m[9]*(h|star-h[10])-Q_dot_sink2
q_check_3=m[12]*(h[13]-h[12])-m[19]*(h[19]-h[18])
q_check_4=m[13]*(h[14]-h[13])-Q_dot_pre
q_check_5=m[14]*(h[15]-h[14])-Q_dot_Boiler
q_check_6=m[15]*(h[16]-h[15])-Q_dot_super
q_check_7=m[17]*(h[18]-h[17])+m[3]*(h[3]-h[2])
q_check_8=m[18]*(h[18]-h[19])-m[13]*(h[13]-h[12])
q_check_9=W_dot_net-m[16]*(h[16]-h[17])+m[2]*(h[2]
-h[1])+m[10]*(h[11]-h[10])
q_check_10=q_boiler+q_super+q_pre
q_check_11=(h[16]-h[13])
q_check_12=m[3]*(h[4]-h[3])-Q_dot_FP2
q_check_13=m[7]*h[7]-m[8]*h[8]-m[20]*h[20]

Q_dot_pre=m[13]*q_pre
Q_dot_boiler=m[14]*q_boiler
```

```
Q_dot_super=m[15]*q_super
Q_dot_solar=Q_dot_pre/eta_HX+Q_dot_Boiler/eta_B
+Q_dot_Super/eta_HX

Q_dot_in=Q_dot_pre+Q_dot_boiler+Q_dot_super+Q_dot_FP
eta_sys=W_dot_net/(Q_dot_in)
T_min=IF(T[1],T[10],T[1],T[1],T[10])
eta_carnot=(1-T_min/T[16])
eta_sys_2=eta_sys/eta_carnot

Q_dot_FP1=m[2]*(h[3]-h[2])
Q_dot_FP2=m[3]*(h[4]-h[3])
Q_dot_FP3=m[4]*(h[5]-h[4])
Q_dot_FP=IF(Q_dot_FP3,0.01,0,0,Q_dot_FP3)
Q_dot_sink1=m[1]*(h[23]-h[1])
Q_dot_Sink2=m[9]*(h|star-h[10])
Q_dot_IPC=m[9]*(h[9]-h|star)
Q_dot_Sink=Q_dot_Sink1+Q_dot_Sink2
Q_dot_rec=m[12]*(h[13]-h[12])

//Check on FT
Q_FT=m[20]*h[20]+m[8]*h[8]-m[7]*h[7]
Q_dot_Source=Q_dot_Boiler+Q_dot_Super+Q_dot_Pre
E_dot_AR=Q_dot_pre+Q_dot_Boiler+Q_dot_super
-Q_dot_sink-W_dot_net+Q_FT

//Source and Sink Calcs
T[29]=T_source
T[24]=T_sink1
T[27]=T_sink2

//STOP1: Checks to make sure that the absorber inlet
 T[23] is greater than the absorber outlet T[1]
STOP_1=IF(T[23],T[1],1311,1,0)
//STOP2: Checks to make sure that the hot stream sink
 inlet of the IPC T[27] is colder than the IPC
 cold stream outlet T[10]
STOP_2=IF(T[10],(T[27]+T_IPCho),1111,1,0)
//STOP3: Checks to make sure that the source inlet
T[29] is greater than the superheater outlet T[16]
STOP_3=IF(T[29],(T[16]+T_PPsource),1111,1,0)
//STOP4: Checks to make sure that the superheater
temperature does not exceed 600 K, the limit on the
data set
STOP_4=IF(600,T[16],1111,1,0)
//STOP5: carnot
STOP_5=IF(eta_carnot,eta_sys,1111,1,0)

//Quality Checks
Qual_1=IF(x_D,x_B,0,1,1111)
Qual_2=IF(x_B,x_WF,0,1,1111)
Qual_3=IF(x_WF,x_V,0,1,1111)

//Price Calcs

C_P1=Pump(Material,1/v[1], 1/v[2],m[1])
C_P2=Pump(Material,1/v[10], 1/v[11],m[10])
C_B=ST(Material, Q_dot_Boiler)
C_pre=IF(q_pre,0,0,0,1)*Interpolate('R22HX','kW','Price',
'kW'=Q_dot_Pre)
C_super=ST(Material, Q_dot_Super)
```

```
C_rec=ST(Material,Q_dot_Rec)
C_FP1=ST(Material, Q_dot_FP1)
C_FP2=ST(Material,Q_dot_FP2)
C_FP3=ST(Material,Q_dot_FP3)
C_sink1=ST(Material,Q_dot_sink1)
C_sink2=ST(Material,Q_dot_sink2)
C_IPC=ST(Material,Q_dot_IPC)
C_FT=Max(C_IPC,C_sink1,C_sink2,C_FP3,C_FP2,C_FP1,
C_super,C_B,C_Pre)

C_turb=Turb(P[6],P[7],3) "3 is the pressure ratio on the
Garrett Turbine"
Area=Q_dot_solar/(eta_Coll*Q_dot_rad)
C_Coll=IF(T_source, 140, C_FPcoll,C_PTC,C_PTC)*Area
C_Tracker=31.88[$/m^2]*Area

Call P_dep(P_turb,P_FT:A_1a,A_1b,A_2a,A_2b, A_3a,A_3b,A_1c,
A_2c,A_3c)

C_tot_1=C_P1+C_P2+C_turb+C_coll+C_tracker+C_sink1+C_FT
+A_1a*C_pre+(C_B+C_rec+C_super+C_IPC+C_sink2)*A_1b
+(C_FP1+C_FP2+C_FP3)*A_1c
C_tot_2=C_P1+C_P2+C_turb+C_coll+C_tracker+C_sink1+C_FT
+A_2a*C_pre+(C_B+C_rec+C_super+C_IPC+C_sink2)*A_2b
+(C_FP1+C_FP2+C_FP3)*A_2c
C_tot_3=C_P1+C_P2+C_turb+C_coll+C_tracker+C_sink1+C_FT
+A_3a*C_pre+(C_B+C_rec+C_super+C_IPC+C_sink2)*A_3b
+(C_FP1+C_FP2+C_FP3)*A_3c

Z_1=C_tot_1/eta_sys
Z_2=C_tot_2/eta_sys
Z_3=C_tot_3/eta_sys

{
flow_1=v[2]*m[2]
flow=flow_1*Convert('m^3/sec','L/min')
flow_GPm=flow*Convert('L/min','gal/min')}

//Entropy Generation
ex[1]=h[1]-T_o*s[1]-b_o
ex[2]=h[2]-T_o*s[2]-b_o
ex[3]=h[3]-T_o*s[3]-b_o
ex[4]=h[4]-T_o*s[4]-b_o
ex[5]=h[5]-T_o*s[5]-b_o
ex[6]=h[6]-T_o*s[6]-b_o
ex[7]=h[7]-T_o*s[7]-b_o
ex[8]=h[8]-T_o*s[8]-b_o
ex[9]=h[9]-T_o*s[9]-b_o
ex[10]=h[10]-T_o*s[10]-b_o
ex[11]=h[11]-T_o*s[11]-b_o
ex[12]=h[12]-T_o*s[12]-b_o
ex[13]=h[13]-T_o*s[13]-b_o
ex[14]=h[14]-T_o*s[14]-b_o
ex[15]=h[15]-T_o*s[15]-b_o
ex[16]=h[16]-T_o*s[16]-b_o
ex[17]=h[17]-T_o*s[17]-b_o
ex[18]=h[18]-T_o*s[18]-b_o
ex[19]=h[19]-T_o*s[19]-b_o
ex[20]=h[20]-T_o*s[20]-b_o
ex[21]=h[21]-T_o*s[21]-b_o
ex[22]=h[22]-T_o*s[22]-b_o
ex[23]=h[23]-T_o*s[23]-b_o
```

```
//Pump
S_dot_gen_pump1=m[1]*(s[2]-s[1])
I_dot_pump1=m[1]*ex[1]-m[2]*ex[2]+w_p1act*m[2]
I_dot_pump1_multi=T_o*S_dot_gen_pump1

//Flash Preheater 1
S_dot_gen_FP1=m[2]*(s[3]-s[2])+m[17]*(s[18]-s[17])
I_dot_FP1=m[2]*ex[2]+m[17]*ex[17]-m[3]*ex[3]-m[18]*ex[18]
I_dot_FP1_multi=S_dot_gen_FP1*T_o

//Flash Preheater 2
S_dot_gen_FP2=m[4]*(s[4]-s[3])+m[20]*(s[21]-s[20])
I_dot_FP2=m[3]*ex[3]+m[20]*ex[20]-m[21]*ex[21]-m[4]*ex[4]
I_dot_FP2_Multi=S_dot_gen_FP2*T_o

//Flash Preheater 3
DELTA_s_45=IF(s[5]-s[4],0.001,0.001,0.001,s[5]-s[4])
T_eff_FP3=IF(T[4]-T[5],0.01,T[4],T[4],(h[5]-h[4])/DELTA_s_45)
S_dot_gen_FP3=Q_dot_FP3/T_eff_FP3+m[5]*s[5]-m[4]*s[4]
I_dot_FP3=Q_dot_FP3*(1-T_o/T_eff_FP3)+m[4]*ex[4]-m[5]*ex[5]
I_dot_FP3_multi=S_dot_gen_FP3*T_o

//Flash Tank
//Assume this is an adiabatic process
S_dot_gen_FT=m[8]*s[8]+m[20]*s[20]-m[7]*s[7]
I_dot_FT=-m[20]*ex[20]-m[8]*ex[8]+m[7]*ex[7]
I_dot_FT_multi=S_dot_gen_FT*T_o

//Mixing 1
S_dot_gen_mix1=m[9]*s[9]-m[8]*s[8]-m[6]*s[6]
I_dot_mix1=m[6]*ex[6]+m[8]*ex[8]-m[9]*ex[9]
I_dot_mix1_multi=T_o*S_dot_gen_mix1


//IPC
S_dot_gen_IPC1=m[10]*s|star+m[12]*s[12]-m[9]*s[9]-m[11]*s[11]
I_dot_IPC1=m[11]*ex[11]-m[12]*ex[12]+m[9]*ex[9]
-m[10]*(h|star-T_o*s|star-b_o)
I_dot_IPC1_multi=T_o*S_dot_gen_IPC1

T_eff_IPC=(h[10]-h|star)/(s[10]-s|star)
S_dot_gen_IPC2=Q_dot_sink2/T_eff_IPC-m[9]*s|star
+m[10]*s[10]
I_dot_IPC2=-Q_dot_sink2*(1-T_o/T_eff_IPC)+m[10]*(h|star
-T_o*s|star-b_o)-m[10]*ex[10]
I_dot_IPC2_multi=T_o*S_dot_gen_IPC2

I_dot_IPC=I_dot_IPC1+I_dot_IPC2

S_dot_gen_IPC=S_dot_gen_IPC1+S_dot_gen_IPC2

//Pump2
S_dot_gen_pump2=m[10]*(s[11]-s[10])
I_dot_pump2=m[10]*ex[10]-m[11]*ex[11]+w_p2act*m[11]
I_dot_pump2_multi=T_o*S_dot_gen_pump2

//Recuperator
//Assumed Adiabatic
S_dot_gen_recup=m[13]*(s[13]-s[12])+m[18]*(s[19]-s[18])
I_dot_recup=m[12]*ex[12]-m[13]*ex[13]+m[18]*ex[18]
-m[19]*ex[19]
I_dot_recup_multi=T_o*S_dot_gen_recup

//Preheater
T_eff_pre=(h[14]-h[13])/(s[14]-s[13])
```

```
S_dot_gen_pre=IF(T[14],T[13],0,0,-Q_dot_pre/T_eff_pre
+m[13]*(s[14]-s[13]))
I_dot_pre=IF(T[14],T[13],0,0,Q_dot_pre*(1-T_o/T_eff_pre)
+m[13]*ex[13]-m[14]*ex[14])
I_dot_pre_multi=T_o*S_dot_gen_pre

//Boiler
T_eff_boiler=(h[15]-h[14])/(s[15]-s[14])
S_dot_gen_boiler=-Q_dot_boiler/T_eff_boiler+m[14]*(s[15]-s[14])
I_dot_boiler=Q_dot_boiler*(1-T_o/T_eff_boiler)
-m[15]*ex[15]+m[14]*ex[14]
I_dot_boiler_multi=T_o*S_dot_Gen_boiler

//Superheater
T_eff_super=(h[16]-h[15])/(s[16]-s[15])
S_dot_gen_super=-Q_dot_super/T_eff_super+m[15]*(s[16]-s[15])
I_dot_super=Q_dot_super*(1-T_o/T_eff_super)+m[15]*ex[15]
-m[16]*ex[16]
I_dot_super_multi=T_o*S_dot_Gen_super

//Turbine
S_dot_gen_turb=m[16]*(s[17]-s[16])
I_dot_turb=m[16]*ex[16]-m[17]*ex[17]-w_t_act*m[16]
I_dot_turb_multi=T_o*S_dot_Gen_turb

//Valve
//Assumed adiabatic
S_dot_gen_valve=m[22]*(s[22]-s[21])
I_dot_valve=m[21]*ex[21]-m[22]*ex[22]
I_dot_valve_multi=T_O*S_dot_gen_valve

//Second Mixing State
S_dot_gen_mix2=m[23]*s[23]-m[22]*s[22]-m[19]*s[19]
I_dot_mix2=m[19]*ex[19]+m[22]*ex[22]-m[23]*ex[23]
I_dot_mix2_multi=T_o*S_dot_gen_mix2

//Absorber
T_eff_abs=(h[1]-h[23])/(s[1]-s[23])
S_dot_gen_abs=Q_dot_sink1/T_eff_abs+m[23]*(s[1]-s[23])
I_dot_abs=-Q_dot_sink1*(1-T_o/T_eff_abs)+m[23]*ex[23]
-m[1]*ex[1]
I_dot_abs_multi=T_o*S_dot_gen_abs

S_dot_gen=S_dot_gen_pump1+S_dot_gen_FP1+S_dot_gen_FP2
+S_dot_gen_FP3+S_dot_Gen_FT+S_dot_gen_mix1
+S_dot_gen_IPC+S_dot_gen_pump2+S_dot_gen_recup
+S_dot_gen_pre+S_dot_gen_boiler+S_dot_gen_super
+S_dot_gen_turb+S_dot_gen_valve+S_dot_gen_abs
+S_dot_gen_mix2
I_dot=I_dot_pump1+I_dot_FP1+I_dot_FP2+I_dot_FP3+I_dot_FT
+I_dot_mix1+I_dot_IPC+I_dot_pump2+I_dot_recup
+I_dot_pre+I_dot_boiler+I_dot_super+I_dot_turb
+I_dot_valve+I_dot_abs+I_dot_mix2
I_dot_calc=S_dot_gen*T_o
(Q_dot_pre+Q_dot_Boiler+Q_dot_Super)/T_eff_H=
Q_dot_pre/T_eff_pre+Q_dot_boiler/T_eff_boiler
+Q_dot_super/T_eff_Super
(Q_dot_sink1+Q_dot_sink2)/T_eff_L=Q_dot_sink1/T_eff_abs
+Q_dot_sink2/T_eff_IPC
eta_Check=(1-T_eff_L/T_eff_H)/(1+(T_eff_L*S_dot_gen)
/(W_dot_net))
```

```
eta_check_2=(1-T_eff_L/T_eff_H)-(T_eff_L*S_dot_gen)
/(Q_dot_pre+Q_dot_Boiler+Q_dot_Super+Q_dot_FP)
```

B.5 Kalina II CAT Code

```
Procedure HX_TPP(P_c,T_c_in,h_c_in,x_c,P_h,T_h_in,h_h_in,
x_h,T_PP:T_h_out,T_c_out)
N=0
T_Hout=T_C_In+T_PP

10: N=N+1
IF T_Hout>=T_H_in THEN
T_H_out=T_h_in
T_c_out=T_c_in
h_H_out=h_h_in
h_C_out=h_h_in
ELSE
Call NH3H2O(123,T_Hout,P_H,x_H:T_h_out,P_h_out,x_h_out,
h_h_out,s_h_out,u_h_out,v_h_out,chi_h_out)
h_cout=h_c_in+(h_h_in-h_h_out)
Call NH3H2O(234,P_c,x_c,h_cout:T_c_out,P_c_out,x_c_out,
h_c_out,s_c_out,u_c_out,v_c_out,chi_c_out)
DELTA=T_H_in-T_c_out

IF DELTA<T_PP THEN
T_hout=T_hout+1[K]
GOTO 10
ENDIF

T_PP_cohi=T_h_in-T_c_out
T_PP_ciho=T_h_out-T_c_in

ENDIF
END

Procedure HX_TPP2(P_c,T_c_in,h_c_in,x_c,m_c,P_h,T_h_in,
h_h_in,x_h,m_h,T_PP:T_h_out,T_c_out)
N=0
T_Hout=T_C_In+T_PP

10: N=N+1
IF T_Hout>=T_H_in THEN
T_H_out=T_h_in
T_c_out=T_c_in
h_H_out=h_h_in
h_C_out=h_h_in
ELSE
Call NH3H2O(123,T_Hout,P_H,x_H:T_h_out,P_h_out,x_h_out,
h_h_out,s_h_out,u_h_out,v_h_out,chi_h_out)
h_cout=(m_c*h_c_in+m_h*(h_h_in-h_h_out))/m_c
Call NH3H2O(234,P_c,x_c,h_cout:T_c_out,P_c_out,x_c_out,
h_c_out,s_c_out,u_c_out,v_c_out,chi_c_out)
DELTA=T_H_in-T_c_out

IF DELTA<T_PP THEN
T_hout=T_hout+1[K]
GOTO 10
ENDIF

T_PP_cohi=T_h_in-T_c_out
T_PP_ciho=T_h_out-T_c_in

ENDIF
END
```

```
Procedure q_coll(h_pre_out,h_sat,h_boil_out,h_super_out:
 q_pre,q_boil,q_super)
IF (h_sat>h_pre_out) THEN
q_pre=h_sat-h_pre_out
q_boil=h_boil_out-h_sat
ELSE
q_pre=0
q_boil=h_boil_out-h_pre_out
ENDIF
q_super=h_super_out-h_boil_out
END

Function Pump(M,rho_in,rho_out,m_dot)
rho=(rho_in+rho_out)/2
gpm=(m_dot/rho)*Convert('m^3/s','gal/min')
IF (M=1) AND (gpm<4) THEN
Pump=720
ELSE
IF (M=1) AND (gpm>=4) AND (gpm<25) THEN
Pump=3488
     ELSE
     IF (M=2) AND (gpm<4) THEN
     Pump=1899
          ELSE
          IF (M=2) AND (gpm>-4) AND (gpm<25) THEN
          Pump=6512
ELSE
Pump=1000000
          ENDIF
     ENDIF
ENDIF
ENDIF

END

Function ST(M,kW)
N=0
IF kW<=0 THEN
ST=0
N=10000
GOTO 10
ENDIF
IF M=1 THEN
ST=Interpolate('S&T Brass','kW','Price','kW'=kW)
ELSE
ST=Interpolate('S&T SS', 'kW','Price','kW'=kW)
ENDIF
10: end=N
END

Function Turb(P_in,P_out,P_R)
N=0
REPEAT
P=P_in/P_R
N=N+1
UNTIL (P<=P_in)
Turb=N*632.90 [$]
```

```
END

Procedure P_dep(P_t,P_FTbar:A_1a,A_1b,A_2a,A_2b, A_3a,
A_3b,A_1c,A_2c,A_3c)
P_turb=Convert('bar','kPa')*P_t
P_FT=Convert('bar','kPa')*P_FTbar

"Shell and Tube"
IF P_turb<1000[kPa] THEN
A_1a=1
A_2a=1
A_3a=1
ELSE
A_1a=1*P_turb/1000 "Linear"
A_2a=0.08333333*(P_turb/1000)^2+0.9166666667 "Polynomial"
A_3a= 4.316627*(P_turb/1000)^0.5-3.3166667 "Power Series"
ENDIF

"R22/Recuperator"
IF P_turb<3000 [kPa] THEN
A_1b=1
A_2b=1
A_3b=1
ELSE
A_1b=1*P_turb/1000-2 "linear"
A_2b=0.071428575*(P_turb/1000)^2+0.35742857 "Polynomial"
A_3b=5.04867559792*(P_turb/1000)^(0.5)-7.74456264654 "Power"
ENDIF

{
"Shell and Tube"
IF P_turb<1000[kPa] THEN
A_1a=1
A_2a=1
A_3a=1
ELSE
A_1a=3*P_turb/1000-2 "Linear"
A_2a=0.6*(P_turb/1000)^2+0.4 "Polynomial"
A_3a= 9*(P_turb/1000)^0.5-8 "Power Series"
ENDIF

"R22/Recuperator"
IF P_turb<3000 [kPa] THEN
A_1b=1
A_2b=1
A_3b=1
ELSE
A_1b=2*P_turb/1000-5 "linear"
A_2b=0.2857*(P_turb/1000)^2-1.5714 "Polynomial"
A_3b=7.4641*(P_turb/1000)^(0.5)-11.9282 "Power"
ENDIF
}

"Shell and Tube: P_FT"
IF P_FT<1000[kPa] THEN
A_1c=1
A_2c=1
A_3c=1
ELSE
A_1c=1*P_FT/1000 "Linear"
A_2c=0.08333333*(P_FT/1000)^2+0.9166666667 "Polynomial"
A_3c= 4.316627*(P_FT/1000)^0.5-3.3166667 "Power Series"
ENDIF

END
```

```
//Define Cycle Parameters
//Define the turbine and absorber pressures
P_turb=10 [bar]
P_abs=1.0 [bar]

//Define the ammonia Concentration in the working fluid
X_WF=0.426

//Define the Flash Tank Parameters
P_FT=3 [bar]
T_FT=ConvertTemp('C','K',75)

//Define the sink and source temperatures
T_Sink1=ConvertTemp('C','K',25)
T_sink2=ConvertTemp('C','K',25)
T_Source=ConvertTemp('C','K',325)

//Define the medium
T_o=ConvertTemp('C','K',25)
P_o=Convert('kPa','bar')*101.35[kPa]
b_o=enthalpy(air,T=T_o)-T_o*entropy(air,T=T_o,P=P_o)

//Define the net work output from the turbine
W_dot_net="763.4 "14.7 [kW]

//Define the component efficiencies
eta_t=0.85
eta_p1=.7
eta_p2=.7
eta_HX="1"0.97
eta_B="1"0.97

//Material Selection: 1=Brass, 2=Stainless Steel
Material=2
C_FPcoll=C_PTC "[$/m^2]"
C_PTC=33"44" [$/m^2]
eta_Coll=.6" 0.65"
Q_dot_rad=1 [kW/m^2]


//Define the Pinch Point/Closest Approach Temperatures
//Pinch Points used in cycle calculations
T_PP=5 [K]
T_PPABSho=10 [K] "The pinch point between the hot stream
outlet T[1] and the cold stream inlet T[??] of the
absorber"

T_PPpreci=10 [K] "The pinch point between the cold strem
inlet at T[13] and the source stream outlet at T[32]
of the Preheater"
T_FP3ho=10 [K] "The pinch point between the hot stream
outlet T[26] and the cold stream inlet T[3] of the
Flash Preheater II"
T_IPChi=10[K] "The pinch point between the hot stream
inlet T[9] and the cold stream outlet T[28] of the
IPC"
T_IPCho=10 [K] "The pinck point between the hot stream
outlet T[10] and the cold stream inlet T[27] on the IPC"
T_PPsource=10 [K] "The pinch point between the source T[29]
and the max cycle temp"
//T_PPFP3=5 [K] "The pinch point beteen T[25] and T[5]"}

//Determine the basic concentration from the parameters at
 the absorber (state 1)
T_1=T_sink1+T_PPABSho
```

```
P_1=P_abs
Call NH3H2O(128,T_1,P_1,0:T[1],P[1],x[1],h[1],s[1],u[1],
v[1],Qu[1])
x_B=x[1]
ex[1]=h[1]-T_o*s[1]-b_o

//Determine the pump work (process 1 to 2)
Call NH3H2O(235, P_FT, x_B, s[1] : T_2s, P_2s, x_2s,
 h_2s,s_2s, u_2s, v_2s, Qu_2s)
w_p1s=h_2s-h[1]   "v[1]*(P_FT-P[1])*(100 [kPa/bar])
 vdP work for an isentropic pump."
w_p1act=w_p1s/eta_p1
h_2actinput=w_p1act+h[1]
Call NH3H2O(234, P_FT, x_B, h_2actinput: T[2], P[2], x[2],
 h[2],s[2], u[2], v[2], Qu[2])
ex[2]=h[2]-T_o*s[2]-b_o

//Determine the WF concentration from the condensation
parameters for state 8
Call NH3H2O(238, P_FT,x_WF,0:T[8], P[8], x[8], h[8],s[8],
 u[8], v[8], Qu[8])
ex[8]=h[8]-T_o*s[8]-b_o

//Determine the pump work (process 8 to 9)
Call NH3H2O(235, P_turb, x_WF, s[8] : T_9s, P_9s, x_9s,
h_9s,s_9s, u_9s, v_9s, Qu_9s)
w_p2s=h_9s-h[8]   "v[1]*(P_FT-P[1])*(100 [kPa/bar])
 vdP work for an isentropic pump."
w_p2act=w_p2s/eta_p2
h_9actinput=w_p2act+h[8]
Call NH3H2O(234, P_FT, x_WF, h_9actinput: T[9], P[9],
x[9], h[9],s[9], u[9], v[9], Qu[9])
ex[9]=h[9]-T_o*s[9]-b_o

//Determine the preheater input heat (process 9 to 10)
Call NH3H2O(238, P_turb,x_WF,0:T[10],P[10],x[10],h[10],
s[10],u[10],v[10],Qu[10])
ex[10]=h[10]-T_o*s[10]-b_o

//Detemine the evaporator input heat (process 10 to 11)
Call NH3H2O(238, P_turb,x_WF,1:T[11],P[11],x[11],h[11],
s[11],u[11],v[11],Qu[11])
ex[11]=h[11]-T_o*s[11]-b_o

//Determine the superheat input heat
//Determine the turbine specific work (process 12 to 13)
Call QualKal(P_turb, P_abs, eta_t,x_WF: T_super,h_12,w_t_act,
h[13],Qu[13] ,T[13],T_12,s[13],u[13],v[13],P[13])
x[13]=x_WF
Call NH3H2O(123,T_12, P_turb,x_WF:T[12],P[12],x[12],h[12],
s[12],u[12],v[12],Qu[12])
ex[12]=h[12]-T_o*s[12]-b_o
ex[13]=h[13]-T_o*s[13]-b_o

//w_net=w_t_act-w_p1act-w_p2act
//m_dot_WF=W_dot_net/w_net
W_dot_net=m_dot_WF*w_t_act-w_p1act*m_dot_WF*(1+g)
-w_p2act*m_dot_WF

//Determine the vapor and dilute concentrations and the
 inlet conditions to the Flash Tank (states 6,7 and 8)
```

```
Call NH3H2O(128,T_FT,P_FT,1:T[6],P[6],x[6],h[6],s[6],
u[6],v[6],Qu[6])
x[6]=x_V
ex[6]=h[6]-T_o*s[6]-b_o
Call NH3H2O(128,T_FT,P_FT,0:T[15],P[15],x[15],h[15],s[15],
u[15],v[15],Qu[15])
x[15]=x_D
ex[15]=h[15]-T_o*s[15]-b_o
//Call NH3H2O(123,T_FT,P_FT,x_B:T[6],P[6],x[6],h[6],s[6],
u[6],v[6],Qu[6])

//The intensive properties at 2 are equal to the intensive
 properties at 3 and 4.  The flow rates change.
T[3]=T[2]
P[3]=P[2]
x[3]=x[2]
h[3]=h[2]
s[3]=s[2]
u[3]=u[2]
v[3]=v[2]
Qu[3]=Qu[2]
ex[3]=ex[2]
T[4]=T[2]
P[4]=P[2]
x[4]=x[2]
h[4]=h[2]
s[4]=s[2]
u[4]=u[2]
v[4]=v[2]
Qu[4]=Qu[2]
ex[4]=ex[2]

//Define the mass balance terms
f=g*(X_V-X_D)/(X_V-X_B)
g=(X_WF-X_B)/(X_B-X_D)

"The normalized mass balance"
m[1]=m_dot_WF*(1+g)
m[2]=m_dot_WF*(1+g)
m[3]=m_dot_WF*(1+g-f)
m[4]=f*(m_dot_WF)
m[5]=f*(m_dot_WF)
m[6]=(f-g)*m_dot_WF
m[7]=m_dot_WF
m[8]=m_dot_WF
m[9]=m_dot_WF
m[10]=m_dot_WF
m[11]=m_dot_WF
m[12]=m_dot_WF
m[13]=m_dot_WF
m[14]=m_dot_WF
m[15]=g*m_dot_WF
m[16]=g*m_dot_WF
m[17]=m_dot_WF*(1+g)
m_dot_B=m[1]
m_dot_D=m[15]
m_dot_V=m[6]

//Flash Preheater
//Since the FT temperature is defined (state 5), the inlet
 to the cold side (state 4) and the turbine hot side inlet,
 a simple entahlpy balance yields state 14
```

```
Call NH3H2O(123, T_FT,P_FT,X_B:T[5],P[5],x[5],h[5],s[5],
u[5],v[5],Qu[5])
ex[5]=h[5]-T_o*s[5]-b_o
h_14*m[14]+h[5]*m[5]=h[4]*m[4]+h[13]*m[13]
Call NH3H2O(234,P_abs,x_WF,h_14:T[14],P[14],x[14],h[14],s[14],
u[14],v[14],Qu[14])
ex[14]=h[14]-T_o*s[14]-b_o

//Mixing at State 7
h_7*m[7]=m[6]*h[6]+m[3]*h[3]
Call NH3H2O(234,P_FT,x_WF,h_7:T[7],P[7],x[7],h[7],s[7],
u[7],v[7],Qu[7])
ex[7]=h[7]-T_o*s[7]-b_o

//Throttling Valve
Call NH3H2O(234,P_abs,x_D,h[15]:T[16],P[16],x[16],h[16],
s[16],u[16],v[16],Qu[16])
ex[16]=h[16]-T_o*s[16]-b_o

//Mixing at State 17
h_17*m[17]=h[16]*m[16]+h[14]*m[14]
Call NH3H2O(234,P_abs,x_B,h_17:T[17],P[17],x[17],h[17],
s[17],u[17],v[17],Qu[17])
ex[17]=h[17]-T_o*s[17]-b_o

Call q_coll(h[9],h[10],h[11],h[12]:q_pre,q_boiler,q_super)
Q_dot_pre=m[11]*q_pre
Q_dot_boiler=m[12]*q_boiler
Q_dot_super=m[13]*q_super
Q_dot_Sink_1=m[1]*(h[17]-h[1])
Q_dot_Sink_2=m[8]*(h[7]-h[8])
Q_dot_in=Q_dot_pre+Q_dot_boiler+Q_dot_super
Q_dot_rec=m[13]*(h[13]-h[14])
Q_dot_FP1=m[4]*(h[5]-h[4])
Q_dot_IPC=m[7]*(h[7]-h[8])


eta_sys=W_dot_net/(m[11]*(h[12]-h[9]))

FT_CHECK=-m[5]*h[5]+m[6]*h[6]+m[15]*h[15]
STOP_1=IF(FT_CHECK,0.001,0,0,11111)
STOP_2=IF(T[12],T_source-T_PP,0,0,1111)

Q_dot_solar=Q_dot_pre/eta_HX+Q_dot_Boiler/eta_B
+Q_dot_Super/eta_HX
E_dot_AR=Q_dot_in-Q_dot_sink_1-W_dot_net-Q_dot_sink_2
Q_mixing=-m[6]*h[6]+m[7]*h[7]-m[3]*h[3]

eta_Carnot=1-(T[1]/T[12])
eta_sys_2=eta_sys/eta_carnot

eta_sys_93=0.93*eta_sys

//STOP1: Checks to make sure that the absorber inlet T[23]
is greater than the absorber outlet T[1]
STOP_3=IF(T[17],T[1],1311,1,0)
//STOP2: Checks to make sure that the hot stream sink inlet of
the IPC T[27] is colder than the IPC cold stream outlet T[10]
//STOP_4=IF(T[10],(T_source+T_IPCho),1111,1,0)
//STOP3: Checks to make sure that the source inlet T[29] is
greater than the superheater outlet T[16]
//STOP_5=IF(T[29],(T[16]+T_PPsource),1111,1,0)
//STOP4: Checks to make sure that the superheater temperature
does not exceed 600 K, the limit on the data set
```

```
//STOP_6=IF(600,T[16],1111,1,0)
//STOP5: carnot
//STOP_7=IF(eta_carnot,eta_sys,1111,1,0)

//Quality Checks
Qual_1=IF(x_D,x_B,0,1,1111)
Qual_2=IF(x_B,x_WF,0,1,1111)
Qual_3=IF(x_WF,x_V,0,1,1111)

//Price Calcs

C_P1=Pump(Material,1/v[1], 1/v[2],m[1])
C_P2=Pump(Material,1/v[10], 1/v[11],m[10])
C_B=ST(Material, Q_dot_Boiler)
C_pre=IF(q_pre,0,0,0,1)*Interpolate('R22HX','kW','Price',
'kW'=Q_dot_Pre)
C_super=ST(Material, Q_dot_Super)
C_rec=ST(Material,Q_dot_Rec)
C_FP1=ST(Material, Q_dot_FP1)
//C_FP2=ST(Material,Q_dot_FP2)
//C_FP3=ST(Material,Q_dot_FP3)
C_sink1=ST(Material,Q_dot_sink_1)
C_sink2=ST(Material,Q_dot_sink_2)
C_IPC=ST(Material,Q_dot_IPC)
C_FT=Max(C_sink1,C_sink2,C_super,C_B,C_Pre)

C_turb=Turb(P[6],P[7],3) "3 is the pressure ratio on the
Garrett Turbine"
Area=Q_dot_solar/(eta_Coll*Q_dot_rad)
C_Coll=IF(T_source, 140, C_FPcoll,C_PTC,C_PTC)*Area
C_Tracker=31.88[$/m^2]*Area

Call P_dep(P_turb,P_FT:A_1a,A_1b,A_2a,A_2b, A_3a,A_3b,A_1c,
A_2c,A_3c)

C_COL=C_coll+C_tracker
C_other=C_P1+C_P2+C_turb+C_sink1+C_FT+A_3b*C_pre+(C_B
+C_rec+C_super+C_sink2)*A_3a+(C_FP1+C_IPC)*A_3c
eff_multi=eta_sys*eta_coll

C_not=C_P1+C_P2+C_turb+C_coll+C_tracker+C_sink1+C_FT+C_pre
+(C_B+C_rec+C_super+C_sink2)+(C_FP1+C_IPC)
C_tot_1=C_P1+C_P2+C_turb+C_coll+C_tracker+C_sink1+C_FT
+A_1b*C_pre+(C_B+C_rec+C_super+C_sink2)*A_1a
+(C_FP1+C_IPC)*A_1c
C_tot_2=C_P1+C_P2+C_turb+C_coll+C_tracker+C_sink1
+C_FT+A_2b*C_pre+(C_B+C_rec+C_super+C_sink2)*A_2a
+(C_FP1+C_IPC)*A_2c
C_tot_3=C_P1+C_P2+C_turb+C_coll+C_tracker+C_sink1+C_FT
+A_3b*C_pre+(C_B+C_rec+C_super+C_sink2)*A_3a
+(C_FP1+C_IPC)*A_3c

Z_not=C_not/eta_sys
Z_1=C_tot_1/eta_sys
Z_2=C_tot_2/eta_sys
Z_3=C_tot_3/eta_sys

//Entropy Analysis
//Pump 1
S_dot_gen_pump1=m[2]*(s[2]-s[1])
I_dot_pump1=m[1]*ex[1]-m[2]*ex[2]+w_p1act*m[2]
```

```
I_dot_pump_multi=T_o*S_dot_gen_pump1

//Flash Preheater 1
S_dot_gen_FP1="0"m[5]*s[5]+m[14]*s[14]-m[4]*s[4]-m[13]*s[13]
I_dot_FP1="0"m[4]*ex[4]-m[5]*ex[5]+m[13]*ex[13]-m[14]*ex[14]
I_dot_FP1_multi=S_dot_gen_FP1*T_o

//Flash Tank
S_dot_gen_FT=m[15]*s[15]+m[6]*s[6]-m[5]*s[5]
I_dot_FT=m[5]*ex[5]-m[6]*ex[6]-m[15]*ex[15]
I_dot_FT_multi=S_dot_gen_FT*T_o

//Mixing 1
S_dot_gen_mixing1=m[7]*s[7]-m[6]*s[6]-m[3]*s[3]
I_dot_Mixing1=ex[3]*m[3]-ex[7]*m[7]+m[6]*ex[6]
I_dot_Mixing1_multi=S_dot_gen_mixing1*T_o

//IPC
T_eff_IPC=(h[8]-h[7])/(s[8]-s[7])
S_dot_gen_IPC=Q_dot_sink_2/T_eff_IPC+m[8]*s[8]-m[7]*s[7]
I_dot_IPC=-Q_dot_sink_2*(1-T_o/T_eff_IPC)-m[8]*ex[8]
+m[7]*ex[7]
I_dot_IPC_calc=T_o*S_dot_gen_IPC

//Pump 2
S_dot_gen_pump2=m[8]*(s[9]-s[8])
I_dot_pump2=m[8]*ex[8]-m[9]*ex[9]+w_p2act*m[8]
I_dot_pump2_multi=T_o*S_dot_gen_pump2

//Preheater
T_eff_Pre=(h[9]-h[10])/(s[9]-s[10])
S_dot_gen_Pre=-Q_dot_pre/T_eff_Pre+m[10]*s[10]-m[9]*s[9]
I_dot_Pre=Q_dot_pre*(1-T_o/T_eff_Pre)-m[10]*ex[10]
+m[9]*ex[9]
I_dot_Pre_multi=T_o*S_dot_gen_pre

//Boiler
T_eff_Boiler=(h[11]-h[10])/(s[11]-s[10])
S_dot_gen_Boiler=-Q_dot_boiler/T_eff_Boiler+m[11]*s[11]
-m[10]*s[10]
I_dot_Boiler=Q_dot_boiler*(1-T_o/T_eff_Boiler)+m[10]*ex[10]
-m[11]*ex[11]
I_dot_Boiler_Multi=S_dot_Gen_Boiler*T_o

//Superheater
T_eff_Super=(h[12]-h[11])/(s[12]-s[11])
S_dot_gen_Super=-Q_dot_super/T_eff_super+m[12]*s[12]
-m[11]*s[11]
I_dot_super=Q_dot_super*(1-T_o/T_eff_super)+m[11]*ex[11]
-m[12]*ex[12]
I_dot_super_multi=T_o*S_dot_gen_super

//Turbine
S_dot_gen_turbine=m[13]*s[13]-m[12]*s[12]
I_dot_turbine=-w_t_act*m[13]+m[12]*ex[12]-m[13]*ex[13]
I_dot_turb_Multi=T_o*S_dot_gen_turbine

//Throtling Valve
S_dot_gen_valve=m[15]*(s[16]-s[15])
I_dot_valve=m[15]*(ex[15]-ex[16])
I_dot_valve_multi=S_dot_gen_valve*T_o

//Mixing 2
S_dot_gen_mixing2=m[17]*s[17]-m[14]*s[14]-m[16]*s[16]
```

```
I_dot_mixing2=m[14]*ex[14]+m[16]*ex[16]-m[17]*ex[17]
I_dot_mixing2_multi=T_o*S_dot_Gen_mixing2

//Absorber
T_eff_abs=(h[17]-h[1])/(s[17]-s[1])
S_dot_gen_abs=Q_dot_sink_1/T_eff_abs+m[1]*s[1]-m[17]*s[17]
I_dot_abs=-Q_dot_sink_1*(1-T_o/T_eff_abs)+m[17]*ex[17]
-m[1]*ex[1]
I_dot_abs_multi=T_o*S_dot_gen_abs

S_dot_gen=S_dot_gen_pump1+S_dot_gen_FP1+S_dot_gen_FT
+S_dot_gen_Mixing1+S_dot_gen_IPC+S_dot_gen_pump2
+S_dot_gen_pre+S_dot_gen_Boiler+S_dot_gen_super
+S_dot_gen_turbine+S_dot_gen_valve+S_dot_gen_mixing2
+S_dot_gen_abs

I_dot=I_dot_pump1+I_dot_FP1+I_dot_FT+I_dot_Mixing1
+I_dot_IPC+I_dot_pump2+I_dot_pre+I_dot_Boiler
+I_dot_super+I_dot_turbine+I_dot_valve
+I_dot_mixing2+I_dot_abs

I_dot_multi=T_o*S_dot_gen

(Q_dot_pre+Q_dot_Boiler+Q_dot_Super)/T_eff_H=
Q_dot_pre/T_eff_pre+Q_dot_boiler/T_eff_boiler
+Q_dot_super/T_eff_Super
(Q_dot_sink_1+Q_dot_sink_2)/T_eff_L=Q_dot_sink_1/T_eff_abs
+Q_dot_sink_2/T_eff_IPC

eta_Check=(1-T_eff_L/T_eff_H)/(1+(T_eff_L*T_o*S_dot_gen)
/(T_o*W_dot_net))

eta_check_2=(1-T_eff_L/T_eff_H)-(T_eff_L*S_dot_gen)/(Q_dot_in)
```

APPENDIX C

HEAT EXCHANGER LOSS CALCULATION CODE

The evaluation of the loss parameter from the heat exchangers is completed through a radial conduction analysis. The code is set for a heat exchanger material of brass but the EES property call for Stainless Steel can also be used. The EES code used to complete this analysis follows:

```
T_s_in=ConvertTemp('C','K',500)
T_infinity=ConvertTemp('C','K',25)
T_s_outter=T_infinity+125[K]

//Rated Heat for this HXer
Q_rate=Convert('BTU/hr','W')*(240000[BTU/hr])

//Dimensions of HXer
r_1=r_2-Convert('in','m')*0.25[in]
r_2=r_3-Convert('in','m')*0.5[in] "Insulation thickness"
r_3=r_4-Convert('in','m')*0.25[in]
//r_4=convert('in','m')*0.25[in]+r_3
D=2*(r_4)
D=convert('in','m')*4.5[in]
L=convert('in','m')*((10*8+7)/8)[in]

//Resistances
k_met=k_('Brass"Stainless_AISI302"', (600[K]))
Res_1=(ln(r_2/r_1))/(2*Pi*L*k_met)
k_ins=0.24 "Incropera and Dewitt"
Res_2=(ln(r_3/r_2))/(2*Pi*L*k_ins)
Res_3=(ln(r_4/r_3))/(2*Pi*L*k_met)
Res_4=1/(2*Pi*L*r_4*h_air)
Res_Eq=Res_1+Res_2+Res_3+Res_4

//solve for h_air using natural convection
T_f=(T_s_outter+T_infinity)/2
g=g#
Beta=1/(T_f)
rho=Density(Air,T=T_f,P=101.35[kPa])
k_air=Conductivity(Air,T=T_f)
mu=Viscosity(air,T=T_f)
nu_air= mu/rho
Pr=Prandtl(air,T=T_f)
Pr=nu_air/alpha_air

Ra_d=(g*Beta*(T_s_outter-T_infinity)*(2*r_4)^3)
/(nu_air*alpha_air)
Nus_d=(0.6+((0.387*Ra_d)^(1/6))/((1+(0.559/Pr)^(9/16))^(8/27)))^2
Nus_d=h_air*2*r_4/k_air

q=(T_s_in-T_infinity)/Res_Eq

Ratio=q/Q_rate*100[%]
```

REFERENCES

[1] Abengoa Solar, "Sulcar Platform, PS10: The first commercial tower of the World," May 2009. http://www.abengoasolar.com/sites/solar/en/ourprojects/solucar/ps10/index.html.

[2] Acciona North America, "Nevada Solar One." http://www.acciona-na.com/About-Us/Our-Projects/U-S-/Nevada-Solar-One.aspx.

[3] Bakos, G. C., "Design and construction of a two-axis sun tracking system for parabolic trough collector (PTC) efficiency improvement," *Renewable Energy*, vol. 31, no. 15, pp. 2411 – 2421, 2006.

[4] Bejan, A., Tsatsaronis, G., and Moran, M., *Thermal Design & Optimization*. New York: John Wiley & Sons, Inc., 1996.

[5] Bobkova, E., Grilikhes, V., Soluyanov, A., and Shvarts, M., "A method of choosing optimal parameters of flat fresnel lenses for solar radiation concentration," *Applied Solar Energy (English translation of Geliotekhnika)*, vol. 42, no. 3, pp. 32 – 35, 2006.

[6] Brighman Young University-Thermophysical Properties Laboratory, "American Institute of Chemical Engineers, Design Institute for Physical Properties (DIPPR), project 801," November 2007. http://dippr.byu.edu.

[7] Brodyanskii, V. M., "Improving the efficiency of nuclear and geothermal power stations by using low environment temperatures," *Thermal Engineering (English translation of Teploenergetika)*, vol. 53, no. 3, pp. 201–207, 2006.

[8] Cengel, Y. A. and Boles, M. A., *Thermodynamics: An Engineering Approach*. Boston: McGraw Hill, 4 ed., 2002.

[9] Chou, M.-C., Pan, C., Shen, S., Chen, M.-F., Lin, K., and Wu, S.-T., "A novel method to fabricate gapless hexagonal micro-lens array," *Sensors and Actuators, A: Physical*, vol. 118, no. 2, pp. 298 – 306, 2005.

[10] Colonna, P. and van Putten, H., "Dynamic modeling of steam power cycles. Part I-modeling paradigm and validation," *Applied Thermal Engineering*, vol. 27, no. 2-3, pp. 467 – 480, 2007.

[11] Department of Energy/Enegy Information Administration, "International Energy Outlook 2008," Tech. Rep. DOE/EIA-0484(2008), Energy Information Administration, US Government, Washington, DC, 2008.

[12] Department of Energy/Enegy Information Administration, "Electricity market module," Tech. Rep. DOE/EIA-0554(2009), Energy Information Administration, US Government, Washington, DC, 2009.

[13] DiPippo, R., "Second law assessment of binary plants generating power from low-temperature geothermal fluids," *Geothermics*, vol. 33, no. 5, pp. 565–586, 2004.

[14] Drescher, U. and Bruggemann, D., "Fluid selection for the Organic Rankine Cycle (ORC) in biomass power and heat plants," *Applied Thermal Engineering*, vol. 27, no. 1, pp. 223–228, 2007.

[15] Eck, M., Schmidt, H., Eickhoff, M., and Hirsch, T., "Field test of water-steam separators for direct steam generation in parabolic troughs," *Journal of Solar Energy Engineering, Transactions of the ASME*, vol. 130, no. 1, pp. 0110021 – 0110026, 2008.

[16] Edmund Optics, "Fresnel Lenses," March 2008. http://www.edmundoptics.com/.

[17] El-Sayed, Y. M. and Tribus, M., "A theoretical comparison of the Rankine and Kalina cycles," vol. 1 of *American Society of Mechanical Engineers, Advanced Energy Systems Division (Publication) AES*, (Miami Beach, FL), pp. 97–102, ASME, 1985.

[18] Enick, R. M., Donahey, G. P., and Holsinger, M., "Modeling the high-pressure ammonia-water system with WATAM and the Peng-Robinson equation of state for Kalina cycle studies," *Industrial and Engineering Chemistry Research*, vol. 37, no. 5, pp. 1644 – 1650, 1998.

[19] Garrett by Honeywell, "Garrett Turbochargers," February 2009. http://www.turbobygarrett.com/.

[20] Geisz, J., Friedman, D., Ward, J., Duda, A., Olavarria, W., Moriarty, T., Kiehl, J., Romero, M., Norman, A., and Jones, K., "40.8% efficient inverted triple-junction solar cell with two independently metamorphic junctions," *Applied Physics Letters*, vol. 93, no. 12, pp. 123505 (3 pp.) –, 22 Sept. 2008.

[21] Goswami, D. Y., Kreider, J. F., and Kreith, F., *Principles of Solar Engineering*. Philadelphia: Taylor & Francis, 2 ed., 2000.

[22] Grainger Industrial Supply, "2009 Grainger Online Catalog," March 2009), Date=March 2009, Note=http://www.grainger.com,.

[23] Gross, J. and Sadowski, G., "Application of perturbation theory to a hard-chain reference fluid: An equation of state for square-well chains," *Fluid Phase Equilibria*, vol. 168, no. 2, pp. 183 – 199, 2000.

[24] Harr, Gallagher, and Kell, *NBS/NRC Steam Tables*. Hemishpere Publishing Co., 1984.

[25] Heppenstall, T., "Advanced gas turbine cycles for power generation: A critical review," *Applied Thermal Engineering*, vol. 18, no. 9-10, pp. 837–846, 1998.

[26] Ibrahim, O. M. and Klein, S. A., "Thermodynamic properties of ammonia-water mixtures," vol. 99 of *ASHRAE Transactions*, (Chicago, IL), pp. 1495–1502, ASHRAE, 1993.

[27] Ibrahim, O. and Klein, S., "Absorption power cycles," *Energy (Oxford)*, vol. 21, no. 1, pp. 21 – 27, 1996.

[28] Incropera, F. P. and DeWitt, D. P., *Fundamentals of Heat and Mass Transfer*. Hoboken: John Wiley & Sons, Inc., 5 ed., 2002.

[29] Jiayi, H., Chuanwen, J., and Rong, X., "A review on distributed energy resources and microgrid," *Renewable and Sustainable Energy Reviews*, vol. 12, no. 9, pp. 2465 – 2476, 2008.

[30] Johnson, M. G., Sato, H., Williamson, A. G., and Eubank, P. T., "Enthalpies for ethylbenzene, isooctane, and ethylcyclohexane in the fluid state," *Journal of Chemical and Engineering Data*, vol. 35, no. 2, pp. 101 – 107, 1990.

[31] Kalina, A. I., "Combined-cycle system with novel bottoming cycle," *Journal of Engineering for Gas Turbines and Power, Transactions of the ASME*, vol. 106, no. 4, pp. 737–742, 1984.

[32] Kalina, A., "Generation of energy," Tech. Rep. US Patent 4489563, United State Patent Office, 1984.

[33] Kandlikar, S. G., "Fundamental issues related to flow boiling in minichannels and microchannels," *Experimental Thermal and Fluid Science*, vol. 26, no. 2-4, pp. 389–407, 2002.

[34] Kemmoku, Y., Sakakibara, T., Hiramatsu, M., Miyazaki, Y., and Egami, T., "Field test of a concentrator photovoltaic system with flat fresnel lens," vol. C, (Osaka, Japan), pp. 2379 – 2382, 2003.

[35] Kouremenos, D. and Rogdakis, E., "Temperature - entropy (or enthalpy) and the enthalpy entropy (Mollier) diagram of the kalina cycle," vol. 19, (New York, NY, USA), pp. 13 – 19, 1990.

[36] Lee, M. J., Tien, D. L., and Shao, C. T., "Thermophysical capability of ozone-safe working fluids for an organic rankine cycle system," *Heat Recovery Systems & CHP*, vol. 13, no. 5, pp. 409–418, 1993.

[37] Lee, S., Lin, L., Pister, K., Wu, M., Lee, H., and Grodzinski, P., "Passively aligned hybrid integration of 8 1 micromachined micro-fresnel lens arrays and 8 1 vertical-cavity surface-emitting laser arrays for free-space optical interconnect," *IEEE Photonics Technology Letters*, vol. 7, no. 9, pp. 1031 – 1033, 1995.

[38] Leibowitz, H. M. and Micak, H. A., "Design of a 2 MW Kalina cycle binary module for installation in Husavik, Iceland," *Transactions - Geothermal Resources Council*, vol. 23, pp. 75–80, 1999.

[39] Leibowitz, H. and Mirolli, M., "First Kalina combined-cycle plant tested successfully," *Power Engineering (Barrington, Illinois)*, vol. 101, no. 5, p. 4, 1997.

[40] Leutz, R. and Suzuki, A., *Nonimaging Fresnel Lenses: Design and Performance of Solar Concentrators*. Berlin: Springer, 2001.

[41] Lu, S., "Dynamic modelling and simulation of power plant systems," *Proceedings of the Institution of Mechanical Engineers, Part A: Journal of Power and Energy*, vol. 213, no. 1, pp. 7 – 22, 1999.

[42] Lu, S. and Hogg, B., "Dynamic nonlinear modelling of power plant by physical principles and neural networks," *International Journal of Electrical Power and Energy System*, vol. 22, no. 1, pp. 67 – 78, 2000. Power plant modeling;.

[43] Lupfert, E., Geyer, M., Schiel, W., Esteban, A., Osuna, R., Zarza, E., and Nava, P., "Eurotrough design issues and prototype testing at PSA," ASME International Solar Energy Conference, (Washington, DC), pp. 387–391, ASME, 2001.

[44] Mago, P. J., Chamra, L. M., and Somayaji, C., "Performance analysis of different working fluids for use in Organic Rankine Cycles," *Proceedings of the Institution of Mechanical Engineers, Part A: Journal of Power and Energy*, vol. 221, no. 3, pp. 255–264, 2007.

[45] Maloney, J. D. and Robertson, R., "Thermodynamic study of ammonia-water heat power cycles," Tech. Rep. CF-53-8-43, Oak Ridge National Laboratories, Oak Ridge, TN, 1953.

[46] McMaster-Carr Supply Company, "2009 McMaster Carr Online Catalog," March 2009. http://www.mcmaster.com.

[47] Mejbri, K. and Bellagi, A., "Modelling of the thermodynamic properties of the water-ammonia mixture by three different approaches," *International Journal of Refrigeration*, vol. 29, no. 2, pp. 211–218, 2006.

[48] Ministero de Ciencias e Innovación, "La Platforma Solar de Almeria," May 2009. http://www.psa.es.

[49] Mlcak, H., Mirolli, M., Hjartarson, H., Husavikur, O., and Ralph, M., "Notes from the North: A report on the debut year of the 2 MW Kalina cycle geothermal power plant in Husavik, Iceland," Transactions - Geothermal Resources Council, (Reno, NV, United States), pp. 715–718, Geothermal Resources Council, 2002.

[50] Mlcak, H. A., "Kalina cycle concepts for low temperature geothermal," Transactions - Geothermal Resources Council, (Reno, NV), pp. 707–713, Geothermal Resources Council, 2002.

[51] Modern Automotive Performance, "Garret GT1241," February 2009. http://www.maperformance.com/garrett-gt1241-turbocharger-50-130-hp.html.

[52] Montes, M., Abnades, A., and Martnez-Val, J., "Performance of a direct steam generation solar thermal power plant for electricity production as a function of the solar multiple," *Solar Energy*, vol. 83, no. 5, pp. 679 – 689, 2009.

[53] National Renewable Energy Laboratory, "National Solar Radiation Database 1991-2005 Update," October. http://rredc.nrel.gov/solar/old_data/nsrdb/1991-2005/.

[54] National Renewable Energy Laboratory, "Photovoltaics," September 2007. http://www.nrel.gov/learning/re_photovoltaics.html.

[55] O'Gallagher, J., *Nonimaging optics in solar energy:Synthesis lectures on energy and the environment: technology, science, and society.* San Rafael, Calif.: Morgan & Claypool Publishers, 2008.

[56] O'Neill, M. J., "Transmittance-optimized, point-focus Fresnel lens solar concentrator," (Indian Wells, CA, USA), pp. 25 – 37, 1984.

[57] RenewableEnergyWorld.com, "Solar cell breaks the 40% efficiency barrier," November 2008. http://www.renewableenergyworld.com/rea/news/story?id=46765.

[58] Rogdakis, E. D., "Thermodynamic analysis, parametric study and optimum operation of the Kalina cycle," *International Journal of Energy Research*, vol. 20, no. 4, pp. 359–370, 1996.

[59] Rogdakis, E. D. and Antonopoulos, K. A., "High efficiency NH3/H2O absorption power cycle," *Heat Recovery Systems & CHP*, vol. 11, no. 4, pp. 263–275, 1991.

[60] Saleh, B., Koglbauer, G., Wendland, M., and Fischer, J., "Working fluids for low-temperature organic Rankine cycles," *Energy*, vol. 32, no. 7, pp. 1210–1221, 2007.

[61] Sandler, S. I., *Chemical and Engineering Thermodynamics*. New York: John Wiley & Sons, Inc., 3 ed., 1999.

[62] Smith, R. W., Ranasinghe, J., Stats, D., and Dykas, S., "Kalina combined cycle performance and operability," vol. 30 of *American Society of Mechanical Engineers, Power Division (Publication) PWR*, (Houston, TX, USA), pp. 701–728, ASME, 1996.

[63] Stecco, S. S. and Desideri, U., "Thermodynamic analysis of the Kalina cycles: Comparisons, problems and perspectives," American Society of Mechanical Engineers, (Toronto, Ont), pp. 149–8, ASME, 1989.

[64] Stirling Energy Systems, Inc., "Suncatcher: Pure power made simple," June 2009. http://www.stirlingenergy.com/.

[65] Thome, J. R., "Boiling in microchannels: a review of experiment and theory," *International Journal of Heat and Fluid Flow*, vol. 25, no. 2, pp. 128–139, 2004.

[66] Thome, J. R., "State-of-the-art overview of boiling and two-phase flows in microchannels," *Heat Transfer Engineering*, vol. 27, no. 9, pp. 4–19, 2006.

[67] Tillner-Roth, R., *Fundamental Equation of State*. Verlad, Aachan: Shaker, 1998.

[68] US Department of Energy, "A consumer's guide to energy efficiency and renewable energy: Estimating appliance and home electronic energy use," October 2007. http://apps1.eere.energy.gov/consumer/your_home/appliances/index.cfm/mytopic=10040.

[69] US Department of Energy: Energy Efficiency and Renewable Energy, "A consumer guide: Get your power from the sun," June 2009. http://www.nrel.gov/docs/fy04osti/35297.pdf.

[70] US Environmental Protection Agency, "2001 dupont Safety Health & Environment Robust Summary for HCFC-123," June 2009.

[71] US Environmental Protection Agency and US Department of Energy, "Energy star: Boilers for consumers," 2009.

[72] US Naval Research Laboratory, "Vanguard Project," June 2009. http://www.nrl.navy.mil/content.php?P=VANGUARD.

[73] van Putten, H. and Colonna, P., "Dynamic modeling of steam power cycles: Part ii - simulation of a small simple rankine cycle system," *Applied Thermal Engineering*, vol. 27, no. 14-15, pp. 2566 – 2582, 2007.

[74] Vidal, A., Best, R., Rivero, R., and Cervantes, J., "Analysis of a combined power and refrigeration cycle by the exergy method," *Energy*, vol. 31, no. 15, pp. 3401–3414, 2006.

[75] Vijayaraghavan, S. and Goswami, D. Y., "A combined power and cooling cycle modified to improve resource utilization efficiency using a distillation stage," *Energy*, vol. 31, no. 8-9, pp. 1177–1196, 2006.

[76] WattSun Solar Trackers, "Wattsun solar tracke retail price and data sheet," December 2008.

[77] Wei, D., Lu, X., Lu, Z., and Gu, J., "Performance analysis and optimization of organic Rankine cycle (ORC) for waste heat recovery," *Energy Conversion and Management*, vol. 48, no. 4, pp. 1113–1119, 2007.

[78] White, F. M., *Fluid Mechanics*. Boston: McGraw Hill, 5 ed., 2002.

[79] Yoshioka, K., Kobayashi, M., Suzuki, A., Endoh, K., Ohe, N., and Saitoh, T., "Optimum design and properties of a static concentrator with a non-imaging lens," vol. 1, (Waikoloa, HI, USA), pp. 1119 – 1122, 1994.

[80] Zarza, E., Valenzuela, L., Len, J., Hennecke, K., Eck, M., Weyers, H. D., and Eickhoff, M., "Direct steam generation in parabolic troughs: Final results and conclusions of the DISS project," *Energy*, vol. 29, no. 5-6, pp. 635 – 644, 2004.

[81] Zhang, P., Londe, G., Sung, J., Johnson, E., Lee, M., and Cho, H., "Microlens fabrication using an etched glass master," *Microsystem Technologies*, vol. 13, no. 3-4, pp. 339 – 342, 2007. Conformal antiadhesion layer;Hot embossing;Isotropic etching;Numerical aperture;.

VITA

Suzanne E. Price was awarded her Bachelors Degree in Mechanical Engineering from North Carolina State University in May 2003. At NC State, Ms. Price was a member of the women's gymnastics team, the corresponding secretary for the NC Alpha Chapter of Tau Beta Pi, and a member of Pi Tau Sigma Honors Society. Ms. Price continued her education at Georgia Institute of Technology at the Woodruff School of Mechanical Engineering where she received her MS degree in Mechanical Engineering on August 1, 2009. Ms. Price has accepted a position with the GreenTech group at MPR, a nuclear engineering consulting firm in Alexandria, Virginia.